amU
Aix Marseille Université

NNT : 2024AIXM0001

THÈSE DE DOCTORAT

Soutenue à AMU — Aix-Marseille Université
le 18 decembre 2024 par

Borana DOLLOMAJA

Modélisation de la stimulation pour l'épilepsie réfractaire

Modeling brain stimulation for drug-resistant epilepsy diagnosis

Discipline
Biologie Santé

Spécialité
Neurosciences

École doctorale
ED62 - Sciences de la Vie et de la Santé

Laboratoire/Partenaires de recherche
Institut de Neurosciences des Systèmes (INS)

Composition du jury

John Terry University of Birmingham, UK	Rapporteur
Premysl JIRUSKA Charles University, Czech Republic	Rapporteur
Julien MODOLO Université de Rennes, France	Examinateur
Agnes TREBUCHON Aix Marseille Université (INS), Service de neurophysiologie clinique - Hôpital de la Timone (AP-HM), France	Présidente du jury
Viktor JIRSA Aix Marseille Université (INS), France	Directeur de thèse

Institut de Neurosciences des Systèmes

Affidavit

I, undersigned, Borana Dollomaja, hereby declare that the work presented in this manuscript is my own work, carried out under the scientific supervision of Viktor Jirsa and Huifang Wang, in accordance with the principles of honesty, integrity and responsibility inherent to the research mission. The research work and the writing of this manuscript have been carried out in compliance with both the French national charter for Research Integrity and the Aix-Marseille University charter on the fight against plagiarism. This work has not been submitted previously either in this country or in another country in the same or in a similar version to any other examination body.

Marseille, le 15/10/2024 [Signature]

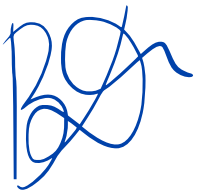

This work is licensed under Creative Commons Attribution-NonCommercial-NoDerivatives 4.0 International Public License

Liste de publications et/ou bervets et participation aux conferences

1. Liste des publications et/ou brevet réalisées dans le cadre du projet de thèse :
   (a) **Dollomaja, B.**, Wang, H., Makhalova, J., Guye, M., Bartolomei, F., Jirsa, V., Virtual Epilepsy Patient Cohort : Generation and Evaluation. medRxiv 2024.10.02.24314607 ; doi : https ://doi.org/10.1101/2024.10.02.24314607
   (b) **Dollomaja, B.**, Makhalova, J., Wang, H., Bartolomei, F., Jirsa, V., Bernard, C. (2023). Personalized whole brain modeling of status epilepticus. Epilepsy & Behavior, 142, 109175.
   (c) Wang, H. E., **Dollomaja, B.**, TRIEBKORN, J. P., Duma, G. M., Williamson, A., Makhalova, J., ... Jirsa, V. (2024). Virtual brain twins for stimulation in epilepsy. medRxiv, 2024-07.
   (d) Wang, H. E., Triebkorn, P., Breyton, M., **Dollomaja, B.**, Lemarechal, J. D., Petkoski, S., ... Jirsa, V. K. (2024). Virtual brain twins : from basic neuroscience to clinical use. National Science Review, 11(5), nwae079.
   (e) Wang, H. E., Woodman, M., Triebkorn, P., Lemarechal, J. D., Jha, J., **Dollomaja, B.**, ... Jirsa, V. (2023). Delineating epileptogenic networks using brain imaging data and personalized modeling in drug-resistant epilepsy. Science Translational Medicine, 15(680), eabp8982.
2. Participation aux conférences et écoles d'été au cours de la période de thèse :
   (a) OHBM Conference - Seoul, South Korea,
   June 2024, Poster Presenter and Speaker
   (b) Brain connectivity workshop - Shanghai, China
   June 2024, Participant
   (c) OHBM Educational Course on Whole-brain Models
   July 2023, Online Speaker
   (d) Atelier AVIESAN "Neurosciences computationnelles" - Paris, France
   January 2023, Junior Presenter
   (e) SfN Conference - San Diego, USA
   November 2022, Poster presenter
   (f) ICTALS Conference - Bern, Switzerland
   July 2022, Poster Presenter
   (g) 14th European Epilepsy Congress - Geneva, Switzerland
   July 2022, Participant
   (h) School of Brain Cells & Circuits "Camillo Golgi" - Erice, Italy
   December 2021, Participant and Poster presenter

Résumé

L'épilepsie se caractérise par des crises récurrentes et un tiers des patients sont résistants aux traitements médicamenteux. La chirurgie cérébrale ciblant les zones épileptogènes (EZ) offre une alternative avec un taux de réussite de 60%, souvent entravé par un mauvais diagnostic des EZ. Les électrodes intracérébrales (SEEG) aident à localiser les EZ avant la chirurgie, mais les enregistrements de crises spontanées ne fournissent pas toujours suffisamment d'information. Pour mieux délimiter les EZ, la stimulation cérébrale est utilisée pour déclencher des crises, mais cette méthode repose sur une approche par essai et erreur, nécessitant une meilleure compréhension des effets des paramètres de stimulation.

Cette thèse s'est concentrée sur les modèles de stimulation à l'échelle du cerveau entier pour le diagnostic de l'épilepsie avec trois résultats principaux. Premièrement, le modèle Epileptor a été étendu pour prendre en compte les crises stimulées. En utilisant ce modèle, nous avons virtualisé un ensemble de données de 30 patients atteints d'épilepsie pharmacorésistante. L'hypothèse d'EZ a été estimée par le pipeline Virtual Epileptic Patient, actuellement utilisé dans un essai clinique "EPINOV". Pour chaque patient virtuel, nous avons généré et validé des copies synthétiques de leur activité interictale, ainsi que de leurs crises spontanées et stimulées. Deuxièmement, en utilisant des modèles de champ neuronal à haute résolution, nous avons simulé des crises déclenchées par la stimulation SEEG et une par une nouvelle méthode non invasive appelée stimulation par interférence temporelle. Ces modèles à haute résolution permettent de calculer les champs électriques générés par la stimulation. Cette avancée nous a permis d'établir et de valider le premier pipeline diagnostique pour estimer l'EZ à partir des crises stimulées. Troisièmement, nous avons construit des jumeaux cérébraux virtuels pour 5 patients atteints d'épilepsie ayant subi 1363 stimulations, dont 16 ont déclenché des crises. Nous avons systématiquement étudié la relation entre les paramètres de stimulation et l'EZ. Cela pourrait ouvrir la voie à l'optimisation des paramètres de stimulation pour aider les cliniciens dans le diagnostic de l'épilepsie.

De plus, en utilisant des modèles cérébraux personnalisés, nous avons montré pour la première fois que l'état de mal épileptique se propage selon les connexions structurelles du cerveau. En résumé, nos travaux démontrent que les modèles de stimulation du cerveau entier peuvent capturer les caractéristiques des données réelles et expliquer les effets des paramètres de stimulation. À l'avenir, ces modèles pourraient devenir un outil précieux pour la neuromodulation des réseaux épileptiques.

Mots clés : épilepsie, stimulation cérébrale, modélisation, dynamique des crises, SEEG

Abstract

Epilepsy involves recurrent seizures and one-third of patients are resistant to medication. Brain surgery targeting epileptogenic zones (EZ), offers an alternative treatment with 60% success rate, often hindered by EZ misdiagnosis. Intracerebral depth electrodes (SEEG) help localize EZ pre-surgery, but spontaneous seizure recordings may not provide enough data. To better delineate the EZ, brain simulation is used to trigger seizures but is done by trial-and-error and requires a better understanding of stimulation parameter effects.

This thesis focused on whole-brain stimulation models for epilepsy diagnosis with three main results. First, the Epileptor model was extended to account for stimulated seizures. Using this model, we virtualized a dataset of 30 drug-resistant epilepsy patients. The EZ hypothesis was estimated by the Virtual Epileptic Patient pipeline, currently used in a clinical trial. For each virtual patient, we generated and validated synthetic copies of their interictal activity, spontaneous and stimulated seizures. Then we examined the effects of stimulation amplitude and location, finding that higher amplitudes increased seizure likelihood, and location effects varied with seizure network organization. Second, using high-resolution neural field models we simulated seizures triggered by SEEG stimulation and a novel non-invasive method called Temporal Interference stimulation. High-resolution neural field models enable the calculation of electric fields introduced by stimulation. This advancement allowed us to establish and validate the first diagnostic pipeline for estimating the EZ during stimulations. Third, we built virtual brain twins for 5 epileptic patients, who underwent 1363 stimulations, of which 16 triggered seizures. We systematically investigated the relationship between stimulation parameters and EZ. This could pave the way for optimal stimulation parameters to assist clinicians in diagnosing epilepsy.

Additionally, using personalized brain modeling, we showed for the first time that status epilepticus spreads according to the brain's structural connections. In summary, our work demonstrates that whole-brain stimulation models can capture real data features and explain stimulation parameter effects. In the future, these models could be a guiding tool for neuromodulation of seizure networks.

Keywords : epilepsy, brain stimulation, modeling, seizure dynamics, SEEG

Acknowledgements

As much as we all say it and know it, time flies. Still, I find it difficult to grasp that these four years have flown by. This PhD started from a series of inconspicuous events, spanning over many years, and it would not have been possible without the generosity of my thesis supervisor, Viktor Jirsa. Thank you for being an individual of great character, resilience, and optimism. Thank you for your honest answers when I asked all sorts of questions. Thank you for your guidance, your patience in explaining concepts, and all your support throughout the years.

My thesis ultimately focused on stimulation for epilepsy, which meant having the chance to work with my co-supervisor, Huifang Wang. This thesis defense would not have taken place without her, as well as the projects described here. Thank you, Huifang, for always checking in, for working patiently with me and for all the laughter and honest conversations. Thank you for teaching me about Chinese culture and allowing me to experience it firsthand. Thank you for your honest vision of science, for leading by example, and for always striving to be the best scientific version of yourself.

To all the people that helped me along the way, Carmela and Gian Marco, thank you for working with me on TI modeling. I was happy to no longer be struggling alone. To Fabrice Bartolomei and Julia Makhalova, thank you for your immensely valuable clinical insights. To Christophe Bernard, I really admire you ; thank you for working with me for a bit and helping me write my first academic paper. To Flavius, thank you for helping me with the clinical stimulation data and for being such a great individual. To Paul and your brilliant disco brains, thank you for all your pre-processing and your invaluable help ; you are a fine scientist.

To the person that made me take a leap of faith in joining this lab, Lionel, thank you for always taking the time to share your experience and knowledge. To the first people I got to share my office with, Bahar, Mario, Marcel, thank you for your support (you had to handle a young lady who had zero clue about what she was doing and was internally, quietly, panicking). To Sawssan and Sophie, thank you for your friendship and support, you were the first friends I made here. To Camille, thank you for quickly becoming one of my dearest friends. To Kashyap, thank you for your being a (much better than me) sport buddy after work and a great friend. To Lisa, Hiba, Viktor Sip, Giovanni, thank you for the memorable hikes, trips, conversations and friendship. To Amir, Manef, Giovanna, Nariman, Nina, Meysam, Tasos thank you for the cool barbecues and fun conversations. Spase, thank you for always stopping by and saying hi and always being open for a chat. To Jean-Didier, thank you for being the only French person in the epilepsy team, and for your valuable advice. To Martin, thank you for the insightful conversations and your unique perspective. To Aitakin, Claudio, Damien, thank you for your kindness and sunny personality. To Marmaduke and Jan, thank you for being sooo cool. Marisa, I greatly admire your work and am really happy to have met you in person. I hope the scientific community continues to benefit from your

contributions for many years to come. Also, the cool kids : Giacomo, Chloe, Sofia, Pietro, Daniela, Sara, Maria, Matteo, Gabriele and more - thank you for letting me join in some of your adventures, you really know how to enjoy your PhD and I love seeing that. Giacomo and Chloe, thank you for making our office a better place, I will miss you. Speaking of cool, Christophe, Anton, Antoine, Pascale, Marco, Myriam, Vinicius, Maeva, Melany, Akanksha thank you for making my time in the lab so enjoyable and sweet (I'm thinking of all the cakes, of course). To Pierpaolo, thank you for your friendship and for giving me a home for the last year of my PhD - from where I am writing this. I saw you as a new postdoc that was always ready to make silly jokes and I'm proud and lucky to see the great researcher and mentor you've become, but most importantly, I am so proud of the risotto you make.

To my friends, thank you for standing by me. Romain, thank you for growing into adulthood with me and for being such a generous and kind friend. Alexandre et Elia, merci pour votre précieuse amitié, et j'ai hâte de vous revoir, ainsi que Desara, Manon, Myriam, Stefan, Mamadou. Polikseni, Faustine, thank you for your encouraging words to stop being hard on myself ; you're the kind of friends anyone would be lucky to have. Greisa, thank you for hanging out in Tirana with Poli over the years ; I hope the tradition will continue. Amela, thank you for your friendship and advice – my thesis is definitely not a page over 120.

Finally, and most importantly, to my family, thank you for your constant support. To my mom Trendelina, thank you for your unconditional support and love, for putting our education and independence first when you didn't get the same opportunities. To my sisters, Anxhela, Anisa, thank you for always being there for me. To my dad, Ramadan, thank you for your support. To my grandparents, thank you for your love and precious childhood memories. Gjysh Hyseni, nuk i harroj bisedat tona dhe pasionin e perbashket per shkencen.

I will really miss the INS, and hope many more will have the chance to experience this great academic environment, as I did.

Contents

I Framework **1**

1 Introduction **2**
1.1 Objectives of the thesis 3
1.2 Structure of the thesis 4

2 Epilepsy **6**
2.1 Clinical and biological aspects of epilepsy 6
2.1.1 Introduction 6
2.1.2 From ancient cultures to modern neurology 6
2.1.3 Seizures 7
2.1.4 Epilepsy treatment 8
2.1.5 Epileptogenic zone concept in drug-resistant epilepsy 8
2.1.6 Diagnosis of drug-resistant epilepsy 10
2.1.7 Summary 13
2.2 Models of epilepsy 13
2.2.1 Computational models of the brain 13
2.2.2 Phenomenological neural mass models of seizures 18
2.2.3 The Virtual Epileptic Patient 22

3 Brain stimulation in epilepsy **27**
3.1 Clinical relevance of brain stimulation 27
3.1.1 Overview of stimulation methods 27
3.1.2 Invasive brain stimulation in epilepsy 30
3.1.3 Non-invasive brain stimulation in epilepsy 34
3.2 Models of brain stimulation 38
3.2.1 Modeling the stimulation electric field 38
3.2.2 Modeling the brain's response 41
3.2.3 Important challenges in brain stimulation models 43
3.3 Summary 44

II Original work **45**

4 A model for stimulated seizures **46**
4.1 Context 46
4.2 A hypothesis based on empirical observation 47
4.3 Modeling the accumulatory effect with the 3D Epileptor 48

4.4 Conclusion 50

5 Virtual Epileptic Patient Cohort **52**
5.1 Introduction 52
5.2 Results 54
5.2.1 Workflow of the virtual epileptic cohort 54
5.2.2 Overview of virtual epileptic cohort 56
5.2.3 Spontaneous seizures 56
5.2.4 Stimulated seizures 61
5.2.5 Interictal spikes 65
5.3 Discussion and conclusions 65
5.4 Materials and methods 68
5.4.1 Study design 68
5.4.2 Patient data 69
5.4.3 Data processing 70
5.4.4 Neural mass models 71
5.4.5 The Epileptor model 72
5.4.6 The Epileptor-stimulation model 73
5.4.7 Calculation of the electric field of SEEG stimulation 74
5.4.8 Spontaneous seizures 74
5.4.9 Stimulated seizures 75
5.4.10 Interictal spikes 77
5.4.11 Randomized cohort 78
5.4.12 Comparing simulated and empirical SEEG traces 78
5.4.13 Permutation test 80
5.5 Data availability 80
5.6 Supplementary Material 81
5.6.1 BIDS structure of the virtual epileptic cohort 81
5.6.2 Example of two different seizure types for the same patient . 81
5.6.3 Epileptor-stimulation model 83
5.6.4 Changing stimulation parameters 83
5.6.5 Data features for comparing simulated and empirical SEEG . 85
5.6.6 Cohort statistics based on the clinical hypothesis 85
5.6.7 Complete set of metrics used to compare simulated and empirical seizures 86
5.6.8 Grouping metrics by surgical outcome 90

6 High-resolution stimulation models **92**
6.1 Introduction 92
6.2 Results 93
6.2.1 Virtual epileptic patient pipeline for SEEG stimulation . . . 93
6.2.2 Virtual epileptic patient pipeline for TI stimulation 95
6.2.3 Applying the pipeline to a second patient 95
6.3 Discussion and conclusions 99
6.3.1 Summary 99
6.3.2 Future scientific studies 99
6.4 Methods 103

6.4.1 Patient data . . . 103
6.4.2 Data processing . . . 103
6.4.3 High resolution simulation of the Epileptor-Stimulation model 104
6.4.4 Calculation of the electric field of SEEG stimulation . . . 105
6.4.5 Calculation of the electric field of the TI stimulation . . . 106

7 Applications to clinical data 108
7.1 Optimizing the stimulation model based on empirical data . . . 108
7.1.1 Context and project goal . . . 108
7.1.2 Methods . . . 109
7.1.3 Preliminary results . . . 110
7.1.4 Conclusion . . . 112
7.2 Clinical trial Epinov . . . 116
7.2.1 Context and project goal . . . 116
7.2.2 Methods . . . 116
7.2.3 My contributions to the clinical trial . . . 116

8 Modelling status epilepticus 118
8.1 Introduction . . . 118
8.2 Results . . . 119
8.2.1 Virtualizing Status Epilepticus Patient . . . 119
8.2.2 Status Epilepticus Network Dynamics . . . 121
8.3 Discussion . . . 124
8.4 Conclusion . . . 125
8.5 Methods . . . 125
8.5.1 Patient data . . . 125
8.5.2 Data processing . . . 125
8.5.3 VEP model construction . . . 126
8.5.4 Neural mass modeling . . . 127
8.5.5 Modeling status epilepticus . . . 127
8.5.6 Forward solution . . . 128
8.6 Supplementary figures . . . 128

9 Conclusions 132
9.1 Summary . . . 132
9.2 Discussion . . . 133
9.3 Perspectives . . . 135
9.4 Personal thoughts . . . 135

List of figures

2.1 Classification of epilepsies according to ILAE 7
2.2 The evolving representations of the epileptogenic zone 9
2.3 Network organization of partial seizures 10
2.4 Presurgical methods to locate the epileptogenic area 11
2.5 Placement of SEEG electrodes in the 70s 12
2.6 Models of epileptiform activity 15
2.7 Onset dynamical mechanisms 20
2.8 The Epileptor model 23
2.9 The Virtual Epileptic Patient with different types of seizure 24
2.10 VEP pipeline 26

3.1 Typical placement of a DBS electrode 28
3.2 Timing of DBS effects across disorders 29
3.3 tES electric field on realistic brain model 35
3.4 Temporal Interference Stimulation 36
3.5 Temporal Interference from mouse to human 37
3.6 Examples of non-invasive brain stimulation estimation with realistic head models and finite-element modeling calculations. Taken from [147]. 41
3.7 Activating function monopolar cathodic stimulation 42

4.1 Empirical example of stimulation and accumulation phenomenon . . 47
4.2 3D Epileptor model with varying m 49
4.3 Accumulatory behavior of variable m 49
4.4 Stimulation examples with the Epileptor model 50

5.1 Workflow of the virtual epileptic patient cohort 55
5.2 Empirical and simulated spontaneous seizure activity 59
5.3 Comparing simulated and empirical SEEG spontaneous seizures . . 60
5.4 Empirical and simulated seizures triggered by stimulation 62
5.5 63
5.5 Comparison of simulated and empirical SEEG signals for stimulation induced seizures 64
5.6 Empirical and simulated SEEG interictal activity 66
5.7 BIDS-IEEG structure of the virtual epileptic cohort 81
5.8 Two different seizure types from the same patient 82
5.9 Example time series for Epileptor-stimulation model 83
5.10 Simulation examples with different stimulation amplitudes 84

5.11 Simulation examples with different stimulation locations 85
5.12 Comparing simulated and empirical SEEG 86
5.13 Cohort statistics based on the clinical hypothesis 87
5.14 All statistics for the VEC dataset as compared to the control dataset for spontaneous seizures 87
5.15 All statistics for the VEC dataset as compared to the control dataset for stimulated seizures 88
5.16 Grouped metrics following surgical outcome 91

6.1 VEP diagnostic mapping for spontaneous seizures 94
6.2 VEP diagnostic mapping for SEEG stimulation 96
6.3 Epileptor-Stimulation time series with SEEG stimulation 97
6.4 VEP diagnostic mapping from TI stimulation 98
6.5 Epileptor-Stimulation time-series with TI stimulation 99
6.6 VEP diagnostic mapping from SEEG stimulation for a second patient with frontal lobe epilepsy 100
6.7 VEP diagnostic mapping from TI stimulation for second patient with frontal lobe epilepsy 101

7.1 Neural mass versus neural fields electric fields 110
7.2 Stimulating pairs inducing seizure and not-inducing seizure 111
7.3 Stimulation field inducing seizure and not inducing seizure 112
7.4 High-resolution stimulation field inducing seizure versus not inducing seizure 113
7.5 Using estimated EZ and global coupling K distributions, we parametrized our virtual brain model for patient 1. We then ran simulations for each clinical stimulation setting and compared the outcome with the empirical data. The panel "Stimulations", compares the outcome between simulated timeseries and empirical recordings in terms of triggered seizures (dark blue) or no triggered seizure. In A), we estimated the aforementioned parameters using the first spontaneous seizure of the patient. In B), we used the second spontaneous seizure of the patient, and in C) their third spontaneous seizure. 114
7.6 One example of simulations performed. Each number corresponds to a simulation where a seizure was triggered. On the right, we show the simulated timeseries on the whole-brain level and plot the region where the seizure was triggered, alongside the slow-evolving parameters, in particular m which crossed the seizure threshold. 115

8.1 Personalised brain model for a patient with status epilepticus 120
8.2 SEEG recording and simulated time-series of SE 122
8.3 Connections where refractory status epilepticus is observed 122
8.4 Epileptogenicity map of x0 values 123
8.5 Circular graph of 300 strongest region-to-region connection strengths 124
8.6 Simulation time series on the source level and on the sensor level . . 129
8.7 Simulation time series on the source level and on the sensor level . . 130
8.8 Simulation of SE using a different set of parameters 131

List of tables

5.1 Patient information of the virtual epileptic cohort. Abbreviations : FCD, focal cortical dysplasia ; HS, hippocampal sclerosis ; L, left ; NA, not applicable ; PMG, polymicrogyria ; PNH, periventricular nodular heterotopia ; R, right ; R>L : right hemisphere onset propagating to left hemisphere ; R&L : right and left onset ; NSS, number of simulated spontaneous seizures ; NIS, number of simulated induced seizures ; NII, number of simulated interictal timeseries. 57

7.1 Overview of the empirical dataset. SS : spontaneous seizures, SIS : stimulation-induced seizures, HS : hippocampal sclerosis, FCD : focal cortical dysplasia, DNET :dysembryoplastic neuroepithelial tumor, M :male, F :female, R :right, L :left. 111

Liste des abréviations

CT	Computed Tomography
EZ	Epileptogenic Zone
DRE	Drug-resistant epilepsy
dMRI	diffusion Magnetic Resonance Imaging
MRI	Magnetic Resonance Imaging
SEEG	Stereoelectroencephalography
ECoG	Electrocorticography
SE	Status Epilepticus
PZ	Propagation Zone
TI	Temporal Interference
ILAE	International League Against Epilepsy
NMM	Neural mass model
NFM	Neural field model

Première partie

Framework

Chapter 1

Introduction and thesis goals

Brain disorders are numerous, and epilepsy is one of the most common, with symptoms documented in some of the oldest inscriptions. It is also a universal disorder of neural systems, sharing common patterns between species, from flies and fish to cats, dogs, and humans [93]. This inherent property of brain systems is characterized by abrupt and yet recurrent abnormal electrical activity of the brain. Current progress allows for the electrical features of the disorder to be phenomenologically modeled [67] and spatio-temporal seizure propagation patterns can be modeled at the whole brain level [66]. This is achieved thanks to developments in brain imaging and analysis of electrophysiological seizure patterns [10, 142]. In this thesis, we focus on modeling stimulated seizures using personalized virtual brain models, integrating them into virtual brain datasets, and comparing our simulations to empirical data.

There exist multiple models to describe seizures in epilepsy, from the neural level, or the microscale, up to the whole brain level, or macroscale [30, 143]. At one end of spatial resolution, microscale models describe intricate dynamics of ion channels, synaptic transmission, and glial-neuron cell interactions [31, 110, 132]. In the middle, mesoscale models describe neural network interactions, where different cell types interact and give rise to ensemble dynamics [133, 146]. At the other end, macroscale models describe neural population interactions both within individual regions and between brain regions. One of the most common mesoscale models are neural mass models, which capture the global dynamics of neural populations by describing local field potentials or mean membrane potential [29, 67].

The brain contains an immense number of neurons, around 86 billion, and an estimated 171 billion cells in total. The intricate interactions between chemical and electrical synapses, along with ion channels, make it extremely challenging to fully understand the biophysical processes behind seizure generation. Neural mass models simplify this complexity by concentrating on specific neurophysiological patterns. In this study, we used the Epileptor neural mass model, which focuses on the dynamic features of seizures at the neural population level [67]. This phenomenological model is particularly useful in describing spatio-temporal seizure organization and has been used to estimate the networks of seizure generation from empirical data [51].

In addition, although seizures share common patterns across individuals, they also express important levels of intra- and inter-subject variability [107, 117]. To express variability across subjects, personalized brain models are needed. In particular,

brain network models can capture individual brain connectivity from white-matter fiber distributions, which are captured by diffusion-MRI [98]. In addition, neural field models can also capture the cortical geometry of the gray matter from T1-MRI [97]. Such personalized models have been shown to have predictive power over subject averages [82]. They are particularly useful in epilepsy because they can model seizure propagation networks following individual brain connectivity [66]. This increases their precision when estimating epileptogenic networks responsible for seizure generation at the individual level [81, 142].

In the clinic, seizures can be triggered by applying electrical current stimulation through intracranial electrodes. By systematically varying the stimulation parameters, seizures are triggered in regions thought to be involved or highly connected to epileptogenic networks [128]. This approach is particularly useful for delineating the epileptogenic network and has been associated with a better post-surgical outcome [127]. However, finding the right stimulation configuration to trigger the seizure network is time-consuming and not optimized. Understanding how clinical stimulation parameters affect seizure networks could help clinicians find the optimal stimulation paradigm that can inform about the seizure network.

In this context, models of stimulated seizures embedded within patient-specific whole-brain networks could allow for a better understanding of the complex interactions between intracranial electrical stimulation and seizure generation and propagation. Personalized whole-brain network models have been used to model spontaneous seizure dynamics and estimate the possible sources of seizure onset based on empirical data features [51, 142]. However, so far they have not been used to model stimulated seizures [141]. We extended the Epileptor model to account for seizure generation by external electrical stimulation. We based our implementation on an accumulation hypothesis, based on observations from empirical intracranial recordings. We then integrated this model into personalized whole-brain network models of patients with epilepsy and generated synthetic copies of stimulated seizures but also spontaneous seizures and interictal activity with spikes. This approach allowed us to systematically interrogate whole-brain responses following different sets of stimulation parameters and potentially improve our ability to control stimulation outcome.

1.1 Objectives of the thesis

In this thesis, we propose a model of brain stimulation for drug-resistant epilepsy. Our aim is two-fold : (1) to have a better understanding of electrical brain stimulation and its effect on brains with epilepsy, and (2) to improve diagnostic methods of the epileptogenic zone using stimulated seizures. In addition, we also used personalized brain modeling for one patient with status epilepticus (SE) intracranial recordings and showed for the first time that SE propagates under the constraint of the structural connectome.

To have a better understanding of the effects of electrical brain stimulation in drug-resistant epilepsy, we extend the Epileptor model. This phenomenological neural mass model can generate seizures autonomously, and it describes seizure dynamics by reproducing specific universal features of the electrical signal at the local field

potential level. In particular, during seizures, fast discharge phenomena and spike-and-wave dynamics are present. During the transition between the interictal and ictal states, a baseline shift is captured, as observed in direct current (DC) recordings [67]. This model can also generate seizures by stimulation, but the phenomenon occurs abruptly. In empirical intracranial recordings of stimulated seizures, weak currents are applied for several seconds. In this paradigm, to achieve the seizure onset state, instead of a single short pulse stimulation, a longer-lasting bipolar pulse stimulation is needed to induce a seizure. In addition, we have observed that this transition to seizure is accompanied by a slow increase of the oscillatory response to the stimulus. We hypothesized then that electrical brain stimulation, which generates seizures, is caused by a slow build-up or accumulation of ion imbalances, which destabilizes the brain regions it affects until pushing them to the critical point of seizure onset. We implemented this behavior in the Epileptor model and tested our hypothesis by simulating empirical stimulation paradigms. Using this simple phenomenological model, we were able to show that we could capture empirical data features in-silico. We then systematically varied the main parameters that are varied clinically, namely stimulation location and amplitude, and compared our simulated responses to the empirical ones.

To contribute to epileptogenic zone diagnosis, we integrated our approach into a pipeline that uses high-resolution neural field models. In this pipeline, we used our model for stimulated seizures for both intracranial stimulation and a novel non-invasive temporal interference (TI) stimulation. TI stimulation consists of combining two simultaneous transcranial direct current stimulations at very high frequencies ($> 1kHZ$), f_1 and $f_2 = f_1 + \Delta f$, that overlap in a region of interest. At the locations of overlap, the combined electric fields will produce amplitude modulation at low frequency Δf. TI assumes that neurons do not respond to very high stimulation frequencies but that they will only respond to the amplitude modulation frequency [48]. We implemented this phenomenon and mapped the estimated electric field onto subject-specific cortical surfaces. We showed that non-invasive stimulation could be used to trigger seizures without being limited to the implanted electrodes. This pipeline is a first proof-of-concept that could become a clinical tool for epilepsy diagnosis.

1.2 Structure of the thesis

The thesis is structured as follows. In chapter 2, we describe the basic landscape of epilepsy and the most relevant knowledge relative to this thesis topic. Next, in chapter 3, we give an overview of the current knowledge and progress relative to brain stimulation in epilepsy.

Chapter 4 describes the construction of the extended model for stimulated seizures. This chapter is short but contains the underlying model, which is then applied to both whole-brain neural mass modeling in chapter 5 and whole-brain neural field modeling in chapter 6.

In chapter 5 we construct a virtual cohort of 30 patients with drug-resistant epilepsy as an open dataset with ground truth epileptogenic zone parameters for the scientific community. This dataset can be used for hypothesis testing and validation.

For each virtual brain twin, the dataset contains stimulated seizures, spontaneous seizures and interictal spikes. We describe the metrics we used to try and compare our synthetic data to empirical time series and we interrogate stimulation amplitude and location parameters within the dataset.

Next, in chapter 6, we model stimulated seizures using high-resolution neural field models. In addition, we model both invasive intracranial electrical stimulation and non-invasive TI stimulation. We establish in this work the first diagnostic pipeline for estimating the EZ during stimulations.

In chapter 7, we show some exciting ongoing work, where we use an empirical dataset of 5 patients with drug-resistant epilepsy, who underwent 1363 stimulations, of which 16 triggered seizures. In this work, we study the relationship between the estimated epileptogenic zone and the stimulation parameters outcome. We then show some preliminary work on systematic investigations of the relationship between stimulation parameters and brain responses depending on how the virtual brain models are parametrized.

Chapter 8 describes our first attempt at modeling status epilepticus at the whole-brain level using personalized brain modeling. SE is a rare but very hard to control and dangerous condition where a person with epilepsy experiences a seizure that lasts for at least 20 minutes. It is unclear whether SE propagates in the brain similarly to spontaneous seizures. Here we show for one patient, using our personalized whole brain modeling approach for SE seizures and comparing it to the empirical data, that SE propagates under the constraint of the structural connectome. This result needs to be repeated on multiple subjects, but we achieved a first demonstration that SE propagates similarly to spontaneous seizures.

Finally, in chapter 9, we conclude on the results we have obtained so far and discuss the future perspectives and what we have learned while stumbling along the way.

Chapter 2

Epilepsy

2.1 Clinical and biological aspects of epilepsy

2.1.1 Introduction

Epilepsy is one of the most prevalent and second most burdensome neurological disorder worldwide, in terms of disability-adjusted life years [36]. This disorder affects 70 million people, of all sexes, age groups and nationalities, with a higher prevalence in low-to-middle income countries [36]. The main characteristic of the disorder are unprovoked and brief abnormal electrical activities of the brain, known as *seizures*. Up to 10% of people will experience one occasional seizure in their lifetime [52]. A person is diagnosed with epilepsy when two or more unprovoked seizures occur at least 24h apart [13]. People with epilepsy can suffer from injuries during seizures, or suffer from anxiety and depression. The stigma they face can make it difficult for them to live a fully normal life. Certain types of epilepsy are caused by brain injuries, fever, cerebrovascular disease, metabolic insults, infections or complications at birth [13]. Yet in about one half of the cases, the causes of epilepsy are unknown [13].

2.1.2 From ancient cultures to modern neurology

Epilepsy is one of the few disorders with written records spanning nearly 4,500 years, documented across multiple ancient cultures, including the Babylonians (circa 2000 BC), Egyptians (circa 1700 BC), and Greeks (5th century BC) [93]. For a long time, this disorder was mystified and attributed to divine punishment. Reportedly, the first scientific mind to consider epilepsy as non-divine was Hippocrates (460-390 BC), providing an objective explanation of the disorder and considering it to have similar origins as other illnesses [93]. However, due to the lack of an obvious cause, the belief that epilepsy was a mystical or supernatural phenomenon persisted, especially throughout the Middle Ages. It was only at the beginning of the 18th century, that the general opinion of epilepsy was one of an idiopathic condition residing in the brain and other inner organs. As a result, the first modern book on epilepsy was written by Samuel August Tissot, a Swiss neurologist [126]. Since then, alongside the development of electroencephalography (EEG) in the 19th century, epileptic

attacks were associated with abnormal electrical brain activity, what we call today as *seizures* [93].

2.1.3 Seizures

Seizures manifest as loss of body control, in various ways across people, such as body stiffness, jerking and shaking, strange sensations, breathing problems and even loss of consciousness. Symptoms depend on the spatial and temporal organization of the abnormal activity in the brain. The International League Against Epilepsy (ILAE) classifies seizures into three main types [38, 115]. Seizures that arise within one hemisphere of the brain are categorized as *focal*, whereas when starting in both brain hemispheres simultaneously, they are categorized as *generalized*, and otherwise as *unknown* when the onset is unclear [38] (Figure 2.1). Focal seizures are the most common type across age groups [13].

Seizures typically last for a few seconds or minutes. In a few cases, seizures can be abnormally prolonged, producing an enduring epileptic condition known as *status epilepticus (SE)* [130]. According to the ILAE, the treatment of an SE condition should start 5 minutes after the start of a generalized tonic-clonic seizure and 10 minutes after a focal seizure [130]. SE is difficult to control and can have long-term consequences in the brain, such as neuronal injury and network alterations, and in the worst cases can increase the risk of death [13].

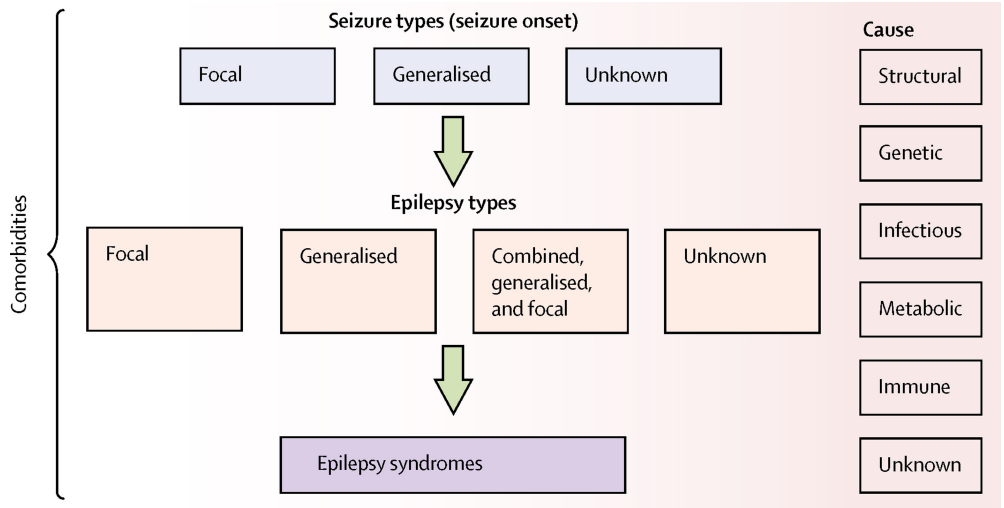

FIGURE 2.1 – Framework for the classification of epilepsies according to the International League Against Epilepsy. The classification is based on three levels : seizure type, epilepsy type and epilepsy syndrome. Additionally, epilepsy cause, made of six subgroups, is incorporated alongside each level to inform diagnosis and treatment. Figure from [125].

Depending on the seizure type, epilepsy is classified into four types (Figure 2.1). When seizures originate from one hemisphere, the epilepsy is *focal*. When seizures involve both sides of the brain, the epilepsy is considered *generalized*. A person can happen to have both types of seizures, in which case their epilepsy is *combined,*

generalized and focal. Lastly, when seizure type is not clearly defined, the epilepsy is *unknown*.

Finally, epilepsy syndromes are diagnosed when a distinct combination of seizure types, EEG findings, age of onset, and other clinical characteristics are present. However, there has never been a formal classification of this category by the ILAE, but it rather serves as a diagnostic guide [115]. Some examples include childhood absence epilepsy, Dravet syndrome or Lennox-Gastaut syndrome to name a few.

2.1.4 Epilepsy treatment

People suffering from epilepsy are mainly treated with anti-epileptic drugs. There are over 25 available anti-epileptic drugs, with an ever-increasing number each year [125]. Despite such developments, the efficacy rate of drug treatments remains constant : about 66% of people with epilepsy experience seizure remission (complete cessation of seizures for at least one to two years) [125]. Consequently, about one-third of people with epilepsy are drug-resistant. Drug-resistant epilepsy (DRE) is diagnosed after *"failure of adequate trials of two tolerated, appropriately chosen and used antiseizure drug schedules to achieve sustained seizure freedom"* [125]. In such cases, alternative treatments are considered, such as surgery, neurostimulatory interventions or dietary treatments (e.g., ketogenic diet) [125]. Drug-resistant focal epilepsy is most commonly treated with brain surgery, where brain regions responsible for seizure generation are surgically removed, known as *epileptogenic zones (EZ)*. The success rate of surgery in achieving seizure freedom ranges from 50-80% of patients in well-selected groups [125]. Post-surgical seizure relapse is often due to misdiagnosis or incomplete resection of the epileptogenic zone (EZ). As a result, accurate identification of the EZ is a critical step in the pre-surgical evaluation of DRE. Improving diagnostic techniques tailored to each patient has the potential to significantly increase the number of individuals who can be cured of DRE through surgery.

2.1.5 Epileptogenic zone concept in drug-resistant epilepsy

For a long time, epilepsy was considered to be a divine disorder, and treatments varied from religious (fasting, prayer, exorcisms) to magical (phases of the moon) and botanical remedies [93]. Ever since epilepsy was attributed as a brain disorder, the focus of treatment shifted to medical and neurological approaches. Nowadays, a central aspect of epilepsy treatment is the localization of the *epileptogenic zone (EZ)*, especially in drug-resistant cases.

In the beginnings of epilepsy surgery by Wilder Penfield and Herbert Jasper in the 1940s, cortical imaging was not yet available. Instead, they relied on direct intraoperative observation of the cortex and recording of acute electrocorticography (ECoG) discharges [92]. Presurgical information was mainly based on semiological descriptions and interictal spikes detected on scalp/sphenoidal EEGs [92]. Therefore, intraoperative information was crucial to refine localization, in particular by mapping interictal spikes in the ECoG and their relationships to structural abnormalities. They also attempted to reproduce patients' auras and localize the eloquent cortex

through acute electrical cortical stimulation [92, 94]. In a letter Penfield wrote to Lennox in 1940, he expressed that by epileptogenic lesion one should not mean "the foreign tissue lesion itself" but rather "the structurally and functionally disturbed but still viable surrounding gray matter", thus extending beyond the immediate structural brain pathology [61, 92]. Additionally, Jasper described in simple terms the lesion area, epileptogenic focus, and spike zone as 3 concentric circles (Figure2.2) [61].

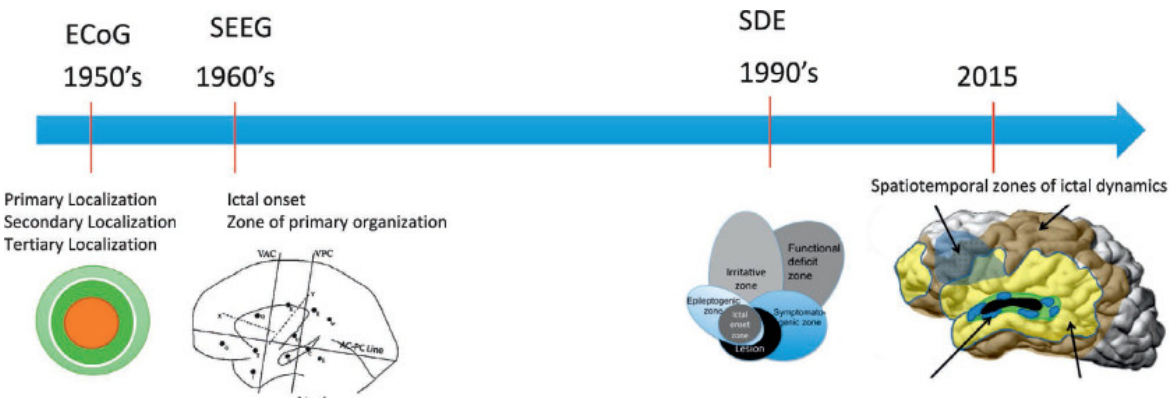

FIGURE 2.2 – Evolution of the epileptogenic zone concept over the years, going from a focus-based approach, to a spatio-temporal network concept. Figure from [61].

As of the 1960s, Talairach and Bancaud introduced the "epileptogenic zone" concept as *"the site of the beginning of epileptic seizures and of their primary organization"* and highlighted the inadequacy of the epileptogenic lesion definition [123]. They believed that it was critical to understand how ictal patterns led to clinical symptoms, referring to anatomo-electro-clinical correlations. By introducing the stereo-electro-encephalographical (SEEG) method, they allowed for a three-dimensional exploration of brain areas. SEEG recordings of patients during seizures allowed for a better understanding of how seizures start and spread, thus focusing on the spatiotemporal organization of epileptic discharges in the brain [61].

From 1993, Lüders et al. defined the EZ as *"the area of cortex that is necessary and sufficient for initiating seizures and whose removal is necessary for complete abolition of seizures"* [80]. Later on, they simplify their definition of EZ as *"the minimum amount of cortex that must be resected to produce seizure freedom"* [80]. They define five cortical zones with partial overlap : (1) the irritative zone generating interictal spikes, (2) the seizure onset zone generating clinical seizures, (3) the symptomatogenic zone producing ictal symptoms, (4) the epileptogenic lesion, and (5) the functional deficit zone, which has abnormal function during the interictal period (Figure 2.2). In this definition, removal of the seizure onset zone is necessary but not sufficient for achieving seizure freedom. A potential seizure onset zone capable of generating seizures in the future exists beyond the actual seizure onset zone that triggers the patient's current seizures. The EZ is considered to evolve in time in this context. A removal of both current and potential seizure onset zones is needed to achieve seizure freedom [80]. However, it is only after the surgery that one can be sure that the EZ was correctly identified.

From the 2000s until now, the concept of EZ has been transformed to that of a

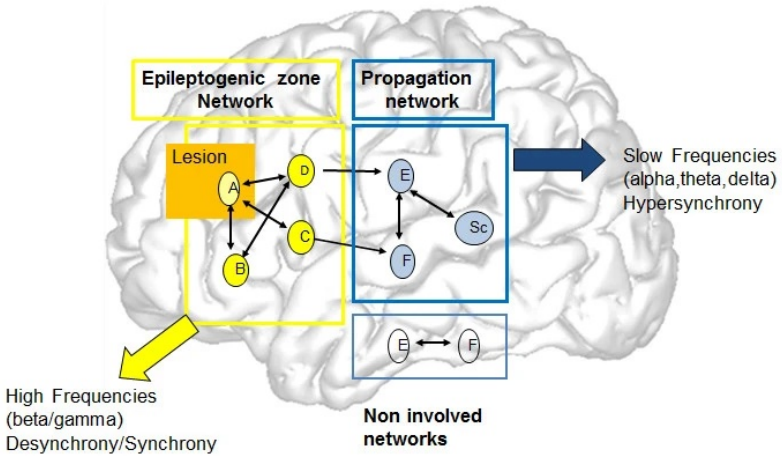

FIGURE 2.3 – Illustration of the network organization of partial seizures, with different connected structures in the epileptic brain. In particular, the EZ network generates seizures and in particular fast discharges during seizure onset. The propagation zone (PZ) network is less epileptogenic and ictal activity occurs only following seizure onset in the EZ. During the course of the seizure, the EZ and PZ networks can synchronize before an abrupt seizure offset. Figure from [11].

network, where pathological and healthy brain regions are connected and influence each other's activity (Figure 2.3) [11, 120]. This implies that the network as a whole is responsible for the emergence of seizures. Therefore, any modification applied to the network in any location, be it structural (e.g., brain surgery) or functional (e.g., brain stimulation) will alter seizure expression or recurrence [120]. Spencer showed that patients with implanted intracranial electrodes had the same clinical expressions but variable spontaneous seizure dynamics, which could be explained by a seizure network that can be entrained from any of its various parts [120]. Therefore, rather than referring to an epileptogenic zone, it could be more pertinent to refer to an epileptogenic zone network (Figure 2.3). The epileptogenic zone network concept will be a central concept of this thesis, where brain models describing local brain activity embedded within a structural brain network give rise to whole-brain seizure dynamics.

Finally, Jehi points out that the visual representation in figure 2.2 seems to include progressively more parts of the brain, saying, "in some patients, the epileptogenic zone *is* the brain : it is in the genetic, molecular, subcellular structure of the brain predisposing some of our surgical patients to redevelop epilepsy even after we remove their current EZ. The future may be in our focusing more on the *epileptogenic* rather than on the *zone* component of the EZ".

2.1.6 Diagnosis of drug-resistant epilepsy

Treatment of drug-resistant epilepsy with brain surgery involves a multitude of brain examination techniques, to arrive at a surgical decision that can stop seizures and avoid neurological deficits. Initially, patients undergo non-invasive procedures.

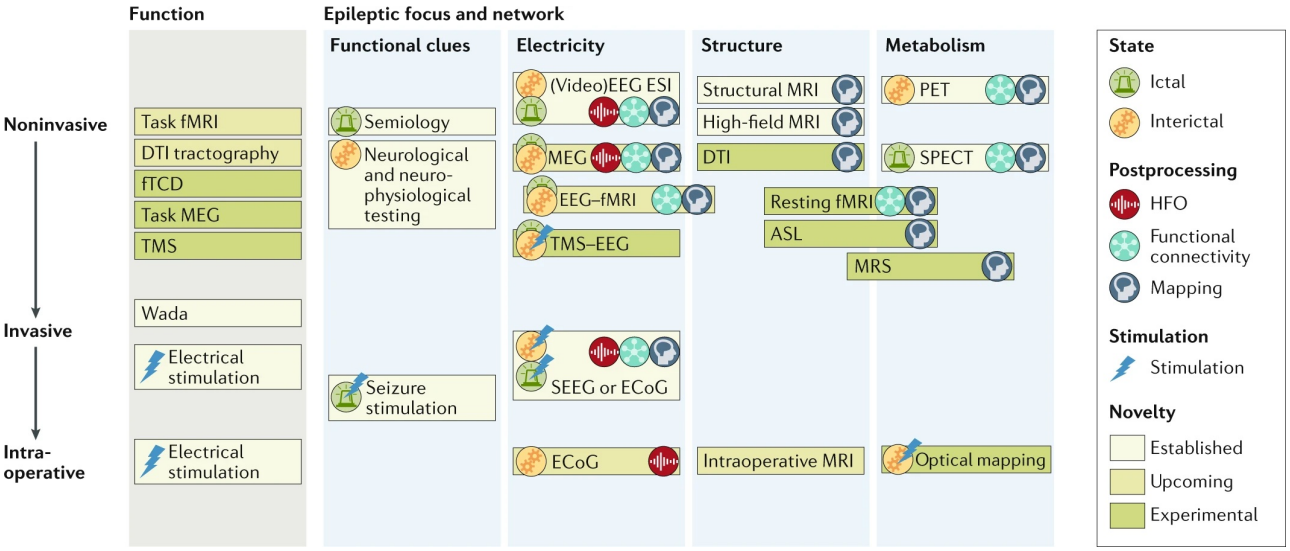

FIGURE 2.4 – Presurgical methods to locate the epileptogenic area. Taken from [149]. Each column lists methods for localization and delineation of the epileptogenic network. Non-invasive methods are performed prior to intracranial electrode placement, whereas invasive methods are performed following electrode placement. Finally, intraoperative methods are performed during surgery. ASL, arterial spin labeling ; DTI, diffusion tensor imaging ; fMRI, functional MRI ; fTCD, functional transcranial Doppler sonography ; MRS, magnetic resonance spectroscopy ; SPECT, single-photon emission CT ; SPES, single-pulse electrical stimulation ; TMS, transcranial magnetic stimulation.

These include video-EEG recordings (examining symptoms during seizures), MRI scans and source localization methods using whole-brain recordings from EEG or MEG, to name a few (Figure 2.4) [125, 149]. While these techniques provide a preliminary diagnosis, they are not precise enough for a surgical decision to be made. This is because, until now, they lack the necessary resolution to make a precise delineation of the epileptogenic network, especially when it involves deep brain regions. An exception is when the anatomical MRI reveals a clear lesion or tumor, which can significantly aid the diagnosis. However, 20 to 40% of epilepsy surgery candidates have no visible abnormalities in their MRI [76].

To address the precise EZ diagnosis problem, neurosurgeon Talairach and neurologist Bancaud invented the SEEG in 1960s in Paris [122, 123]. They created a method to implant long thin electrodes intracranially, which record local electrical brain activity of the surrounding tissue (Figure 2.5). These electrodes have a diameter of 0.8 mm and span a length of 10-15 cm, thus reaching deep brain structures for recording which is not possible with non-invasive methods. These electrodes are only placed in brain areas suspected to be epileptogenic or important for a complete picture of the EZ landscape to be made. The SEEG implantation is an individualized procedure, where video-EEG recordings contribute to the implantation scheme of each patient. Recorded interictal and ictal brain activity is then analyzed by expert clinicians to make a diagnosis of the EZ. Additionally, the intracerebral electrical signals are correlated in time and space with clinical semiology, aiming to provide

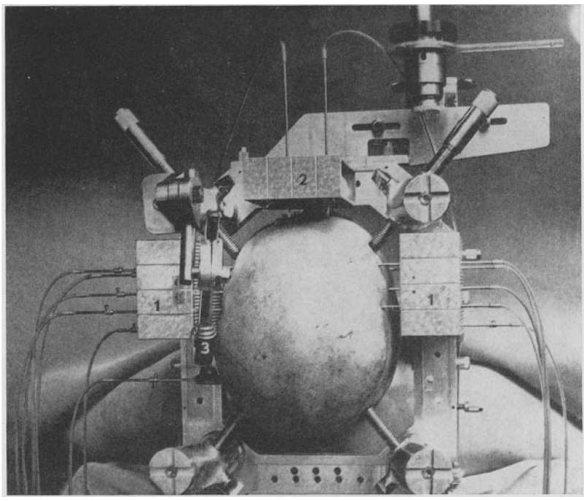

FIGURE 2.5 – Placement of SEEG electrodes in the 70s. Cranial view of a person with (1) lateral and (2) anterior perpendicular electrode implantation placement. Figure taken from [122].

an accurate interpretation of the SEEG [23].

In particular, the correlations of electrical stimulation with SEEG and the anatomo-electro-clinical responses are used to compensate for the sparse nature of the implantation [23]. Electrical stimulation is delivered using two neighboring contacts of the SEEG, thus sending focal stimulation currents to the brain. There are two main goals in performing this procedure. First, it is done for functional mapping before surgery, to determine the functional role of each brain region and ensure that areas included in the surgical resection are safe to operate on and remove. Secondly, due to the sparse spatial sampling of the SEEG, spontaneous seizure recordings can be insufficient to make a clear diagnosis of the EZ. It can also occur for patients to have no spontaneous seizures during the hospitalization period with the implanted SEEG. In both cases, brain stimulation is performed to delineate the EZ, by inducing seizures [128] and has been shown to improve surgical outcome [127]. This procedure is applied through a trial-and-error approach, by regularly varying the location and amplitude of stimulation. Stimulation frequencies are typically set at either 1 Hz or 50 Hz, with standard ranges applied to the remaining parameters [59]. A key challenge is identifying the stimulation parameters that most accurately reproduce the natural triggers of spontaneous seizures while avoiding the triggering of seizures in healthy tissue [149]. Clinically, it is generally assumed that stimulated seizures, which closely mimic the electrical patterns and symptoms of spontaneous seizures, are the best approximation of this "natural stimuli" [59].

The use of SEEG has enabled the simultaneous recording of electrical brain activity from both superficial and deep layers of the brain, which has given support to the existence of epileptogenic networks involved in seizure organization [149]. By analyzing seizure propagation pathways to trace their origins, the epileptogenic network can be mapped [23]. These insights, combined with imaging modalities such as PET, MRI, and MEG, help constrain the hypothesis regarding the EZ network and guide decisions regarding surgical strategy.

2.1.7 Summary

Epilepsy is a complex disorder with many unanswered questions. As we discussed above, while most people with epilepsy are treated with antiseizure medication, these treatments are ineffective for about one-third of patients. When people with drug-resistant epilepsy undergo surgical treatment, nearly 50% of them experience seizure relapse after surgery [125]. We emphasized the importance of improving EZ diagnosis, which may require novel approaches. One promising avenue is the use of computational brain models, which could provide a new perspective by integrating multiple imaging modalities into a personalized virtual brain model of the patient's brain. These models could also provide more insight into the interactions between brain stimulation and seizure organization, which could help improve stimulation strategies for diagnosis.

Although many hypotheses exist, the precise biological mechanisms underlying seizure generation and their spatiotemporal evolution are not clearly underpinned. Of course, the main culprit of such complexity is the brain itself, for which we are still at the very beginning of its understanding. And yet, we cannot overlook the patterns : epilepsy has existed for a very long time, as far as written records go, and seizures exist and share common patterns across multiple species. As Jirsa et al. noted : *"the invariance of seizures from flies to rodents to humans clearly argues that seizures are a* ***universal*** *behavior of neural systems"*[67]. In the following section, we will explore epilepsy from a theoretical perspective and examine some models of epilepsy.

2.2 Models of epilepsy

2.2.1 Computational models of the brain

Brain activity can be modeled using mathematical frameworks and dynamical systems theory. More particularly, differential equations are used to describe how a certain variable evolves in time. In the context of the brain, depending on the focus of the study, such a variable could be a neuron's firing rate, the mean membrane potential of a neural population, or the electrical activity of a specific brain region. We use these equations to perform simulations. To achieve this, we compute the evolution of the variable in time, starting from an initial condition, which represents the variable's starting value. Once defined, the variable's trajectory is calculated based on the equations governing its evolution, resulting in a simulated representation of brain activity. Nowadays, this can be easily calculated on our modern computers using numerical integration methods. These methods approximate the continuous evolution of the variable at discrete time points. They calculate, from an initial point, the path taken by the variable at each discrete point in time, constrained by the parameters of the model. Additionally, the implemented algorithms can be shared on the internet, making brain modeling more accessible to fellow humans. The virtual brain (TVB) platform is one such collection of algorithms that allows for simulations of whole-brain activity to be performed [111].

The equations governing brain dynamics, at any given scale, provide a framework

for interpreting observed activity and making hypotheses about unobservable or hidden variables. For instance, in clinical epilepsy, we typically observe electrical brain activity from neural populations using intracranial electrodes (see Figure 2.6). Models such as the Epileptor [67], hypothesize that slow-varying processes guide the brain into and out of the seizure (ictal) state. When embedded within whole-brain models and coupled across brain regions, these models can be used to estimate the EZ network using data fitting methods such as Bayesian inference [51, 142]. However, models are always approximations, capturing only specific phenomena of interest. This is both their strength, as they allow for a new understanding of a complex system like the brain to be achieved, but their simplicity means that a lot of other relevant phenomena will not be explained. This is why, in computational neuroscience, we build models at different scales and of different types (Figure 2.6). As Deco et al. explain : *"Computational models at different space–time scales help us understand the fundamental mechanisms that underpin neural processes and relate these processes to neuroscience data"* [29].

Models at different scales

In epilepsy, there exist many models to understand how seizures occur, where they spread in the brain, and when they occur, to name a few [25, 31, 66]. Modeling approaches are also performed on multiple scales, from the microscopic neural level up to the whole brain level. The choice of spatial scale largely depends on the behavior of interest one seeks to reproduce and the nature of the empirical data (Figure 2.6) [143]. For instance, to understand single neuron activity in epilepsy, microscopic models would be appropriate. Whereas to understand seizure propagation in the brain, macroscopic whole-brain models would be more useful.

Microscopic scale

At the microscopic scale, **detailed neuron models** focus on neuronal morphology and function (Figure 2.6D). The cellular structure is described in terms of dendrites, soma, and axon using multi-compartmental models. For instance, such models have been used to investigate the impact of neuronal morphology on the excitability of neuronal networks and generation of self-sustained seizure activity [110]. The electrical properties, on the other hand, include, for instance, membrane capacitance, membrane time constant, reversal potential, axial resistivity, and voltage-dependent ion channels [143]. In most cases, these models are based on the Hodgkin-Huxley conductance-based formalism [55, 143]. Although this formalism assumes constant intra- and extra-cellular ionic concentrations, it is not always the case in reality. In normal functioning, these concentrations are mostly constant thanks to glial buffering, spatial diffusion and ionic pumps, but in pathological conditions (such as epilepsy) they can be dramatically altered. When ionic concentrations vary, they can change the amount of ions flowing in and out of ion channels, thus changing ionic currents and impacting the voltage dynamics of the neural membrane. For instance, this approach has been used to model at the single neuron level the relationship between different levels of extracellular potassium and the generation of seizures, status epilepticus and depolarization block [31]. Other approaches have

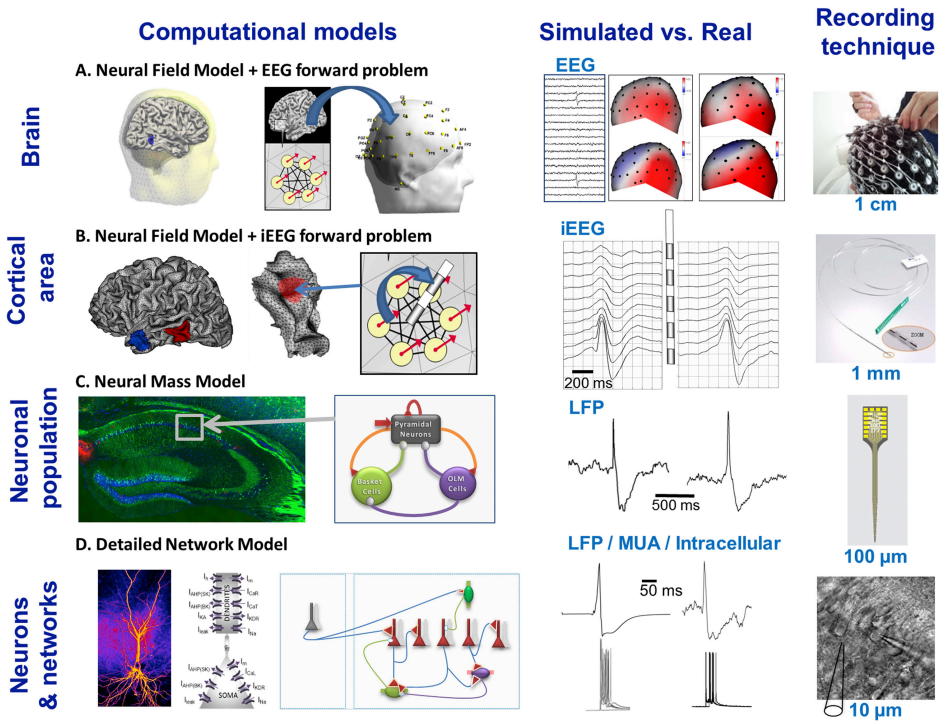

FIGURE 2.6 – Models of epileptiform activity across scales, from the neural level up to the whole brain. On the right, recording techniques at various spatial scales determine the level of detail and the constraints upon the computational models. On the left, different modeling techniques are adapted to each spatial scale : detailed models account for neuronal morphology whereas large-scale models approximate neural population activity. Simulated activity is projected to recording sensors, using forward modeling, to be comparable to real recordings. In the middle, comparisons between simulated and real signals can be done to validate the models. Figure from [143].

shown that the interaction between sodium-potassium pumps, glial cells, and intrinsic neuronal currents can produce changes in ionic concentrations that give rise to dynamics observed physiologically in seizures [25]. They emphasize the importance of ion concentration homeostasis to ensure normal neuronal function [25].

Mesoscopic scale

Simpler models are obtained by reducing the more complex ones and describing only a few key aspects of the neuron, such as its membrane excitability and interaction with the extracellular environment through changes in ionic concentrations [30]. This approach has been used to model the behavior of **networks of neurons** composed of single-compartment excitatory and inhibitory neurons, as well as glia and the extracellular environment [133]. They showed that when glial cells failed to absorb excess ions (in particular K^+) and thus regulate excessive excitation, seizure-like activity emerged from these networks [133].

However, at the neural population level, interactions between neurons and other cells such as glia create additional complexity. As the number of neurons we wish to model increases, the number of model variables and parameters linearly increases as well. This makes it difficult to extract useful information from such models, and simulations require a lot of computational power. In addition, whole-brain recordings with EEG, MEG, or fMRI are difficult to link with such microscopic models. This justified the usage of models where the activity of neural populations is collapsed to an averaged value of their simultaneous activity. These models are called lumped models, or **neural mass / neural population models** (Figure 2.6C). They are defined using differential equations, where variables evolve in time following specific nonlinear constraints depending on the equation's parameters and functions. Such models assume that the collective dynamics of neural populations can be captured well enough using their averaged temporal and spatial activity. They justify this as coming from a high degree of local redundancy in the brain, where many cells have nearly identical responses to the same stimuli [146]. As Willson and Cowan justify in their seminal work [146], introducing a deterministic model for neural population dynamics : *"if a fluid is observed at the molecular level, what is seen is Brownian motion, whereas the same fluid, viewed macroscopically, may be undergoing vert orderly streamlined flow"*. In their model, the main assumption is that excitatory (E) and inhibitory (I) cells are fundamental to all neural processes, using two variables to represent the mean activity of these cell types. In epilepsy, a disruption of the E/I balance is thought to be related to seizure generation [114]. Other neural mass models focus on capturing specific phenomena that are observed in empirical data. For instance, the Epileptor model focuses on reproducing universal seizure dynamics as observed in LFP recordings across different species [67]. We have based this thesis work on this model and we will explain it in more detail in the following section.

One of the main limitations of neural mass models (NMM) is that the cortical tissue captured by the model is approximated as a point-like source. Models that also take into account the continuous spatial cortical geometry are called **neural field models** (NFM) (Figure 2.6B). They can be seen as an extension of NMM that

takes into account cortico-cortical connections between neural populations [64, 143]. They use integro-differential equations (NMMs use differential equations), where the integral term describes how activity at distant locations of the cortical surface influences the activity at a given point (e.g., via synaptic connections) [143]. This allows for particular phenomena such as traveling waves to be studied, which have been observed during seizure propagation of synchronous discharges [24, 134].

Macroscopic scale

At the macro-scale, models of large-scale brain regions allow for whole-brain activity to be simulated. This allows for the modeled activity to be related to whole-brain imaging recordings such as EEG, MEG, or fMRI (Figure 2.6A). To model brain activity at the whole-brain scale, the cortical and subcortical gray matter of the brain is typically divided into brain regions based on brain atlases, which characterize the brain space according to anatomical features. Each brain region is then represented by a meso-scale model, which can either be a **neural mass** model or a **neural field** model. The models are coupled to each other following estimations of long-range white matter fiber connectivity, allowing for whole-brain activity to be simulated [112].

The global equation at the whole-brain level for such a model using **neural masses** is given by :

$$\dot{\psi}_i(t) = F(\psi_i(t)) + K \sum_{j=1}^{L} W(i,j) S(\psi_i(t), \psi_j(t - \tau_{ij})) + noise \tag{2.1}$$

where $\psi_i(t)$ is a state vector of neural activity at brain region i and time t. $\dot{\psi}$ is the temporal derivative of the state vector, and F is a function of the state describing the local neural activity. W is a matrix of heterogeneous connection strengths between node i and j. S is a coupling function of the local state ψ_i and the distant delayed state ψ_j, where τ_{ij} is the time delay between the two regions (typically depending on fiber tract length and propagation velocity) [112]. The neural masses are connected to each other following the connectivity matrix. Each neural mass receives input from all other L neural masses connected to it, represented as the sum of their activities and scaled by a constant K [142].

Neural fields extend the previous equations to account for the spatial continuity of the cortical surface. They allow for higher resolution simulations to be performed because they take into account not only the temporal evolution of brain activity but also the spatial resolution along the cortical sheet (i.e., corticocortical connectivity). Therefore, such models are computationally heavier than neural mass models. The global equation at the whole brain level for such a model using the **neural fields** is given by :

$$\begin{aligned} \dot{\psi}_i(x,t) = F(\psi_i(x,t)) + K_{het} \sum_{j=1}^{L} W_{het}(i,j) S_{het}(\Psi_i(t), \Psi_j(t - \tau_{ij})) \\ + K_{hom} \int_{\Gamma} W_{hom}(|x-y|) S_{hom}(\psi(y,t)) dy + noise \end{aligned} \tag{2.2}$$

where $\psi_i(x,t)$ describes the neural state of a region i, at a position vertex x and time t. The subscripts i and j define two brain regions, both containing multiple vertices. Vertices belong to two closed surfaces representing the pial cortex of the right and left hemispheres of the brain. Typically, the surface is discretized by $\approx 260,000$ vertices. The heterogeneous coupling, capturing long-range white matter connectivity, through W_{het} and S_{het}, is similar to the NMM approach, with the additional input to the coupling S_{het} being the average neural state of all vertices belonging to regions i and j, represented by Ψ_i and Ψ_j. The homogeneous coupling, models corticocortical connections and is represented by the integral across the spatial domain Γ, where W_{hom} is a translationally invariant coupling strength function based on the geodesic distance between vertices located at position x and y along the surface [64, 112]. S_{hom} is a nonlinear activation function, often a sigmoidal function of the incoming activity ψ at position y and time t (regardless of the region assignment of the vertices) [64]. K_{het} and K_{hom} are the scaling parameters for heterogeneous and homogeneous couplings [142]. Time delays between two regions τ_{ij} in TVB are only taken into account for heterogeneous (long-range white matter fibers) connectivity, whereas for homogeneous (corticocortical) connectivity, signal transmission is considered instantaneous [112].

The simulated whole-brain activity can be mapped onto EEG/MEG/fMRI sensors using forward modeling approaches, which use head models to describe signal propagation from the brain through various tissues (e.g., scalp, skull, etc.) until reaching the sensors. This allows for a direct comparison of synthetic and empirical data to be performed at the whole brain level, and has opened avenues into estimating specific model parameters linked to local brain features, such as the epileptogenic network [66, 142].

Phenomenological and biophysical models

Phenomenological models focus on a particular phenomenon they wish to model ; therefore, the model's variables and parameters can have little to no direct relationship with biology. On the other hand, biophysical models have a different approach, where capturing biophysical processes is primary and their model's variables and parameters represent biological processes and features.

Both approaches have their own usefulness. On the one hand, phenomenological models have the advantage of focusing on very specific features of an observation, allowing them to have a low model complexity, generally with a low number of variables and parameters. On the other hand, biophysical models have the advantage of describing biophysical processes in a detailed manner, allowing for insights coming from the model to be related directly to biological mechanisms. However, they require for this a much higher number of variables and parameters, making them highly complex to work with.

2.2.2 Phenomenological neural mass models of seizures

In this section, we focus on phenomenological models at the mesoscale, i.e., at the brain region scale. In this thesis, we used one particular phenomenological neural

mass model, the Epileptor [67] which will be described in the next section. Here, we want to give a more general overview of such modeling approaches and focus on the hypotheses these models provide regarding seizure onset mechanisms. This section is based on the insightful review of Saggio and Jirsa [108], where the brain is viewed as a complex dynamical system and an overview of the possible ways such a system can generate seizures is elegantly and systematically illustrated.

Seizures from a dynamical systems perspective

The simplest way to think of an epileptic brain is to imagine it contains two states : a seizing state (ictal state) and a normal state (interictal state). An epileptic brain then moves from one state to the other, which describes the recurrent seizures in time. From a dynamical systems perspective, electrical brain activity can be described using variables that evolve in time based on mathematical differential equations. This evolution in time of the variables is called a *trajectory* (Figure 2.7C). Essentially, the variable's trajectory can either converge or diverge as $t \to \infty$. When a variable converges, it settles to a particular behavior (steady/oscillatory). When a variable diverges, its value becomes increasingly large and without bound. To study all the possible trajectories of a variable, one can find the *equilibrium points* of the dynamical system describing it. Equilibrium points are described within the *phase space*, which spans all possible states of the dynamical system, and a particular state at a given time is represented by a point. If the system starts at the equilibrium point, it remains there. An equilibrium point can be an *attractor* (trajectories are drawn towards them), a *repeller* (trajectories are pushed away) or a *saddle* (trajectories are drawn in some directions and pushed away in others). Attractors and repellers can be either a point, a limit cycle or more complex structures in chaotic systems. When a trajectory evolves towards a stable fixed point, its value evolves towards a steady state in time. When a trajectory evolves towards a stable limit cycle, its activity becomes oscillatory. Multiple equilibrium points can exist in the same phase space, in which case we can have multistability (Figure 2.7B). The phase space is then comprised of basins of attraction, which describe the states where the variable will evolve towards if it starts within that portion of the space. The boundary between two basins of attraction in phase space is typically defined by a *separatrix*, which is often comprised of saddle/unstable equilibrium points (Figure 2.7C, middle).

In addition to variables, the differential equations of a dynamical system also contain parameters, which are constant values in time. A change of a parameter in the equation can impact the nature of the equilibrium points of the dynamical system and therefore impact the trajectory of the variable(s). One can systematically calculate all the fixed points of a variable for each unique parameter value. This can be described using a plot called a *bifurcation diagram* (Figure 2.7A), which describes the dynamical repertoire of the system depending on the parameter values and initial conditions [108]. A *bifurcation* occurs when a change of parameter value causes a change in the type and/or number of attractors. For instance, if we imagine the state of a drop of water to be described using a variable x, it will depend on the temperature parameter λ. The state of the drop of water is liquid for $\lambda = 1°C$

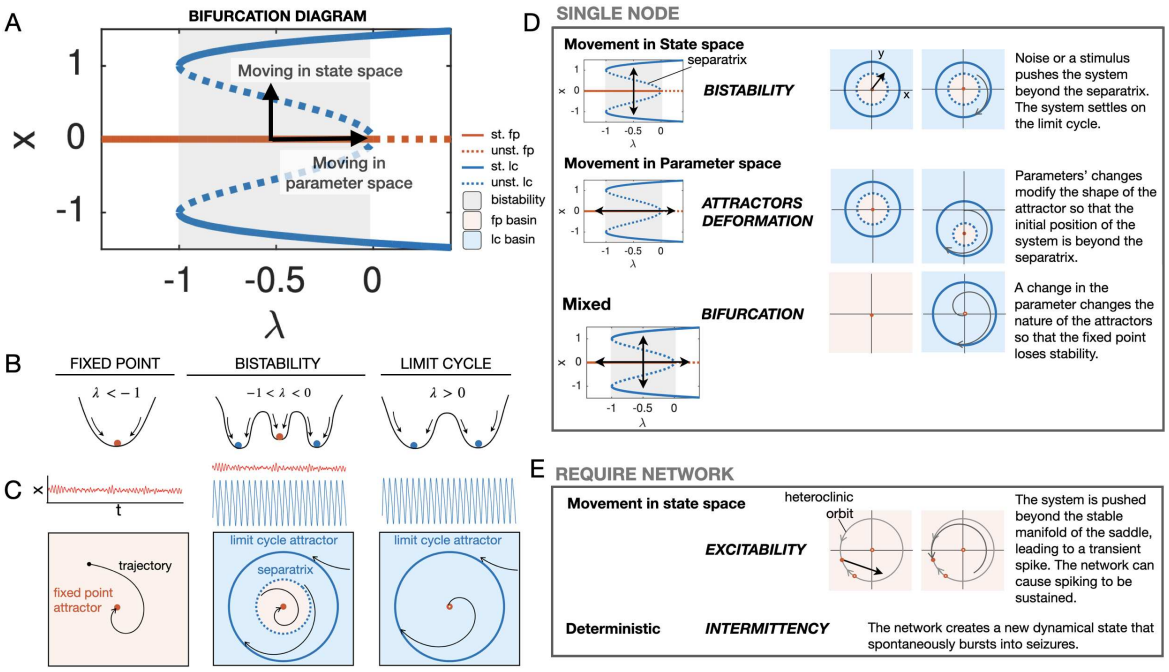

FIGURE 2.7 – A) A bifurcation diagram of a dynamical system, which describes in a compact way all the equilibrium points of a variable x for each value of a parameter λ. The diagram contains attractors (full lines) where trajectories evolve towards and repellers (dashed lines) where trajectories evolve away from. The coexistence of a fixed point and a limit cycle for the same parameter λ is called bistability, which can be used in particular for models of seizure onset and offset. As the parameter value λ varies, for some specific values the nature and number of attractors changes. For these values, the system undergoes a bifurcation. B) Fixed points and limit cycles for different value ranges of λ are visualized as valleys, where gravity pushes the system to the lowest point of the valley, depending on the initial condition of the system. C) Slight perturbations, for example from noise, move the system around the fixed point in time. Timeseries for $x(t)$ are shown in red for such a behavior. When trajectories converge to a limit cycle, the behavior becomes oscillatory, shown in blue for $x(t)$. D) Mechanisms acting at the single node level for state switching. On the left, the same bifurcation diagram is plotted. On the right, two plots of the state space are shown, one before and one after state switch. Movement in state space pushes the trajectory of the variable beyond the separatrix, thus changing its basin of attraction from a fixed point to a limit cycle. Movement in parameter space instead changes the shape (attractors deformation) or the nature (bifurcation) of the attractors, therefore causing a change in the trajectory of the variable, from a steady state behavior to an oscillatory behavior. Both mechanisms can happen together and cause a state change. E) Mechanisms at the network level for state switching. The excitability mechanism happens when multiple excitable nodes (close to a SNIC bifurcation) are coupled together such that noise or a stimulus perturbation leads to sustained oscillatory activity, which is a model for spontaneous seizures. The intermittency mechanism occurs when a heterogeneous network creates a new dynamical state which produces brief spontaneous seizures. Figure adapted from [108] with permission.

but it becomes solid for $\lambda = 0°C$. In between these two values, a bifurcation occurs for the variable x. Similarly, in epilepsy, we can imagine that a parameter change (e.g., excitability) causes a bifurcation in the electrical brain activity, from a normal state to a seizure. In its simplest form, we can represent the normal brain activity in time as evolving around a constant value (converging to a stable fixed point) and the seizure state as sustained oscillatory activity (converging to a stable limit cycle). In most cases, these two states co-exist in a bistable regime, and trajectories can move from one state to another in several different ways. In the following section we describe the different ways this switching of states can be modeled.

Mechanisms for seizure onset (and offset)

Seizures can either be modeled as starting in a single node representing a brain region, or they can emerge from a network of brain region nodes.

At the level of a single node, there are at least two ways for the system to move from the interictal (fixed point) state to the ictal (limit cycle) state, causing a seizure to start. One way is by changing the value of the variable by applying a perturbation, such as noise or a stimulus (Figure 2.7A, vertical arrow), which can cause the system to cross the separatrix (i.e., the boundary between two basins of attraction). We can call this mechanism for seizure onset, *movement in state space*, which requires bistability. A movement in the opposite direction, from the ictal to the interictal state can be similarly obtained by moving in state space in the opposite direction. A second way for state switching, is by changing the value of the parameter, such that it changes the nature of the attractors, by transforming the fixed point attractor where the variable has converged, to an unstable fixed point, thus making the variable change trajectory and converge towards a limit cycle (Figure 2.7A, horizontal arrow). In this case, a bifurcation has occurred. We call this mechanism *movement in parameter space*, which does not require bistability. Movement in parameter space can also change the shape of the attractor, which can place the position of the variable from one basin of attraction to another, thus changing the state it converges to. Such mechanisms have also been described by Lopes da Silva et al. [27] and they were linked to seizure prediction. In particular, movements in state space in a bistable system caused by random noise fluctuations, make seizures unpredictable. On the other hand, movements in parameter space from either endogenous or exogenous factors, can make critical parameters gradually change in time, causing attractors to deform either gradually or suddenly, such that the distance between the normal basin of attraction and the separatrix tends to zero, causing the system to transition to a seizure. In this case, seizures can be predictable, by measuring gradual changes in dynamics that can be detectable before the sudden seizure onset [27].

At the network level, two mechanisms are proposed [7, 108] : *excitability* and *intermittency* [108] (Figure 2.7E). The excitability mechanism typically happens when multiple nodes close to the excitability threshold are coupled together and sustain oscillatory activity following a stimulus or noise perturbation. In isolation, a single excitable node (typically close to a SNIC bifurcation), can produce a single large amplitude oscillation. When several excitable nodes are coupled together, the

transient oscillation becomes sustained such that spontaneous seizures can occur in the network [45]. The intermittency mechanism is produced when network heterogeneities can create a new dynamical state at the whole network level that produces brief generalized seizures without the need of noise [108].

2.2.3 The Virtual Epileptic Patient

In this section, we are going to describe how the Epileptor neural mass model [67] is used to model personalized whole brain seizure dynamics. The approach combines multiple patient-specific imaging modalities within the so-called Virtual Epileptic Patient (VEP) model. We then describe the different elements that are part of this framework, and how this approach is used in a clinical trial aiming to improve surgical prognosis for patients with drug-resistant epilepsy [142].

The Epileptor model

In our case, we used the Epileptor model, which is a phenomenological model for seizure dynamics (Figure 2.8) [67]. This model focuses on specific dynamical features of electrical brain activity recordings on the LFP level of epileptic brains. Interestingly, common dynamical features of recorded brain activity during seizures are found across species, such as human, rat, and zebrafish, indicating a universality of seizure dynamics across species. In particular, the epileptor captures high-frequency discharges and spike and wave events during seizures. It also captures interictal spikes before and after seizure events. Finally, it also captures DC shifts between the interictal and ictal state switching, commonly found during DC recordings of seizures but not present during the more common AC recordings. The model manages to capture such features of the signal during the ictal and interictal state using only five variables, which all evolve on different time scales. In particular, the slow-evolving variable z of the model, the so-called permittivity variable, guides the system from one state to another (the two states being the interictal and the ictal state).

Other parameters, such as m, play a role in the oscillatory nature of the seizure state. They manipulate the frequency and amplitude of oscillations during seizure events [33].

Personalized Virtual Brain Models

Virtual brain models are a concept born after tractography was invented in the early 2000s [65]. Tractography is an imaging method that provides estimated white-matter fiber orientations for a person's brain. It is extracted from diffusion-weighted imaging (DW-MRI), where the diffusion of water molecules constrained by the white matter fibers allows for an indirect estimation of the orientations of these long fibers to be made. Each person's tractography is unique, although the method is not perfect and its limitations are known. A tractography can be used to represent a person's connection pathways of their entire brain. Since tractography typically estimates millions of fibers across the brain, these connections are grouped by brain regions, which are estimated using brain atlases, such as the VEP atlas [140]. Thus, we can obtain a connectome, a region-to-region connectivity matrix of a person's brain.

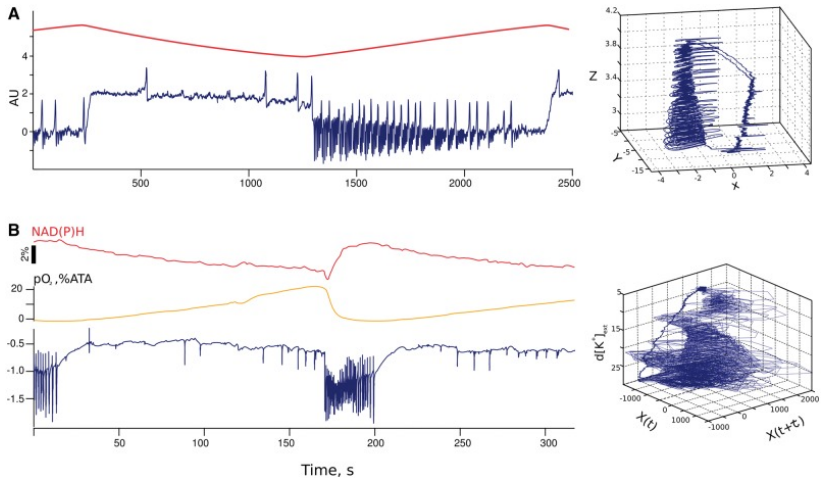

FIGURE 2.8 – Example of simulated timeseries with the Epileptor model and experimental recordings on the mouse hippocampus. The model is divided into fast-evolving variables, representing fast discharges and spike-wave phenomena during seizures and slow-evolving variables. Interestingly, the slow-evolving variable guides the system in and out of seizures and captures experimentally observed dynamics of oxygen, ATP and extracellular potassium during seizure events. On the right, the manifold of the model is mapped in 3D alongside a 3D representation of experimental signals (LFP recordings and extracellular potassium). Figure taken from [67].

Although such a connectome is non-directional, it allows for a brain network model to be constructed.

Based on this virtual brain structure, brain activity can be simulated. To achieve this, the brain region nodes of the brain network are equipped with neural mass models to describe the average population activity of the neurons in that region. The virtual epileptic patient pipeline integrates patient-specific data modalities to construct virtual whole brain models for patients with epilepsy (Figure 2.9). It uses the Epileptor model to describe seizure dynamics on spatial and temporal scales.

Inferred Epileptor parameters from real data

Empirical iEEG recordings are fitted against the model's simulations using Bayesian inference techniques, allowing to obtain estimations of the epileptogenic zone. Here, the empirical iEEG recordings are simplified into envelope data features, using band-pass filtering which reduces the signals into envelopes which when jumping from their baseline indicate a seizure event in time. They are fitted against a reduced version of the Epileptor, the 2D Epileptor model, which uses 2 variables only, namely the fast variable x_1 and the slow variable z. Here the fast variable jumps from the baseline when a seizure event occurs and the slow variable controls the system by guiding it between the ictal and the interictal states. Both the full 6D Epileptor model and the reduced 2D Epileptor model are parameterized easily via the parameter x_0, which represents the excitability of the system, thus determining the brain state of the system. Therefore, when the simulated data are adjusted to the envelope data features of the empirical data, the parameter x_0 plays an impor-

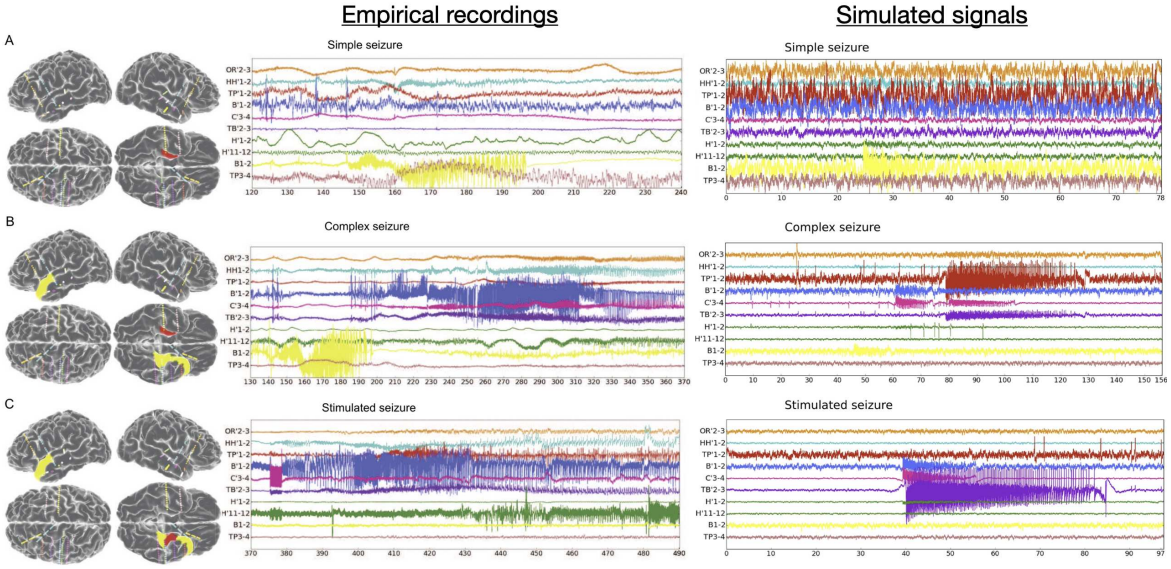

FIGURE 2.9 – Different types of seizures in the same patient : A) Simple seizure in the right hippocampus, B) Complex seizure with propagation in the contra-lateral hemisphere and C) Stimulated seizure with stimulation in the right hippocampus. Figure taken from [66].

tant role. The simulations that best match the empirical data features are related to distributions of the parameters x_0 but also the parameter K, corresponding to the global coupling factor.

To infer the epileptogenicity parameters from the empirical seizure, the Maximum a Posteriori (MAP) optimization is used. This method estimates the most probable parameters of a model given observed data (here the SEEG seizure recording) and prior knowledge. The optimization finds the parameter values that maximize the posterior distribution.

The posterior distribution, based on Bayes' Theorem, is mathematically defined as :

$$p(\theta|D) = \frac{p(D|\theta)p(\theta)}{p(D)} \tag{2.3}$$

where the posterior distribution $p(\theta|D)$ is the probability of parameters θ (here regional x_0, K) given the data D. $p(D|\theta)$ is the likelihood, or probability of observing the data D given the parameters θ. This in our case is our virtual model. The prior distribution $p(\theta)$ is our belief about the parameters before observing the data, which can, for instance, be an observed lesion on the T1-MRI / HFOs / interictal spikes, etc. Finally, $p(D)$ is the evidence or marginal likelihood, the probability of the data D integrated over all possible parameters. In our case, this is a constant value [51].

The MAP optimization seeks to find the values θ_{MAP} that maximize the posterior distribution :

$$\theta_{MAP} = \underset{\theta}{\operatorname{argmax}}\, p(\theta|D) \tag{2.4}$$

The θ_{MAP} is computed via an iterative process that starts with an initial guess and moves through parameter space following the direction of the gradient of the

probability distribution.

A limitation of MAP is that it provides a point estimate based on the data and prior, but it does not fully capture the uncertainty in the parameter estimation. Full Bayesian inference methods like Markov Chain Monte Carlo (MCMC) sample from the entire posterior distribution, thus providing a more complete representation of parameter uncertainty or even multi-modal distributions, which are not captured by MAP. However, MAP is much faster to compute than MCMC.

Clinical trial

The Virtual Epileptic Patient (VEP) pipeline (Figure 2.10) is currently being used in the EPINOV clinical trial (Improving Epilepsy Surgery Management and Prognosis Using Virtual Epileptic Patient Software) [81, 142]. This is the first epilepsy trial to incorporate virtual brain models. The primary goal is to assess the ability of VEP algorithms to enhance surgical outcomes. The trial is a multi-center, controlled, randomized, and prospective study, with 356 enrolled participants [63]. Half of them are assigned to a VEP group, where VEP is integrated into multidisciplinary decision-making, while the other half follow standard clinical practices [63].

The results from the VEP consist of epileptogenicity distributions across brain regions and confidence diagnostics [142]. They are provided in the form of a clinical report to clinicians during their decision-making process for the EZ diagnosis. The main goal is to see the difference between the VEP group and the control group in terms of seizure freedom (Engel class I) without disabling side effects at 12-month follow-up. Secondary objectives include differences in surgical strategy and surgical safety. I have also been part of the scientific team that uses the VEP pipeline to provide clinical reports for patients of this trial. This ongoing work and my contributions are described in Chapter 7.

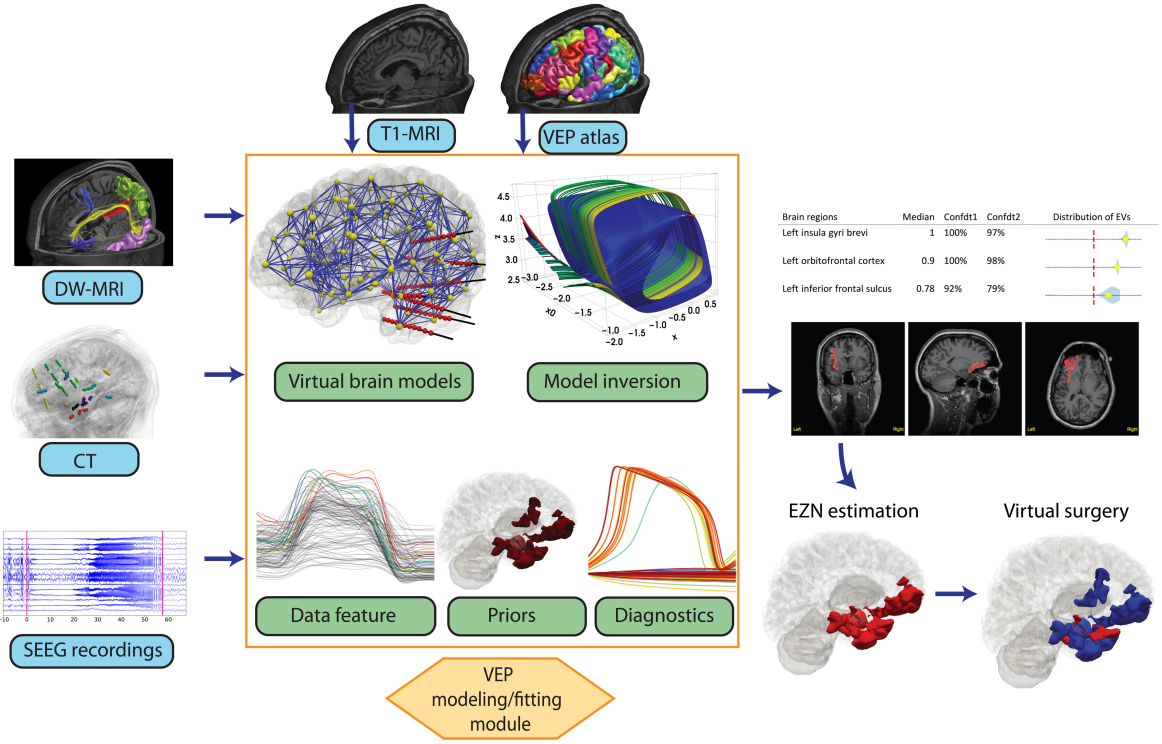

FIGURE 2.10 – Virtual epileptic patient pipeline. This pipeline first combined structural brain imaging to build a personalized virtual brain model. In particular, a brain atlas was overlaid on the T1-MRI to parcellate the brain into regions. Then, the DW-MRI was used to estimate white matter fiber bundles connecting the different brain regions. This resulted in a whole-brain network model, unique to each patient. The Epileptor model was employed on each brain region to model brain dynamics. SEEG electrode locations were reconstructed from a CT scan. From seizure SEEG recordings, envelope data features were extracted and fitted against simulated data from the virtual brain model. This resulted in estimated excitability parameter distributions for each Epileptor model. These distributions were represented using a threshold as either epileptogenic or non-epileptogenic within a clinical report. In addition, virtual surgery can be performed on these virtual brain models. Figure taken from [142].

Chapter 3

Brain stimulation in epilepsy

3.1 Clinical relevance of brain stimulation

3.1.1 Overview of stimulation methods

Brain stimulation has nowadays become a tool for treatment and diagnosis of various neurological disorders. It is divided into two main categories : (i) invasive stimulation, which requires surgery, where stimulating electrodes are placed in direct contact with the brain and (ii) non-invasive stimulation, requiring no surgery, where stimulating electrodes/coils are placed on the scalp.

In both cases, brain stimulation has immediate effects, including membrane polarization, neurotransmitter release, spike timing and spike timing-dependent plasticity. It also has long-lasting effects, which can be neurogenesis, cortical reorganization, and synaptic plasticity.

Invasive brain stimulation

The main invasive brain stimulation method is deep brain stimulation (DBS). DBS is a neurosurgical procedure involving electrode implantation in a specific brain area and delivering constant or intermittent current from an implanted battery source [79]. The electric field is typically focal and targets directly the brain tissue where the electrode is located. However, the effects of the electric field also influence the network of neurons connected to the local tissue. Typically targets are located in deep brain regions rather than cortical areas (Figure 3.1). It is both a probe and modulator of brain activity and it is mainly used as a therapeutic treatment for brain disorders involving motor, limbic, memory, and cognitive functions [79]. In particular, DBS has become the standard of care for patients with movement disorders, such as Parkinson's disease (PD). It can control the motor symptoms of PD by targeting regions such as the subthalamic nucleus (STN) or globus pallidus internus (GPi) but is ineffective for treatment of gait symptoms and does not improve speech and affective and cognitive symptoms.

Regarding mechanisms, most theories focus on stimulation-induced disruption of pathological brain circuit activity, which occurs at the ionic, protein, cellular, and network level [79]. On the ionic level, an electrode inside the brain polarized to a negative potential (i.e., a cathode) redistributes ions (Na^+ and Cl^-) in the

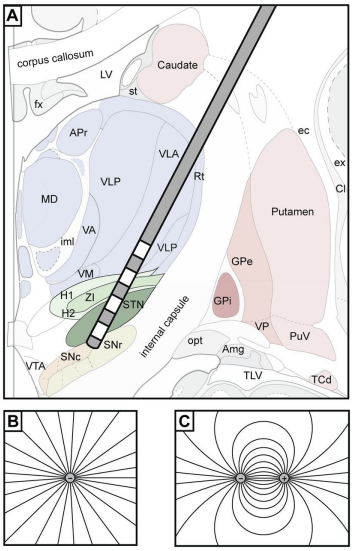

FIGURE 3.1 – This figure, from [53], shows a typical placement of a DBS electrode. In B) the electric field produced in a "monopolar" configuration is illustrated, with a single cathode in the electrode and the anode is located in the chest, in the implantable pulse generator. In C) the electric field produced in a "bipolar" configuration is illustrated, where the cathode and anode are located in two neighboring DBS contacts, creating a focal electric field.

extracellular space, which creates an electric field. This electric field then manipulates the voltage sensor of the neuron's sodium channels, which can generate an action potential. The action potential typically initiates in the axon and propagates in both directions (orthodromic and antidromic) along the axon. Stimulation with DBS involves stimulation of multiple axons, which follow with high fidelity the typical frequencies of $\sim$ 100 Hz [79]. In addition, synaptic transmission between neurons occurs and this is a much more complicated process [79]. Neurotransmitter release from DBS can occur both on the local and network level. For instance, DBS of the anterior thalamus in epilepsy could be dependent on the stimulation-induced release of adenosine [53]. In PD, stimulation of the dorsal STN results in dopamine release in the caudate nucleus [53].

In addition, under high-frequency activity, the releasable pool of neurotransmitters in the axon terminals can be exhausted and a postsynaptic receptor depression can occur. Another phenomenon known as 'synaptic filtering' is thought to have a key role in DBS, where pathological oscillations of brain activity (e.g., beta-band oscillations in PD) are not allowed to propagate in connected regions. More generally, DBS is thought to disrupt the pathological brain oscillations. However, the effects of DBS can take many months before achieving maximal benefit in disorders such as epilepsy, dystonia, and depression (see Figure 3.2). It is thought that symptoms that respond on longer timescales are mediated by slow-evolving mechanisms such as synaptic plasticity and anatomical remodeling [53]. Therefore, understanding neuro-plasticity changes induced by DBS is an important avenue.

One of the main challenges in DBS clinical practice is programming the stimulation parameters, which is done by a trial-and-error, time-consuming approach.

Typically, the parameters are set based on experience, and once the patient's response is observed, the parameters are re-adjusted on the basis of clinical outcome [79]. In disorders that respond rapidly to parameter changes such as Parkinson's, this procedure can be reliable and efficient (Figure 3.2). But for circuit disorders like epilepsy where the efficacy of stimulation treatment can only be observed after many months, this approach creates many complications, in particular an inappropriate overdose of DBS (Figure 3.2) [79]. Therefore, it is important to go beyond empirical studies and understand acute and long-term mechanisms of brain stimulation in the brain. So far, computational models can estimate and visualize the volume of brain tissue activated by DBS based on its dosing. **The next, more difficult step, would be building predictive models of the complex dynamic interactions between temporal pulse parameters and neural communication within the pathological and healthy brain networks** [53, 79].

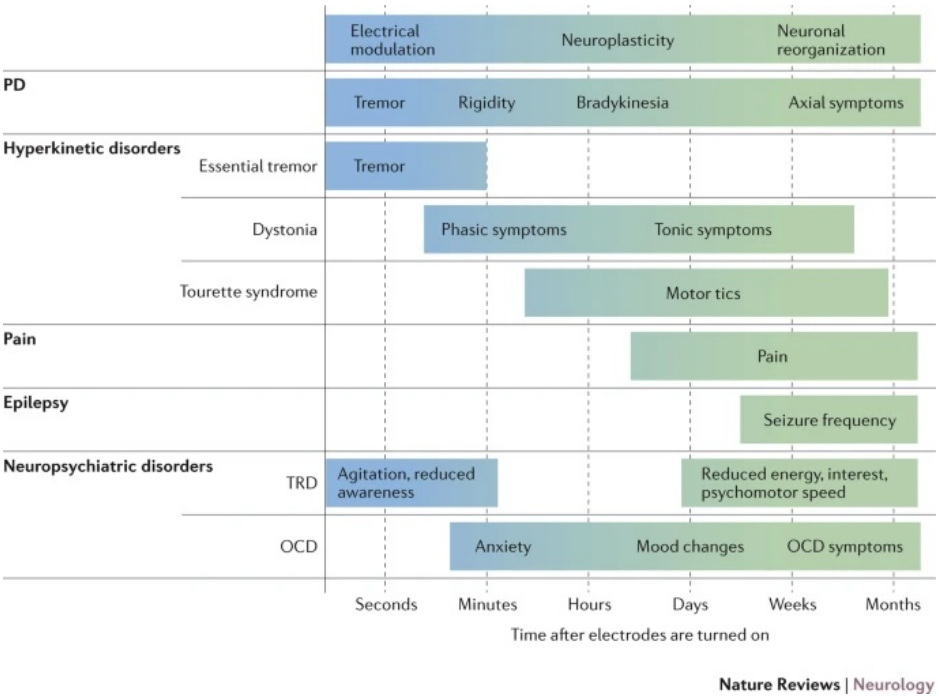

FIGURE 3.2 – This figure, from [5], shows in logarithmic scale when symptom improvement can be observed following DBS treatment for patients with various brain disorders. Notice how for epilepsy, multiple months are needed to observe any symptom improvement. OCD – obsessive-compulsive disorder ; TRD – treatment-resistant depression.

Non-invasive brain stimulation

Non-invasive brain stimulation (NIBS) originated over 40 years ago, where it was demonstrated for the first time that human brain function could be electrically influenced without opening the skull, by running brief electrical currents through the human scalp [83]. Since then, the two main NIBS methods are transcranial magnetic stimulation (TMS) and transcranial electrical stimulation (tES). In TMS, based on

the principles of electromagnetism, a magnetic coil is placed against the scalp to send magnetic pulses to the brain and activate nerve cells in a specific region. In tES, two pairs of electrodes are used as anode and cathode to generate an electric field, just like in DBS, but here the electrodes are placed directly on the head. Contrary to invasive stimulation methods, TMS and tES generate electric fields that span larger areas of tissue (in order of centimeters). In addition, they can only directly affect activity in cortical regions [96].

TMS elicits temporally restricted bursts of action potentials and can be used during task performance to study temporal dynamics of brain function at high temporal resolution [96]. For example, TMS pulses applied on V1 can induce suppression of conscious visual perception of visual stimuli [96].

TES can be induced either by transcranial direct current stimulation (tDCS), or transcranial alternating current stimulation (tACS). TDCS applies a weak tonic direct current between two electrodes placed on the scalp, allowing for current to partially pass through large areas of cortical tissue. The current can either de- or hyper-polarize the resting membrane potential of neurons and modulate cortical excitability (which depends also on the field direction and neuronal morphology) [96]. This technique has a low temporal resolution, since the neural response to tDCS occurs after a few seconds and continues throughout the current application, and aftereffects can last for several hours [96]. On the other hand, tACS uses oscillatory electrical stimulation and can induce neural activation in specific frequency bands. For instance, tACS has been used to study the causal role of theta-gamma cross-frequency coupling for working memory, or link beta and gamma oscillations to motor behavior [96].

A new NIBS methodology, called temporal interference (TI), promises to go further and allow for neural activity entrainment of deep brain structures without recruitment of the overlying cortex [48]. So far, this has been achieved only with invasive stimulation methods, but TI stimulation has been shown to be able to achieve similar results purely non-invasively [2, 85]. TI stimulation is performed by coupling at least two pairs of tACS electrodes which are simultaneously stimulating at slightly different frequencies.

In terms of the neurophysiological processes stimulated by NIBS, there is an ongoing debate [96]. Neural activation by electrical current depends on multiple factors, such as direction of the electrical field relative to the neuron, stimulation intensity, penetration depth into excitable tissue, and more [96]. Computational models can estimate the electric fields induced by NIBS methods [113]. However, these models need further physiological validation [96].

3.1.2 Invasive brain stimulation in epilepsy

Invasive brain stimulation methods in epilepsy include DBS, ECoG, and SEEG stimulation. Invasive brain stimulation in epilepsy is used for the following purposes :

1. In cases of epilepsy where anti-epileptic drugs and surgery are not a treatment option, stimulation as palliative treatment for seizure reduction.
2. In cases of drug-resistant epilepsy where surgery is a treatment option :
   — For functional brain mapping prior to brain surgery.

— To improve delineation of the epileptogenic zone during diagnosis.

— To perform radiofrequency thermocoagulation.

Invasive brain stimulation for seizure reduction

In patients with epilepsy that cannot be treated by medication or by brain surgery, brain stimulation is an alternative treatment option. The main neuromodulation therapies that have been tested appropriately and approved are vagus nerve stimulation (VNS), DBS of the anterior nucleus of the thalamus (ANT-DBS) and closed-loop responsive neurostimulation (RNS) [106]. All of them are mostly palliative, with only a few individuals achieving complete seizure freedom for more than 12 months from these treatments [106]. Overall, more than half of individuals have long-term reduction of seizure frequency of more than 50% [106].

VNS treatment is applied to the left vagus nerve following either routine schedules (e.g., 30s stimulation every 5 min) or following closed-loop protocols, where stimulation is performed following changes in heart rate that might reflect an ongoing seizure [106]. Stimulation can also be applied on demand by passing a magnet in front of an implanted stimulator. Its mechanisms are thought to be related to neuromodulation of the brainstem, thalamic, and cortical afferent projections. Long-term effects could be related to GABAergic modulation and neuroinflammation [105]. Systematic reviews of VNS show a responder rate (>50% reduction in seizure frequency) at 1 year of 37%, which progressively increases with an increase in treatment years [106].

DBS has been shown to be a useful treatment in epilepsy, for instance in clinical trials targeting the anterior nucleus of the thalamus (ANT) [37]. The mechanisms of this treatment are thought to be related to the ANT's role within the Papez circuit and high-frequency stimulation can interfere with brain activity synchronization [105]. In this trial, by 2 years, 54% of patients had a seizure reduction of at least 50% and complication rates were modest. As a continuation of these results, a 10-year-long SANTE trial using the same approach, investigated whether seizure frequency continued to improve over time [109]. Their results showed a responder rate ($>$ 50% reduction in seizure frequency) at 1 year of 43% and at 5 years of 68%, where seizure freedom for at least 6 months happened only for 16% of subjects [109]. As we notice, despite the efficacy of DBS therapy, most patients did not become seizure-free.

More recent approaches involve responsive neurostimulation (RNS) treatment, where sensing electrodes detect seizure activity and deliver stimulation to prevent seizure propagation [86]. The electrodes are placed at the zone(s) of suspected seizure onset and can both record and deliver short bursts of electrical stimulation. This treatment has been shown to influence long-term neuromodulation of seizure network activity [105]. Studies have shown responder rates at 1 year of 44%, similar to DBS [106]. However, in a study using RNS for 9 years of follow-up, the responder rate was 73%, and 35% of subjects had a >90% reduction in seizure frequency. Seizure freedom for more than 1 year happened for 18% of subjects [86].

Brain stimulation for epilepsy treatment is still under development. Clinical trials have shown responder rates to brain stimulation treatment at 1 year follow-up of around 40%, which tends to increase each additional treatment year [106]. However,

long-term outcomes can have multiple biases, such as loss of participants, which can alter the final results, especially when the participants drop out due to experiencing treatment ineffectiveness. Despite clinical trials showing partial effectiveness and a majority of patients not becoming seizure-free, brain stimulation is thought to be a promising therapy. In particular, given its current empirical approach, if stimulation effects are better understood, treatment effectiveness could greatly improve. In addition, biomarkers that can predict which patients are more likely to respond are also missing and would be of great clinical relevance [106].

Invasive brain stimulation for epilepsy surgery

People with drug-resistant epilepsy who are candidates for brain surgery undergo multiple examinations, from non-invasive to invasive measurements until a surgical decision is made. Each step is followed in order to achieve a precise diagnosis of the EZ, which is thought to be crucial for seizure freedom post-surgery.

In this light, SEEG electrode implantation is performed as a minimally invasive step prior to brain surgery. Each patient has an individualized implantation scheme based on their non-invasive measurements. These electrodes allow for a 3D exploration of the brain networks hypothesized to be involved in the patient's epilepsy condition and should aid in refining the clinical EZ hypothesis.

Aside from recording electrical brain activity, SEEG electrodes can also send electrical current to the brain. The technique of stimulation using SEEG was founded by the same people who pioneered the method of SEEG, Talairach and Bancaud, in the Sainte Anne hospital in Paris. Using two neighboring contacts with identical opposite charges, a focal electric field is induced in the surrounding tissue. The stimulation modality of choice is using bipolar biphasic pulse stimulation. Brain stimulation can be performed across all possible contiguous contact pairs in the implanted SEEG leads. In addition to stimulation location, stimulation amplitude, frequency, duration and pulse width are the parameters that can be tuned by the clinician. Guidelines have been put in place by some centers to aid in following safe practices [59].

There are two main reasons to perform brain stimulation with SEEG contacts. Firstly, for **functional brain mapping** prior to brain surgery. By identifying cortical structures related to language and motor function, post-surgical brain function complications can be avoided [128]. Electrical stimulation produces a transient functional impairment, which could predict which functions would be disturbed if the stimulated cortex were to be removed [128].

Secondly, stimulation with SEEG contacts is used to **delineate the epileptogenic zone** by inducing seizures. Due to the limited spatial sampling from the SEEG, recorded spontaneous seizures can be insufficient to properly localize the EZ [128]. Exploration with SEEG stimulation can improve the EZ delineation by triggering habitual seizures.

Stimulation induced seizures were first reported during "the early pioneering days of neurosurgery when itraoperative electrical stimulation of the cortex elicited patient's habitual auras" [26, 71, 94]. Later on, induction of seizures by stimulation was used and promoted by Bancaud and Tailarach. Up to the mid-1970s, SEEG was

performed as a single day recording and it was necessary to either have a spontaneous or provoked seizure during the available time window. Therefore triggering a seizure by stimulation or chemical activation became clinical routine. The epileptogenic zone in that context was defined as the region that produced the whole ictal, electroclinical pattern [127].

The idea behind this approach is based on the concept of EZ, which is hypothesized to be structured as a network of regions connected via white matter pathways [41]. Any component of the EZ is able to synchronize the entire epileptogenic network ; therefore, stimulation of any part of the EZ can trigger the patient's seizure [128]. During recorded SEEG seizures, seizure onset can appear as quasi-simultaneous fast discharges across multiple brain regions, possibly extending beyond the EZ. Stimulation can help discriminate which areas are essential to trigger habitual seizures from the rest [128]. However, the site from where a seizure is triggered does not define by itself a seizure focus at that site. Rather, it is how, following stimulation at that site, synchronized activity is produced between the areas involved that informs on EZ organization [128]. A stimulation-induced ictal activity of this network can be informative in two ways depending on the temporal evolution of seizure symptoms relative to the SEEG stimulation and seizure [71]. (i) The ictal symptom occurs during the stimulation, before any significant seizure propagation, which could indicate that the cortical area responsible for the symptom is in close proximity to the brain area being stimulated. (ii) The ictal symptom occurs only during the spread of the SEEG seizure, indicating that there is a connected area or a network of areas activated by the stimulation-triggered ictal discharge which is responsible for the generated symptom. In addition, the anatomic stimulation location and stimulation-induced seizure patterns can be combined with the spontaneous seizure dynamics and observed semiology to provide a greater perspective on the organization of EZ networks [41].

Finally, the procedures for functional mapping and for triggering seizures "should be performed in conjunction to answer the fundamental question whether or not there is a spatio-temporal overlap between the epileptogenic and functional network" [128]. This is crucial to arrive at a surgical decision, which can only be possible if the EZ can be safely resected without compromising brain function for the patient.

Clinical contribution of stimulation-induced seizures

In a review by Kovac and colleagues, the controversy regarding the utility of cortical stimulation-induced seizures is raised [71]. Although this methodology is widely accepted and routinely used for epilepsy surgery in France, in epilepsy centers influenced by the North American approach to epilepsy surgery this is not always the case. Their approach is strongly influenced by the work of Penfield and emphasizes stimulation to be used to "safeguard" function [71].

In a study by Trebuchon and colleagues (largest retrospective post-SEEG epilepsy surgery cohort investigating stimulation-induced seizures as predictors of surgical outcome) [127], the utility of electrical stimulation for seizure induction during SEEG exploration was studied. In this analysis, 346 retrospective patients were operated on for DRE after SEEG exploration included stimulated seizures with either

low-frequency electrical stimulation (LFS) or high-frequency electrical stimulation (HFS). Their analysis concluded that seizure induction by LFS represented a positive predictive factor for seizure outcome after surgery. LFS seems to be more reliable since false positive responses are rare, compared to HFS which is more effective in triggering seizures.

In another study by Orderiz and colleagues, the contribution of SEEG cortical stimulation to surgical outcomes was retrospectively investigated [90]. The good outcome group had a higher proportion of stimulation-induced seizures (Engel I at 42.2 month median follow-up, 31 of 44 (70.5%)) than the bad outcome group (Engel II or greater, 28 of 59 (47.5%)). They concluded that stimulation-induced seizures are just as reliable as spontaneous seizures in localizing the EZ in focal epilepsy.

A systematic exploration of stimulation parameter effects on seizure networks is missing. There are no real standardized procedures, except for the French guidelines in SEEG [59]. As Trebuchon and Chauvel conclude in their paper : *"because stimulation is necessarily disrupting a network, may the effect of stimulation at any given site really be considered as focal ? Although precise analysis of local effects of stimulation is important, it seems very likely that other effects distant to the stimulation site are involved. A systemic effect of stimulation is an important question to consider for interpretation."*[128].

3.1.3 Non-invasive brain stimulation in epilepsy

In epilepsy, non-invasive brain stimulation, using tDCS/tACS is used as therapy for drug-resistant epilepsy. However, the method is still in its early stages and multiple studies show only partial efficacy. A new option that promises to go beyond the capabilities of transcranial current stimulation (tCS) is TI stimulation.

Transcranial current stimulation in epilepsy

Transcranial brain stimulation methods are generally safe, well tolerated and reversible. In epilepsy, the first technique for treating pharmacoresistant epilepsy was with repetitive transcranial magnetic stimulation (rTMS) [124]. Follow-up studies however reported a lack of evidence in seizure frequency decrease and a risk of inducing seizures in patients and healthy subjects [119].

More recent techniques of transcranial current stimulation (tCS) promise to be a safer option, in addition to being less expensive and can even become an "at-home" usage device. Using scalp electrodes, weak electric currents can be sent to the brain which do not induce action potentials but rather modulate neural activity (Figure 3.3A). More concretely, when these electrodes are placed in the region of interest, the current induces intracerebral current flow. In a traditional electric circuit of metal wires, negatively charged electrons flow from cathode to anode. However, in the brain, current is created by the motion of ions, which can be positive or negative. Positive ions flow towards the cathode (V-, negative charge) and negative ions flow towards the anode (V+, positive charge).

Consequently, current flow can change neuronal excitability in the stimulated area based on the type of stimulation. It has been demonstrated that anodal brain

stimulation increases neuronal excitability and cathodal brain stimulation is inhibitory [89]. Therefore in the case of epilepsy treatment, in order to inhibit epileptogenic areas with high excitability, cathodal electrodes are placed over them, whereas anodal electrodes are carefully chosen to avoid the EZ.

The effects of tCS are mediated by the electrical fields they create in the cortex. The created electrical field depends on multiple parameters, such as electrode locations, stimulation current, cortical anatomy and tissue conductivity. The electric field causes ions to displace and accumulate, with the highest charge accumulation occurring in the dendritic-soma direction of pyramidal neurons (see Figure 3.3B) [119]. Pyramidal neurons are aligned perpendicular to the cortical surface, therefore the highest modulation effects of the electric field would come from its normal component to the cortical surface.

In a review by Simula and colleagues [119], the development of tCS in epilepsy treatment is shown to have some promising results, but they require larger patient cohorts, longer-term follow up, and further understanding of stimulation effects in patients with epilepsy. Experimental designs and stimulation parameters are inconsistent across studies and findings are at times contradictory [119].

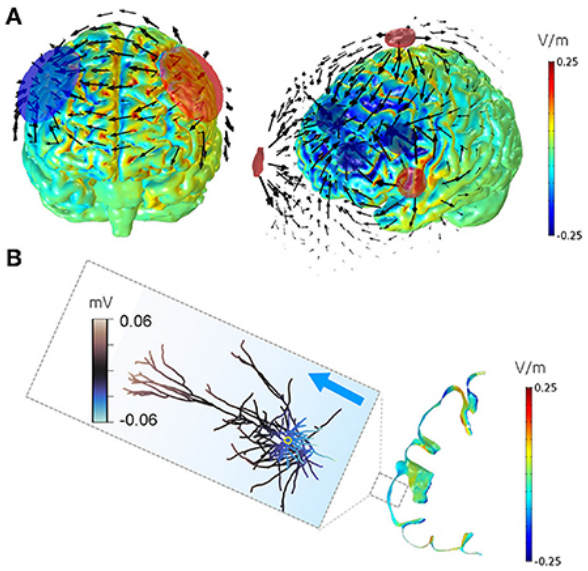

FIGURE 3.3 – This figure, from [119] shows estimated tES electric fields on a realistic head model. A) Bipolar montage with two scalp electrodes with stimulation current 1 mA and multichannel montage of six electrodes with stimulated current 4 mA. The estimated electric field component directed perpendicularly to the cortical surface is diplayed. B) The membrane polarization from the electric field is directed outwards from the cortex on a pyramidal neuron with realistic morphology.

Temporal interference stimulation in epilepsy

Until recently, non-invasive stimulation of deep brain areas could not be achieved without also stimulating the superficial cortex under the scalp electrodes. Temporal interference (TI) is a novel non-invasive stimulation method, based on the physiological phenomenon of neurons not being activated by stimulation frequencies beyond

1 kHz [48]. By combining two simultaneous tACS stimulations at high frequencies f_1 and $f_2 = f_1 + \Delta f$, where Δf is a low frequency, the method assumes that the combined field will modulate its amplitude at frequency Δf at the location of overlap between the two tACS fields (Figure 3.4). This assumes that neurons will only respond to the low-frequency signal modulation despite the actual applied currents at much higher frequencies. Depending on the electrode arrangement, the field of overlap can stimulate deep brain structures focally, such as the hippocampus [48, 85].

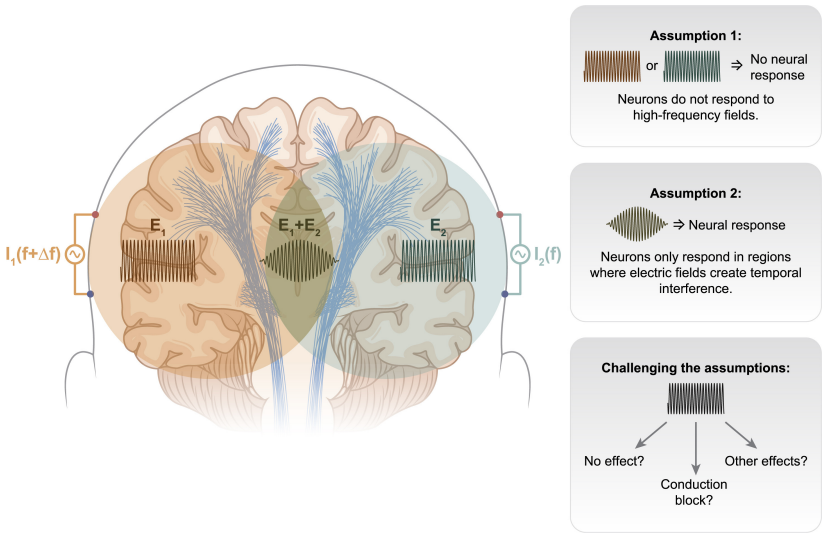

FIGURE 3.4 – This figure illustrates the concept of temporal interference. The main assumptions are (1) no neural response from high frequency stimulation (beyond 1 kHz) and (2) two electric fields which can modulate at their location of overlap with lower frequencies, will have an influence on neural responses at that lower frequency. Taken from [84].

This method could replace SEEG stimulation for EZ delineation, with the advantage of being non-invasive and capable of exploring the whole-brain rather than just the locations of SEEG implantation. In addition, the orientation of TI fields relative to the brain structure being stimulated is important for activating neural response for seizure onset [85]. This was demonstrated in alive mice, where TI fields targeting the hippocampus structure at the same location but at different orientations (medio-lateral vs. anterior-posterior) yielded different responses [85].

It has also been shown that TI can suppress epileptic biomarkers by focally targeting the hippocampus in a mouse model of epilepsy and its capability for focal stimulation of the hippocampus was also demonstrated in a human cadaver (Figure 3.5)[2]. As a continuation, TI was used alongside fMRI demonstrating that it can focally modulate hippocampal activity and have behavioral effects by enhancing episodic memory in humans [139].

The focality of TI using two tACS fields is not optimal as compared to DBS using two adjacent contacts. To increase focality, multiple TI is another approach, consisting of combining multiple pairs of simultaneous tACS fields [1, 16]. This significantly increases the focality of TI and allows for comparability with DBS yet

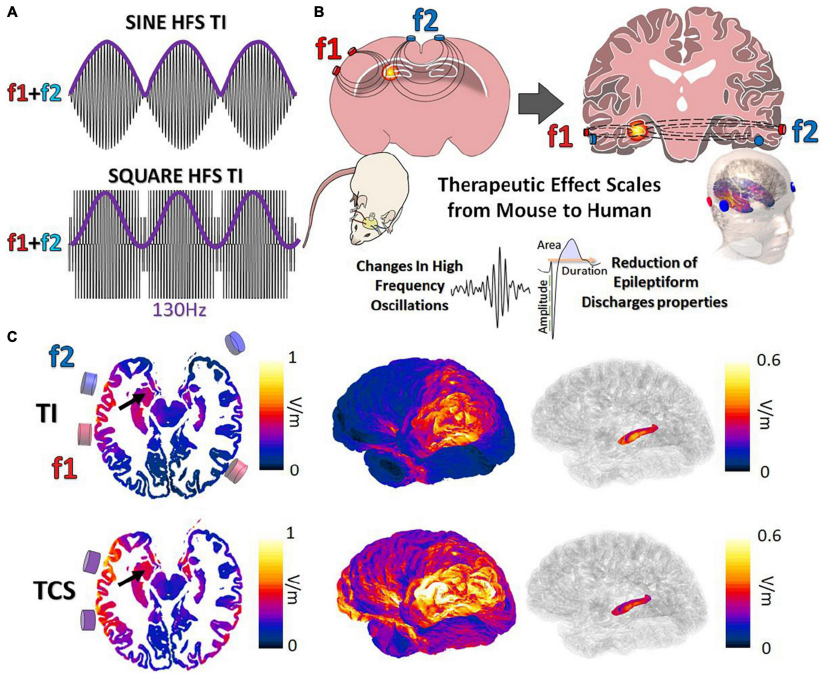

FIGURE 3.5 – This figure, from [2] illustrates how TI can be obtained by using sine waveform and square waveforms in (A), and how it can be translated from mouse to human to reach the same deep brain structure, in this case the hippocampus in (B). In (C), the TI envelope modulation amplitude distribution is shown for TI and tCS, indicating that TI is capable of reaching deep brain structures more focally and at a higher field strength.

with the advantage of non-invasiveness and allowing for more spatial flexibility.

The method is still under development and has only been applied to a few first human subjects to prove its safety and efficacy. The assumptions behind the method of TI have been questioned [84]. Although TI uses the assumption that neural membranes do not respond to stimulation fields beyond 1 kHz, research has shown that they do respond but with complex dynamics (i.e. neurons can have an initial response to the stimulation or fire continuously during the stimulation) and lead to phenomena such as conduction block (i.e. blocking action potential propagation) [84]. The physics of TI were studied to test the assumptions of the methodology, showing that indeed neural structures can be excited at the overlap between the two high-stimulation fields but this could also lead to conduction block in off-target neural structures (Figure 3.4) [84]. Their study showed that the absence of activity outside brain regions of electric field overlap during TI, could also be due to conduction block rather than the low-pass filtering property of neurons (Figure 3.4). Therefore, more precise control experiments are required to systematically explore all the properties of TI stimulation. For example, in one animal study that triggered seizure-like events (SLEs) with TI stimulation (1200/1250 Hz), control stimulations were performed (1200/1200 Hz and 50/50 Hz) and observed no SLEs [85]. Further tests outside of the TI focus could be relevant to prove the efficacy of TI and observe whether there are any side effects from this type of stimulation. In the future, if this method proves to be efficacious, it has the potential to become a non-invasive clinical tool for epilepsy diagnosis and treatment.

3.2 Models of brain stimulation

Brain stimulation modeling has two essential compartments that need to be addressed. First, an external current applied to the brain generates an electric field, which can be estimated using Maxwell's equations of electromagnetism. This field depends on the stimulating electrode, stimulation parameters and tissue conductivity. However, the electric field is not the only component driving neural response to external stimulation [84]. The physiological and anatomical properties of neurons determine the brain's active tissue response to the stimulus, also known as "activating function". Brain stimulation has both local and non-local effects, acute and long-term effects. We will explore them in the following sections.

3.2.1 Modeling the stimulation electric field

The electric field generated from electrical brain stimulation can be estimated using Maxwell's equations. These equations describe how electric and magnetic fields interact over time and space. They can explain diverse phenomena in electromagnetism, from simple electric circuits to the propagation of light waves.

Quasi-static approximation of Maxwell's equations

A simplification of Maxwell's equations can be done when dealing with electromagnetic phenomena that vary slowly in time, typically for frequencies below 1000

Hz. For example, we can apply such a simplification in the case of stimulation with intracerebral electrodes in drug-resistant epilepsy, which is typically performed at frequencies below 100 Hz.

In such cases, the wavelength for those frequencies is much larger than the system's size, therefore propagation effects can be neglected. The displacement current ($\frac{\delta E}{\delta t}$) can be ignored in comparison to the conduction current and the magnetic field effects are minimal.

Gauss' law in differential form describes the divergence of the electric field, i.e. the volume density of the outward flux of a vector field from an infinitesimal volume around a given point :

$$div\vec{E} = \nabla \cdot \vec{E} = \frac{\rho_V}{\epsilon} \tag{3.1}$$

where ρ_V is the charge density and ϵ the vacuum permittivity
Faraday's law :

$$curl\vec{E} = \nabla \times \vec{E}(\vec{r}) = 0 \tag{3.2}$$

Using the irrotational theorem, we deduce from 3.2 :

$$\vec{E} = -\nabla V \tag{3.3}$$

Therefore,

$$\begin{aligned} \nabla \cdot \vec{E}(\vec{r}) &= -\nabla[\nabla V(\vec{r})] \\ &= -\nabla^2 V(\vec{r}) = \frac{\rho_V(\vec{r})}{\epsilon} \end{aligned} \tag{3.4}$$

We get Poisson's equation :

$$\nabla^2 V(\vec{r}) = -\frac{\rho_V(\vec{r})}{\epsilon} \tag{3.5}$$

If the volume charge density is zero (i.e. in all parts of space where there is no electric charge), then we get Laplace's equation :

$$\nabla^2 V = 0 \tag{3.6}$$

Laplace's equation is a partial differential equation, typically depending on (x, y, z) coordinates in 3D space. This equation has two important properties. (i) According to the uniqueness' theorem, it has unique solutions once a suitable number of boundary conditions are specified. (ii) Its solutions satisfy the superposition principle, where any number of potentials $V_1, V_2, V_3, \ldots$, where $V = a_1V_1 + a_2V_2 + a_3V_3 + \ldots$ where a_j are constants, satisfies $\nabla^2 V = \nabla^2(a_1V_1 + a_2V_2 + a_3V_3 + \ldots) = a_1\nabla^2 V_1 + a_2\nabla^2 V_2 + a_3\nabla^2 V_3 + \cdots = 0$. Solving Laplace's equation allows for an estimation of the electric field distribution in space to be performed.

Electric potential of a point charge in the electrostatic case

From Gauss's law 3.1 we have $\vec{E}(\vec{r}) = \frac{Q}{4\pi\epsilon r^2}\hat{r}$. We can deduce the electric potential of a point charge being :

$$V(\vec{r}) = \frac{Q}{4\pi\epsilon r} \tag{3.7}$$

Using the principle of superposition, we can estimate the electric potential for N point charges :

$$V(\vec{r}) = \frac{1}{4\pi\epsilon} \sum_{k=1}^{N} \frac{Q_k}{|\vec{r} - \vec{r_k}|} \tag{3.8}$$

Electric potential using detailed electrode and head geometries

More detailed approaches use detailed electrode geometries and head models to have a more accurate estimation of the electric field. This is based on the assumption that the induced electric field has a complex spatial distribution which depends on the individual brain anatomy, requiring individual variability for the same stimulation protocol across subjects [99, 113]. The focus on personalized modeling of the induced electric field stems from reported variability in stimulation effects both within and between individuals [50, 60]. This can be explained by the complex interplay between individual anatomy, electric field propagation and brain state dependence.

We are going to overview some literature that has tried such approaches at the scale of whole-brain.

One example is SimNIBS, released in 2013, an open source and free software package to simulate non-invasive brain stimulation, allowing for realistic calculation of the electric field induced by transcranial electric and magnetic stimulation (Figure 3.6). It first computes high-quality head models from MRI images as well as accurate stimulation electrode geometries. Then, it builds a volume conductor model, which describes how electric fields are transmitted from a current source through biological brain tissue to measurements sensors. This model consists of a finite element mesh, consisting of tetrahedrons belonging to different tissue segments (Figure 3.6a). There are 15 different segmented tissue types from T1/T2-MRI, including skin, bone, cerebral white and gray matter, veins, visual nerve and spinal cord to name a few [99]. Finite element method (FEM) solvers are then used to estimate the electric field at each tetrahedral element of the subject's head mesh, and interpolates them to the cortical surface (Figure 3.6b)[113, 147].

Another open-source platform has a focus on modeling deep brain stimulation is OSS-DBS [21]. It uses volume conductor models for the head and electrodes and FEM solvers to estimate the induced electric field. In addition, it allows for placement of neuron models to increase spatial resolution in specific locations of interest, typically near the stimulation electrode.

Another specialized simulation tool which analyses the interaction between physical fields (e.g. electromagnetic fields) and biological tissues is Sim4Life. It handles complex multiphysics problems and has a focus on medical applications. One such application is temporal interference stimulation, where this tool has been used to model the effects of this novel stimulation method [48]. This tool helps to optimize the safety and efficacy of stimulation protocols and includes detailed models of human head and brain, using over 130 segmented tissues [58].

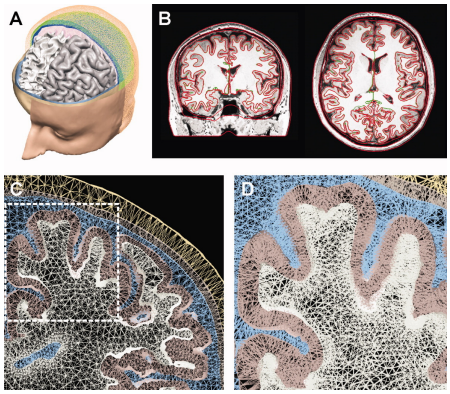

(a) Accurate head model extracted from T1-MRI and its voulme mesh zoomed-in. Each color indicates a different surface type (skin, skull, cerebrospinal fluid, GM and WM).

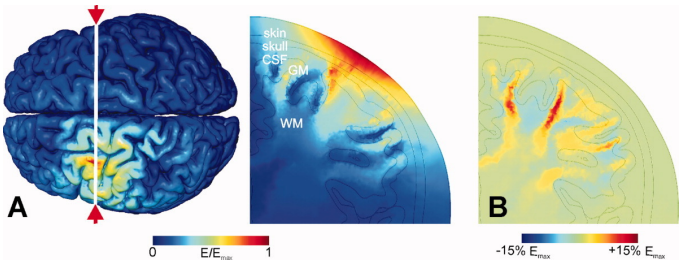

(b) Estimated electric field induced by TMS. In A, the field is shown on the GM surface and on a coronal slice. In B, the difference between electric fields with anisotropic versus homogeneous GM and WM conductivities is shown. Anisotropic conductivities were derived from DTI data.

FIGURE 3.6 – Examples of non-invasive brain stimulation estimation with realistic head models and finite-element modeling calculations. Taken from [147].

3.2.2 Modeling the brain's response

The activating function

To describe how neurons respond to external electrical stimulation, Frank Rattay developed the "**activating function**" formalism [84, 102]. This theory allows to understand how electrical fields applied to the brain induce neural responses. In particular, it estimates which parts of a neuron are more likely to fire an action potential. The activating function is proportional to the second spatial derivative of the electric field [102]. Positive values of the activating function suggest a depolarization of the membrane potential and negative values a hyperpolarization of the membrane potential (Figure 3.7).

Why the second spatial derivative ? When an electric field is generated (e.g. with DBS) it causes ions to move around, resulting in current flow (positive ions move towards the negative charge and negative ions move towards the positive charge). When a **uniform** electric field across space is applied, ions move uniformly along the neuron without a net difference in how much current is entering or leaving at different points along the neuron. A **non-uniform** electric field, which varies in strength/direction along the neuron, creates an uneven current flow along the neuron. The regions where there is the greatest difference in current flow are where local depolarization or hyperpolarization occurs. Therefore, *the spatial locations where the electric field changes more rapidly are the ones where neural activation is more likely to occur*. The **first spatial derivative** of the electric field describes the **slope** of the field or how the field changes from one point to the other along the axon. The **second spatial derivative** describes the **velocity** at which this slope changes, or the curvature of the electric field (see Figure 3.7). This second derivative corresponds to locations where there is the greatest imbalance in current flow in and out of the neural membrane, i.e. locations where action potentials can be triggered

[18].

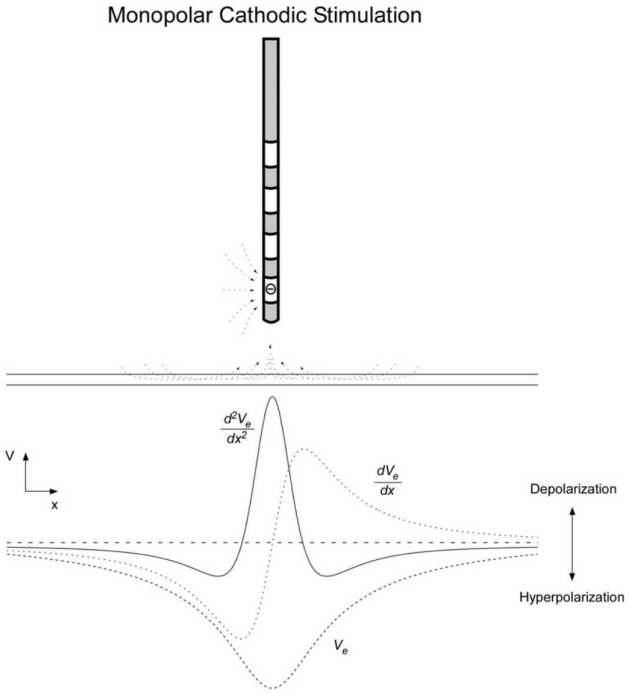

FIGURE 3.7 – This figure, from [18], illustrates the activating function along an axon during cathodic stimulation.

The activating function depends on neuron geometry

The distribution of the activating function depend on the shape and orientation of the neuron.

Along the myelinated axon membrane, the more abrupt changes in local electric field happen along the nodes or Ranvier, because there the geometry of the neuron changes abruptly. An action potential will be fired if the local depolarization exceeds a certain threshold. Once the activating function determines where an action potential is triggered, it propagates along the axon shaft. At the axon terminal, an action potential leads to neurotransmitter release. Therefore here, the activating function does not generate action potentials but rather modulates membrane potential which affects synaptic transmission.

The neuron's orientation relative to the electric field is also important. Locations where the neuron is oriented perpendicular to the electric field are more sensitive to stimulation. If the neuron is aligned parallel to the electric field, the forces it exerts on ion movement will be evenly distributed along the neuron, resulting in small changes in membrane potential. When the neuron is aligned perpendicular to the electric field, ions will move non-uniformly along the neuron leading to a greater voltage gradient between points along the axon or dendrite. The voltage difference results in non-uniform current flow (inducing depolarization and hyperpolarization at various points) and makes the neuron more likely to generate an action potential.

The volume of tissue activated

The volume of tissue activated (VTA) estimates the three-dimensional spatial extent of neural tissue that is stimulated by an electric field. It is typically estimated during DBS stimulation. Unlike the activating function, it is a macroscopic measure of the population of neurons that are most likely to be activated. Activated neurons are depolarized beyond their threshold and can trigger action potentials. The VTA depends on electrode geometry, stimulation parameters and tissue properties like conductivity.

It is mathematically derived from aggregating neurons which respond to external electrical stimulation based on the activating function. To derive the VTA, the strength of the electric field at different spatial locations is combined with the threshold needed for neurons in each location to fire and with their distribution and orientation relative to the electric field. As a general principle, since the electric field decreases with distance from the stimulation source, also the VTA decreases proportionally to the distance from the stimulating electrode.

Active tissue response

The active tissue response (ATR) refers to the physiological response of the neural tissue to stimulation, including neuronal firing, synaptic transmission, neurotransmitter release and network effects. This term requires us to go beyond the action potential firing of individual neurons or populations of them, and consider the more detailed and complex neural responses to stimulation, which are both local (ion dynamics, synaptic modulation) and global (neuronal communication, plasticity).

The brain response to stimulation can be modeled at different resolutions and scales, depending on the paradigm and question at hand. It can be done using either phenomenological, biophysical or data-driven models.

There is a variability in brain response to stimulation which increases the complexity of such an endeavor. Therefore, it is important to interpret brain responses to stimulation in terms of probabilities rather than discrete phenomena.

3.2.3 Important challenges in brain stimulation models

Advancing scientific understanding and improving clinical efficacy in brain stimulation modeling can be achieved through several key avenues. First, comparing model responses to real-world data and scenarios can provide valuable insights into how well these models reflect actual brain dynamics. Optimizing stimulation parameters is crucial for increasing the effectiveness of treatments. Additionally, gaining a deeper understanding of the mechanisms of brain stimulation, particularly its short- and long-term effects, is essential for minimizing potential side effects. Investigating plasticity induced by brain stimulation may also play a significant role in enhancing treatment outcomes.

3.3 Summary

In this thesis, we seek to model brain stimulation in epilepsy using personalized whole-brain models. This modeling approach could hopefully get us closer to understanding stimulation parameter effects in epilepsy and be a first step to build a stimulation guiding tool for clinicians.

We have used clinical data from patients with drug-resistant epilepsy which are candidates to brain surgery. These patients have undergone SEEG electrode implantation and weak stimulating currents have been used to delineate their EZ. Our goal was two fold : on the one hand, we seek to understand the underlying mechanisms for stimulation to lead to seizure generation ; on the other hand, understand the role of stimulation parameters on seizure networks which can optimize the stimulation procedure.

In the following chapters, we introduce a framework to model stimulated seizures phenomenologically. We use this approach to build a virtual cohort of patients with epilepsy, using virtual brain twins. Next, we use high-resolution brain modeling for invasive and non-invasive brain stimulation. Finally, we used systematical empirical stimulation data to compare them against our model. We discuss limitations and future improvements in the final chapter.

Deuxième partie

Original work

Chapter 4

Extending the Epileptor model for stimulated seizures

4.1 Context

People with drug-resistant epilepsy that are candidates for brain surgery treatment undergo intracranial electrode (SEEG) implantation. During this period, their brain activity is recorded with these electrodes and their resting state activity and spontaneous seizures are recorded. In addition, brain stimulation is applied with these same electrodes to delineate the epileptogenic zone (EZ) network. During SEEG stimulation, bipolar biphasic electrical stimulation is applied using two adjacent contacts and varying stimulation location, amplitude and frequency, among others. In particular, stimulation is applied to induce habitual seizures, with the goal of triggering the same clinical symptoms and electrical brain activity of spontaneous seizures. This additional information makes up for the limited sampling provided from the implanted intracranial electrodes and can distinguish the excitability levels of different brain structures during synchronous ictal activity [128].

So far, Jirsa and colleagues have modeled seizure dynamics by capturing universal features of ictal brain activity, namely fast discharges and spike and wave phenomena but also baseline shift at seizure onset [67]. From this, personalized whole-brain models of patients with epilepsy were constructed to study seizure dynamics and estimate their EZ [51, 66, 142]. Seizures induced by SEEG stimulation were not yet represented in this framework. In this thesis, we introduce an extension of the phenomenological Epileptor model to account for stimulated seizures. We base our approach on empirical patient recordings of stimulated seizures and build an hypothesis. In this short chapter, the basic assumptions and logic behind the extended model are presented. The model has been used in Chapter 4 and Chapter 5 to build a virtual cohort for epilepsy and to model brain stimulation at the high-resolution level for epilepsy diagnosis.

4.2 A hypothesis based on empirical observation

To model stimulation-induced seizures, we first needed to start with a plausible mechanism relating stimulation to seizure onset. We started with empirical recordings of patients with drug-resistant epilepsy undergoing stimulation with SEEG, as shown in Figure 4.1. During low-frequency stimulations that triggered a seizure, we observed a slow change in the tissue's response between stimulation pulses. As the stimulation approached seizure onset, the post-stimulation oscillatory response continuously rises up until the system destabilizes and goes into a seizure. We hypothesized that these oscillations could be related to slow accumulation effects in the background, for instance, extracellular potassium.

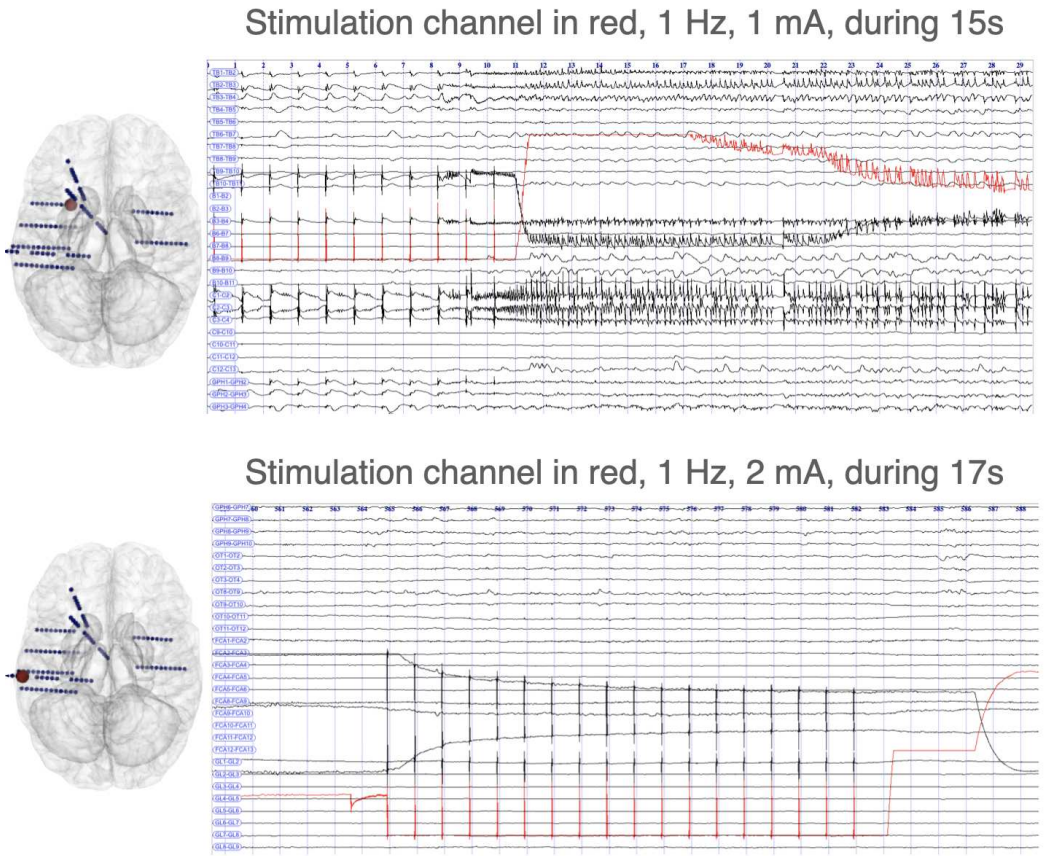

FIGURE 4.1 – In this example, we show two SEEG recordings from the same patient with temporal lobe epilepsy. In the upper figure, stimulation in channel B1-B2 triggered an habitual seizure. In the lower figure, stimulation in FCA11-12 did not trigger a seizure.

There is no consensus about the precise biophysical mechanism of ion exchanges that leads to seizure onset. Previous studies demonstrated an increase in excitability, spike frequency and oscillation power [22, 103, 135, 136] when an external perturbation was applied. Experimental studies have linked seizure onset to specific changes in ion dynamics such as extracellular potassium or intracellular chloride [39, 78, 129]. Thus, recorded stimulated seizures seem to be an abrupt electrical phenomenon, but the physiological, unobserved, processes are slow-evolving and can push the system

to a critical bifurcation leading to the seizure state. We hypothesized that exposure of repetitive stimulation/perturbation generates a slow accumulation effect, which can push the system to the seizure state when a seizure threshold is reached.

4.3 Modeling the accumulatory effect with the 3D Epileptor

We modeled the accumulation effect phenomenologically via the parameter m, which influences the oscillatory dynamics in the seizure onset state in the Epileptor model [33].

We began by extending the simpler 3-dimensional Epileptor model, using only the very fast population (x_1, y_1) which captures fast discharges during the seizure-like state and the slow variable z which guides the system between the ictal and interictal states, in particular by using the parameter x_0. The equations are the following :

$$\begin{aligned} \dot{x}_1 &= y_i - f_1(x_i) - z_i + I_{ext} \\ \dot{y}_1 &= c - dx_i^2 - y_i \\ \dot{z} &= r(4(x_i - x_0) - z_i) \end{aligned} \tag{4.1}$$

where :

$$f_1(x_1) = \begin{cases} ax_1^3 - bx_1^2 & \text{if } x_1 < 0 \\ -(m + 0.6(z-4)^2)x_1 & \text{if } x_1 \geq 0 \end{cases}$$

The default parameters of the system are $I_{ext} = 3.1, m = 0, a = 1, b = 3, c = 1, d = 5, r = 0.00035$.

In figure 4.2, we display the behavior of the 3-dimensional Epileptor model with varying values of m (default value $m = 0$). As also pointed out by El Houssaini et al., the parameter m plays a role in the stability of the equilibrium points of the model and the behavioral patterns of the time series [33].

We rendered m time dependent, $m = m(t)$, and introduced an exponentially decaying memory kernel of length λ through a linear ordinary differential equation, which slowly builds up when an external stimulus is applied, until the seizure threshold is reached. In the absence of stimulus $m(t)$ slowly returns back to baseline.

$$\dot{m} = \lambda(-m + k|I_{stim}|) \tag{4.2}$$

We chose to always consider the stimulus to have a positive accumulatory effect on the variable m, and scaled it with the parameter k. This parameter adjusts the impact of the stimulus intensity the variable m, whereas the parameter λ controls the overall (slow) evolution of m in time, as shown in Figure 4.3.

We demonstrate examples of simulated time series using this approach in figure 4.4. The extended Epileptor-stimulation model is as follows :

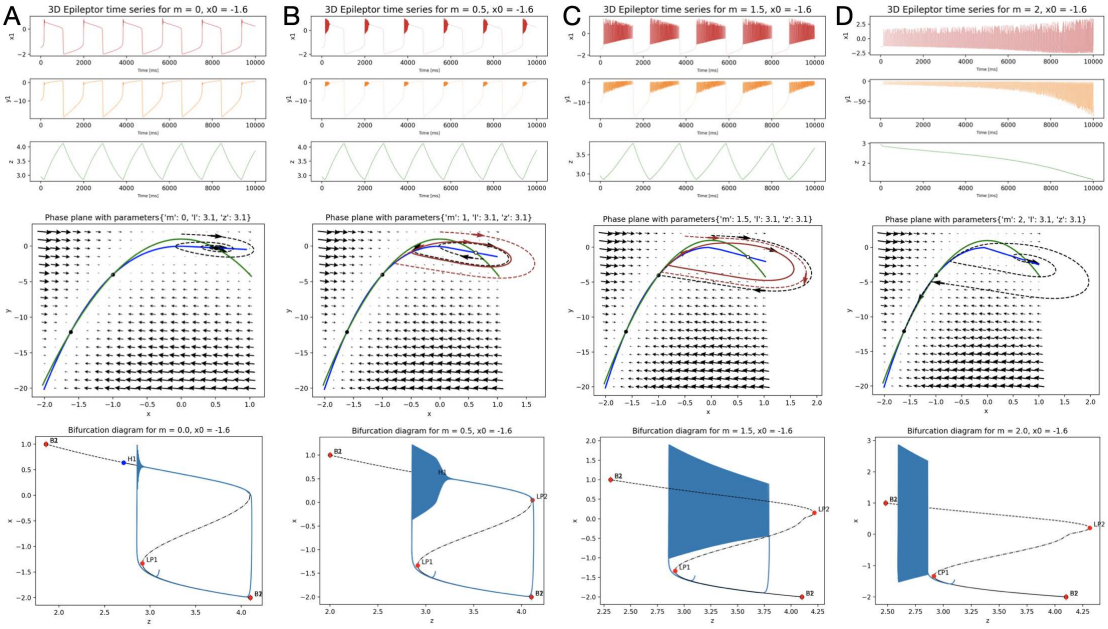

FIGURE 4.2 – The 3D Epileptor model with varying m. Each row, from top to bottom : time series for each variable (x_1, y_1, z), phase plane plot with nullclines x_1 and y_1 for $z = 3.1$ and a complete bifurcation diagram for varying values of z (dotted line : unstable fixed points, continuous line : stable fixed points). A) $m = 0$, the oscillations in the upstate are brief because the equilibrium in the upstate is a stable spiral. B) $m = 0.5$, oscillations in the upstate are of higher amplitude and longer because the equilibrium in the upstate is an unstable spiral with a limit cycle (in red in the phase plane plot). C) $m = 1.5$, oscillations in the upstate have an even higher amplitude and last for the entire duration of the upstate, the limit cycle, shown in red in the phase plane has a greater diameter. D) $m = 2$, the system exhibits unstable spiral behavior.

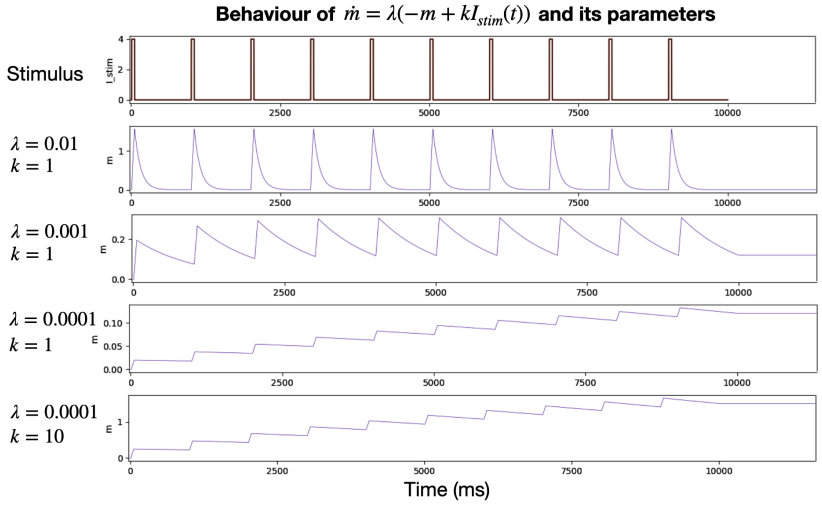

FIGURE 4.3 – Simple illustration of the different behaviors of m depending on λ and k parameters depending on the same stimulus input.

$$\begin{aligned}
\dot{x}_1 &= y_i - f_1(x_i) - z_i + I_{ext} + I_{stim} \\
\dot{y}_1 &= c - dx_i^2 - y_i \\
\dot{z} &= r_1(4(x_i - x_0 + H(m_i - m_{thresh})) - z_i) \\
\dot{m} &= r_2(k|I_{stim}| - m)
\end{aligned} \tag{4.3}$$

where :

$$f_1(x_1) = \begin{cases} ax_1^3 - bx_1^2 & \text{if } x_1 < 0 \\ -(m + 0.6(z-4)^2)x_1 & \text{if } x_1 \geq 0 \end{cases}$$

The default parameters of the system are $m_{thresh} = 1.5, I_{ext} = 3.1, a = 1, b = 3, c = 1, d = 5, r_1 = 0.00035, k = 1, r_2 = 0.001$.

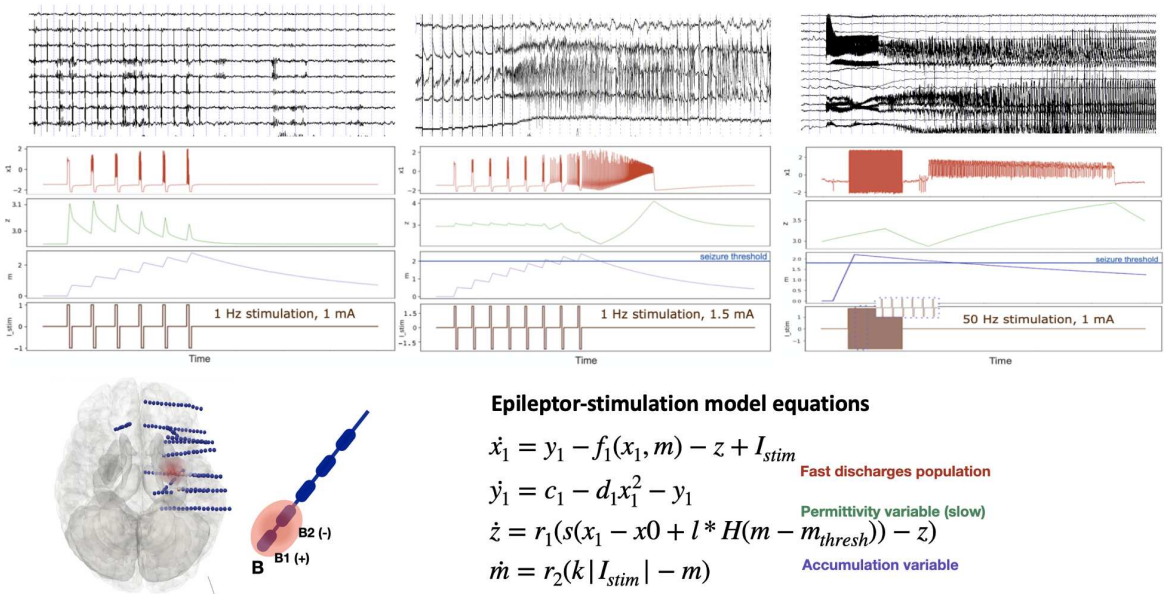

FIGURE 4.4 – Empirical SEEG recording with stimulation and simulated time series with the extended model. A) Stimulation at 1 Hz frequency, 1 mA amplitude with no induced seizure. In the simulated time series, the variable m increases due to the applied stimulus but does not cross the seizure threshold. The system remains in the normal state. B) Stimulation at 1 Hz frequency, 1.5 mA amplitude induced a seizure. In the simulated time series, the variable m crosses the seizure threshold and kicks the system to the seizure-like state. C) Stimulation at 50 Hz frequency, 1 mA amplitude induced a seizure.

4.4 Conclusion

In this short chapter, we explained the simple notions behind the extended Epileptor model for seizures induced by stimulation. We focused here only at the single neural mass level, where the very basic assumption of this work focuses on the effects an external stimulation has on the brain relative to seizure onset. Although seizure

onset is a very abrupt phenomenon, we hypothesize that the biological processes happening in the background are slow-evolving and push the system to a critical bifurcation, which then destabilizes the system and brings it to the seizure state. In Chapter 5, we use this model on personalized virtual brains to build synthetic copies of empirical stimulated seizures. We systematically evaluate our approach and test the effects of stimulation parameters in-silico. In Chapter 6, we use high-resolution personalized virtual brain to model stimulated seizures and model both invasive SEEG and non-invasive TI stimulation.

Chapter 5

Virtual epileptic patient cohort : generation and evaluation

Abstract Epilepsy is a prevalent brain disorder, characterized by sudden, abnormal brain activity, making it difficult to live with. One-third of people with epilepsy do not respond to anti-epileptic drugs. Drug-resistant epilepsy is treated with brain surgery. Successful surgical treatment relies on identifying brain regions responsible for seizure onset, known as epileptogenic zones (EZ). Despite various methods for EZ estimation, evaluating their efficacy remains challenging due to a lack of ground truth for empirical data. To address this, we generated and evaluated a cohort of 30 virtual epilepsy patients, using patient-specific anatomical and functional data from 30 real drug-resistant epilepsy patients. This personalized modeling, based on the patient's brain data, is called a virtual brain twin. For each virtual patient, we provided data that included anatomically parcellated brain regions, structural connectivity, reconstructed intracranial electrodes, simulated brain activity at both the brain region and electrode levels, and key parameters of the virtual brain twin. These key parameters, which include the EZ hypothesis, serve as the ground-truth for simulated brain activity. For each virtual brain twin, we generated synthetic spontaneous seizures, stimulation-induced seizures and interictal activity. We systematically evaluated these simulated brain signals by quantitatively comparing them against their corresponding empirical intracranial recordings. Simulated signals based on patient-specific EZ captured spatio-temporal seizure generation and propagation. Through in-silico exploration of stimulation parameters, we also demonstrated the role of patient-specific stimulation location and amplitude in reproducing empirically stimulated seizures. The virtual epileptic cohort is openly available, and can be directly used to systematically evaluate methods for the estimation of EZ or source localization using ground truth EZ parameters and source signals.

5.1 Introduction

Epilepsy is one of the most common neurological disorders, affecting 1% of the global population. It is characterized by recurrent spontaneous seizures, which are sudden bursts of abnormal electrical activity of the brain. Anti-epileptic drugs are the most common treatment option, however one-third of patients with epilepsy are

drug-resistant. In such cases, brain surgery is the main alternative treatment, which seeks to resect brain zones responsible for seizures, known as epileptogenic zones (EZ) [105, 125].

For precise localization of the EZ pre-surgery, intracranial depth electrodes (stereoelectroencephalography, SEEG), are inserted in the patient's brain to locally record electrical brain activity [59]. Spontaneous seizures recorded with intracranial electrodes are used to define the EZ. However, due to partial sampling from the intracranial electrodes, spontaneous seizures may not be sufficient to make a clear diagnosis. Intracranial electrical stimulation is performed to contribute to the EZ localization by triggering seizures and for functionality mapping of regions explored [127]. Outside of seizure events and when a patient is at rest, interictal activity is recorded, where interictal spikes are analyzed to contribute to the EZ localization. Both ictal and interical activities are used to constrain and define the epileptogenic zone.

Despite huge research and clinical efforts to tackle drug-resistant epilepsy, brain surgery has a failure rate of about 50% [105]. Treatment failure is attributed to a misdiagnosis or a incomplete diagnosis of the EZ. Therefore, a precise EZ diagnosis is crucial to improve treatment of drug-resistant epilepsy. Many methods have been proposed to diagnose the EZ based on analysis of empirical brain recordings [10, 43]. However, they are difficult to evaluate due to absence of ground truth information for empirical data. Recent studies evoke the need for synthetic datasets in order to benchmark scientific methods [42, 44]. When synthetic datasets capture the structure and features of empirical data, they can be useful for hypothesis testing and validation before accessing the real dataset [44]. Furthermore, synthetic health care datasets protect patient privacy and are easier to access compared to empirical data for which strict privacy laws are in place [40, 54].

We aimed to build a reliable synthetic dataset of patients with drug-resistant epilepsy, based on parameterized epileptogenic zone information, inferred from empirical spontaneous seizures. This resource could be used by the scientific community to test and validate their EZ diagnosis methods. To achieve this, we built for each patient a virtual brain twin, using their own anatomical and functional data [141]. T1-weighted magnetic resonance imaging (T1-MRI) and diffusion-weighted MRI (DW-MRI) defined the structural scaffold with network nodes (brain regions) and links (structural connectivity). SEEG electrode locations are reconstructed from post-operative CT. To model brain activity at each node, the Epileptor model is employed, which describes spatio-temporal seizure dynamics [67]. Finally, to determine the EZ parameters for each patient, we used the Virtual Epileptic Patient (VEP) pipeline [142]. The VEP estimates the epileptogenic zone from empirical seizure recordings, using personalized whole-brain modeling and machine learning methods [51]. This pipeline is currently used in a clinical trial, with the goal of improving surgical outcome for DRE (EPINOV NCT03643016) [81, 142]. In addition, we used the clinical EZ estimation from expert epileptologists as a second approach.

As a result, we generated a virtual cohort of 30 drug-resistant epilepsy patients. We introduced metrics to systematically compare this virtual cohort against the corresponding empirical cohort. We provided for the first time, an extended model for stimulated seizures on the whole-brain level. For each patient, we used one

virtual brain twin to generate synthetic spontaneous seizures, stimulated seizures and interictal activity. We also provided the personalized brain network models and parameters used to simulate the data. Additionally, we interrogated the influence of stimulation location and simulation amplitude on seizure networks. We shared this dataset publicly in iEEG-BIDS format [56] to help the scientific community when systematically evaluating and validating their EZ estimation methods. The unique feature of the virtual cohort lies in its known ground-truth from the modeling setting and detailed parameters.

Despite being an emerging technology, synthetic datasets can enhance clinical research, protect patient privacy, and reduce costs [42]. Synthetic SEEG data have been used to validate dynamical network biomarkers [104] and validate methods for estimating epileptogenic zones [51, 142]. The novelty of our work is the generation of a comprehensive virtual patient cohort, enabling researchers to evaluate their methods using synthetic data that mimic empirical data. Each virtual brain twin contains synthetic spontaneous seizures, stimulated seizures and interictal activity at the whole-brain level and at the SEEG level. Here, we present for the first time synthetic seizures triggered by SEEG stimulation. Each patient's estimated EZ serves as model parameters, providing ground-truth data for the virtual cohort. This makes our synthetic cohort a valuable tool for assessing data analysis methods. We have made this dataset publicly available to help the scientific community test and refine their techniques.

The paper begins by outlining the workflow for building personalized brain models for drug-resistant epilepsy. It then provides an overview of the cohort, examples of simulated time series, and a systematic comparison between simulated and empirical SEEG data. We also assess the significance of key model parameters, focusing on the EZ hypothesis and stimulation parameters. Finally, the discussion addresses limitations and future applications for synthetic data in epilepsy.

5.2 Results

5.2.1 Workflow of the virtual epileptic cohort

The workflow of the virtual epileptic cohort in Figure 5.1 illustrates the process of generating patient-specific synthetic data using a personalized whole-brain network model derived from patient-specific brain imaging data, and conducting a systematic comparison.

First, we used patient-specific T1-MRI alongside the VEP atlas [140] to parcellate the brain into anatomo-functional relevant regions, represented as point-like sources. The DW-MRI was used to derive the region-to-region connectivity, by counting white matter streamlines to and from each brain region. Secondly, regional brain activity was simulated using the Epileptor model [67]. Based on the EZ hypothesis, we parametrized the model's excitability for each region. We employed two EZ hypotheses : the VEP hypothesis and a clinically defined hypothesis. The VEP hypothesis is estimated from spontaneous seizures using Bayesian inference methods [51, 142]. The clinical hypothesis is defined by clinical experts (JM and FB). Finally, from post-implantation CT scan we estimated the coordinates of SEEG electrodes. The

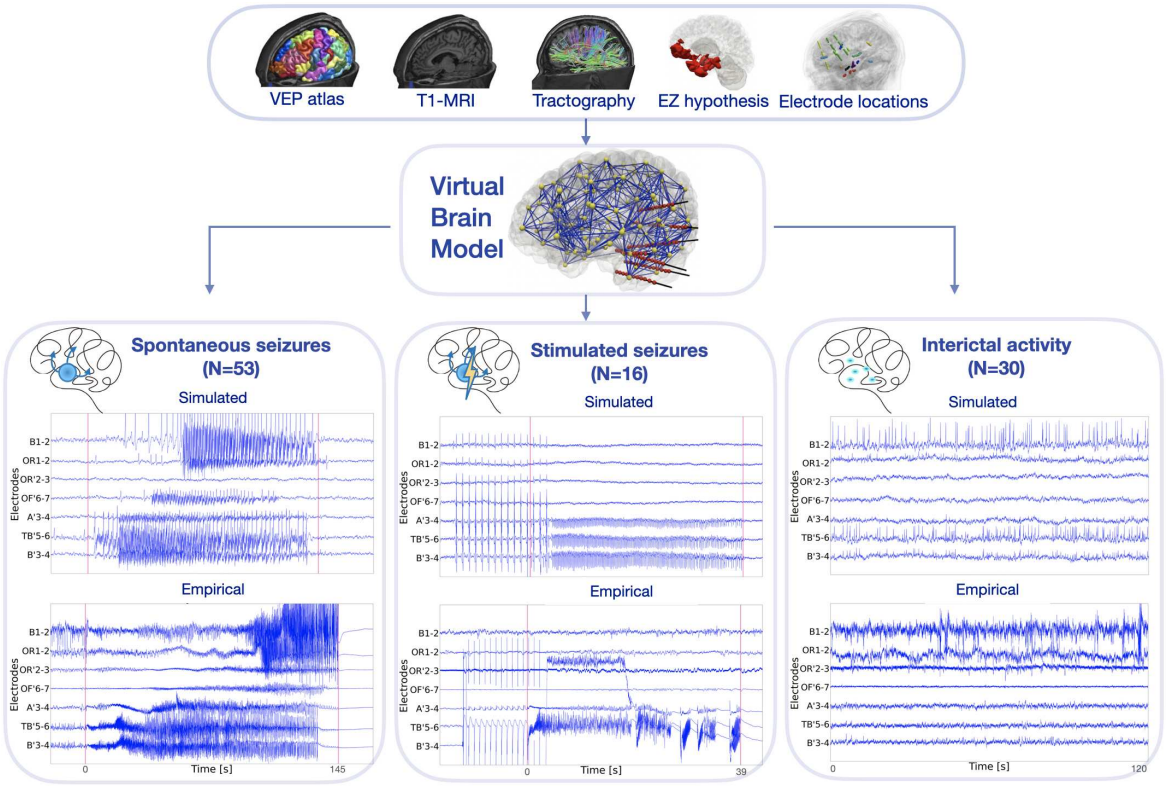

FIGURE 5.1 – Workflow of the virtual epileptic patient cohort. Patient-specific T1-MRI, dw-MRI and CT-scan are integrated within a common virtual brain model. The VEP atlas is applied on the T1-MRI to parcellate the brain into anatomical regions, represented as network nodes. From the dw-MRI a tractography is computed, made of estimated white matter fiber connections, from which region-to-region connectivity is derived, represented as network edges. On each node of the virtual brain a neural mass model is used to simulate field potentials. The EZ hypothesis informs the excitability parameter for each brain region. Based on this brain model, three different states can be simulated : spontaneous seizures, stimulation-induced seizures and interictal spikes. Whole-brain network activity is mapped onto the reconstructed SEEG electrodes using the source-to-sensor forward solution, thus obtaining simulated SEEG time series. The simulated SEEG time series are systematically compared against the empirical SEEG recordings using spatio-temporal data features.

distance between brain sources and SEEG sensors and the size of source regions is used to evaluate the source-to-sensor gain matrix. The gain matrix maps simulated source-level activity to sensors, obtaining synthetic SEEG activity. For each patient, one personalized brain model was used to simulate three different states : spontaneous seizures, stimulated seizures and the interictal period with spikes (Figure 5.1). In the following sections, we propose several metrics to systematically compare the synthetic and empirical data features for each of these three types of brain dynamics.

5.2.2 Overview of virtual epileptic cohort

The virtual epileptic cohort consists of 30 virtualized drug-resistant epilepsy patients (5.1) and follows standardized BIDS-IEEG structure [56]. For a detailed overview of this structure, see supplementary Figure 5.7. Following this standard, the data was categorized into *simulated* data and *derived* data. The simulated data contain simulated brain activity at the SEEG electrode level, with three modalities : spontaneous seizures, stimulated seizures and interictal activity. See 5.1 for a summary of the number of simulations for each modality per patient. The derived data are extracted from MRI and CT-scan brain imaging, capturing the brain anatomy of each patient. This includes : (i) spatial coordinates of brain regions, (ii) coordinates of implanted SEEG electrodes, (iii) region-to-region connectivity matrix, and (iv) source-to-sensor gain matrix. Finally, personalized model parameters (including the EZ hypothesis) and simulations at the whole-brain level are made available. In this paper, we define *ground truth* as the chosen model parameters which gave rise to simulated brain activities at the SEEG level.

5.2.3 Spontaneous seizures

Simulation of spontaneous seizures

We simulated spontaneous seizure data for each patient in the virtual epileptic cohort. As a first approach to parameterize the epileptogenic network, we used the VEP hypothesis estimated from the VEP pipeline [142]. This pipeline uses patient-specific data to build virtual brain models and bayesian inference algorithms to obtain estimated distributions of excitability for each brain region, in the $[0, 1]$ range. We linearly transformed epileptogenicity values to the excitability parameter x_0 into a range $[-2.2, -1.2]$ in the Epileptor model (5.3). The critical value x_{0c} is approximately -2.0 depending on the global connectivity matrix [142]. For any given region, if $x_0 > x_{0c}$ the region can autonomously generate seizures, otherwise it remains in the normal state. For each patient, we simulated one seizure for each empirical seizure type. We defined each seizure type qualitatively based on the seizure spatial propagation patterns observed at the SEEG level. While the seizure onset network was the same, the seizure propagation network varied across seizure types (see also supplementary Figure 5.8). As a second approach, the clinical hypothesis was used to parameterize the epileptogenic network. Epileptogenic, propagation and healthy regions were coupled according to the structural connectome, which gave rise to whole-brain seizure dynamics. We simulated a total of 53 spontaneous seizures for each EZ hypothesis ($1 - 3$ per patient).

TABLE 5.1 – Patient information of the virtual epileptic cohort. Abbreviations : FCD, focal cortical dysplasia ; HS, hippocampal sclerosis ; L, left ; NA, not applicable ; PMG, polymicrogyria ; PNH, periventricular nodular heterotopia ; R, right ; R>L : right hemisphere onset propagating to left hemisphere ; R&L : right and left onset ; NSS, number of simulated spontaneous seizures ; NIS, number of simulated induced seizures ; NII, number of simulated interictal timeseries.

ID	Sex	Age	Epilepsy type	MRI	Histopathology	Side	NSS	NIS	NII
1	F	34	Temporal	Normal	HS	R	2	0	1
2	F	29	Temporo - occipital	L temporo - occipital PNH	NA	L	2	1	1
3	M	36	Temporo - frontal	R temporo - occipital scar	FCD I	R	1	1	1
4	F	26	Temporal	R temporal mesial ganglioglioma	Ganglioglioma	R	2	0	1
5	M	21	Parietal	L postcentral - parietal gyration asymmetry	NA	L	2	0	1
6	M	59	Frontal	Normal	NA	L	2	0	1
7	M	60	Temporal	Normal	mild gliosis	R>L	1	1	1
8	F	46	Temporal	L amygdala enlargement	mild gliosis	L	3	1	1
9	F	45	Bifocal : parietal temporal	R parietal lesion	mild gliosis	R	2	1	1
10	F	45	Temporal	L hippocampal sclerosis	HS	L	3	1	1
11	F	41	Frontal	L frontal scar(abcess)	Gliosis	L	1	1	1
12	F	28	Bilateral temporo - frontal	Bilateral hippocampal and amygdala T2-hypersignal	NA	R&L	2	2	1
13	M	19	Frontal	Normal	mild gliosis	L	1	0	1
14	F	23	Premotor	Normal	FCD IIb	L	1	0	1
15	M	41	Temporal	R temporal PMG and multiple PNH	NA	R	2	1	1
16	M	29	Temporo - fronto - parietal	R temporo-parieto-insular & L temporo-parietal necrosis	NA	R>L	3	0	1
17	M	26	Temporal	L temporo-polar hypothrophy and HS	HS	L	2	0	1
18	M	24	Parieto - temporal	"L Parieto - occipital necrosis"	NA	L	1	0	1
19	M	44	Temporo - insular	Normal	NA	L>R	1	0	1
20	F	27	Temporal	Normal	HS	R	1	1	1
21	F	23	Occipital	Normal	FCD Ic	L	2	0	1
22	F	30	Parietal	L parietal FCD	FCD IIb	L	1	1	1
23	M	63	Temporal	Normal	NA	L	1	0	1
24	M	29	Temporal	Normal	NA	R	3	0	1
25	M	42	Insular	Normal	NA	L	3	2	1
26	F	28	Occipital	PNH	NA	R	1	0	1
27	M	29	Frontal	R prefrontal gliotic scar (arteriovenous malformation)	Gliosis	R>L	1	1	1
28	F	22	Temporo - frontal	Anterior temporal necrosis	Gliosis	R	1	0	1
29	F	30	Bilateral temporal	Bilateral posterior PNH	NA	R>L	3	1	1
30	M	56	Temporo - frontal	R Frontal FCD	FCD IIb	R	2	0	1

Examples of spontaneous seizures from two patients of the VEC are shown in Figure 5.2.Empirical and simulated seizure activity are shown for patient 1 with temporal lobe epilepsy (Figure 5.2A). Empirical recordings indicated an early recruitment in the hippocampus of the right hemisphere. The estimated epileptogenic network using the VEP pipeline included the hippocampus-anterior, hippocampus-posterior and amygdala of the right hemisphere. The propagation network included the right-STS-anterior, the left-supramarginal-anterior, the left-temporal-pole, the left-rhinal-cortex and the left-Heschl-gyrus. From this estimation, we determined the excitability parameters for all brain nodes and simulated the SEEG time series. The SEEG signal power over the whole activity is visualized on the reconstructed electrodes. Secondly, the same data are shown for patient 5 with parietal epilepsy in Figure 5.2B. Here, the estimated epileptogenic network included the postcentral-gyrus, superior-parietal-lobule, and angular-gyrus of the left hemisphere. The propagation network extended to both right and left hemisphere brain regions.

Evaluating spontaneous seizures

To evaluate the spatio-temporal information captured by the virtual epileptic cohort, we compared simulated and empirical SEEG time series for 53 spontaneous seizures (Figure 5.3). In addition, to evaluate the importance of personalized parameters in the subsequent simulated data, we built a randomized cohort (RC) of 15 simulated spontaneous seizures. This cohort was constructed using virtual brain models from the VEC cohort and changing only their EZ hypothesis by random selection from another patient.

We showed four metrics to compare empirical and simulated spatio-temporal seizure dynamics in Figure 5.3 (all 16 metrics shown in supplementary Figure 5.14). We captured high frequencies of the signal during seizure activity using a high-pass filter followed by envelope smoothing using a low-pass filter. When the envelope crossed a defined threshold, we marked the corresponding electrode as seizure electrode. By marking the timestamps when the envelope jumps from and returns to baseline, we estimated the seizure onset and offset times, respectively (see Figure 5.3A). Next, each electrode's activity was binarized in time at each timestep (0-no seizure activity ; 1- seizure activity) (see Figure 5.3B). The binarized synthetic and empirical SEEG were compared using Pearson correlation. We also compared the intersection of SEEG seizure channels between the empirical and synthetic time series, resulting in our overlap metric. Finally, based on seizure onset times, we categorized each channel as either seizure onset (SO), seizure propagation (SP) or no seizure. Each category was compared using the Jaccard similarity coefficient (see Figure 5.3D, see also Materials and methods). We performed a permutation test for each metric (H_0 : mean(VEC) $\leq$ mean(RC), H_1 : mean(VEC) $>$ mean(RC)). The virtual epileptic cohort performs significantly better than the randomized cohort ($p < 0.0001$). In addition, results with EZ hypothesis based on the clinical hypothesis are presented in supplementary Figure 5.13A.

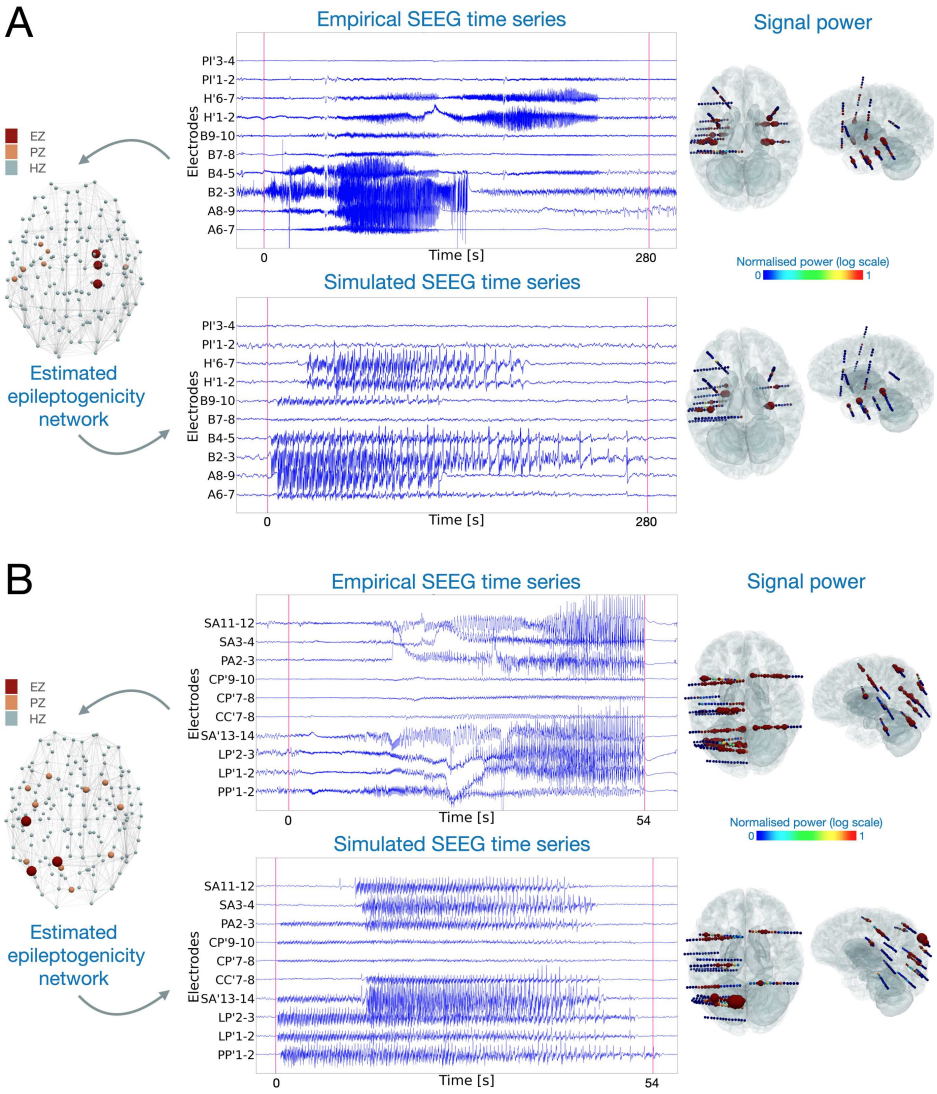

FIGURE 5.2 – The corresponding empirical and simulated spontaneous seizure activity for : A) Patient 1 with temporal lobe epilepsy showing right-hemisphere hippocampal early involvement propagating after several seconds in the contra-lateral hemisphere, and B) Patient 5 with parietal epilepsy. In both A) and B), on the left-side panel, the estimated epileptogenic network from the empirical spontaneous seizure is plotted for each brain region. Red, orange and light blue represent EZ, PZ and HZ respectively. The top middle panels display empirical SEEG recordings. The bottom middle panels represent corresponding simulated recordings based on the EZ network. Red vertical lines denote the seizure onset and offset, determined by clinicians for the empirical recordings and by our model in the simulated time series. Right-side panels show the signal power distribution for all channels. The color bar displays normalized signal power, where blue and red represent low and high signal power, respectively.

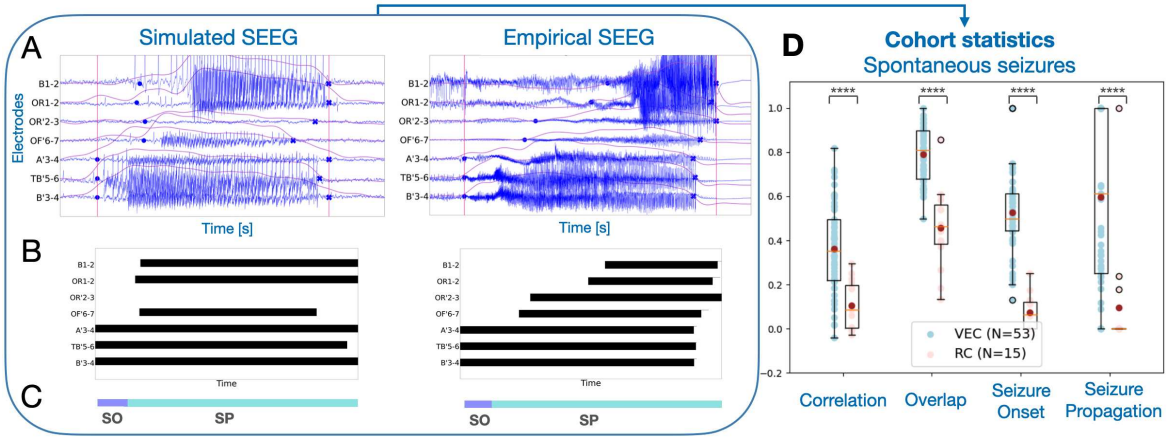

FIGURE 5.3 – Comparing simulated and empirical SEEG spontaneous seizures. A) Left, simulated SEEG seizure. Right, empirical SEEG timeseries of seizure dynamics. For each electrode, the envelope data feature is computed by band-pass filtering the electrical brain signal. Seizure onset and seizure offset time points, shown as blue circles, are computed for each electrode based on the envelope's jump from and return to baseline. B) Each empirical and simulated SEEG electrode is binarized in time, where 0 (white) corresponds to no seizure activity and 1 (black) corresponds to seizure activity. C) The time reference bar is used for both empirical and simulated SEEG to categorize recording electrodes into two groups : SO (Seizure Onset) and SP (Seizure Propagation). An electrode is labeled as SO when its onset time point aligns with the horizontal purple line, typically within the first few seconds of the entire seizure duration. Whereas an electrode is labeled as SP when its onset time point aligns with the horizontal light blue line. D) Four metrics to quantify the comparison of SEEG recordings in virtual epilepsy cohort (VEC, N = 53 in blue) and the randomized cohort (RC, N=15 in red) against the empirical SEEG recordings. Each point in the plot corresponds to one metric for one empirical and simulated SEEG pair. The dark red point in each metric represents the mean value for each category. Results are shown in box plots, overlayed over individual data points. Middle box represents the interquartile range (IQR), with a line at the median. The whiskers extend from the box to the data point lying within 1.5x the IQR. Points past the whiskers are marked as fliers. $^{****}p - value < 0.0001$; permutation test.

5.2.4 Stimulated seizures

Simulation of stimulated seizures

We provided 16 SEEG stimulated seizures for 14 patients. We used the EZ hypothesis estimated from spontaneous seizures and the same stimulation parameters which clinicians used in the clinical recordings. In Figure 5.4A, we show an example of a focal temporal seizure from patient 3, triggered by stimulation of electrodes B2 and B3, as anode and cathode, respectively.

The epileptogenic network is estimated from the spontaneous seizure of the same patient using the VEP pipeline. The epileptogenic zones are T2-anterior and hippocampus-anterior of the right hemispheres. The propagation zones are SFS-rostral, amygdala and fusiform gyrus of the right hemisphere. Following the stimulation period, a seizure is triggered in the stimulating electrodes and other nearby electrodes. The second example consists of a bilateral temporo-frontal seizure from patient 12, applied using electrodes B3 and B4 (Figure 5.4B). The epileptogenic network is estimated from the spontaneous seizure of the same patient. The epileptogenic zones are left orbito-frontal-cortex, right F3-pars-opercularis and right occipito-temporal-sulcus. Propagation zones have an extended network including the right hippocampus-anterior where the stimulating electrodes are located. Seizure activity is first observed in the right-temporal-lobe, and later propagates to frontal regions and the contra-lateral hemisphere (B' electrodes located in the left temporal lobe). In both examples, normalized signal power distribution on reconstructed SEEG electrodes displays the large network of seizure organization.

Evaluating stimulated seizures

We used three approaches to evaluate synthetic stimulated seizures (Figure 5.5). Before comparison, we removed the time series corresponding to the stimulus current and only compared the post-stimulus time series. In the first approach, similarly to spontaneous seizures, four metrics were compared against a randomized cohort (all 16 metrics shown in supplementary Figure 5.15). The randomized cohort was generated using random EZ hypothesis and contains in total 15 stimulated seizures. Thus, for the same patient, an EZ hypothesis was chosen from a random patient. Then, we applied the same stimulation parameters to simulate seizure dynamics induced by stimulation. We employed a permutation test on the comparative metrics that specifically compared means. The results demonstrate a significantly better performance for the virtual epileptic cohort compared to the randomized cohort ($p<0.001$), as shown in Figure 5.5A. Results with EZ hypothesis based on the clinical hypothesis are presented in supplementary Figure 5.13B.

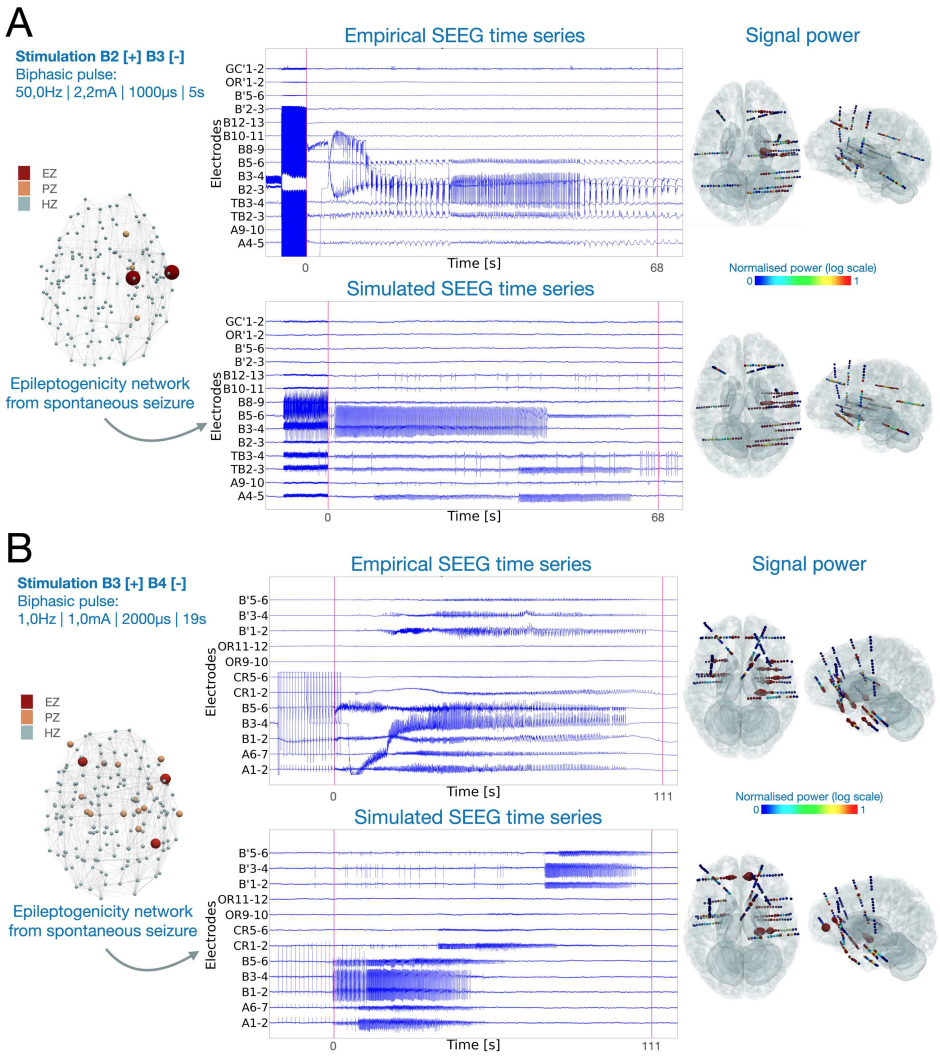

FIGURE 5.4 – Stimulated seizures induced by adjacent SEEG electrodes for two patients with different propagation patterns. A) Focal temporal seizure of patient 3, induced by high-frequency stimulation of electrode pairs B2-B3, located in the right hippocampus anterior. Stimulation waveform is a bipolar pulse applied at 50 Hz frequency, 2.2 mA amplitude, with pulse width of 1 millisecond and 5 second duration. B) Bilateral seizure of patient 12, induced by low-frequency stimulation of electrode pairs B3-B4, also located in the right hippocampus anterior. Stimulation waveform is a bipolar pulse applied at 1 Hz frequency, 1 mA amplitude, with pulse width of 2 milliseconds and 19 second duration. In both A) and B), left-side panels display stimulation parameters and the epileptogenic network estimated from the spontaneous seizure of the same patient. Red, orange and light blue represent EZ, PZ and HZ respectively. The middle panels show empirical and simulated SEEG time series for a few electrodes. Red vertical lines denote the seizure onset and offset, determined by clinicians for the empirical recordings and by our model in the simulated time series. The right-side panels show the normalized signal power distribution for all channels. Color bar represents signal power, where blue and red represent low and high signal power, respectively.

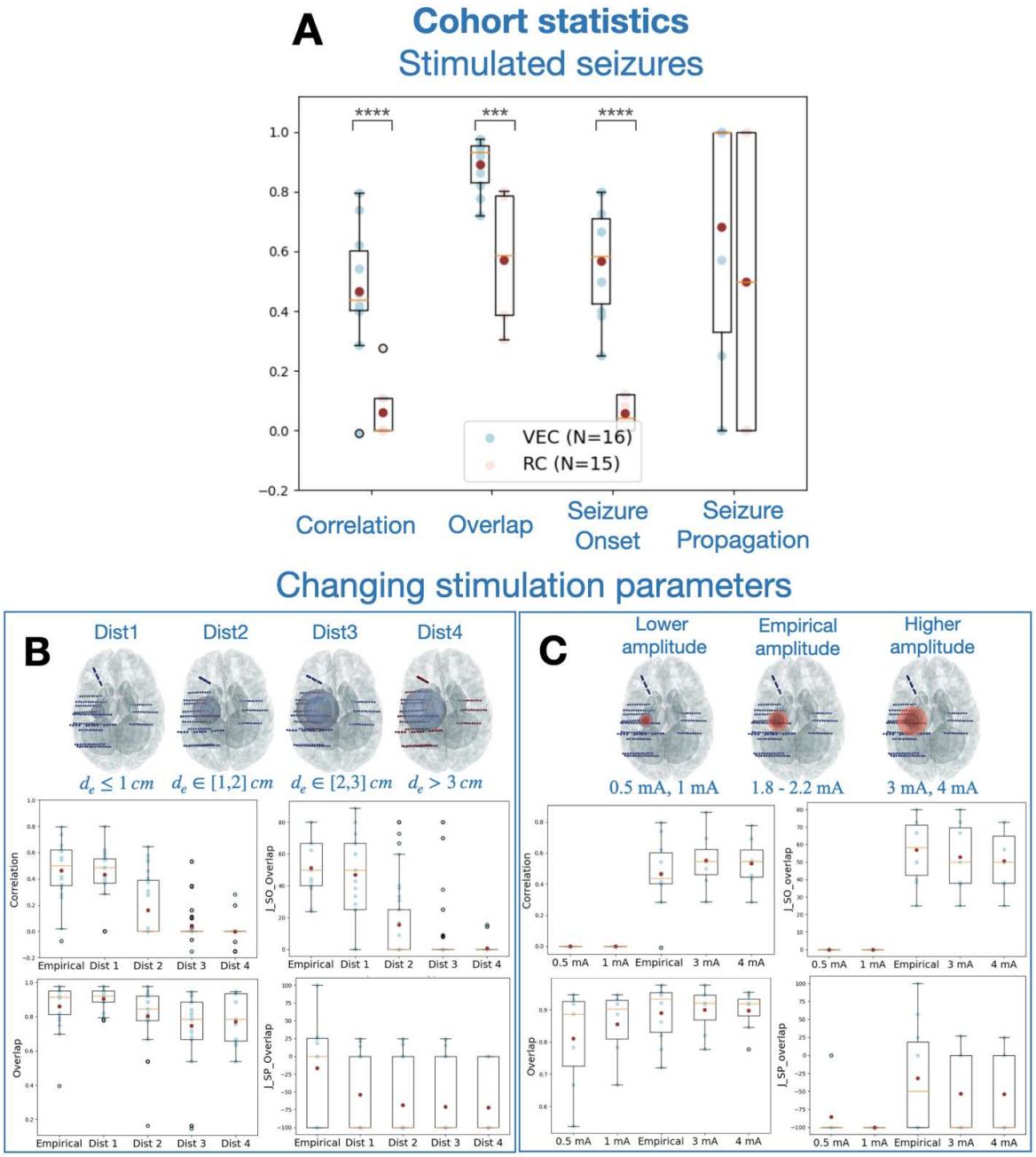
A
Cohort statistics
Stimulated seizures
****
***
****
1.0
0.8
0.6
0.4
0.2
0.0
−0.2
VEC (N=16)
RC (N=15)
Correlation
Overlap
Seizure Onset
Seizure Propagation
Changing stimulation parameters
B
Dist1
Dist2
Dist3
Dist4
$d_e \leq 1\,cm$
$d_e \in [1,2]\,cm$
$d_e \in [2,3]\,cm$
$d_e > 3\,cm$
Correlation
J_SO_Overlap
Overlap
J_SP_Overlap
Empirical Dist 1 Dist 2 Dist 3 Dist 4
C
Lower amplitude
Empirical amplitude
Higher amplitude
0.5 mA, 1 mA
1.8 - 2.2 mA
3 mA, 4 mA
Correlation
J_SO_overlap
Overlap
J_SP_overlap
0.5 mA 1 mA Empirical 3 mA 4 mA

Figure 5.5 *(previous page)* – Comparison of simulated and empirical SEEG for stimulation induced seizures. A) Four metrics compare the stimulation-induced SEEG seizure time-series in virtual epileptic cohort (VEC, N=16 in blue) and the randomized cohort (RC, N=15 in red). Each point in the plot corresponds to one metric comparing one empirical and simulated SEEG pair. Dark red points in each metric represent the mean value. $^{****}p-value < 0.0001$, $^{***}p-value < 0.001$; permutation test. B) Performance metrics for varying only stimulation locations in seven patients, measured by the distance from the empirical stimulation locations. We randomly stimulated up to 10 pairs of electrodes within four main distance groups located outside of the empirical locations. If d_e is the distance in cm from the empirical locations, Dist1 : $d_e \leq 1$; Dist2 : $d_e \in [1, 2]$; Dist3 : $d_e \in [2, 3]$; and Dist4 : $d_e \geq 3$. Each distance group is compared using four metrics, displayed in box plots and overlaid individual data points (in blue). In total, 243 simulations were generated and compared against the empirical recordings. C) Performance metrics for varying only stimulation amplitude in seven patients. Empirical stimulation amplitude varied from $1.8 - 2.2mA$. Then we performed four simulations per patient, using the same stimulation parameters but 2 lower amplitudes (0.5 mA, 1 mA) and 2 higher amplitudes (3 mA, 4 mA). Four metrics are used to compare across the five amplitude groups. In total, 28 simulations were generated and compared against empirical recordings. In all cases, results are shown in box plots, overlayed over individual data points. Middle box represents the interquartile range (IQR), with a line at the median. Whiskers extend from the box to the data point lying within 1.5x the IQR. Points past whiskers marked as fliers.

In the two other approaches, we investigated the role of two stimulation parameters in inducing seizures : stimulation location and stimulation amplitude. We varied these stimulation parameters and compared the simulated outcome against the empirical stimulated seizure. We varied stimulation location by randomly selecting 10 electrode pairs from each of four distance groups to stimulate for seven patients, shown in Figure 5.5B. The distance groups are defined by d_e the distance from the empirical stimulation location : Dist1 : $d_e \leq 1$; Dist2 : $d_e \in [1, 2]$, Dist3 : $d_e \in [2, 3]$ and Dist4 : $d_e \geq 3$. For each patient, stimulation parameters are all the same as their empirical cases, except for the stimulation locations. As stimulation location was selected incrementally further away from the empirical location, the similarity between the simulated and empirical seizure dynamics deteriorated, as observed across our four metrics (see also supplementary Figure 5.11). Both structural connectome and EZ network configurations determined the stimulated seizure patterns.

For varying stimulation amplitude, we could evaluate the capacity of our model in generating seizure dynamics for a particular stimulation amplitude (5.5C). For each patient, first, we adjusted the model parameters to induce seizures by stimulation using the same stimulation amplitude as the empirical case. Then, we varied stimulation amplitude using common amplitudes used clinically (two lower and two higher amplitudes than the empirical one) to simulate the signals and evaluate the post-stimulus response by comparing it with the empirical stimulated seizure. Lower stimulation amplitudes did not induce a seizure, which translated to low simila-

rity values across metrics. Higher stimulation amplitudes induced synthetic seizures which were similar to the empirical amplitudes, but longer lasting (see supplementary Figure 5.10).

In summary, on average of seven patients, the virtual epileptic cohort is capable of capturing spatio-temporal features of stimulated seizure data based on its personalized EZ hypothesis, stimulation location and stimulation amplitude.

5.2.5 Interictal spikes

Simulation of interictal spikes

In our virtual epileptic cohort, we simulated brain activity and SEEG recordings during the interictal period for all 30 patients. We simulated interictal time series based on the EZ hypothesis, such that the EZ network could generate interictal spiking. We illustrated simulated SEEG and empirical SEEG for patient 8, shown in Figure 5.6A. The detailed shapes of interracial spikes in both simulated and empirical SEEG are illustrated as well. We also mapped interictal spike counts across all implanted SEEG electrodes in 3D space (Figure 5.6B).

Comparing empirical and simulated interictal spikes

To evaluate the simulated interictal spikes, we measured interictal spike count for each SEEG electrode, which is the fraction of spikes in each electrode compared to all detected spikes. Spikes are detected after bandpass filtering the signal and detecting peaks above calculated thresholds as described by [100]. Next, we compared the empirical and simulated spike counts across all patients of the virtual epileptic cohort and calculated the correlation of their spike counts in the left box of Figure 5.6C. In addition, we generated a randomized cohort for 15 patients by using the same brain models but randomly selecting an EZ network from other patients in the cohort. We also calculated spike count correlation with the empirical data in the randomized cohort. Our second approach using the clinical hypothesis was also evaluated in supplementary Figure 5.13C. Permutation testing showed a significant difference between the two groups (H_0 : mean(VEC) $\leq$ mean(RC) ; p-value < 0.001).

5.3 Discussion and conclusions

We provided a cohort of 30 virtualized drug-resistant epilepsy patients for hypothesis testing and validation. For each patient, we used one virtual brain model to generate synthetic spontaneous seizures, stimulation-induced seizures and interictal activity with spikes. Here, we present for the first time synthetic seizures induced by stimulation. In addition, we systematically evaluated our synthetic SEEG time series by comparing them against their corresponding empirical SEEG recordings. The synthetic SEEG data are simulated using personalized brain models, based on patient-specific brain connectivity, alongside reconstructed brain sources and SEEG sensors [98]. We used the Epileptor model, which captures spatio-temporal seizure dynamics and interictal spikes. We showed that the synthetic data respect the structure and

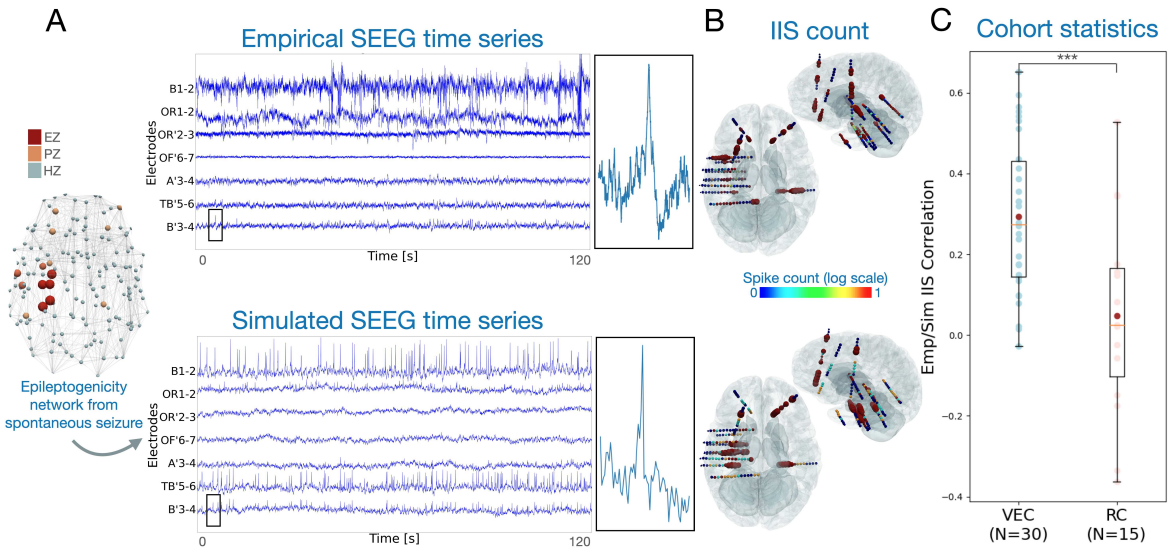

FIGURE 5.6 – A) Interictal activity of one patient shown by SEEG signals in empirical and simulated cases, with interictal spikes in multiple electrodes. One interictal spike is shown by zooming in on channel B'3-4 for both the simulated and empirical cases. B) Interictal spike (IIS) count across all implanted SEEG electrodes are displayed in axial and sagittal view for the simulated and empirical SEEG time series. Spike count values are normalized and displayed in logarithmic scale. C) Boxplots for correlation of simulated and empirical IIS count. Correlation values are plotted for all virtual epileptic cohort patients (VEC, N=30, in blue) and randomized cohort (RC, N=15, in red). Middle box represents the interquartile range (IQR), with a line at the median. The whiskers extend from the box to the data point lying within 1.5x the IQR. Points past the whiskers are marked as fliers. $^{***}p - value < 0.001$; permutation test.

features of the empirical dataset. In particular, we demonstrated that the parameters used to simulate synthetic SEEG data are important in capturing spatio-temporal features of epileptic activity, such as seizure propagation, stimulation outcome and interictal spike count. These parameters serve as ground truth for evaluating data analysis methods in clinical epilepsy research.

The precise mechanisms contributing to seizure emergence are still not fully understood. Studies have shown that the transition to seizure is a slow process, characterized by a progressive loss of neural network resilience [22, 103], a build-up of low-amplitude high-frequency activity and a progressively increasing sensitivity of the network to electric stimulation [68]. In addition, seizure generation has been linked to specific changes in ion dynamics such as extracellular potassium [39], intracellular chloride [78] and extracellular calcium [144], although ion dynamics are highly intertwined [101]. We hypothesized that repetitive stimulation leads to a slow accumulation of ion imbalances which can trigger a seizure. We implemented this behaviour using the Epileptor model and making m time-varying, which influences the oscillatory dynamics of the seizure state [33, 67]. When stimulation is applied, m slowly increases and when reaching a defined seizure threshold, it pushes the system to the seizure state (see supplementary Figure 5.9). In our approach, we tuned the seizure threshold parameter based on the EZ hypothesis and the empirical stimulation parameters. Therefore, when modifying only stimulation amplitude the response depends on the accumulation variable crossing the seizure threshold. Lower stimulation amplitudes failed to cross the defined seizure threshold, whereas empirical and higher stimulation amplitudes cross this threshold (see supplementary Figure 5.10). In future studies, this approach can be extended and be more precise for each patient when more empirical stimulation data are integrated for model inversion.

To ensure the quality and usefulness of the synthetic data, we implemented a set of comparative metrics, although to the best of our knowledge there is no standard method for validating synthetic data. We focused on specific data features of the real SEEG signal such as the envelope function, seizure onset and offset times and interictal spikes. Although these features are important for understanding epileptic brain activity, they could not account for all the complexity of recorded brain activity. We focused on simple spatio-temporal network features because, although the Epileptor captures common properties of brain activity during seizures [67], it does not account for all seizure dynamotypes [107]. This was shown by our metrics, where empirical data features were captured by the synthetic data, albeit only to a certain extent. However, the same metrics were applied to a randomized cohort and demonstrated that non-informative parameters fail to capture the same empirical data features. In addition, our simulations were not biased by surgical outcome (supplementary Figure 5.16).

Furthermore, for stimulated seizures, we systematically varied stimulation location and amplitude and compared the outcome against the empirical data. In the clinical setting, these parameters exhibit the greatest variation. Other parameters such as stimulation frequency are typically chosen as either 1 Hz or 50 Hz, while a standard range is adhered to for pulse width (0.5-3 ms) and stimulation duration (20-60 sec for 1 Hz stimulation ; 3-8 s for 50 Hz stimulation) [59]. However, the seizure propagation metric (SP) did not perform as well for stimulated seizures com-

pared to spontaneous seizures, highlighting a limitation of our study. Additionally, we compared spike count correlations between simulated and empirical interictal data. Despite using the same EZ parametrization, the average correlation was lower than that of seizure dynamics. This discrepancy may be explained by studies indicating that propagation zones can generate independent interictal spikes, suggesting the epileptogenic and irritative zone overlap but are not identical [12, 17]. The main contribution of these simulated interictal data is their ground truth information that can be used to evaluate data analysis methods for interictal spikes (e.g. source localization).

We simulated spatio-temporal seizure dynamics on 162 brain regions defined in VEP atlas[140]. This low spatial resolution constrains the complexity of simulated propagation patterns, as compared to empirical SEEG data. Each brain source represents on average $\sim 16\,cm^2$ of the cortical surface. Conversely, neural field models use finer spatial scales ($\sim 1\,mm^2$ of the cortical surface) and consider short-range cortical connections in addition to long-range white matter connectivity. In addition, dipole orientations of brain sources are not taken into account by the forward solution used to compute the SEEG time series. The current dipole is mainly attributable to pyramidal cells in the cortical gray matter and is aligned perpendicular to the brain surface [**buzsaki-eeg**]. Neural field models provide more realistic source to sensor mapping by considering both orientation and distance between the dipole sources and the sensors [64, 97]. However, unlike neural field models, neural mass models are typically more efficient in terms of computational resources, simulation duration and parameter exploration. They remain reliable in capturing various features of brain activity, including seizure dynamics [67, 97].

The current dataset can be enriched by other data imaging modalities, such as EEG, MEG and fMRI, directly through the forward solution on the provided brain source signals in this cohort. Additional data modalities can also be integrated to better inform the virtual brain twins and improve the personalized synthetic data, such as PET/SPECT [75], sodium MRI [6], MEG [95] and high-resolution EEG [74]. The models that account for a vast combination of clinical seizure patterns [107], or other biophysically grounded models [3, 9] that link parameters closer to underlying biological mechanisms, can also be utilized. Replacing neural mass models by neural field models which account for cortical geometry and short-range connectivity is an additional future goal. This would allow for the integration of high-resolution brain imaging data (e.g. ultra-high field MRI [$\geq 7T$]) which can improve model creation and patient specificity [63]. Overall, these informative features and modeling approaches can be integrated in the virtual epileptic cohort to provide a richer repertoire of simulated seizure dynamics.

5.4 Materials and methods

5.4.1 Study design

This study consisted of using a cohort of 30 patients with drug-resistant epilepsy alongside a methodology of personalized virtual brain modeling to build a synthetic copy of the dataset, called the virtual epileptic cohort. The objective of this study

was to provide researchers and other potential users a virtual dataset with ground truth for testing and validation of their methods. We provided this dataset alongside comparative metrics between the synthetic and empirical data to gauge the capacity of the virtual cohort in capturing relevant data features.

We used noninvasive T1-MRI and DW-MRI to reconstruct patient-specific whole-brain network models. The Epileptor [67] model was used to simulate brain activity for each network node. The Epileptor was extended to account for stimulated seizures, alongside its existing dynamical regimes for interictal and spontaneous ictal dynamics. The model's excitability parameter was defined using the EZ hypothesis, which was estimated using the VEP pipeline [142]. A second EZ hypothesis was defined from a team of clinical experts (JM and FB). For each empirical SEEG recording, a synthetic copy was simulated and was either interictal activity (N=30), spontaneous seizure (N=54) or stimulated seizure (N=16). Simulations were performed on the whole-brain level and were mapped onto reconstructed SEEG electrodes using a source-to-sensor gain matrix. Electrode locations were obtained from cranial CT-scan after electrode implantation. The synthetic SEEG time series were compared against empirical SEEG recordings using 16 metrics comparing spatio-temporal seizure network dynamics and interictal spike organization. We selected four metrics to describe the main data features that were captured, but provided all of them in the supplementary material. To assess to what extent a personalized EZ hypothesis captured features of the empirical recordings, we constructed a surrogate cohort of 15 patients using random EZ hypothesis. The randomized cohort was also compared against the empirical recordings. Then, the virtual epileptic cohort and the randomized cohort metrics were compared and a permutation test was applied for significance testing. Finally, stimulation location and amplitude were systematically varied in-silico and compared against empirical stimulated seizures.

5.4.2 Patient data

Empirical patient data

A total of 30 retrospective patients with drug-resistant epilepsy underwent a standard presurgical protocol at La Timone hospital in Marseille, France. Informed written consent was obtained for all patients in compliance with ethical requirements of the Declaration of Helsinki. The study protocol was approved by the local Ethics Committee. All patients underwent comprehensive presurgical assessment, including medical history, neurological examination, neuropsychological assessment, fluorodeoxyglucose-PET, high-resolution 3T-MRI, long-term scalp-EEG, and invasive SEEG recordings. All patients had invasive SEEG recordings obtained by implanting multiple depth electrodes, each containing 10-18 contacts (2mm long) separated by 1.5- or 5-mm contact spacing. The SEEG recordings were performed as part of routine clinical management, in line with French national guidelines [59]. Recordings were stored separately for each seizure, with seizure onset and offset times marked by expert epileptologists. For stimulation-induced seizures, stimulation parameters (channels, frequency, amplitude, pulse width and duration) were additionally provided. SEEG recordings during rest were stored separately. Following electrode implantation, a cranial CT-scan was performed to obtain locations of electrodes in

the brain.

Virtual Epileptic Cohort data

The virtual epileptic cohort of 30 patients is provided in a BIDS-iEEG compatible format [56]. Following this format, each patient's synthetic data are saved into two categories : simulated data and derived data. The simulated data contains simulated SEEG time series. The derived data contains structural information extracted from brain imaging scans (T1-MRI, DW-MRI and CT-scan) and underlying model parameters used to generate the simulated data.

For each patient, synthetic SEEG time series are provided in BrainVision format (**ieeg** folder in supplementary Figure 5.7). These synthetic time series are grouped into three different folders for each type (*ses-01* : simulated seizure, *ses-02* : stimulated seizure, *ses-03* : stimulated interictal spikes). Each synthetic SEEG file contains the EZ hypothesis type used in its filename (*VEPhypothesis* or *Clinical-Hypothesis*). Also, if multiple synthetic SEEG files are provided, they each have a unique run number (starting from run-01). For all synthetic SEEG files, electrode names and coordinates are provided as *tsv* files. For every patient, the number of simulated brain activities for each condition are summarized in Table 5.1.

In addition, we provided structural information (**struct** folder in supplementary Figure 5.7), notably their connectome and gain matrix. The connectome comes in the form of a zip file (TVB-compatible data format) and contains information about connectivity weights (MxM matrix, M=162 brain regions), connectivity centers, center orientations, connectivity areas and volumes, tract lengths and cortical/non-cortical region flags (for more information, see [131]). The gain matrix is saved as a *tsv* file, this MxN matrix contains M regions and N sensors and maps the simulated brain activity from the brain region level to the SEEG sensors, thus obtaining synthetic SEEG time series.

Finally, corresponding model and simulator parameters are provided for each synthetic SEEG file (**parameters** folder in supplementary Figure 5.7). Stimulation parameters are also provided for stimulation-induced synthetic seizures. The synthetic time series on the brain source level are also provided for each synthetic SEEG file. A VEP atlas [140] is provided as a tsv file for mapping source labels to brain region names.

5.4.3 Data processing

The data processing method used here has been described in [142]. Here, we briefly explain the method used. To construct the virtual epileptic patients, we first preprocessed the T1-MRI and DW-MRI data. Volumetric segmentation and cortical surface reconstruction were obtained from the patient-specific T1-MRI data using the recon-all pipeline of the FreeSurfer software package. The cortical surface was parcellated according to the VEP atlas (code available at `https://github.com/HuifangWang/VEP_atlas_shared.git`). We used the MRtrix software package to process the DW-MRI, employing an iterative algorithm to estimate the response functions and subsequently used constrained spherical deconvolution to de-

rive the fiber orientation distribution functions. The iFOD2 algorithm was used to sample 15 million tracts. The structural connectome was constructed by assigning and counting the streamlines to and from each VEP brain region. This results in a 162x162 connectivity matrix which is symmetric (there is no directionality information available in the white matter fibers). The diagonal entries of the connectome matrix were set to 0 to exclude self-connections within areas and the matrix was normalized so that the maximum value was equal to one. We obtained the location of the SEEG contacts from post-implantation CT scans using GARDEL as part of the EpiTools software package [138]. Then we coregistered the contact positions from the CT scan space to the T1-MRI scan space of each patient.

5.4.4 Neural mass models

A neural mass model describes the activity of a population of neurons, thus it can describe the local activity of a brain region. It is defined by a set of differential equations that govern their dynamics. Just like brain regions are connected through long range white fibers, neural masses are linked through the structural connectome to form a whole brain network. The global equation for such a model can be given by

$$\dot{\psi}_i(t) = F(\psi_i(t)) + K \sum_{j=1}^{L} W(i,j) S(\psi_i(t), \psi_j(t)) \tag{5.1}$$

where $\psi_i(t)$ is a state vector of neural activity at brain region i and time t. $\dot{\psi}$ is the temporal derivative of the state vector. F is a function of the state and captures the local neural activity. In our case, F reflects the Epileptor model, described above. W is a matrix of heterogeneous connection strengths between node i and j. S is a coupling function of the local state ψ_i and the distant delayed state ψ_j. That a node receives input through the network is given by the sum across the number of nodes L and scaled by a constant K. In this paper, this set of differential equations is solved using an Euler integration scheme with a step size of 0.5 ms.

Forward solution with neural mass models

Mapping the neural activity from the sources (VEP brain regions) to the sensors (SEEG contacts) is done by solving the forward problem and estimating a source-to-sensor matrix (gain matrix). As sources for our model, we used the vertices of the pial surface and volume bounding surfaces for the cortical and subcortical regions respectively. Surfaces are represented as triangular meshes. We estimate that the matrix $g_{j,k}$ from source brain region j to sensor k is equal to the sum of the inverse of the squared Euclidean distance $d_{i,k}$ from vertex i to sensor k weighted by the area a_i of the vertex on the surface.

$$g_{j,k} = \sum_{i=0}^{N_j} \frac{a_i}{d_{i,k}^2} \tag{5.2}$$

Here vertex i belongs to region j which has N_j vertices in total. The area a_i of vertex i is obtained by summing up one-third of the area of all the neighboring

triangles. Vertices belonging to the same brain region are summed to obtain the gain for a single region of our brain network model. The resulting gain matrix has dimensions MxN, with M being the number of regions and N the number of sensors. Matrix multiplication of the simulated source activity with the gain matrix yields the simulated SEEG signals.

5.4.5 The Epileptor model

We used whole brain network models to generate synthetic SEEG time series. Within a brain network model, each brain region is represented as a node and the connections between regions are represented as edges. The brain regions are obtained by the FreeSurfer parcellation using the VEP atlas. The connection strength between regions is inferred from the structural connectome derived from DW-MRI data. The brain activity of each brain region is represented by a neural mass model, here we used the phenomenological 6D Epileptor model. There are 6 coupled differential equations in this model, which model 3 neural populations acting on a fast, intermediate and slow time scale.

$$
\begin{aligned}
\dot{x}_1 &= y_1 - f_1(x_1, x_2) - z + I_{ext1} \\
\dot{y}_1 &= c - dx_1^2 - y_1 \\
\dot{x}_2 &= -y_2 + x_2 - x_2^3 + I_{ext2} + 0.002g - 0.3(z - 3.5) \\
\dot{y}_2 &= \frac{1}{\tau}(-y_2 + f_2(x_2)) \\
\dot{z} &= r(4(x_1 - x_0) - z + f_3(z) + K \sum_{j=1}^{N} C_{i,j}(x_1^j - x_1^i)) \\
\dot{g} &= -0.01(g - 0.1x_1)
\end{aligned}
\tag{5.3}
$$

where

$$
f_1(x_1, x_2) = \begin{cases} ax_1^3 - bx_1^2 & \text{if } x_1 < 0 \\ -(m - x_2 + 0.6(z-4)^2)x_1 & \text{if } x_1 \geq 0 \end{cases}
$$

$$
f_2(x_2) = \begin{cases} 0 & \text{if } x_2 < -0.25 \\ a_2(x_2 + 0.25) & \text{if } x_2 \geq -0.25 \end{cases}
$$

$$
f_3(z) = \begin{cases} -0.1z^7 & \text{if } z < 0 \\ 0 & \text{if } z \geq 0 \end{cases}
$$

The state variables x_1 and y_1 describe the activity of the neural population acting on a fast time scale to model fast discharges during epileptic seizures. The state variables x_2 and y_2 describe the activity of the neural population acting on an intermediate time scale to to model spike and wave phenomena during seizures. The state variable z acts on a slow time scale and drives the system autonomously in and out of the ictal state. In addition, the state variable g acts as a low-pass filter of the coupling from x_1 to x_2 and generates the preictal and ictal spikes.

The excitability parameter x_0 represents the degree of epileptogenicity and determines whether the system converges towards an ictal or healthy state. If $x_0 > x_0c$,

where x_0c is the critical value of epileptogenicity, the Epileptor shows seizure activity autonomously and is referred to as epileptogenic ; otherwise the Epileptor is in its (healthy) equilibrium state and does not trigger seizures autonomously. The default parameters are $r = 0.00035$, $\tau = 10$, $I_{ext1} = 3.1$, $I_{ext2} = 0.45$, $a = 1$, $a_2 = 6$, $b = 3$, $c = 1$, $d = 5$ and $m = 0$.

In addition, the Epileptor model is coupled to N other Epileptors via a linar approximation of permittivity coupling $K \sum_{j=1}^{N} C_{i,j}(x_1^j - x_1^i)$. In this coupling term, K scales the global connectivity and can be varied between simulations to investigate different scenarios. The patient's connectome is represented by $C_{i,j}$ which defines region-to-region connection weights.

5.4.6 The Epileptor-stimulation model

To model stimulated seizures, we needed to determine the relationship between stimulus and brain activity. During stimulated seizures, we observed a slow increase in oscillatory response, followed by a sudden switch to the seizure state, likely due to ion imbalances (e.g., extracellular potassium) reaching a critical threshold. To model this, We used the phenomenological Epileptor model. We transformed the parameter m into a variable that accumulates stimulus effects slowly which influences the excitability of the model. When reaching a critical seizure threshold value m_{thresh}, it can push the system from its normal state to the seizure state via the permittivity variable z, which guides the system in and out of seizures (see supplementary 5.9). The extended Epileptor-stimulation model is as follows :

$$
\begin{aligned}
\dot{x}_1 &= y_1 - f_1(x_1, x_2) - z + I_{ext1} + nI_{stim} \\
\dot{y}_1 &= c - dx_1^2 - y_1 \\
\dot{x}_2 &= -y_2 + x_2 - x_2^3 + I_{ext2} + 0.002g - 0.3(z - 3.5) \\
\dot{y}_2 &= \frac{1}{\tau}(-y_2 + f_2(x_2)) \\
\dot{z} &= r(4(x_1 - x_0 - H(m - m_{thresh})) - z + f_3(z) + K \sum_{j=1}^{N} C_{i,j}(x_1^j - x_1^i)) \\
\dot{g} &= -0.01(g - 0.1x_1) \\
\dot{m} &= r_2(k|I_{stim}| - 0.3m)
\end{aligned}
$$

where

$$
f_1(x_1, x_2) = \begin{cases} ax_1^3 - bx_1^2 & \text{if } x_1 < 0 \\ -(m - x_2 + 0.6(z-4)^2)x_1 & \text{if } x_1 \geq 0 \end{cases}
$$

$$
f_2(x_2) = \begin{cases} 0 & \text{if } x_2 < -0.25 \\ a_2(x_2 + 0.25) & \text{if } x_2 \geq -0.25 \end{cases}
$$

$$
f_3(z) = \begin{cases} -0.1z^7 & \text{if } z < 0 \\ 0 & \text{if } z \geq 0 \end{cases}
$$

(5.4)

All default parameters are the same as in the original Epileptor model, except for the additional parameters : $m_{thresh} = 1.5$, $k = 20$, $r = 0.00035$, $r_2 = 0.006$, $n = 3$, $x_0 = -2.2$.

The Epileptor-stimulation model is coupled to N other Epileptors-stimulation using the same permittivity coupling described in the previous section. I_{stim} is a time varying input describing the perturbation signal at each time step, and matches the clinically applied stimulus waveform. Spatially, it is weighted by a scalar corresponding to the estimated electric field magnitude for each brain region (for more detail, see the subsection below). H is the Heaviside function, m_{thresh} is the threshold for m which when crossed changes the state of the system by pushing it in the upstate.

5.4.7 Calculation of the electric field of SEEG stimulation

The French guidelines on SEEG stimulation state that bipolar and biphasic current should be used between two contiguous contacts to target a region of interest [59]. In this setting, one contact acts as a cathode (negative electric potential, sink of current) and the other one as an anode (positive electric potential, source of current). Current flows from the anode to the cathode, hyperpolarizing the neural elements nearest the anode and depolarizing the neural elements nearest the anode. This generates a local electric field in the area where the electrodes are located. A bipolar configuration is preferred for SEEG stimulation because it may be less likely to elicit side effects thanks to the current being more focused than a monopolar configuration and less likely to spread into adjacent structures [72, 73]. A symmetrical biphasic pulse waveform is used to reduce tissue damage by producing a zero net-charge. The parameters used clinically are restricted to frequencies of either 1 Hz or 50 Hz, weak amplitudes ranging from 0.5 to 5 mA, and pulse widths of 500 - 3000 microseconds and duration of 0.5-40 seconds (short duration for 50 Hz stimulation and longer duration for 1 Hz stimulation).

We modeled the stimulus that was clinically applied by generating a bipolar signal following the stimulation parameters. The electric field generated by the stimulus was estimated by approximating the electrode contacts as point sources (q_+ and q_-), which is sufficiently accurate for our neural mass modeling approach [3]. We then mapped the stimulus signal onto the parcellated brain areas based on the distance, resulting in an estimated electric field at the whole-brain level. We used the estimated field magnitude $|\vec{E}(\vec{r})|$ as an input to the I_{stim} parameter of the Epileptor-stimulation model (5.4). The field magnitude at a brain location $\vec{r}$ is computed as :

$$|\vec{E}(\vec{r})| = |kq(\frac{\vec{r} - \vec{r_{q+}}}{|\vec{r} - \vec{r_{q+}}|^3} - \frac{\vec{r} - \vec{r_{q-}}}{|\vec{r} - \vec{r_{q-}}|^3})| \tag{5.5}$$

5.4.8 Spontaneous seizures

To simulate brain dynamics for each patient, we used their virtual brain model and the extended Epileptor model, parametrized by the patient's EZ hypothesis. The EZ hypothesis was based on the VEP pipeline as a first approach and on the clinical hypothesis as a second approach.

To obtain spontaneous seizures, two main parameters were adjusted in the Epileptor model : x_0 and K. Firstly, the x_0 parameter determines regional excitability. To simulate spontaneous seizures, the epileptogenicity heatmap obtained from the EZ hypothesis was translated into x_0 parameter values. For this, normalized epileptogenicity values were linearly transformed into an x_0 range of $[-2.2, -1.2]$, such that seizures occurred autonomously. For x_0 values below -2.062 the model settles into a fixed point in the down-state which corresponds to an interictal state. For $-2.062 < x_0 < -1.025$ the model generates a stable oscillation in the up-state which corresponds to a seizure-like event (SLE). For x_0 values above -1.025 the model settles into a stable fixed point in the up-state. The brain regions that are epileptogenic have x_0 values corresponding to the SLE state and brain regions that are non-epileptogenic have values corresponding to the interictal state.

Secondly, the global coupling parameter (noted as K) is a key parameter which influences the resulting seizure dynamics. This parameter adjusts the coupling strength between nodes, which are connected to each other via a fast-to-slow coupling, also known as permittivity coupling [97]. This parameter is adjusted according to the empirical SEEG recordings. Both x_0 and K determine the simulated spatiotemporal seizure dynamics. For instance, seizures can propagate to non-epileptogenic areas if they're connected to epileptogenic areas. It can also happen than seizures do not propagate to an epileptogenic area in particular cases when that area is connected to multiple healthy regions, which act as seizure inhibitors.

5.4.9 Stimulated seizures

To generate stimulated seizures, we adjusted the parameters x_0, m_{thresh} and I_{stim}. The parameter K value was the same as in the spontaneous seizure. We used the same epileptogenicity heat map from the EZ hypothesis of the spontaneous seizures. To trigger seizures by external stimulation rather then them occuring spontaneously, we set the excitability x_0 values to a sub-critical threshold for seizing, linearly mapping them to an x_0 range of $[-2.2, -2.07]$. The seizure threshold m_{thresh} parameter was also set from the EZ hypothesis, by linearly mapping them to a $[0.5, 10]$ range. Epileptogenic brain regions have lower seizure thresholds than healthy brain regions.

Bipolar current stimulation via SEEG electrodes is applied in order to trigger seizures for epileptogenic zone diagnosis. For this, clinicians stimulate across multiple electrode pairs and across stimulation parameters. This is not done systematically, it rather follows the clinician's hypothesis of the epileptogenic zone and their experience with stimulation parameters. We have selected the clinical stimulation parameters which induced a seizure in the patient. We used the same stimulation electrodes and stimulation parameters in our model. The generated effects of the stimulus are mapped onto the brain regions using the sensor-to-source forward solution. This resulted in an estimated electric field magnitude, represented as scalar weights across brain regions, with the strongest weights located near the stimulating electrode pair. The I_{stim} parameter was defined for each brain region depending on the stimulus weights. It then varied in time following the stimulus bipolar waveform. The variable m is related to regional excitability and it depends on this parameter. When I_{stim} is non-zero, m slowly increases, otherwise it slowly returns to baseline. When $m >$

m_{thresh}, the system is pushed to the seizure state. Then, the structural connectivity influences the spatio-temporal triggered seizure dynamics.

Varying stimulation location

We wanted to interrogate the robustness of our model by systematically changing stimulation location and comparing the outcome to the empirical stimulation-induced seizure. For this we followed the following steps for each of seven patients which had stimulation-induced seizures in the clinic.

We used the same brain models for each patient that were used for the virtual epileptic cohort. We reproduced the same parameters using the VEP hypothesis, taken from the cohort's **derivatives** database, with the only free parameter being stimulation location. To define this parameter, we grouped all SEEG contacts into four categories using the empirical stimulation location as a reference point. If we define d_e as the distance in cm from the empirical stimulation location, Dist1 : $d_e \leq 1$; Dist2 : $d_e \in [1, 2]$; Dist3 : $d_e \in [2, 3]$; and Dist4 : $d_e \geq 3$. Next, we randomly stimulated up to 10 pairs of electrodes within the four main distance groups located outside of the empirical location. This resulted in up to 40 simulations containing the modelled stimulation input and whole-brain response (induced seizure or no seizure).

The comparative metrics between the synthetic SEEG stimulation responses and the empirical SEEG stimulation-induced seizure were performed (Figure 5.5). In total, 243 simulations were generated and compared against the empirical SEEG recordings.

Varying stimulation amplitude

We wanted to interrogate the robustness of our model by systematically changing stimulation amplitude and comparing the outcome to the empirical stimulation-induced seizure. For this we followed the following steps for each of seven patients which had stimulation-induced seizures in the clinic.

We used the same brain models for each patient that were used for the virtual epileptic cohort. We reproduced the same parameters using the VEP hypothesis, taken from the cohort's **derivatives** database, with the only free parameter being stimulation amplitude. In the empirical stimulation parameters, all patients had a stimulation amplitude between 1.8 mA and 2.2 mA (mean=2 mA, std=0.12). We varied this parameter at the following amplitudes : 0.5 mA, 1 mA, 3 mA and 4 mA. We ran simulations for each stimulation amplitude, resulting in four simulations per patient containing the modelled stimulation input and whole brain response (induced seizure or no seizure).

The comparative metrics between the synthetic SEEG stimulation responses and the empirical SEEG stimulation-induced seizure were performed (Figure 5.5). In total, 28 simulations were generated and compared against the empirical SEEG recordings.

5.4.10 Interictal spikes

We generated interictal activity for each patient, containing normal activity with interictal spiking in certain locations. We adjusted the parameters I_{ext} and x_0. We used the same global coupling parameter K of the spontaneous seizures.

We set $I_{ext} = 6.0$ and mapped the epileptogenicity values to an x_0 range of $[-3, -2.8]$, with additive stochastic noise for irregular spiking. This allowed for interictal spikes to be obtained by the model, but it is not the only method [33]. The combination of x_0 values close to the seizure threshold alongside the structural connectivity scaled by K yields the interictal zone network for each patient. This results in interictal spike time series which are personalised to each patient.

The present literature relates the epileptogenic zone network to the interictal spike network [17]. Thus, we used the epileptogenicity heat map obtained from both the VEP hypothesis and the clinical hypothesis to set the EZN close to the critical threshold for seizure-like events.

Interictal spike detection

A spike is defined as a transient distinguished from background activity, with pointed peak and duration between 20-70 ms and varying amplitude typically $> 50\,\mu V$ [70]. A bandpass butterworth noncasual filter was applied on the data (lowcut 1 Hz, highcut 70 Hz). To detect a spike, we looked for the peaks of the signal which crossed a defined threshold. The threshold was defined following the spike detection method in [100]. If we define $|x|$ as the bandpass-filtered signal, then the threshold is equal to 4σ, where $\sigma = median\left\{\frac{|x|}{0.6745}\right\}$. In this case, σ is an estimate of the standard deviation of the background noise. The standard deviation of the signal could lead to very high threshold values, especially in cases with high firing rates and large spike amplitudes. By using the estimation based on the median, the interference of the spikes is diminished (see a demo in [100]). In the empirical spike case, we only took spikes that had an amplitude above $25\,\mu V$. In addition, if two or more peaks were detected within 250 ms (or 256 timesteps in our algorithm) they were counted as a single spike, to ensure that poly-spikes are not counted as multiple spikes.

Estimation of interictal spike count

To evaluate the synthetic interictal time series, we compared their interictal spike count (IIS) against the empirical recording. We used 15 minutes of SEEG interictal activity and 10000 timesteps of synthetic SEEG interictal time series, with a step size 0.05.

If the total number of spikes for a channel i is S_i and there are N channels, then the IIS for that channel was computed as follows,

$$IIS_i = \frac{S_i}{\sum_{i=1}^{N} S_i} \tag{5.6}$$

As a result, we obtained two vectors of length N, containing the interictal spike count for the synthetic and the empirical SEEG time series. We compared these two vectors using the Pearson correlation coefficient.

5.4.11 Randomized cohort

We generated three randomized cohorts for each simulation type : spontaneous seizures, stimulation induced seizures and interictal spikes. Each randomized cohort contained in total 15 synthetic SEEG time series for each EZ hypothesis (VEP hypothesis or Clinical hypothesis). The following approach was applied to generate one randomized cohort.

First, for each patient, the same parameters used to run the virtual epileptic cohort simulations were reused with the exception of the parameter x_0. For this parameter, instead of using the patient's own EZ hypothesis, we select it randomly from another virtual epileptic cohort patient of the cohort. This operation was performed 3 times for each patient. Thus, 3 synthetic simulations are obtained for each patient using a random EZ hypothesis.

Next, we compared the synthetic SEEG seizure from the randomized cohort with the empirical SEEG recording of that patient. If the patient has multiple SEEG recordings for the same type, we select one and we compare all 3 simulations to this SEEG simulation. We do this because seizure features and interictal features within the same patient tend to be more similar than those between patients.

We followed this procedure for 5 patients of our cohort, resulting in 15 simulated seizures for each EZ hypothesis. We used the randomized cohort simulations to compute similarity metrics between the empirical and simulated data. We then compared the same metrics between the virtual epileptic cohort and the randomized cohort. The virtual epileptic cohort cohort showed a significantly higher resemblance with the empirical seizure features as compared to the randomized cohort. This shows that patient-specific EZ hypothesis plays an important role for simulating spatio-temporal seizure dynamics.

5.4.12 Comparing simulated and empirical SEEG traces

To compare the simulated SEEG time series to the empirical SEEG recording we first captured spatio-temporal features in both data. First, we computed an envelope function for each SEEG electrode as explained in [142] (see also supplementary Figure 5.12). We used this envelope to mark each electrode as either seizure (containing seizure activity) or non-seizure (not containing any seizure activity) electrode. If the envelope's peak amplitude crossed a determined threshold, the SEEG electrodes were marked as seizure electrodes, otherwise they were marked as non-seizure electrodes. The threshold was the same for all electrodes and it was manually determined to be higher than the envelope's baseline amplitude . We compared the overlap of seizure and non-seizure electrodes between the simulated and empirical SEEG. In the electrodes where seizure activity was marked, we used the timepoints when the envelope jumped from its baseline and returned back to baseline to mark seizure onset and offset, respectively. Using this information, we binarized all SEEG traces in time : 0 for no seizure, 1 for seizure (5.3B). We then compared the binarized simulated and empirical SEEG using 2D pearson correlation.

Next, we divided SEEG electrodes marked as seizure electrodes into two groups : seizure onset (SO) and seizure propagation (SP) electrodes (5.3C). A seizure electrode was marked as SO when its onset time was belonged to the first few seconds

of the total seizure length (corresponding to the first 5-15% of the total seizure duration), otherwise it was marked as SP. Then, the Jaccard similarity coefficient was employed to compare synthetic and empirical SO groups, and synthetic and empirical SP groups.

We computed these measurements for each pair of simulated SEEG and it's corresponding empirical SEEG, for both the spontaneous and stimulation-induced seizures. We repeated the same measurements for both the Virtual Epileptic Cohort (VEC) and the Randomized Cohort (RC). All measurements were plotted together and a boxplot was overlayed to compare the VEC against the RC (5.3D and 5.5A). The boxplot is constructed as follows. Middle box represents the interquartile range (IQR), with a line at the median. The whiskers extend from the box to the data point lying within 1.5x the IQR. Points past the whiskers are marked as fliers.

We compared how significantly higher the mean for each metric of VEC was to the mean for each corresponding metric of RC using permutation testing [88] (H_0 : mean(VEC) $\leq$ mean(RC), H_1 : mean(VEC) $>$ mean(RC)). For all measurements, p<0.001 therefore it is very unlikely that VEC performs better than RC by chance.

The complete set of all measurements that were performed can be found in the supplementary 5.14.

Computing the 2D pearson correlation

We compare the two binarized images using Pearson correlation and overlap.

$$r = \frac{\sum (x_i - \bar{x})(y_i - \bar{y})}{\sqrt{\sum (x_i - \bar{x})^2 \sum (y_i - \bar{y})^2}} \tag{5.7}$$

Where x_i is the binary value of a pixel in the empirical case, y_i is the binary value of a pixel in the simulated case. Note : r $\in [-1, 1]$.

Binary overlap

$$Binary_{overlap} = \frac{|E_{bin} \cap S_{bin}|}{|E_{bin}|} \tag{5.8}$$

The ratio between the amount of identical timepoints divided by the entire amount of timepoints.

Jaccard similarity coefficient

We compare the seizure onset (SO) and seizure propagation (SP) groups using Jaccard similarity coefficient.

$$SO_{Jaccard} = \frac{|E_{SO} \cap S_{SO}|}{|E_{SO} \cup E_{SO}|} \quad SP_{Jaccard} = \frac{|E_{SP} \cap S_{SP}|}{|E_{SP} \cup E_{SP}|} \tag{5.9}$$

where E_{SO}, E_{SP} are the empirical seizure onset and seizure propagation channels, respectively. S_{SO}, S_{SP} are the simulated seizure onset and seizure propagation channels, respectively.

Signal power

For each SEEG bipolar sensor, the signal power is computed for both the empirical and the synthetic time series and plotted in 3D (e.g. 5.2, right panel).

$$P = \frac{1}{N} \sum_{t=0}^{N} s_t^2 \tag{5.10}$$

where s_t represents the electrode's signal amplitude at timepoint t, N is the total number of time points, P is the signal power for one electrode. The signal power across all electrodes is then normalized between 0 and 1.

5.4.13 Permutation test

We performed a permutation test [88] for each metric ($H_0 : mean(VEC) \leq mean(RC)$, $H_1 : mean(VEC) > mean(RC)$). This test showed the likeliness of the average metric values of the VEC cohort being higher than the RC cohort being attributed to chance.

5.5 Data availability

The virtual epilepsy patient cohort has been uploaded to the European Brain Research Infrastructure [32]. The dataset card can be found using the link : `https://doi.org/10.25493/XWG2-S8X`.

The code used to generate the synthetic data is available at : `https://github.com/BalanceKey/virtual_epilepsy_patient_cohort.git`

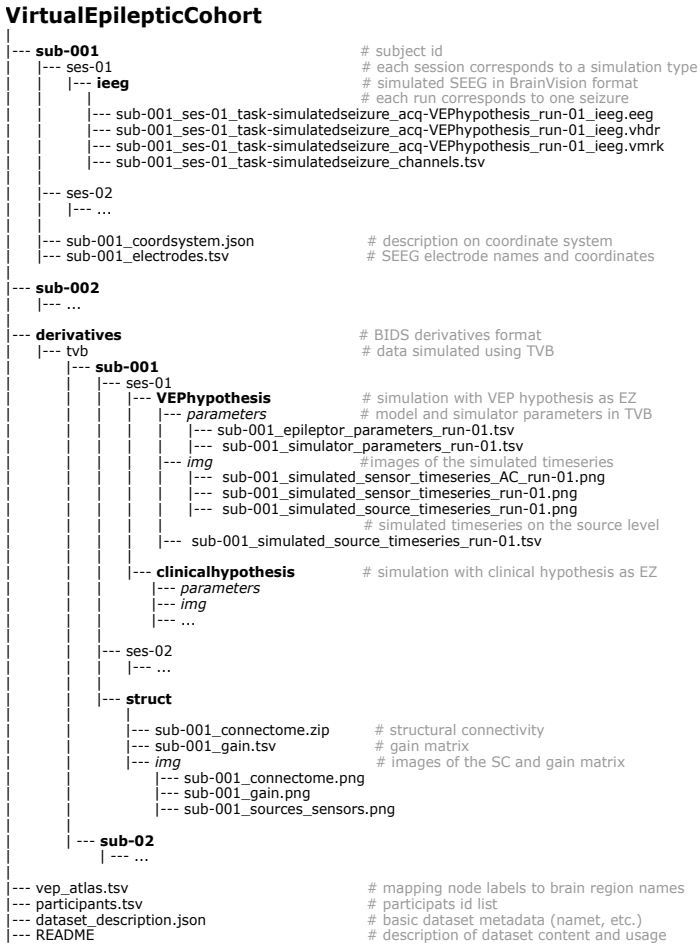

FIGURE 5.7 – BIDS-IEEG structure of the virtual epileptic cohort. The structure contains the simulated SEEG spontaneous seizures, stimulated seizures and interictal spikes in the main folder of each patient (named sub-001, sub-002, etc.). The parameters used to obtain the simulated time series are detailed in the derivatives folder for each of the EZ hypothesis (either VEP hypothesis or clinical hypothesis).

5.6 Supplementary Material

5.6.1 BIDS structure of the virtual epileptic cohort

The BIDS-IEEG structure used for the VEC dataset is illustrated in Figure 5.7.

5.6.2 Example of two different seizure types for the same patient

Two different seizure types from patient 8 of the virtual epileptic cohort are shown in Figure 5.8. In these cases, the EZ network is the same, but the propagation network (PZ) is different.

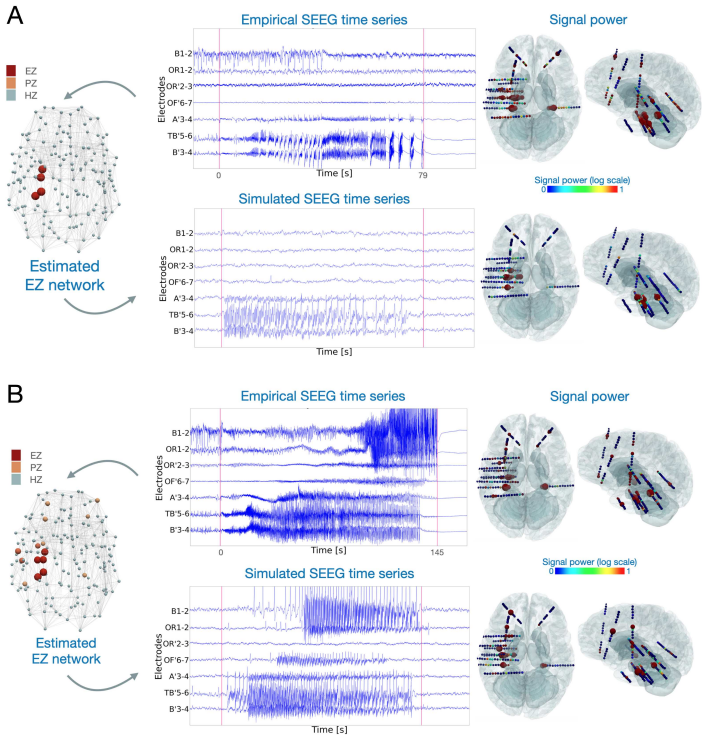

FIGURE 5.8 – Two different seizure types from the same patient. A) Focal seizure occurring in left temporal lobe. B) Propagated seizure with onset in left temporal lobe and propagation to contra lateral hemisphere. For both cases, simulated and empirical SEEG seizures are shown. Red vertical lines indicate seizure onset and seizure offset. Signal power for all SEEG channels is shown in 3D in axial and saggital plane.

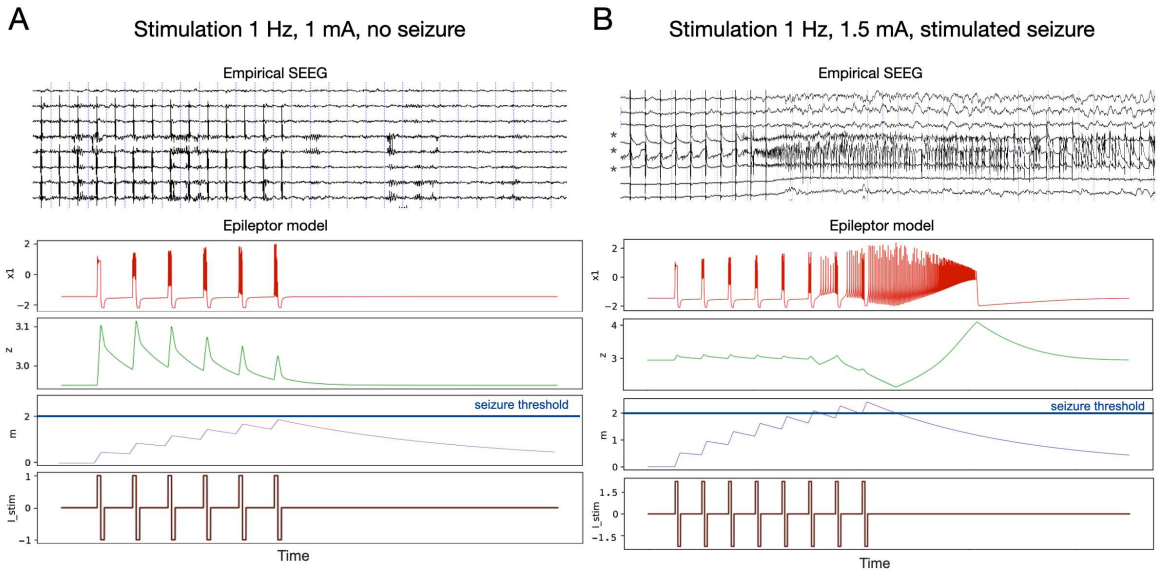

FIGURE 5.9 – Example time series for Epileptor-stimulation model. Above, empirical SEEG recording with stimulation artefact present. Below, simulated time series using the Epileptor-stimulation model. Variables of the model x_1, z, m and I_{stim} are shown. A) Example with 1 Hz, 1 mA stimulation and no seizure being induced. B) Example with 1 Hz, 1.5 mA stimulation and a seizure is induced. Asterisks indicate the time series containing seizure activity.

5.6.3 Epileptor-stimulation model

Time series of the main variables in the Epileptor-stimulation model are shown in Figure 5.9 with 1 Hz stimulation frequency and two different stimulation amplitudes. A higher stimulation amplitude causes a higher increase for the accumulation variable m, which can cross the seizure threshold and push the system from the normal state to the seizure state. When the stimulation stops, the variable m slowly returns to its baseline value.

5.6.4 Changing stimulation parameters

An example from patient 10 of the cohort is shown in Figure 5.10 where different stimulation amplitudes are tested in-silico and compared against the empirical data. Stimulation is applied in electrodes TB'1-TB'2, located in proximity to the left hippocampus region. For all simulations, the EZ hypothesis is estimated from the VEP pipeline and consists of the following regions : Left-Hippocampus-anterior, Left-Hippocampus-posterior, Left-Amygdala. The accumulation hypothesis embedded in the model is such that the effect of the stimulation on the model depends on the seizure threshold. If the critical threshold for seizure onset is reached, the model is kicked to the seizure state (Figure 5.10C) otherwise the model stays in its normal state (Figure 5.10B). Higher stimulation amplitudes will always cross this threshold and destabilise the system to the seizure state (Figure 5.10D).

For the same patient, an example with different stimulation locations is shown in Figure 5.11. The stimulation location is chosen by randomly selecting a pair of

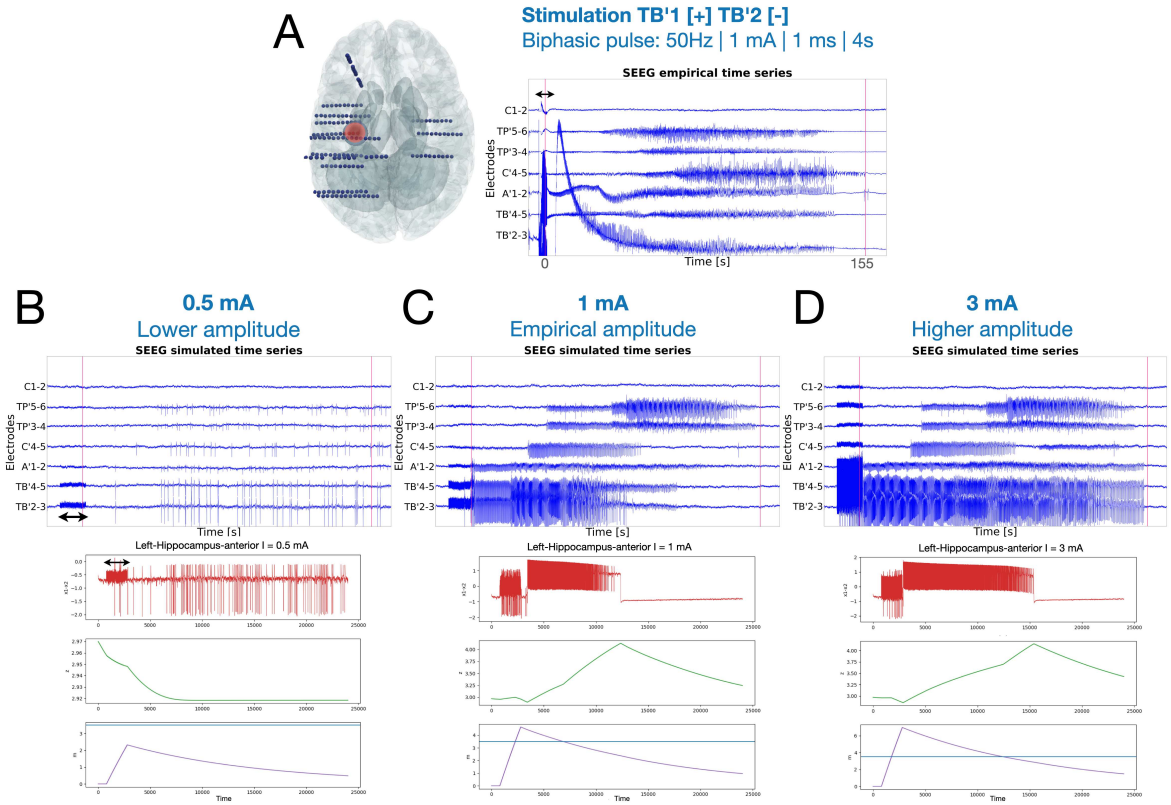

FIGURE 5.10 – Simulation examples with different stimulation amplitude from virtualized patient 10. Double arrow indicates stimulation period. Seven channels are plotted in bipolar montage (out of 116 total bipolar channels). Vertical red lines indicate seizure onset and seizure offset. For all plots B), C) and D), upper plots show simulated time series at the SEEG level with stimulation applied at different amplitudes. Lower plots show variables $x_1 - x_2$ in red, z in green and m in purple evolving for the same simulation for the region left hippocampus anterior. A) Empirical SEEG recording plot of a stimulation-induced seizure. Stimulation was applied at amplitude 1 mA using channels TB'1 [+] and TB'2[-], at frequency 50 Hz, pulse width 1 ms and duration 4 s. Reconstructed SEEG electrodes are shown on the left and stimulation location is plotted in red. B) Upper plot, synthetic SEEG time series of simulated brain activity with stimulation applied at 0.5 mA amplitude. All other stimulation parameters are identical to the empirical parameters. Here, a seizure is not induced after the stimulation is applied. Lower plot, the same simulated activity for the left hippocampus anterior, showing the variable m did not cross the seizure threshold, defined at 3.5 and corresponding variables staying in the normal state. C) Synthetic SEEG time series of the stimulation-induced seizure at 1 mA amplitude. Here, the same stimulation parameters as the ones applied empirically were used. Following the stimulation, a seizure is induced in the left hippocampus anterior, propagating later on to connected brain structures. Lower plot showing the variable m crossed the seizure threshold and the system is kicked to the seizure state. D) Synthetic SEEG time series plot of simulated brain activity with stimulation applied at 3 mA amplitude. Following the stimulation, a seizure is induced in the left hippocampus anterior and propagating later on to connected brain structures. Lower plot showing the variable m crossed the seizure threshold and the system is kicked to the seizure state.

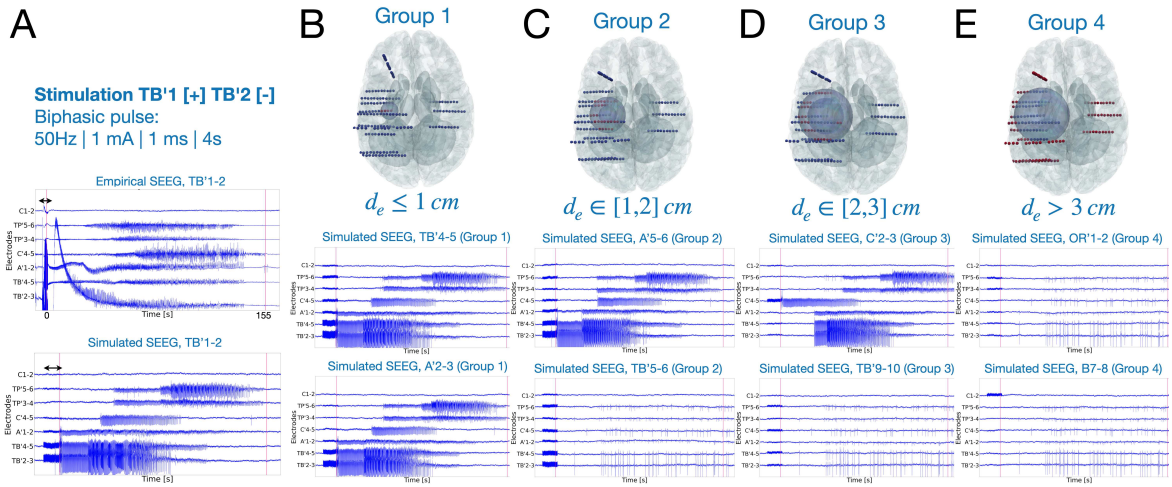

FIGURE 5.11 – Simulation examples with different stimulation locations from virtualized patient 10. Double arrow indicates stimulation period. Seven channels are plotted in bipolar montage (out of 116 total bipolar channels). Vertical red lines indicate seizure onset and offset. A) Upper plot, empirical SEEG recording of a stimulated seizure. Stimulation was applied at $1mA$ using channels TB'1 [+] and TB'2[-], at 50 Hz, pulse width $1ms$ and duration $4s$. Lower plot, corresponding simulated time series of a stimulated seizure. B) Simulated time series of stimulation applied by electrodes within 1 cm distance from the empirical stimulation location (TB'1-2). C) Simulated time series of stimulation applied by electrodes located between 1 and 2 cm distance from the empirical location. D) Simulated time series of stimulation applied by electrodes located between 2 and 3 cm distance from the empirical location. E) Simulated time series of stimulation applied by electrodes located more than 3 cm away from the empirical stimulation location.

electrodes within a certain radius from the empirical stimulation location. As the stimulus is applied increasingly further away from the empirical stimulation location, the seizure dynamics progressively change from the empirical post-stimulation response.

5.6.5 Data features for comparing simulated and empirical SEEG

To compare simulated and empirical SEEG, we extracted data features from the SEEG time series. The approach was similar for both the simulated and the empirical cases, and was based on the envelope function, from which the binarized SEEG data were derived (Figure 5.12).

5.6.6 Cohort statistics based on the clinical hypothesis

We used the clinical hypothesis for the EZ ground truth, as an alternative to the VEP hypothesis. We ran the same simulations on the same personalized virtual brain models and computed the similarity metrics as shown in Figure 5.13. We did

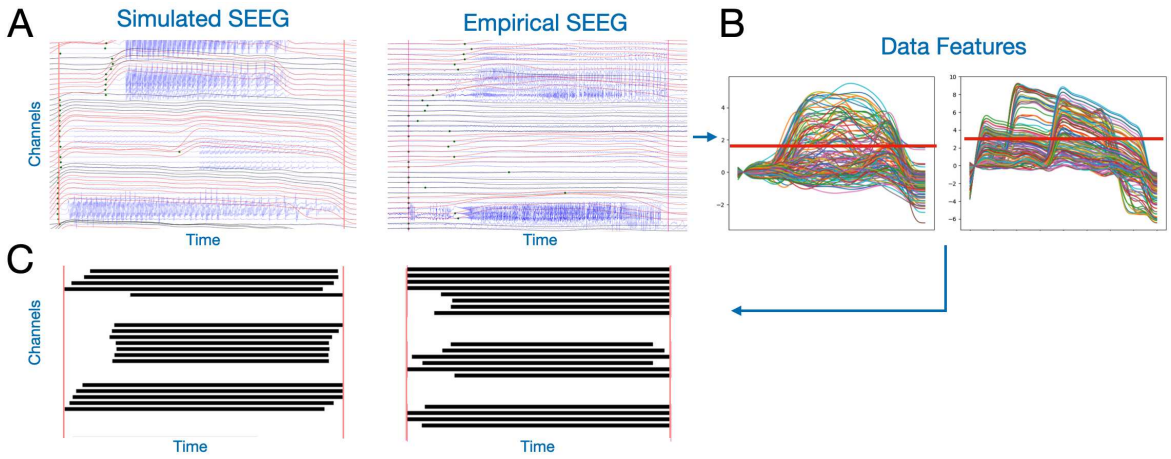

FIGURE 5.12 – Comparing simulated and empirical SEEG : spontaneous seizure example. A) Timeseries plot of a few SEEG channels (right : simulated SEEG time series, left : empirical SEEG time series). Overlayed in red and black are the envelope data features for each SEEG channel, indicating seizure and non seizure channels respectively. Green points indicate estimated seizure onset times. B) Envelope data features overlayed for all SEEG channels (left : simulated, right :empirical). Horizontal red lines indicate chosen threshold to categorize each channel as either seizure (above threshold) or non-seizure channel (below threshold). C) Binary plot of the same SEEG channels, where black indicates seizure activity and white indicates no seizure activity.

not observe a significant difference between the two hypotheses in the computed metrics.

5.6.7 Complete set of metrics used to compare simulated and empirical seizures

To compare the simulated SEEG time series against the empirical SEEG, we tested sixteen metrics in total (Figure 5.14 and Figure 5.15). The metrics are explained in the following subsections, following the same order as in the related figures. In the main article, we selected the following metrics : Binary, Jaccard Seizure Onset, Jaccard Seizure Propagation and Correlation.

Overlap metrics

The overlap metric compares, for any given category, the ratio of common SEEG channels between the empirical and simulated sets, divided by the total number SEEG channels in the empirical set. For any given category, it varies between 0 and 1, where 0 indicates no common channels, and 1 indicates that all channels of the empirical set are present in the simulated set.

For both empirical and synthetic SEEG data, we labelled all SEEG channels (in bipolar montage) as either seizure channel (E_S, S_S for empirical and simulated case respectively) or no seizure channel (E_{NS}, S_{NS} for the empirical and simulated case

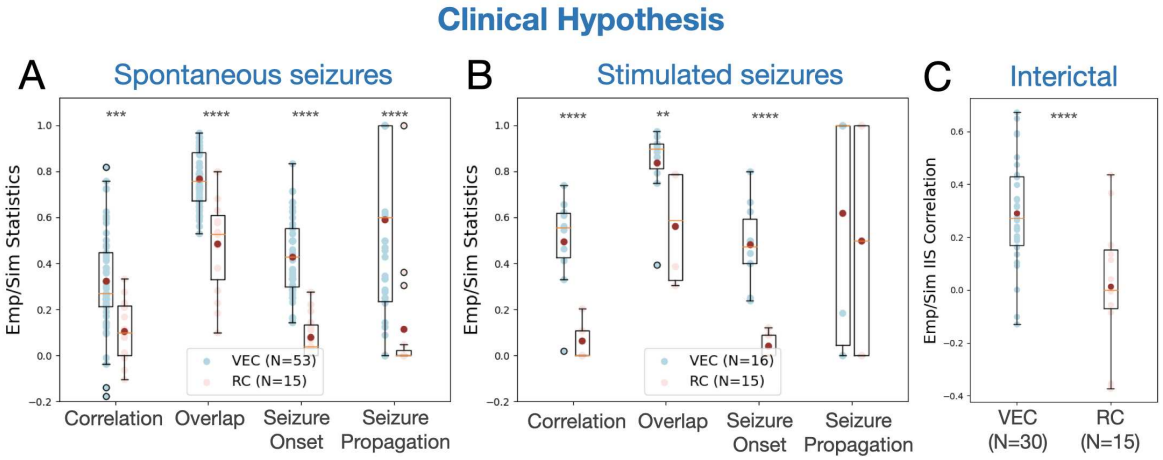

FIGURE 5.13 – Comparison of spontaneous simulated SEEG signals with empirical recordings for the virtual epileptic cohort (VEC, in blue) and the randomized cohort (RC, in red). The clinical hypothesis was used to inform the excitability parameters in the model. A) Boxplot of four main metrics comparing spontaneous seizures against synthetic seizures. Red dots indicate mean values. B) Boxplot of the same metrics comparing synthetic against empirical stimulated seizures. C) Boxplot of interictalspike (IIS) count correlation metric. $^{****}p-value < 0.0001$, $^{***}p-value < 0.001$, $^{**}p-value < 0.01$; permutation test

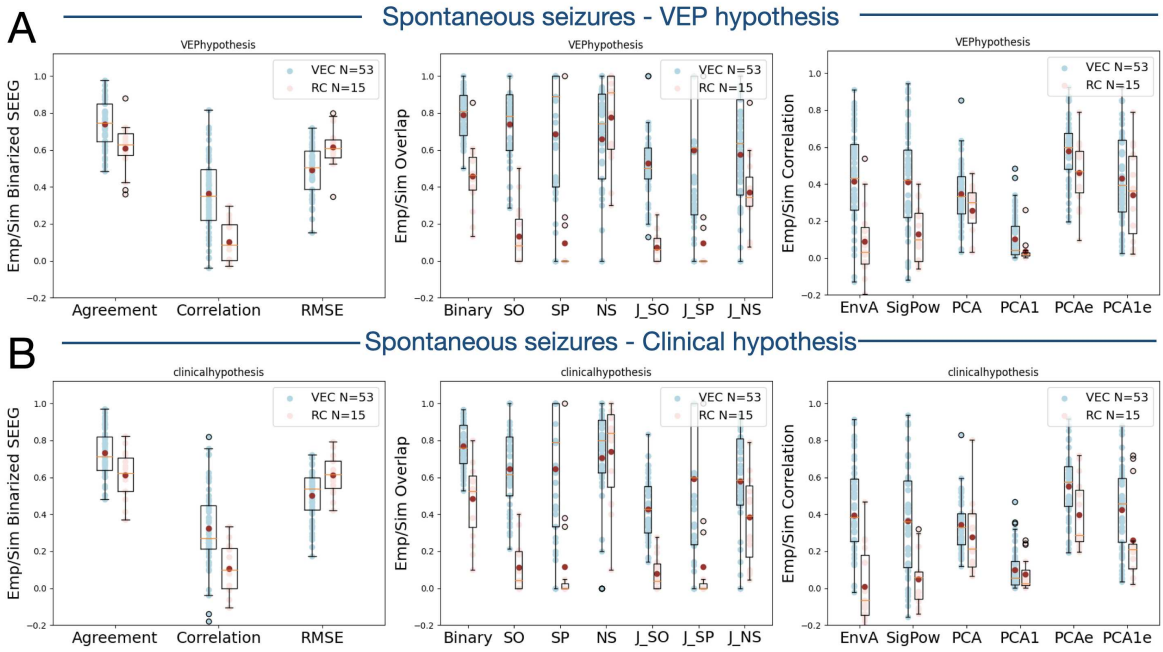

FIGURE 5.14 – Overall statistics for the VEC dataset as compared to the control dataset for spontaneous seizures. In blue, mean and standard deviation for the VEC cohort. In red, mean and standard deviation for the randomized cohort.

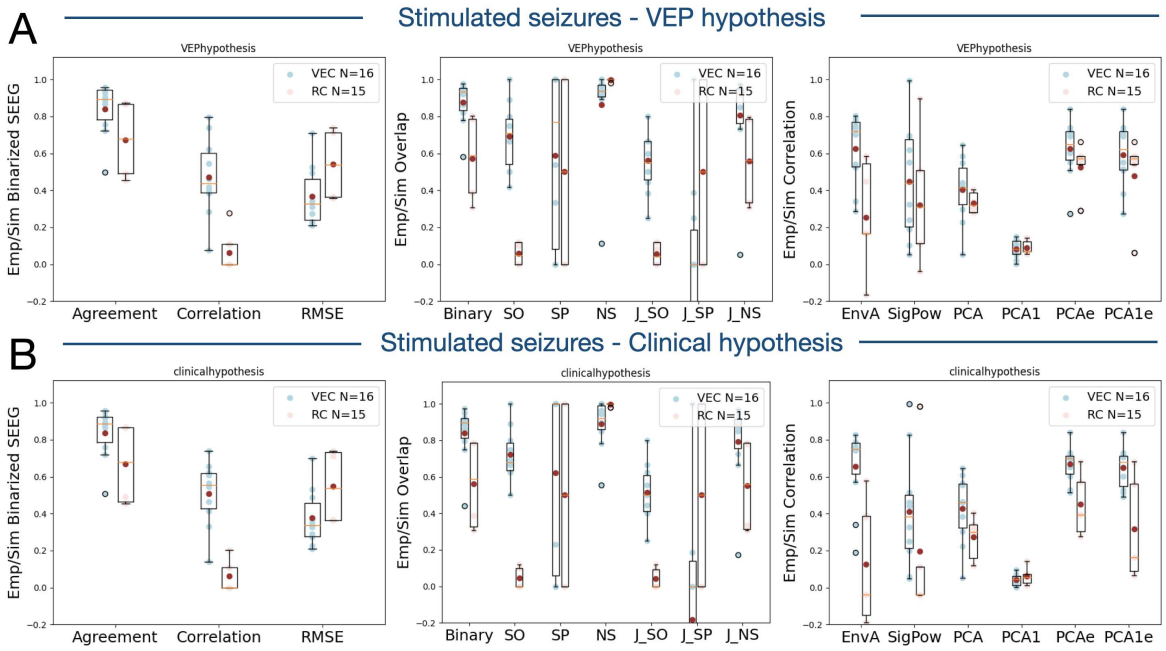

FIGURE 5.15 – Overall statistics for the VEC dataset as compared to the control dataset for stimulated seizures. In blue, mean and standard deviation for the VEC cohort. In red, mean and standard deviation for the randomized cohort.

resp.). A channel is labelled as seizure channel if the envelope data feature crosses the defined threshold, otherwise it is labelled as no seizure channel (as illustrated in Figure 5.12B). The overlap metric used to compare the synthetic and empirical seizure channels is the following :

$$Binary = \frac{|E_S \cap S_S|}{|E_S|} \tag{5.11}$$

which computes the ratio between the number of common seizure channels between empirical and simulated SEEG, divided by the total number of empirical seizure channels.

In addition, for both empirical and synthetic SEEG data, we labelled all seizure channels as either seizure onset channel (E_{SO}, S_{SO} for empirical and simulated case resp.) or seizure propagation channel (E_{SP}, S_{SP} for empirical and simulated case resp.). A seizure channel is labelled as seizure onset channel, if the estimated seizure start time in that channel belongs to the first few seconds of the whole seizure (one-fifth of the total seizure window), otherwise the channel is labelled as seizure propagation channel . The overlap metric used to compare synthetic and empirical data for each category (seizure onset, seizure propagation and no seizure) is as follows :

$$SO = \frac{|E_{SO} \cap S_{SO}|}{|E_{SO}|} \quad SP = \frac{|E_{SP} \cap S_{SP}|}{|E_{SP}|} \quad NS = \frac{|E_{NS} \cap S_{NS}|}{|E_{NS}|} \tag{5.12}$$

The Jaccard similarity coefficient compares the similarity between to sets, by also taking into account the number of non-common items between the two sets

(by computing the union between the two sets). It varies between 0 and 1, where 0 indicates the sets have no elements in common, and 1 indicates the sets are identical. The Jaccard similarity coefficient applied to each category (seizure onset, seizure propagation and no seizure) is as follows :

$$SO_{Jaccard} = \frac{|E_{SO} \cap S_{SO}|}{|E_{SO} \cup E_{SO}|} \quad SP_{Jaccard} = \frac{|E_{SP} \cap S_{SP}|}{|E_{SP} \cup E_{SP}|} \quad NS_{Jaccard} = \frac{|E_{NS} \cap S_{NS}|}{|E_{NS} \cup E_{NS}|} \tag{5.13}$$

where E_{SO}, E_{SP} and E_{NS} are the empirical seizure onset, seizure propagation and no seizure channels, respectively. S_{SO}, S_{SP} and S_{NS} are the synthetic seizure onset, seizure propagation and no seizure channels, respectively.

Correlation metrics

The sample Pearson correlation coefficient is used for all the metrics of this section, where the paired data $(s_1, e_1), ..., (s_n, e_n)$ consisting of n SEEG channels, is used to compute r. The coefficient varies between -1 and 1.

$$r = \frac{\sum_{i=1}^{n}(s_i - \bar{s})(e_i - \bar{e})}{\sqrt{\sum_{i=1}^{n}(s_i - \bar{s})^2}\sqrt{\sum_{i=1}^{n}(e_i - \bar{e})^2}}$$

For both simulated and empirical cases, the envelope peak amplitude is computed for each SEEG channel. Then, the sample Pearson correlation between the two lists of amplitude values is computed, $EnvA$.

For both simulated and empirical cases, the signal variance is computed for each SEEG channel. The sample Pearson correlation between the two lists of variance values is computed.

$$V = \frac{1}{T}\sum_{t=1}^{T}(x_t - \bar{x})^2 \tag{5.14}$$

For both simulated and empirical cases, PCA is performed on the data. First the SEEG timeseries are standardized for each channel, by subtracting the mean and dividing by the standard deviation. Then, PCA is performed on the time series using the same number of components as the number of SEEG channels. Then, the Pearson correlation is computed between the main principal components (i.e. the ones that explain 90% of the variance) of the empirical and simulated data, thus obtaining a correlation matrix. From this matrix, the maximum correlation value is extracted as a comparative value, PCA. As a second approach, the Pearson correlation is computed between the two first components of the empirical and simulated data, $PCA1$.

For both simulated and empirical cases, PCA is performed on the envelope data features, using the exact same approach as above, but replacing the SEEG time series by the envelope time series. The metrics computed are PCA_e and $PCA1_e$.

Comparative metrics for 2D binarized SEEG

We performed four main comparative metrics on the binarized images (E_{bin} for the empirical case, S_{bin} for the simulated case) obtained from the SEEG time series (as illustrated in Figure 5.12C).

First, we performed an overlap metric by measuring the number of identical binary (simulated, empirical) pairs divided by the total number of pixels for one image.

$$agreement = \frac{|E_{bin} \cap S_{bin}|}{|E_{bin}|} \tag{5.15}$$

Second, we performed a Pearson *correlation* on the 2D images, by comparing each binary (simulated, empirical) pair of identical row and column.

Third, we computed the mean squared error and the root mean squared error between the two binary images, with total number of N values :

$$mse = \frac{1}{N}\sum_{i=1}^{N}(E_{bin}(i) - S_{bin}(i))^2 \quad rmse = \sqrt{mse} \tag{5.16}$$

5.6.8 Grouping metrics by surgical outcome

We grouped the patients of the VEC cohort according to the surgical outcome in two groups : seizure-free and not-seizure-free. In figure 5.16, we plot the metrics performance for these two groups. These data were pooled following the Engel score of each patient, where patients with Engel score I were assigned the seizure-free group and patients with Engel scores II, III and IV were assigned the not-seizure-free group. This analysis was purely performed for exploratory purposes. Our interpretation follows that since our purpose was to build synthetic data that best match the empirical recordings, we seem to have little to no bias in whether the data came from patients that were seizure-free or not.

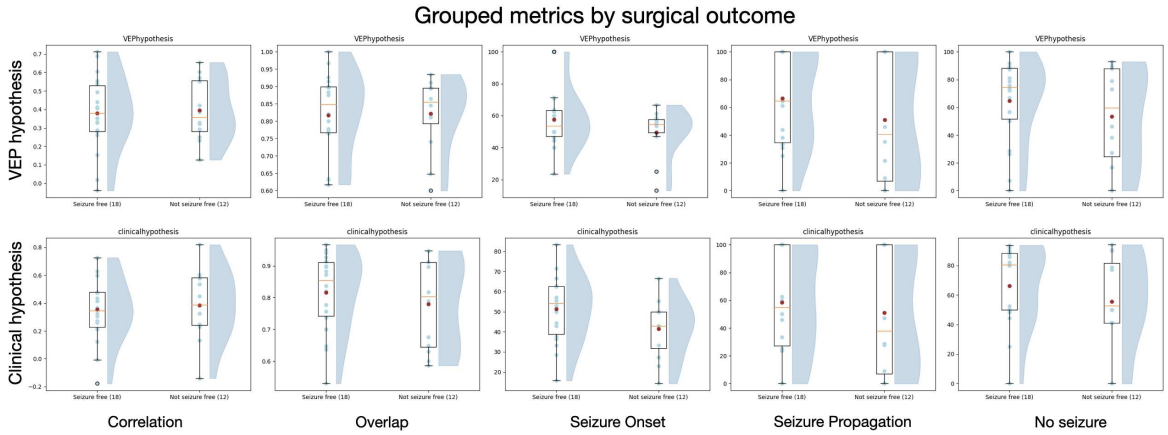

FIGURE 5.16 – Grouped metrics following surgical outcome. Patients were grouped in either the seizure-free group or the not-seizure-free group. First row shows metrics from synthetic data using the VEP hypothesis. The second row uses the clinical hypothesis. In each plot, metrics from seizure-free patients are plotted on the left side, whereas metrics from not-seizure-free patients are plotted on the right side. A boxplot is overlaid over all individual data points and a violin plot is also shown next to it.

Chapter 6

High-resolution brain stimulation modelling : application from invasive SEEG to non-invasive TI

In this chapter, I will outline my contributions to the paper *"Virtual brain twins for stimulation in epilepsy"* focusing specifically on the sections I worked on. I will detail the methods I used for these parts, as well as provide a discussion and conclusion based solely on my contributions. Additionally, I will briefly summarize the overall idea of the paper and explain how my work fits into the broader context of this research.

Abstract Estimating the epileptogenic zone network (EZN) is an important part of the diagnosis of drug-resistant focal epilepsy and plays a pivotal role in treatment and intervention. Virtual brain twins based on personalized whole brain modeling provide a formal method for personalized diagnosis by integrating patient-specific brain topography with structural connectivity from anatomical neuroimaging such as MRI and dynamic activity from functional recordings such as EEG and stereo-EEG (SEEG). Seizures demonstrate rich spatial and temporal features in functional recordings, which can be exploited to estimate the EZN. Stimulation-induced seizures can provide important and complementary information. In our modeling process, we consider invasive SEEG stimulation as the most practical current approach, and temporal interference (TI) stimulation as a potential future approach for non-invasive diagnosis and treatment. This paper offers a virtual brain twin framework for EZN diagnosis based on stimulation-induced seizures. This framework estimates the EZN and validates the results on synthetic data with ground truth. It provides an important methodological and conceptual basis for a series of ongoing scientific studies and clinical usage, which are specified in this paper. This framework also provides the necessary step to go from invasive to non-invasive diagnosis and treatment of drug-resistant focal epilepsy.

6.1 Introduction

In the clinic, patients with drug-resistant focal epilepsy are mainly treated surgically, by resecting their epileptogenic zone (EZ). To properly estimate the EZ,

patients undergo stereo-EEG (SEEG) implantation, allowing for their brain activity to be recorded locally and across brain layers. In addition, SEEG electrodes can stimulate the brain tissue. During SEEG, electrical stimulation is used to map brain function and provoke habitual seizures for diagnosis, helping to localize the EZ and improve post-surgical outcomes [128]. Over the past 15 years, various methods for quantifying EZNs through spectral analysis of SEEG signals have been proposed [10, 46]. In addition to data-driven approaches, methods combining mechanistic models and data analysis have been developed [51, 98]. We created a workflow for estimating a patient's EZN using personalized whole-brain models, known as the virtual epileptic patient (VEP) [66, 81, 142]. The VEP workflow has been retrospectively evaluated with 53 patients and is currently being tested in the EPINOV clinical trial [63, 142]. The virtual brain twin concept, based on the VEP workflow, has been extended to various brain disorders [141]. In this study, we introduce the first high-resolution virtual brain twin workflow for estimating EZNs using a stimulation paradigm.

We propose a personalized whole-brain model, or virtual brain twin, to assess SEEG stimulations. Using a high-resolution model, we compute electric fields from SEEG stimulation, simulate brain responses, and estimate the EZN based on induced seizures. With simulated data as ground truth, we validate the EZN estimation and explore translating the approach from SEEG to non-invasive methods like scalp-EEG and transcranial stimulation, particularly temporal interference (TI). The motivation behind this translation is due to the limited spatial sampling and invasiveness of SEEG. Non-invasive stimulation allows for a full exploration of the brain network. However, noninvasive stimulation is typically limited to brain regions close to the cortical surface, as the electric field gets weaker in deeper cortical layers. Temporal interference stimulation is a novel non-invasive stimulation method that aims at reaching deep brain targets with similar focality to DBS [15, 48]. It uses the brain's insensitivity to high-frequency electric fields (above 1 kHz) [48]. When two slightly detuned high-frequency fields are applied, their interference creates a low-frequency modulation (Δf, typically below 150 Hz) at the target location, effectively stimulating brain regions relevant to functional dynamics.

In this work, we introduced a high-resolution modeling approach to seizures triggered by stimulation. We built personalized high-resolution brain models for either SEEG or TI stimulation. We also estimated the EZ network from stimulated seizures and validated it with simulated data. This research supports transitioning from invasive to non-invasive diagnosis of drug-resistant epilepsy and provides a first proof-of-concept for following studies such as personalized stimulation parameter optimization for diagnosis and treatment in drug-resistant epilepsy.

6.2 Results

6.2.1 Virtual epileptic patient pipeline for SEEG stimulation

We used the data from a right-handed, 23-year-old female patient diagnosed with left occipital lobe epilepsy of unknown origin (negative MRI) to illustrate how to use our workflow. We first extracted the brain geometry, the structural connectivity

matrix, and the source-to-sensor mapping from the T1-MRI, diffusion-weighted MRI, and post-SEEG-implantation CT scans for this patient. We built the whole brain neural mass model based on this anatomical information. Then we ran the HMC algorithms for three spontaneous seizures recorded from this patient (one of the three seizures is shown in Figure 6.1 (**A**)). We pooled the posterior distribution from the three seizures, in which the left lateral occipital cortex (region O2 (in VEP atlas [140]) was consistently identified as part of the EZ. Then we projected the left O2 onto both preoperative and postoperative T1-MRI slides and 3D brain meshes (in Figure 6.1(**C-E**)) to compare its extent with the size of the surgical resection. The patient underwent resective surgery, in which a large portion of the left O2 was removed, and was almost seizure-free after surgery (surgery outcome class of Engel II [145]). Based on this result, we built the high-resolution whole brain model for two types of stimulations with the hypothesis that the left O2 was the EZ of the patient.

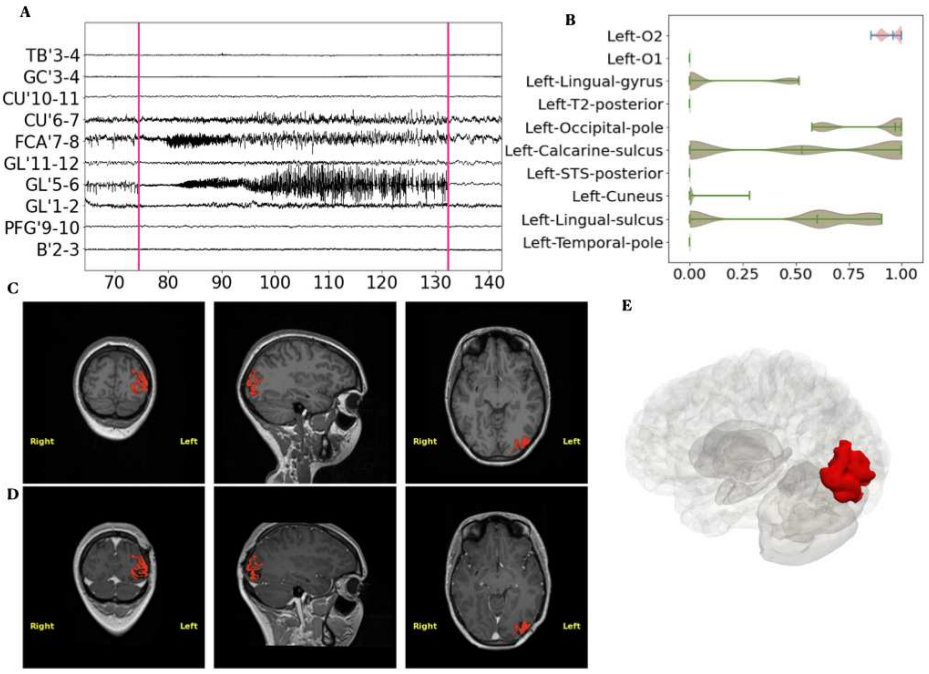

FIGURE 6.1 – VEP diagnostic mapping for spontaneous seizures. (**A**) Selected SEEG recordings from one seizure in a 23-year-old female patient. (**B**) Posterior distribution of the EV (higher value indicates higher probability of seizure) for nine selected regions obtained from the HMC pipeline. (**C**) Heatmap of the left O2 identified by VEP (in red) shown in a preoperative T1-MRI. (**D**) Heatmap of the left O2 identified by VEP (in red) shown in a postoperative T1-MRI. (**D**) The left O2 was projected on the patient's 3D meshes.

To model direct electrical stimulation by SEEG electrodes in the brain, we first mapped the contribution of each SEEG electrode onto the respective brain regions. We retrieved the contribution from a pair of electrodes, in which the perturbation is applied to the brain regions based on the sensor-to-source mapping matrix [142].

Then we calculated the effect of the bipolar pulse stimulation (50 Hz for a duration of 3.5 s on bipolar GL'5-6 electrode leads) on each vertex of the cortex mesh (Figure 6.2**A**). We used the Epileptor stimulation model on each of the 20,284 vertices representing the cortical mesh. The stimulation of the Epileptor leads to an accumulation in a state variable m that pushes the brain to the seizure state (Figure 6.3). The seizures were located around the left O2 regions. From these simulated neural source signals (Figure 6.2**B**), we obtained SEEG signals (Figure 6.2**C**) using the source-to-sensor gain matrix while considering the orientation of dipoles.

We used these synthetic SEEG recordings (Figure 6.2**C**) as an input to the VEP model inversion module to estimate the EZ network. We obtained the left O2 with the highest epileptogenic values out of all the samples according to the posterior distribution of EVs from the HMC algorithm (Figure 6.2**D**). The two neighboring regions (the left-lingual-gyrus and the left-occipital-pole) were the second group of candidates that could belong to the EZ network. The heatmap projected on the patient's T1-MRI revealed the spatial mapping of the EZ network (sagittal, axial and coronal view images shown in Figure 6.2**E**). The spatial mapping of these three regions in 3D brain is shown in Figure 6.2**F**.

6.2.2 Virtual epileptic patient pipeline for TI stimulation

Here we describe how the same pipeline works using TI stimulation. First, we used high-resolution modeling to simulate TI stimulation. We calculated the TI electric field, which is projected onto the cortical surface by stimulating two pairs of EEG electrodes PPO3-PPO5 and P5h-PO5h [91] in Figure 6.4**A**) at the frequencies of 1000 Hz and 1005 Hz, respectively. The stimulation direction is determined based on the assumption that the components of the field that have the greatest impact are those that are parallel to the neurons' axons [69]. We used the amplitude of the TI electric field as input to the Epileptor model on each vertex of the cortical mesh (Figure 6.5). We simulated the brain source signals on each vertex of the whole brain by considering both global and local connectivity (Figure 6.4**B**). We then mapped the signals on the vertices of the cortical surface onto the scalp EEG signals (Figure 6.4**C**) using the source-to-sensor mapping matrix.

We extracted the data features from these synthetic EEG recordings (Figure 6.4**C**) as the input of the VEP model inversion modules to estimate the epileptogenic zone. From the posterior distribution of EVs, we obtained the left O2 with the highest epileptogenic values from all samples and the left O1 as the second candidate belonging to the EZ network (Figure 6.4**D**). The heatmap of these two regions projected on the patient's T1-MRI shows the spatial mapping of the EZ network (sagittal, axial and coronal view images shown in Figure 6.4**E**) and the 3D brain in Figure 6.4**F**, where the left O2 is in red and the left O1 in yellow.

6.2.3 Applying the pipeline to a second patient

To validate that the pipeline can be easily used in other patients, we added the results of a second patient with left frontal lobe epilepsy. The patient underwent resective surgery resulting in seizure freedom (surgery outcome class of Engel I [145]).

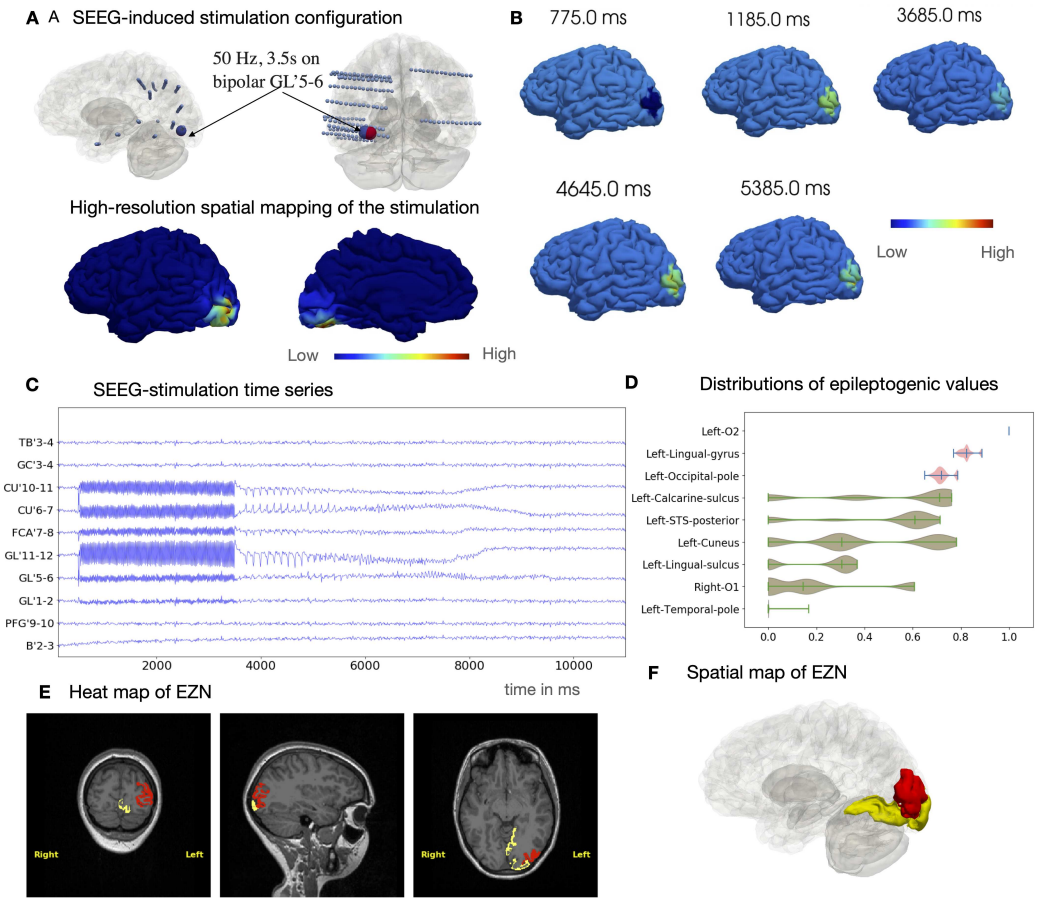

FIGURE 6.2 – VEP diagnostic mapping for SEEG stimulation. (**A**) GL'5-6 (large blue/red sphere) is the stimulated contact in the left occipital lobe, using a bipolar pulse stimulation (50 Hz for a duration of 3.5 s with pulse duration 1ms) (Top). The spatial mapping of the maximum of stimulation values (shown in the colorbar from low (left) to high (right) values) for each vertex of the brain from sensor GL'5-6 (bottom). (**B**) Neural activity is shown on the cortical mesh at 5 different time points. The seizures are located around the left O2 region of the VEP atlas. (**C**) Selected simulated SEEG time-series from a SEEG stimulation-induced seizure in the example patient. (**D**) Posterior distribution of the epileptogenic values (EV) (higher value indicates higher chance for seizure) of 9 selected regions obtained from HMC sampling. Red regions indicate highest chance of being the EZ, other areas are in green. The region of the highest EV posterior distribution is the left O2 in red shown in T1-MRI (**E**) and 3D brain in (**F**). The two regions (the left lingual gyrus and the left occipital pole) are shown in yellow in (**E**, **F**).

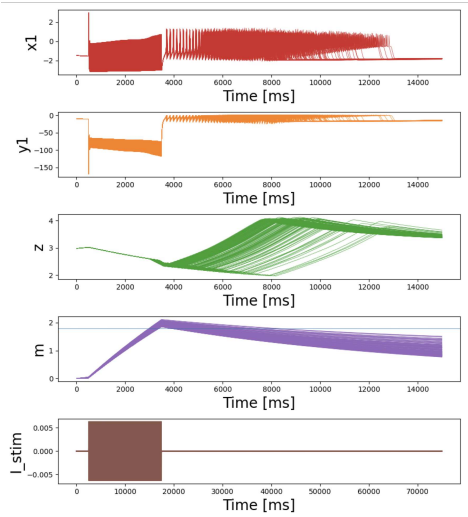

FIGURE 6.3 – The time-series of Epileptor stimulation variables during induced seizures through SEEG stimulation. Five state variables of the model at seizing parts of the cortex and the stimulation time course I_{stim}. The stimulation is accumulating on state variable m of the stimulation-Epileptor equation 6.1. Once m passes a fixed threshold it causes the model to initiate the seizure.

Eight brain regions including the orbito frontal, anterior-cingulate, F1 lateral prefrontal, F2 rostral, SFS rostral, frontal pole and F1-mesial-prefrontal cortex in the left hemisphere were resected. We built the high-resolution whole-brain model for two types of perturbations under the hypothesis that the left F1 lateral prefrontal has the highest x_0 value. To model direct electrical stimulation by SEEG electrodes in the brain, we calculated the electric effect of the bipolar pulse perturbation (50 Hz, for a duration of 3 s on bipolar PM'3-4 electrode leads) 6.6. The seizure was induced around the left F1 lateral prefrontal cortex. From the simulated neural source signals (Figure 6.6**B**), we obtained spontaneous SEEG and EEG signals (Figure 6.6**C**) using the source-to-sensor gain matrix. These synthetic SEEG and EEG signals served as input to the VEP model integration inversion module to estimate the EZ network. We obtained the left-F1-lateral-prefrontal cortex as the region with the highest epileptogenic value from the HMC algorithm (Figure 6.6**D**). The two neighboring regions (the left-F1-mesial-prefrontal and the left-middle-frontal-sulcus) were identified as second group of candidates that could belong to the EZ network.

We also illustrated the results of this frontal lobe epilepsy patient with TI stimulation in Figure 6.7. First, we used high-resolution modeling to simulate TI stimulation. We calculated the TI electric field, which is projected onto the cortical surface by stimulating two pairs of EEG electrodes, AFz-Fpz and AF3-Fp1, in Figure 6.7**A**) at the frequencies of 1000 Hz and 1005 Hz, respectively. The brain source signals on each vertex of the whole brain are shown in (Figure 6.7**B**). We then mapped the neural activity from the cortical surface onto the SEEG and scalp EEG electrodes (Figure 6.7**C**) using the source-to-sensor mapping matrix. We extracted the data features from these synthetic SEEG and EEG recordings (Figure 6.7**C**) which served as input to the VEP model integration inversion modules to estimate the EZ.

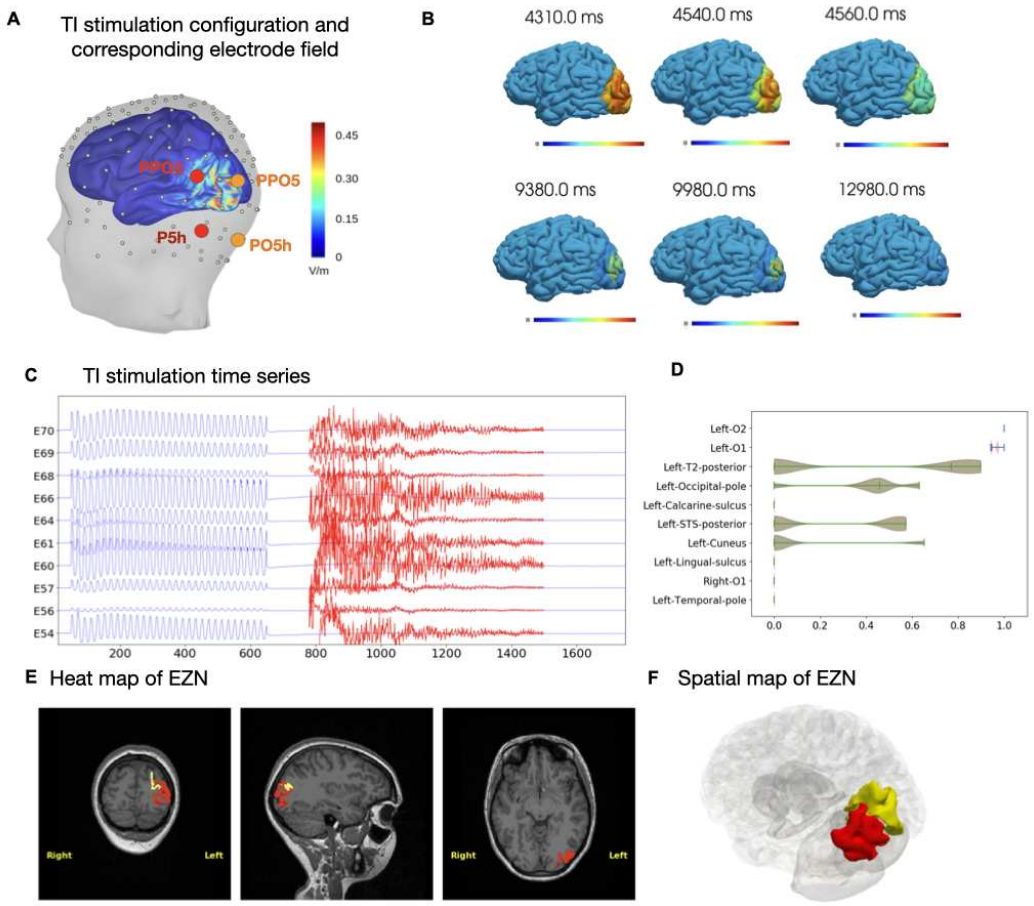

FIGURE 6.4 – VEP diagnostic mapping from TI stimulation. (**A**) The electric field of TI stimulation by two pairs of EEG electrodes (shown in red and orange) is based on the 10-5 international reference system, which is EEG 10-20 extended SPM12 EEG cap from SIMNIBS [91]. We applied a frequency of 1000 and 1005 Hz for the first and second electrode pairs, respectively. The Spatial distribution of the peak activity of the TI envelope is colored in the 3D brain. (**B**) Seizure dynamics were simulated using the stimulation Epileptor through the TI stimulation. Neural activity is shown on the cortical mesh at 6 different time points. The seizures are located around the left O2 regions of the VEP atlas. (**C**) Selected simulated EEG time-series from TI stimulation-induced seizure. The scaled-up time series during the seizure period is shown in red. (**D**) Posterior distribution of the epileptogenic values (EV) (higher value indicates higher chance for seizure) for 10 selected regions obtained from the MCMC sampling. Red regions indicate highest chance of being the EZ network ; the others are in green. The region of the highest EV posterior distribution is the left O2 in red shown in T1-MRI (**E**) and 3D brain in (**F**). The second region (Left O1) is shown in yellow in (**E**, **F**).

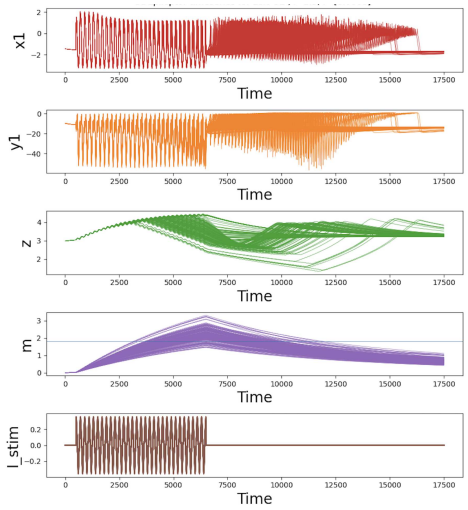

FIGURE 6.5 – The time-series of Epileptor Stimulation equations by inducing seizure through stimulation induced by TI. Five state variables of the model at seizing parts of the cortex and the stimulation time course I_{stim}. The stimulation is accumulating on state variable m of the Epileptor. Once m passes a fixed threshold it causes the model to initiate the seizure.

From the posterior distribution of EVs, we obtained the left middle frontal cortex as the region with the highest epileptogenic values from all samples (Figure 6.7**D**) and shown in red in 3D in Figure 6.7**E**). And the left F1-lateral prefrontal and left-Orbito-frontal-sulcus as the second candidates belonging to the EZ network (Figure 6.7**D**) and shown in yellow in Figure 6.7**E**.

6.3 Discussion and conclusions

6.3.1 Summary

We developed a dedicated stimulation pipeline based on personalized whole brain network modeling for epilepsy. This pipeline integrated empirical patient data and was validated on simulated data from high-resolution network modeling. It estimates EZ networks using model inversion through HMC and Bayesian inference. We demonstrated the estimation of the EZ network from SEEG and EEG signals during seizure activity triggered by direct electrical SEEG or TI stimulation. We introduced model inversion methods integrating a single functional imaging modality (either SEEG or EEG) and multiple, potentially simultaneous, modalities. The stimulation pipeline can provide a methodological and conceptual basis for further scientific studies and clinical translations.

6.3.2 Future scientific studies

The first application of this pipeline can help us answer a crucial diagnostic question : How to infer the underlying EZ networks from stimulated seizures ? To answer

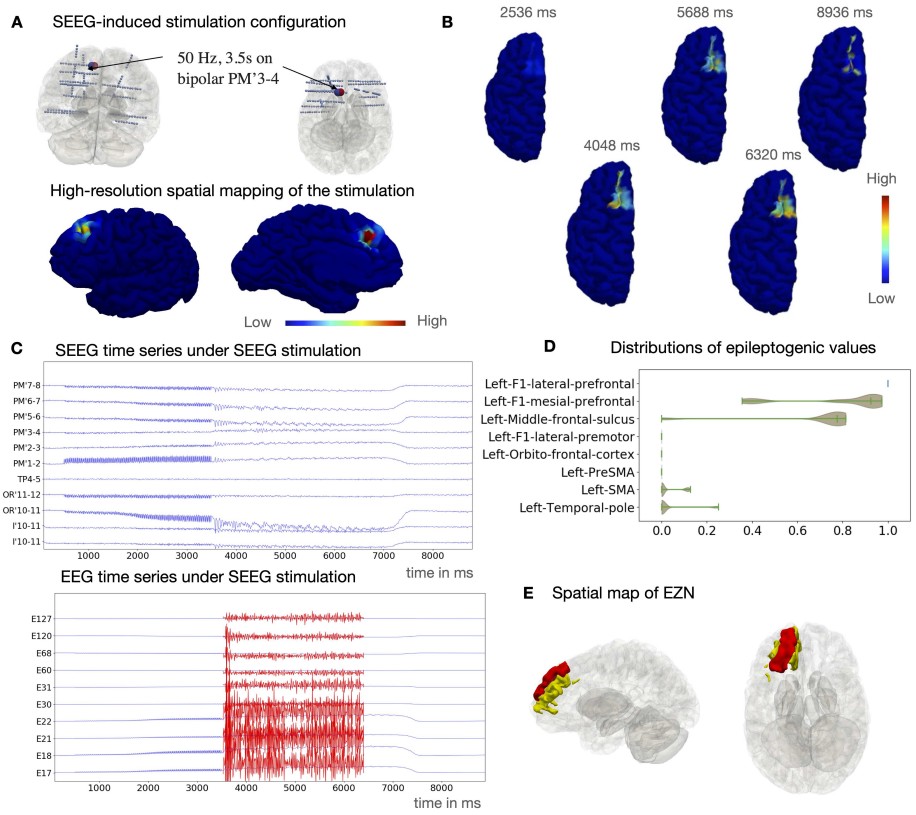

FIGURE 6.6 – VEP diagnostic mapping from SEEG stimulation for a second patient with frontal lobe epilepsy. (**A**) PM'3-4 (large blue/red sphere) is the stimulated contact in the left frontal lobe, using a bipolar pulse stimulation (50 Hz for a duration of 3 s with pulse duration 1ms) (Top). The spatial mapping of the maximum of stimulation values (shown in the colorbar from low (left) to high (right) values) for each vertex of the brain from sensor PM'3-4 (bottom). (**B**) Seizure dynamics were simulated using the stimulation Epileptor and induced through SEEG stimulation. Neural activity is shown on the cortical mesh at 5 different time points. (**C**) Selected simulated SEEG time-series (top) and EEG time-series (bottom) from SEEG stimulation-induced seizure. The scaled-up time series during the seizure period is shown in red. (**D**) Posterior distribution of the epileptogenic values (EV) (higher value indicates higher chance for seizure) for 8 selected regions obtained from the MCMC sampling when analyzing simultaneously SEEG and EEG. (**E**) The highest chance of being the EZ network is left-F1-lateral-prefrontal in red mapped in 3D brain and left-F1-mesial-prefrontal cortex and left-middle-frontal-sulcus in yellow.

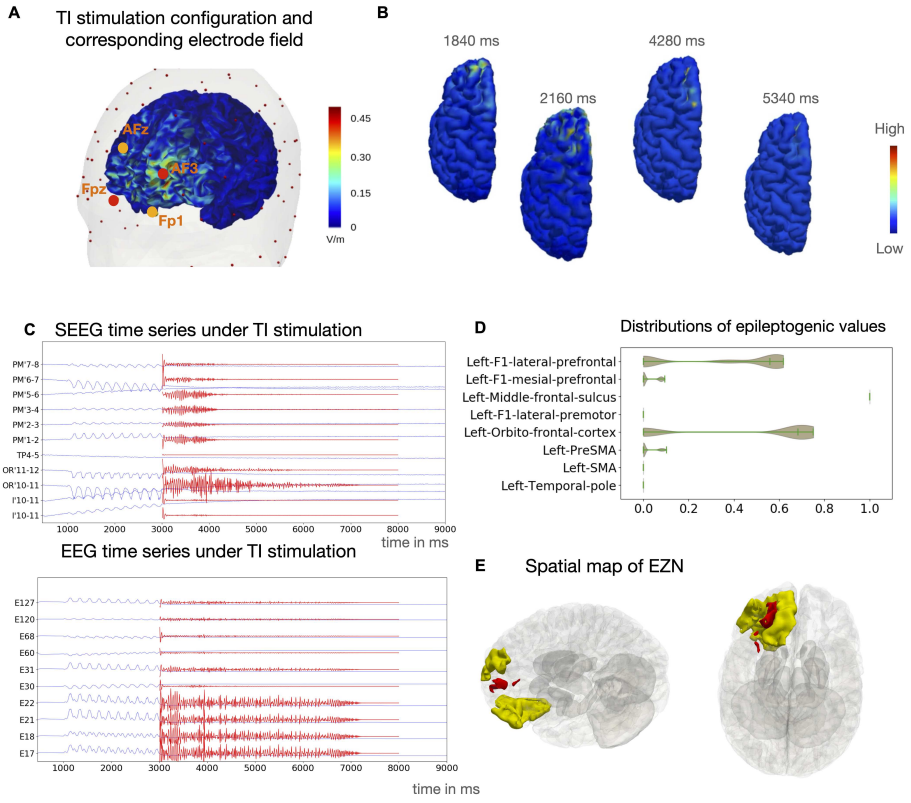

FIGURE 6.7 – VEP diagnostic mapping from TI stimulation for second patient with frontal lobe epilepsy. (**A**) The electric field of TI stimulation by two pairs of EEG electrodes (shown in red and orange). We applied a frequency of 1000 and 1005 Hz for the first and second electrode pairs, respectively. The Spatial distribution of the peak activity of the TI envelope is colored in the 3D brain. (**B**) Seizure dynamics were simulated using the stimulation Epileptor through the TI stimulation. Neural activity is shown on the cortical mesh at 4 different time points. (**C**) Selected simulated SEEG time-series (top) and EEG time-series (bottom) from TI stimulation-induced seizure. The scaled-up time series during the seizure period is shown in red. (**D**) Posterior distribution of the epileptogenic values (EV) (higher value indicates higher chance for seizure) for 8 selected regions the same as Figure 6.6 **D**. (E) The highest chance of being the EZ network as left-middle-frontal-sulcus in red mapped in 3D brain and left-F1-lateral-prefrontal and left-orbito-frontal-cortex in yellow.

this question, it is necessary to investigate the following problems. First, what is the proper range of the stimulation parameters to induce seizures for diagnosis ? Currently, no standardized stimulation protocols exist [41]. The French guidelines suggest parameters for both low-frequency (1 Hz) and high-frequency (50 Hz) stimulation with specified ranges on pulse width, pulse intensity, and stimulation duration [59]. Our personalized whole brain model can predict the stimulation effect for individual patients given specified stimulation parameters. On the patient-specific level, among all feasible stimulation parameters, then what are the optimal stimulation parameters for inducing seizures for diagnosis ? Second, what is the relationship between the EZ network triggered by stimulation and the one occurring during spontaneous seizures ? More specifically, we want to investigate whether the EZ network estimated from stimulation-induced seizures equals the EZ network of spontaneous seizures. It could be possible that stimulation forces seizures in brain regions that would not be epileptogenic otherwise, or that stimulation uncovers only a subset of epileptogenic regions. Even for spontaneous seizures, we have to remember that the limited observations of recordings of spontaneous seizures may also only tell part of the story. Third, how many induced seizures by SEEG stimulation are sufficient for identifying the full underlying EZ network ? We can investigate this question by systematically evaluating the EZ networks on SEEG stimulation-induced seizures generated by VEP models with given EZ networks. The proposed VEP stimulation pipeline with high-resolution modeling provides a reasonable framework as a useful tool to address all these questions.

The diagnostic pipeline for TI stimulation can provide a theoretical basis for the non-invasive diagnosis and treatment of epilepsy. TI stimulation is a good candidate for both diagnosis and treatment in epilepsy within the non-invasive stimulation family. Other non-invasive stimulations, such as tDCS [121], are mostly used only for treatment in epilepsy. The key feature of TI stimulation is that it enables a focused stimulation that can reach deep brain structures non-invasively [47, 48], such as the hippocampus, which quite often is involved in the EZ network in epilepsy. Studies have demonstrated the safety of TI in human participants [148]. Literature and seminars with preliminary results have started to discuss the application of TI stimulation to brain disorders, such as epilepsy [2, 28], Alzheimer's [20], Parkinson's [49] and essential tremor [116]. TI stimulation has evoked seizure-like events in the mouse hippocampus that have been experimentally well controlled [85]. Our study here provides a pipeline for predicting the use of TI for the diagnosis of the EZ network in human epilepsy, and as a basis for an optimization strategy for TI stimulation parameters. Based on this proposed framework, we can further build high-resolution models for individual patients in future therapeutic interventions. Although we obtained a good estimate of the EZ network from non-invasive EEG signals for patient examples whose EZ networks were in cortical regions, for future non-invasive diagnosis of EZ networks in deep structures, we need to explore the non-invasive measurements that can provide useful data features from these deep brain structures.

The current pipeline has several limitations. Model-based approaches are usually computationally expensive and parameter sensitive, which may pose challenges for real-time use in clinical routine, such as the optimization of stimulation parame-

ters. The current pipeline does not consider the dynamics of the epileptic disorders over long timescales nor the long-term effects of the stimulation. Ongoing systematic evaluations and studies will also improve the current pipeline in the following ways. High-resolution modeling of the subcortical structure and a more realistic forward resolution may improve the whole brain modeling. The introduction of regional variations (such as cell density and receptor density) [4, 150] may provide a fundamental way to improve the current VEP pipeline.

6.4 Methods

6.4.1 Patient data

We used the data from two patients who underwent a standard presurgical protocol at La Timone Hospital in Marseille. Informed written consent was obtained in compliance with the ethical requirements of the Declaration of Helsinki and the study protocol was approved by the local Ethics Committee (Comité de Protection des Personnes sud Méditerranée 1). This patient underwent a comprehensive presurgical assessment, which included medical history, neuropsychological assessment, neurological examination, fluorodeoxyglucose positron emission tomography, high-resolution 3T MRI, long-term scalp EEG and invasive SEEG recordings. The patient received non-invasive T1-weighted imaging (MPRAGE sequence, repetition time $=$ $1.9\ s$, echo time $= 2.19\ ms$, voxel size $1.0\times1.0\times1.0\ mm^3$) and diffusion-weighted MRI images (with an angular gradient set of 64 directions, repetition time $= 10.7\ s$, echo time $= 95\ ms$, voxel size $1.95 \times 1.95 \times 2.0\ mm^3$, b-weighting of $1000\ s/mm^2$.) The images were acquired on a Siemens Magnetom Verio 3T MR-scanner. The patient had invasive SEEG recordings obtained by implanting multiple depth electrodes, each containing $10 - 18$ contacts $2\ mm$ long and separated by 1.5 or $5\ mm$ gaps. The SEEG signals were acquired on a 128 channel Deltamed/Natus system. After the electrode implantation, a cranial CT scan was performed to obtain the location of the implanted electrodes.

6.4.2 Data processing

To construct the individual brain network models, we first preprocessed the T1-MRI and diffusion-weighted MRI data. Volumetric segmentation and cortical surface reconstruction were from the patient-specific T1-MRI data using the recon-all pipeline of the FreeSurfer software package `http://surfer.nmr.mgh.harvard.edu`. The cortical surface was parcellated according to the VEP atlas [140]. We utilized the MRtrix software package to process the diffusion-weighted MRI. The structural connectome was constructed by assigning and counting the streamlines to and from each VEP brain region. The diagonal entries of the connectome matrix were set to 0 to exclude self-connections within areas and the matrix was normalized so that the maximum value was equal to one. We obtained the location of the SEEG contacts from post-implantation CT scans using GARDEL (Graphical user interface for Automatic Registration and Depth Electrodes Localization), which is part of the

EpiTools software package [138]. Then we co-registered the contact positions from the CT scan space to the T1-MRI scan space for this patient.

6.4.3 High resolution simulation of the Epileptor-Stimulation model

We modeled epileptic seizures on a patient-specific high-resolution brain model. Although there is no consensus about the precise biophysical mechanism of ion exchanges that leads to seizure onset. Previous studies demonstrated an increase in excitability, spike frequency and oscillation power [22, 103, 135, 136] when an external perturbation was applied. Experimental studies have linked seizure onset to specific changes in ion dynamics such as extracellular potassium or intracellular chloride [39, 78, 129].

We hypothesized that exposure of repetitive stimulation/perturbation generates a slow accumulation effect, which can push the system to the seizure state when a seizure threshold is reached.

We model this accumulation effect phenomenologically via the parameter m, which influences the oscillatory dynamics in the seizure onset state in the Epileptor model [33]. We render m time dependent, $m = m(t)$, and introduce an exponentially decaying memory kernel of length r through a linear ordinary differential equation, which slowly builds up when an external stimulus is applied until the seizure threshold is reached. In the absence of stimulus $m(t)$ slowly returns back to baseline. H is the Heaviside function. When m is greater than the seizure threshold m_{thresh}, the H function equals 1, which kicks the system into the seizure-like state. Otherwise, the H function equals 0.

The pial surfaces of both hemispheres define the spatial domain along which the network activity can unfold. Neural dynamics are governed by an extension of the original Epileptor model [67]. The extended Epileptor-Stimulation model includes a stimulation-accumulating state variable m that can destabilize the system and produce a seizure. The neural activity at every vertex $i = 1, ..., N$ of the network is governed by the following equations :

$$
\begin{aligned}
\dot{x}_i &= y_i - f_1(x_i) - z_i + I_{ext} + I_{stim} + \gamma_{hom} \sum_{j=1}^{N} S(g_{i,j}) H(x_j, \theta_{hom}) + \gamma_{het} \sum_{l=1}^{L} W_{k,l} H(X_l, \theta_{het}) \\
\dot{y}_i &= c - d x_i^2 - y_i \\
\dot{z}_i &= r(4(x_i - x_0 + n H(m_i - m_{thresh})) - z_i) + f_2(z_i) \\
\dot{m}_i &= r(I_{stim} - m_i)
\end{aligned}
\tag{6.1}
$$

where :

$$
\begin{aligned}
f_1(x) &= \begin{cases} ax^3 - bx^2 & \text{if } x < 0 \\ -(m + 0.6(z-4)^2)x & \text{if } x \geq 0 \end{cases} \\
f_2(z) &= \begin{cases} -0.1z^7 & \text{if } z < 0 \\ 0 & \text{if } z \geq 0 \end{cases} \\
H(x,\theta) &= \begin{cases} 1 & \text{if } x \geq \theta \\ 0, & \text{if } x < 0 \end{cases} \\
S(x) &= \frac{1}{2} e^{-|x|}
\end{aligned}
\tag{6.2}
$$

The state variables x and y describe the activity of neural populations on a fast time scale and can model fast discharges. The oscillation of the slow permittivity variable z drives the system autonomously between ictal and interictal states. The parameter x_0 indicates the degree of excitability and directly controls the dynamics of the neural population to produce seizures or not. Each vertex i is connected locally through homogeneous connections and globally through heterogeneous connections to other parts of the brain. Although local connections are actually heterogeneous with a complex variability of interneurons and dendritic arborization, due to lack of personalized measurement in clinical routines, we made an assumption of homogeneity in the local connections while considering only geometric features of brain surface. Local connections, parameters with the subscript hom, are described by a translationally invariant Laplacian coupling kernel $S(g_{i,j})$ where $g_{i,j}$ denotes the geodesic distance along the cortical mesh between vertices i and j. Additionally, global connections, parameters with the subscript het, along white matter fibers, are accounted for by the connectome matrix, where $W_{k,l}$ is the connection strength between brain areas k and l. Each vertex i is assigned to a brain area $k = 1, ..., L$ according to a cortical parcellation. For this study we used the VEP parcellation. The average neural activity X_l of all vertices belonging to area l is coupled throughout the network and projected uniformly to all vertices of area k. The default parameters of the system are $I_{ext} = 3.1, c = 1, d = 5, r = 1, a = 1, m_{thresh} = 1.8, \gamma_{het} = 0.1, \gamma_{hom} = 0.8, \theta_{het} = -1, \theta_{hom} = -1$. The time varying input I_{stim} describes the perturbation signal in each time step depending on stimulation parameters. To accomplish this, we computed the generated electric field from the two types of perturbation a) an invasive SEEG stimulation, and b) a non-invasive TI stimulation. These are described in two separate subsections below.

6.4.4 Calculation of the electric field of SEEG stimulation

The SEEG stimulation is applied to a pair of neighboring sensors, in which one acts as a cathode and the other one as an anode. This generates a bipolar pulse perturbation in the area where the electrodes are located. However, the effects of the stimuli are not only local, because they can propagate through short-range and long-range connections towards other brain areas. The parameters used clinically are restricted to frequencies of either 1 Hz or 50 Hz, weak amplitudes ranging from 0.1 to

3 mA, and pulse widths of 500 – 2000 microseconds. We modeled the same stimulus as had been applied clinically on a personalized digital brain model of the patient. Using the reconstructed brain structure and the overlayed SEEG electrodes, we generated a bipolar signal using the stimulation parameters for the pair of electrodes chosen by the clinician. We then mapped the stimulus signal onto the parcellated brain areas based on the distance, which resulted in an estimated electric field across the brain regions. We used this estimated field as an input to the I_{stim} parameter and simulated the time series on selected vertices from the EZ.

6.4.5 Calculation of the electric field of the TI stimulation

Non-invasive stimulation with TI is a recent method that aims to mimic DBS's capabilities to be both focal and sub-cortical without being invasive. This is done using the assumption that high frequencies (above 500 Hz) have an ignorable effect on neuronal activity [47, 48]. By combining multiple fields of very high-frequency tACS stimulations, such that they interfere maximally in the target of choice, a new electric field can be generated, which modulates at much lower frequencies (e.g. two fields of 1000 and 1050 Hz modulate at 50 Hz at the target of choice). The generated electric field was computed using SimNIBS, as described previously, to compute the generated tACS fields. Then, the vectorial tACS fields are added together, resulting in a TI field estimate for the brain regions. We used this estimated field as an input to the I_{stim} parameter and simulated the time series on one selected vertex from the EZ.

To obtain the distribution of the TI field in the gray matter, we started by computing the electric field distribution from the simulation of a transcranial direct current stimulation (tDCS) via SimNIBS [113]. First, we reprocessed the individual T1-weighted MRI via the SimNIBS process "mri2mesh", which resulted in the segmentation into five head tissues : white and gray matter, cerebrospinal fluid, skull, and scalp. This process creates the tetrahedral meshes necessary for the finite element method (FEM) for the simulation of the electric field distribution. We computed the tDCS field for each pair of electrodes positioned based on the location of the co-registered 128 electrodes EEG cap, using the 10-5 system. Circular electrodes with a diameter of 10 mm and a thickness of 5 mm were directly applied on the head. Then, we projected these electric fields onto the resampled Freesurfer surface (20484 vertices). We extracted the amplitude of the electric field at each vertex of the cortex surface. These fields derived from the coupled electrodes pairs were then modulated by multiplying them with two sinusoids with the frequency of 1000 Hz and 1005 Hz, respectively, for 1 second. Two oscillatory electric fields, which were linearly summed, provided an interference field. To obtain a correct representation of the high frequency activity, the sampling rate was 30 kHz. We extracted the 5 Hz peak envelope by using spline interpolation. Finally, we included this envelope in the virtual brain model as the source of external simulation for the cortex vertices (20484). For this patient, we targeted the highest TI stimulation effect on the left O2 in the VEP atlas [140]. We used the optimization process in SimNIBS to identify the best 4 electrodes configurations (10-5 EEG montage), which maximized the electric field in the left O2. This procedure allowed us to identify, in our case, PPO3-PPO5

and P5h-PO5h ([91]) as the best electrodes couple for the left-O2 stimulation.

Chapter 7

Applications to clinical data

In this short chapter I would like to present two ongoing projects :

(i) The first project uses a small but thorough dataset to evaluate our modeling approach with seizures triggered by SEEG stimulation. I will introduce the dataset, the main goals of our approach, and the progress made so far. However, I would like to emphasize that there is still a lot more to be done, but the writer of this thesis is excited to have empirical data to work with at the moment.

(ii) In the second part, I describe my contribution to the clinical trial Epinov, which began before my PhD and will continue after my thesis. This clinical trial aims to improve surgical prognosis in drug-resistant epilepsy by using computational modeling approaches in estimating the epileptogenic zone. I had the chance to be part of the team responsible for running the VEP pipeline and produce patient reports of estimated epileptogenic zones. I will describe this pipeline and my contributions.

7.1 Optimizing the stimulation model based on empirical data

7.1.1 Context and project goal

Introduction

As we have mentioned in previous chapters, patients with drug-resistant epilepsy who are candidates for brain surgery treatment undergo SEEG implantation. The average recording duration with SEEG is 8.5 days [59]. Brain activity is recorded and spontaneous seizures are expected to occur, which are precipitated under progressive antiepileptic drug withdrawal [59]. After recording spontaneous seizures, intracerebral electrical stimulation is performed for (1) reproducing ictal clinical expression and (2) performing functional mapping of brain areas surrounding the electrodes. Here, we focus on the first aspect of this modality. According to French guidelines on SEEG, the intensity of stimulation and the consequent electroclinical response can be used to evaluate the tissue's excitability [59].

Objectives

As a first objective, we aim to (i) build personalized virtual brain models for each patient and compare their EZ hypothesis to the stimulation outcomes. This first step aims to give a preliminary overview of the predictive potential of our personalized brain modeling approach. As a second step, we aim to (ii) use the same clinically applied stimulation parameters in-silico, and compare the simulated response to the empirical response. Finally, we aim to (iii) build an algorithm for optimal and personalized stimulation parameters for drug-resistant epilepsy diagnosis.

7.1.2 Methods

Estimating the electric field

To estimate the electric field from SEEG stimulation, we use Maxwell's equations. Since the electric field is induced using two adjacent contacts with opposite identical charge $q_+ = q$ and $q_- = -q$, they form an electric dipole. Given the locations for the two charges are in $\vec{r_+}$ and $\vec{r_-}$, the electric field at any location $\vec{r}$, is :

$$\vec{E}(\vec{r}) = \frac{q_+}{4\pi\epsilon}\frac{\vec{r}-\vec{r_+}}{|\vec{r}-\vec{r_+}|^3} + \frac{q_-}{4\pi\epsilon}\frac{\vec{r}-\vec{r_-}}{|\vec{r}-\vec{r_-}|^3} = \frac{q}{4\pi\epsilon}\left(\frac{\vec{r}-\vec{r_+}}{|\vec{r}-\vec{r_+}|^3} - \frac{\vec{r}-\vec{r_-}}{|\vec{r}-\vec{r_-}|^3}\right)\ [V/m] \quad (7.1)$$

Neural mass models

When performing whole-brain simulations with neural mass models, we represent each brain region as a point-like source, located at the centroid of that brain region's volume. A neural mass model (ordinary differential equation evolving in time) is placed in each of these brain nodes. The brain nodes are then connected following connection weights from the structural connectome. Here, we used the VEP atlas parcellation, with 162 brain regions [140]. We estimated the electric field magnitude at each brain region centroid using the formula shown above (see also Figure 7.3). Therefore, the main parameter to take into account was the distance of each brain source to the stimulating electrode pair.

Neural field models

When performing whole-brain simulations with neural field models, the cortical geometry is taken into account, by employing the gray matter surface mesh. Here, a neural field model (partial differential equation evolving in space and time), is placed in each vertex of the cortical mesh. Only the subcortical structures here are represented as point-like sources. We estimated the electric field magnitude at each vertex of the cortical and subcortical mesh. This resulted in much more focal field distributions (see Figure 7.1).

Simulating brain network response to stimulation

To simulate the brain stimulation response, we used the estimated electric field to model the impact of the external stimulus on each brain node. Then, we simulated a bipolar biphasic pulse waveform using the clinical parameters of frequency,

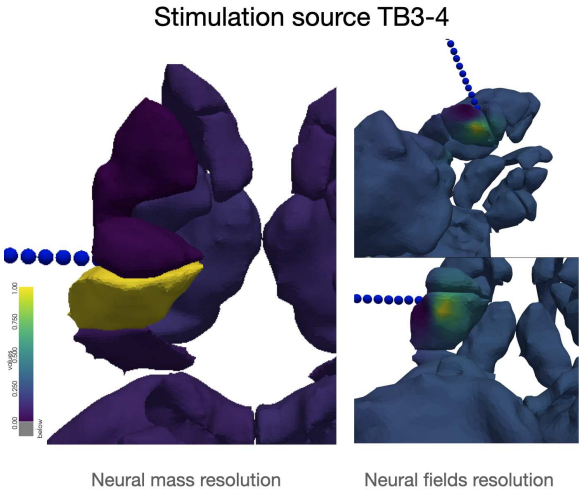

FIGURE 7.1 – Estimations of generated electric field via stimulating electrode TB3[+]-TB4[-]. On the left, the stimulation electric field is mapped to brain region sources corresponding to a single point source. On the right, the stimulation electric field is mapped onto vertices of each brain region's surface mesh.

amplitude, pulse width and duration to vary the external stimulus in time. Then, we ran simulations using this external stimulus applied to the Epileptor-stimulation model to compute a phenomenological response on the whole-brain level. The response was dependent on the interaction between the applied stimulation, the EZ network configuration and the structural connectivity. We compared the simulated outcome to the empirical one in simple binary terms of (0) no seizure induced or (1) seizure induced.

Estimating the EZ network using MCMC

To estimate the EZ network,we employed Markov-Chain Monte Carlo Bayesian inference, a method known for its accuracy, though it can be time-consuming for inferring the posterior distribution of regional excitability x_0 and global coupling K values. Here, we fitted 3 spontaneous seizures from patient 1. We took the median value from each estimated parameter distribution to inform our personalized virtual brain model.

7.1.3 Preliminary results

Empirical dataset

Here, we describe an empirical cohort containing for each patient the complete set of recorded SEEG stimulations and subsequent brain responses. An overview of the empirical dataset is provided in table 7.1.

We built virtual brain twins for 5 epileptic patients, who underwent 1363 stimulations, of which 18 triggered seizures. We systematically investigated the relationship between stimulation parameters and epileptogenic zones. By comparing simulation

ID	Sex	Age	Epilepsy type	MRI	Histopathology	Side	SS	Stimulations	SIS	Engel Class
1	M	53	Temporal	Normal	HS	R	3	158	4	I
2	F	38	Temporal	PNH	FCD1	R>L	3	214	2	I
3	M	20	Fronto-temporo-insular	DNET	DNET	R	3	600	3	II
4	M	31	Temporal	Normal	Mild gliosis	R	2	157	2	I
5	F	21	Prefrontal	Suspected FCD	Mild gliosis	R	2	238	5	II

TABLE 7.1 – Overview of the empirical dataset. SS : spontaneous seizures, SIS : stimulation-induced seizures, HS : hippocampal sclerosis, FCD : focal cortical dysplasia, DNET :dysembryoplastic neuroepithelial tumor, M :male, F :female, R :right, L :left.

results with the outcome of empirical stimulations, we refined the virtual brain twins. This also paved the way to aid clinicians in optimizing stimulation parameters.

Comparing the EZ to the stimulation fields

As a first step, for each patient we grouped stimulations that induced a seizure and stimulations that did not induce a seizure. We visualized the electrode pairs for each stimulation over the reconstructed SEEG electrodes in red in figure 7.2. We also weighted each visualized electrode pair by stimulation amplitude. Additionally, we visualized estimated epileptogenic regions from the VEP pipeline in blue.

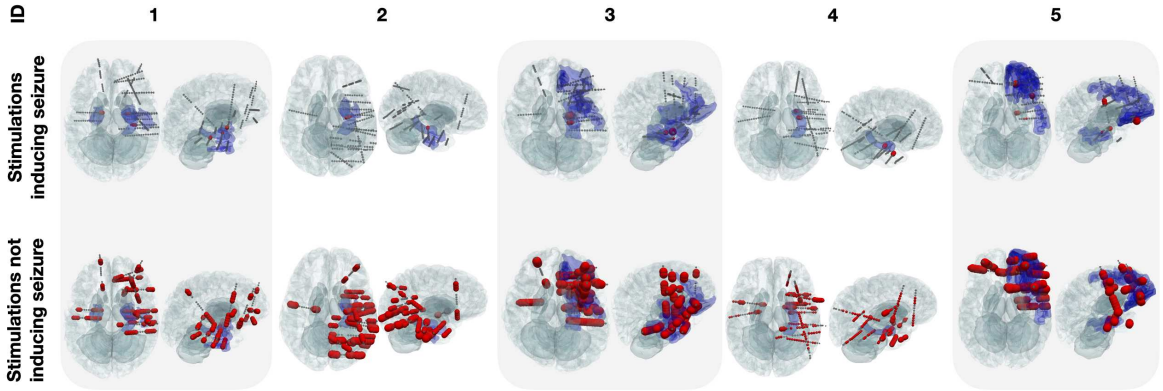

FIGURE 7.2 – Comparison of clinical stimulation electrodes in cases where seizures were triggered versus when seizures were not triggered. In red spheres, SEEG contacts where stimulation was applied are shown. The sphere radius is proportional to the stimulation amplitude. The EZ regions estimated from the VEP pipeline are shown in blue.

Then, we estimated the stimulation weights of each stimulation pair onto the parcellated brain regions using the VEP pipeline in Figure 7.3. The stimulation weights corresponded to electric field magnitudes computed between stimulating electrode pairs and brain region centroids. We summed the normalized stimulation weights of each stimulation session and plotted the estimated fields over the brain region volumes.

We performed the same procedure but using high-resolution brain meshes and computing the electric field magnitudes between stimulating electrodes and each vertex of the brain mesh in figure 7.4.

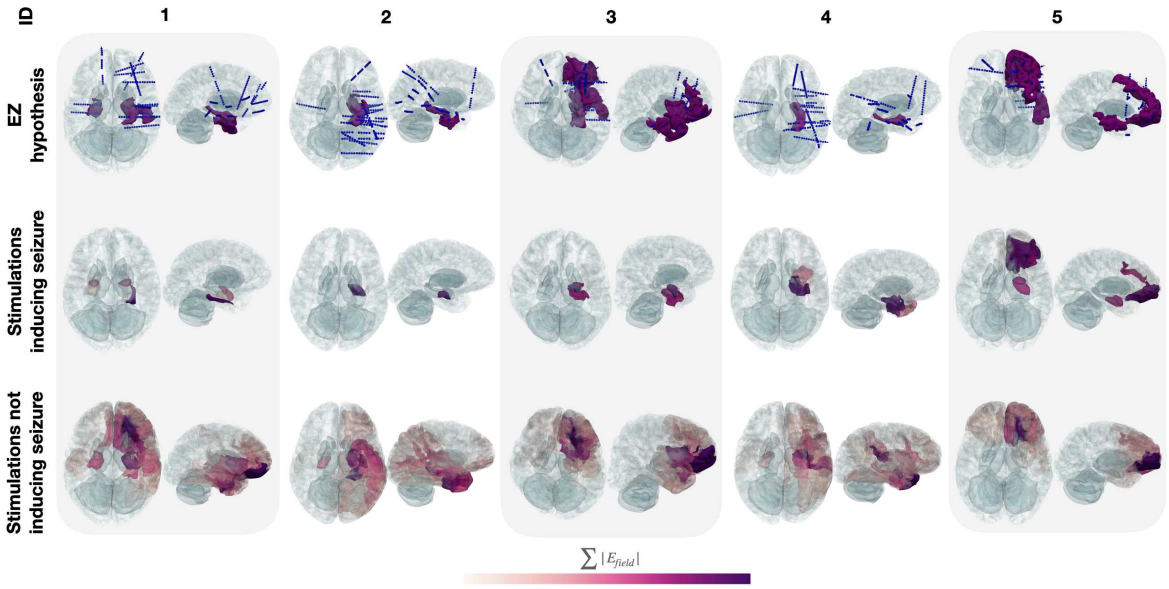

FIGURE 7.3 – In this figure, we illustrate over the reconstructed brain mesh for each patient, their EZ hypothesis from VEP estimation, the summed electric field magnitudes of stimulations that induced a seizure versus those that did not induce a seizure.

Performing simulations and comparing to empirical stimulation outcomes

Using the estimated epileptogenic zone (EZ) and global coupling parameter (K) distributions, we parametrized the virtual brain model for patient 1. Simulations were run for each clinical stimulation setting using whole-brain neural mass modeling, and the outcomes (seizure triggered or not) were compared with the empirical data. Figure 7.5A demonstrates the parameter estimation based on the first spontaneous seizure, while Figures 7.5B and 7.5C show similar estimations using the second and third spontaneous seizures, respectively.

We showed in more detail one example of simulated seizures in Figure 7.6, where each number corresponds to a successful seizure trigger in the simulated data. The right panel illustrates the whole-brain simulated time series, identifying the brain region where the seizure was initiated. We detected when the slow-evolving parameter m crossed the seizure threshold, marking the onset of seizure activity, to automatically compute in the simulated data whether a seizure was triggered.

7.1.4 Conclusion

By building personalized virtual brain models for each patient, we systematically compared empirical SEEG stimulation outcomes with the results of in-silico simulations for one patient. This allowed us to refine the virtual models and better understand the relationship between stimulation parameters and seizure generation. The next steps involve testing the same approach using neural field models over all patients. Moving forward, our final goal is to optimize stimulation parameters for epilepsy diagnosis and treatment, providing a framework for more personalized

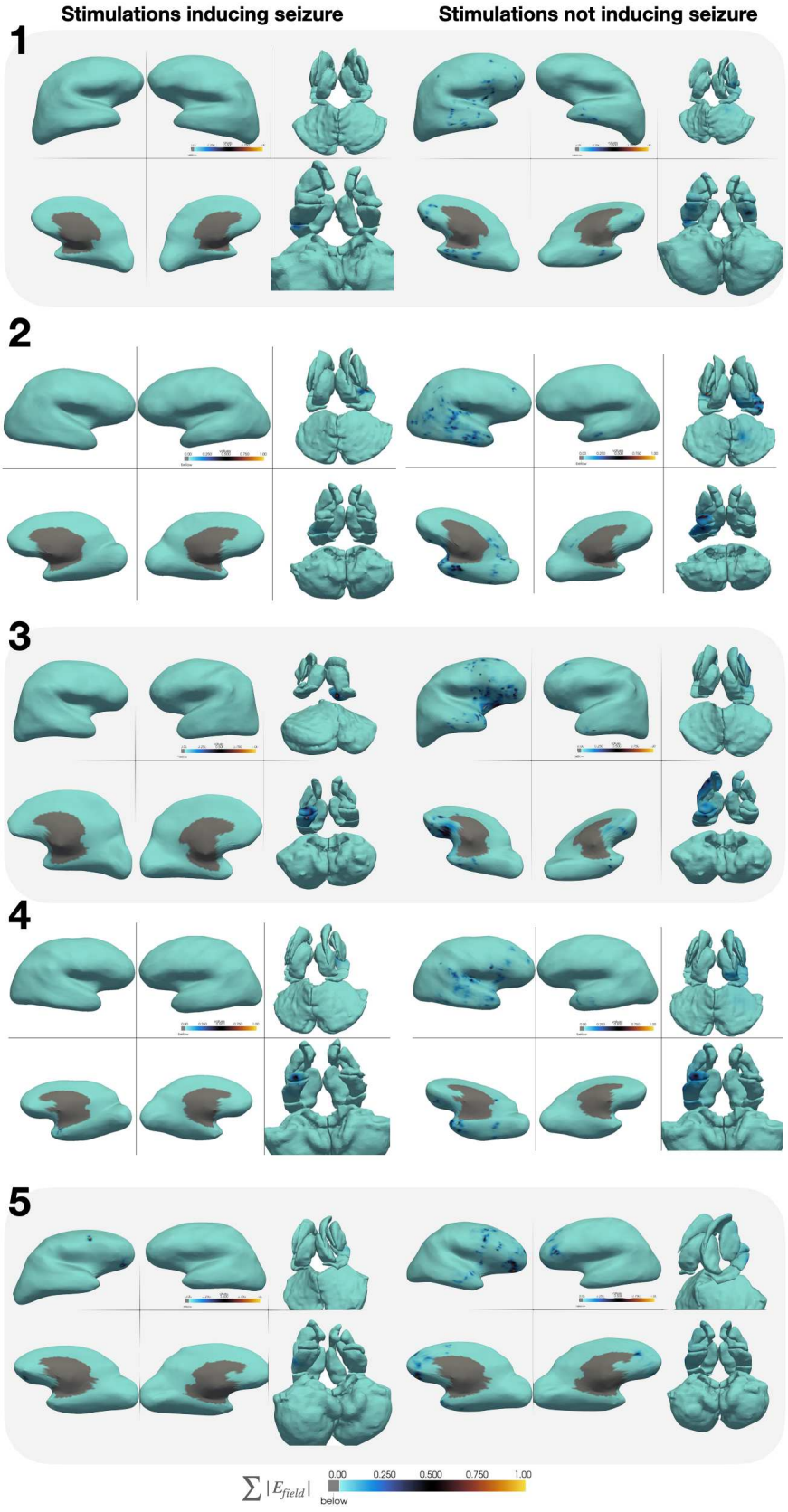

FIGURE 7.4 – In this figure, we illustrate over the reconstructed inflated brain mesh for each patient, the high-resolution summed electric field magnitudes of stimulations that induced a seizure versus those that did not induce a seizure.

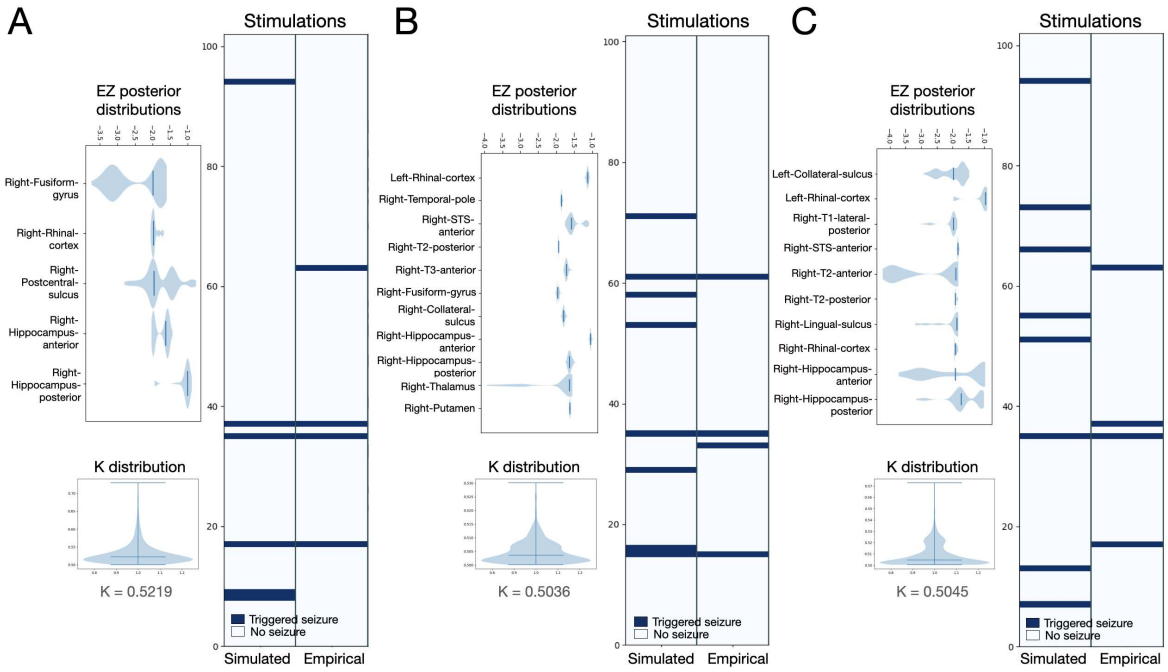

FIGURE 7.5 – Using estimated EZ and global coupling K distributions, we parametrized our virtual brain model for patient 1. We then ran simulations for each clinical stimulation setting and compared the outcome with the empirical data. The panel "Stimulations", compares the outcome between simulated timeseries and empirical recordings in terms of triggered seizures (dark blue) or no triggered seizure. In A), we estimated the aforementioned parameters using the first spontaneous seizure of the patient. In B), we used the second spontaneous seizure of the patient, and in C) their third spontaneous seizure.

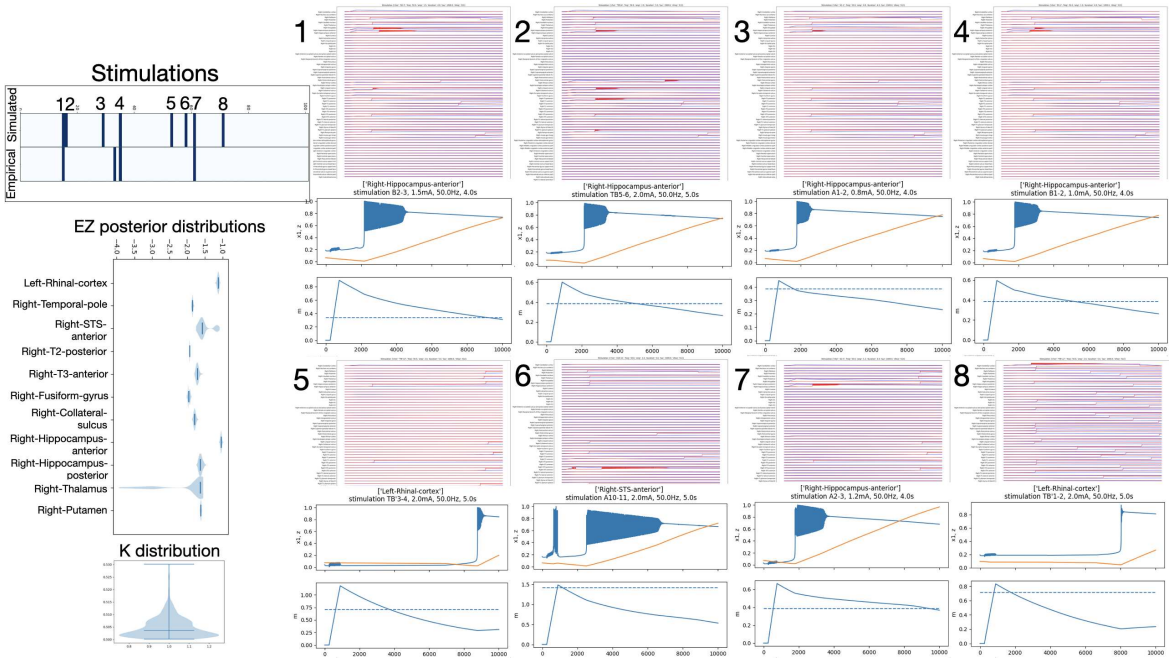

FIGURE 7.6 – One example of simulations performed. Each number corresponds to a simulation where a seizure was triggered. On the right, we show the simulated time-series on the whole-brain level and plot the region where the seizure was triggered, alongside the slow-evolving parameters, in particular m which crossed the seizure threshold.

approaches in clinical settings.

7.2 Clinical trial Epinov

7.2.1 Context and project goal

Currently, people suffering from drug-resistant focal epilepsy can be treated mainly via resective brain surgery. However, seizure freedom rates are around 50%. The clinical trial EPINOV (Improving Epilepsy Surgery Management and Prognosis using Virtual Epileptic Patient Software) started in France in 2018, with its main goal to improve epilepsy surgical prognosis. Its approach centers around the combination of patient-specific imaging data within one virtual brain model and simulating seizure dynamics to estimate the networks responsible for seizure generation in a personalized fashion [63, 142]. The trial included a total of 356 participants from multiple French health centers (Marseille, Lyon, Toulouse, Bordeaux, Lille, Strasbourg, Paris, Grenoble, Nancy and Rennes). Preliminary results from the trial are shared in [142].

7.2.2 Methods

In figure 2.10, the VEP pipeline which was used to estimate the epileptogenic zones for each patient is provided. The pipeline combines patient-specific brain imaging scans (T1-MRI, DW-MRI and CT-scans) within a personalized virtual brain model. Here's a rephrased version of your passage :

The pipeline began by integrating structural brain imaging to create a personalized virtual brain model. Specifically, a brain atlas was mapped onto the T1-MRI to segment the brain into distinct regions. Next, DW-MRI was utilized to estimate the white matter fiber bundles connecting these regions, resulting in a unique whole-brain network model for each patient.

The Epileptor model was applied to each brain region to simulate brain dynamics. SEEG electrode locations were reconstructed using CT scans. Seizure SEEG recordings provided envelope data features, which were then compared to simulated data from the virtual brain model. This allowed for the estimation of excitability parameter distributions for each Epileptor model, which were classified as either epileptogenic or non-epileptogenic in the clinical report. Additionally, virtual surgery could be simulated by severing connections between epileptogenic areas and the rest of the brain, enabling a comparison of brain dynamics before and after surgery.

7.2.3 My contributions to the clinical trial

Here I will describe my involvement in this clinical trial during my PhD period. I was part of a team that used pre-collected patient data from multiple French hospital centers to run the VEP pipeline for each of them. This pipeline had already been implemented and running when I arrived.

Typically, processing a patient's brain imaging data to obtain clinical reports of estimated epileptogenic zones took a few days. The longest computations, which took several hours were : (1) the FreeSurfer recon-all pipeline, which extracted brain anatomical features and performed brain parcellations using the VEP atlas [140],

(2) the tractography estimation and computation of the structural connectome ; and (3) the inference algorithm, which ran parallel processes or chains, to obtain parameter distributions of the virtual brain model that best matched the extracted data features from the SEEG signal. However, both steps were automatic to run for most patients. However, some patients had lesions in their MRI scans, which would make steps (1) and (2) more complicated. For instance, brain lesions inside the white matter would make it confusing for FreeSurfer to make proper distinctions between gray and white cortical volumes. This would also impact the structural connectome estimation, which used gray matter volumes to estimate the links between different brain regions via white-matter pathways. In some rarer cases, patients had already undergone a first brain surgery before enrolling in the trial. In such cases, the parcellation process of step (1) would automatically assign all brain regions to all estimated brain volume in the MRI. Such cases would take longer to deal with and at times were excluded from the trial. Lesional or post-surgical MRIs are still not easy to process automatically, and there is still progress to be made in this direction. We also involved several interns during this period to tackle these problems.

The only step which was semi-automatic, involved the extraction of data features from the seizure recordings with SEEG. This was because of physiological signal artifacts which required human inspection but also due to the large variety of seizure dynamics across patients. Slight adjustments in frequency range to obtain the signal envelopes were required for data features to properly capture seizure dynamics in a 2D-Epileptor fashion. For instance, depending on the seizure length, the same low-pass filter could give a very noisy envelope in longer seizures and a very smooth envelope for shorter seizures. In addition, some channels could show high-frequency activity without there being any seizure, due to other physiological activities that can also occur at similar frequencies as seizures. In those cases, we made sure these channels would not bias the inference algorithm when estimating priors.

In conclusion, I built personalized virtual brain models (automatic), extracted data features from SEEG seizure recordings (semi-automatic), and fit them against simulated data using Bayesian inference methods (automatic). I have done this for about 50 out of 356 enrolled patients of the trial. This resulted in estimated excitability and global coupling parameter distributions [142]. The distributions of regional excitability were then converted to clinical reports of epileptogenic regions proposed by the VEP, alongside a heatmap of those regions overlaid on the T1-MRI of the patient.

Chapter 8

Personalized whole-brain modelling of status epilepticus

Abstract

How status epilepticus (SE) is generated and propagates in the brain is not known. As for seizures, a patient-specific approach is necessary, and the analysis should be performed at the whole brain level. Personalized brain models can be used to study seizure genesis and propagation at the whole brain scale in The Virtual Brain (TVB), using the Epileptor mathematical construct. Building on the fact that SE is part of the repertoire of activities that the Epileptor can generate, we present the first attempt to model SE at the whole brain scale in TVB, using data from a patient who experienced SE during presurgical evaluation. Simulations reproduced the patterns found with SEEG recordings. We find that if, as expected, the pattern of SE propagation correlates with the properties of the patient's structural connectome, SE propagation also depends upon the global state of the network, i.e. that SE propagation is an emergent property. We conclude that individual brain virtualization can be used to study SE genesis and propagation. This type of theoretical approach may be used to design novel interventional approaches to stop SE. This paper was presented at the 8th London-Innsbruck Colloquium on Status Epilepticus and Acute Seizures held in September 2022.

8.1 Introduction

Status epilepticus (SE) is a condition resulting either from the failure of the mechanisms responsible for seizure termination or from the initiation of mechanisms, which lead to abnormally, prolonged seizures. SE can have long-term consequences, including neuronal death, neuronal injury, and alteration of neuronal networks, depending on the type and duration of seizures [130]. SE is a potentially life-threatening neurological emergency that requires intensive care [19]. Although stereoelectroencephalographic (SEEG) recordings of SE are rare, they indicate the involvement of distributed networks [57]. The exact mechanisms underlying SE initiation and propagation remain unknown. Their understanding is crucial for developing individualized therapeutic interventions. A mechanistic approach to stop a focal-onset

SE requires knowing where/how the respective prolonged seizure activity starts and propagates in the brain. We present a first step in this direction.

Since the problem needs to be addressed at the whole brain scale with a high spatial and temporal resolution, the only presently available solution is to use a modeling approach. The Virtual Brain (TVB) platform allows to study seizure genesis and propagation in silico in an individual manner [35, 66, 81]. Anatomical MRI and DTI from a patient are used to create an avatar of the patient's brain [66]. Generative models, such as the Epileptor [67, 87], can then be used to study seizure genesis and propagation, and make predictions with respect to the size and location of the epileptic zone [98].

The Epileptor includes two major parameters, which when varied, allow the Epileptor to generate different patterns of activities, including seizure-like, SE-like and depolarizing block-like events [33, 34]. With ad hoc parameter values, it is thus possible to study SE genesis and propagation in silico. Here we leverage the data recorded in a patient, who experienced an SEEG-recorded SE during the presurgical evaluation. This patient was enrolled in the French ongoing multicenter clinical trial EPINOV (NCT03643016) aiming to estimate the potential impact of the virtual epileptic patient (VEP) brain modeling on improving surgical prognosis in patients undergoing SEEG [81]. Patients undergo high resolution MRI to construct an avatar of their brain. TVB simulations, guided by SEEG recordings, generate predictions regarding the extent of the epileptogenic zone in terms of the epileptogenic brain regions, which are listed in the clinical report and represented on a heatmap in patient's anatomy.

Here we show that SE can be reproduced in TVB with properties similar to those recorded with SEEG recordings. SE propagates in the brain under the constraint of the structural connectome.

8.2 Results

8.2.1 Virtualizing Status Epilepticus Patient

Using the patient's brain imaging data we build a personalised virtual brain model (see Figure 8.1). First, from the T1-weighted MRI (T1-MRI) we extract the patient's brain structure and reconstruct it in 3D space. We overlay the VEP atlas [140] on the reconstructed brain in order to parcellate it into 146 cortical and 16 subcortical brain regions. Each brain region is then represented as a point source. Second, the diffusion-weighted MRI (DW-MRI) is used to estimate the length and density of white matter fibres. We group the fibres according to parcellated brain regions from the VEP atlas to compute the connection strength between areas. This region-to-region connectivity is used to inform connection strength between point sources in the virtual brain network model. Thirdly, we use the patient's post SEEG implantation CT scan to reconstruct the electrode locations in the brain. Finally, we equip this brain network structure with dynamics using mathematical models called neural mass models. The model describes the electrical brain activity of a population of neurons within a region. The neural masses are connected to each other according to the structural connectivity. This allows for complex interactions

between nodes which gives rise to whole-brain dynamics. Here, we use the Epileptor model [67, 87], which can generate seizure-like and SE-lile events [33, 34]. The clinical analysis of SEEG recordings (e.g. the onset zone of the seizure) is used to inform the model's excitability parameter x0, which determines, together with the structural connectivity, where in the brain seizures occur and how they propagate.

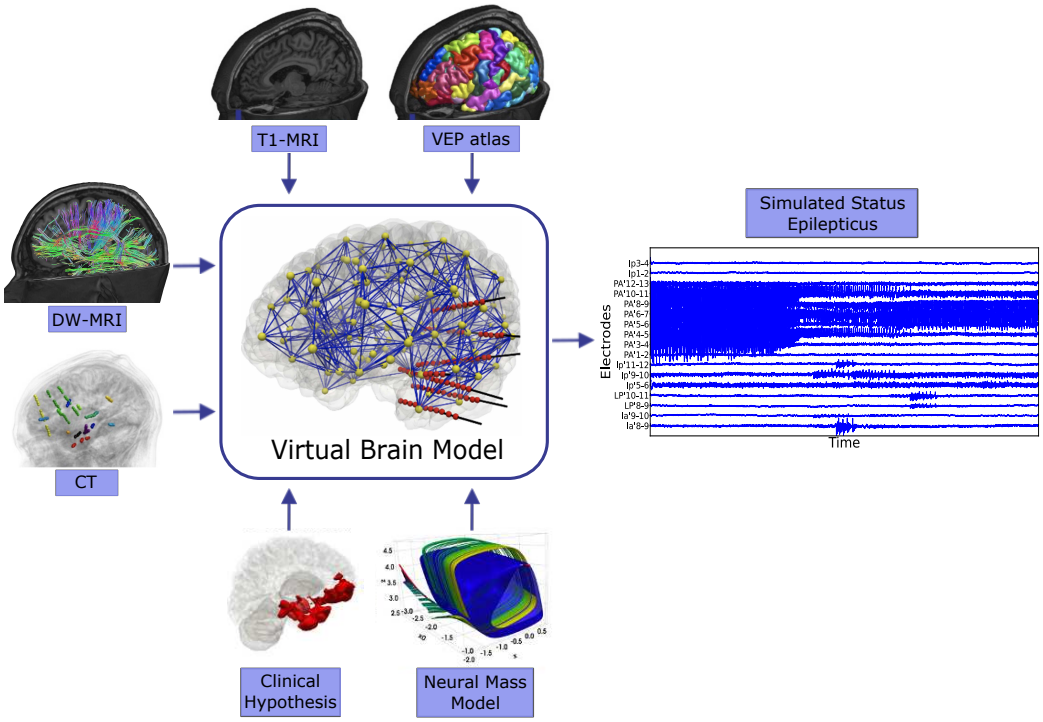

FIGURE 8.1 – We built a personalised brain model for a patient with status epilepticus. A T1-weighted MRI (T1-MRI) is used to extract the individual brain geometry. The distinct brain regions are defined by overlaying the VEP atlas on the T1-MRI, represented as point sources (nodes in yellow). From diffusion weighted MRI (DW-MRI), tractography is performed to estimate the length and density of white matter fibres. By grouping the fibres according to regions obtained from the VEP atlas a structural connectivity matrix is computed, which represents the connection strength between brain regions (edges in blue). From a post-SEEG-implantation CT scan, the SEEG electrode coordinates are reconstructed (in red). The SEEG coordinates are used to compute the source-to-sensor map using the so-called gain matrix. To represent the brain dynamics, in each point source a neural mass model is placed. The neural masses are connected to each other according to the structural connectivity. The clinical hypothesis for the epileptogenic zones informs the model's excitability parameter. A whole-brain simulation of the neural mass network is performed and mapped onto the reconstructed SEEG electrodes. Simulated SEEG time series of SE-like dynamics are plotted.

8.2.2 Status Epilepticus Network Dynamics

During the ten days-long video-SEEG monitoring, the patient presented a single spontaneous, focal onset seizure, evolving into a non-convulsive and then a convulsive SE, with a total duration of 68 min (Figure 8.2). Of note, this seizure recorded under partial tapering of the antiseizure medication, represented his habitual seizures, which tended to evolve to SE in the majority of instances. Electrically, the seizure started with a focal rhythmic polyspikes discharge within the anterior part of the left supramarginal gyrus (contacts PA'10-14) and the adjacent left postcentral sulcus (contacts Ip'9-13), which extended few min later to the left postcentral gyrus, with secondary involvement 20 min later of the left primary sensory-motor regions and the central and parietal operculum, followed by the ipsilateral premotor cortex, the posterior insula, and the left pulvinar. The quantitative SEEG signal analysis using the Connectivity Epileptogenicity Index, cEI [8], showed maximal epileptogenicity values within the left postcentral sulcus and the anterior part of the left supramarginal gyrus. Therefore, the hierarchy of the epileptogenic and the propagation networks was clearly present in the empirical SE dataset. Here we demonstrate this hierarchical organization of subnetworks involved in the initiating and propagation of ictal activity during the focal-onset SE in our virtual brain model by simulating the SE network dynamics. We observe that SE propagates in silico following the strongest estimated white matter connections within left parietal regions where the seizure starts but also between parietal regions and sensory-motor regions, subcortical regions (such as thalamus) and temporal regions (such as insula) (see Figure 8.3 and Figure 8.4).

First, we use the Epileptor model's capability of simulating SE, which in the model co-exists with seizures (i.e. SE and seizures are two different attractors, which exist in the same parameter space). El Houssaini et al. [33, 34], used specific parameters (in particular x0 and m) and showed that only by changing initial conditions, the simulated dynamics converged towards either seizures or SE. Following that study, we chose parameters to model SE in our virtualized patient (see Methods). We used a set of parameters to illustrate the propagation pattern. By slightly changing the parameters we can obtain a self-sustained SE (Supplementary figure 8.8).

We set high excitability x0 values for clinically estimated areas where the seizure recorded in the patient started, namely, the Left-Postcentral-gyrus and the Left-Postcentral-sulcus. We then set the following regions of the left hemisphere close to critical threshold for seizure onset but not enough for a seizure to start spontaneously : Supramarginal-posterior, Central-sulcus-head-face, Precentral-gyrus-upper-limb, Precentral-gyrus-head-face, Central-sulcus-upper-limb, F2-Caudal.

We run the simulations in TVB using a deterministic Heun integrator with time step 0.1 (see Supplementary figure 8.7). The time series obtained by the simulation are mapped onto the SEEG electrodes by a matrix multiplication with the source-to-sensor gain matrix. The simulated time series and the empirical recording of SE are shown in Figure 8.2a. The simulated SE starts in the same regions (the Left-Postcentral-sulcus and Left-Postcentral-gyrus), and, later, propagates to other regions.

The Epileptor describes seizure dynamics, which accounts for relative changes in signal frequency and amplitude, and not for their absolute value [67, 87], which

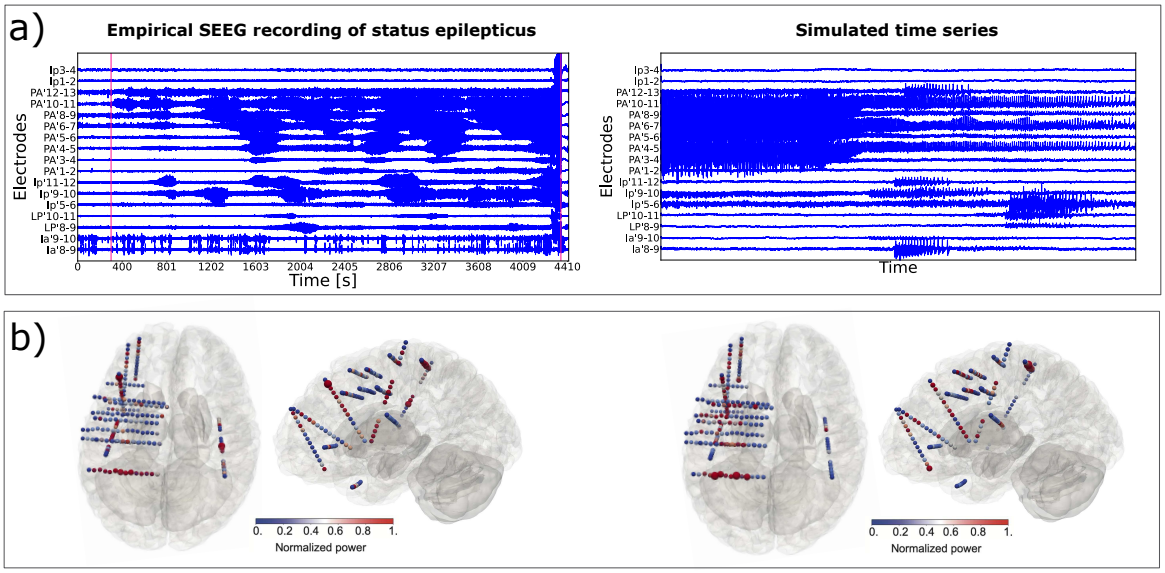

FIGURE 8.2 – a) On the left, SEEG electrode recording of SE. Red vertical lines indicate start and end of status epilepticus, which lasted for about 67 minutes. On the right, simulated status epilepticus like event using the Epileptor model. b) SEEG signal power across reconstructed electrodes is shown for both empirical (left) and simulated (right) SEEG time series. The signal power is normalized between 0 and 1. The colormap displays the SEEG channels with the highest signal power in red. The radius of each SEEG electrode is proportional to its signal power.

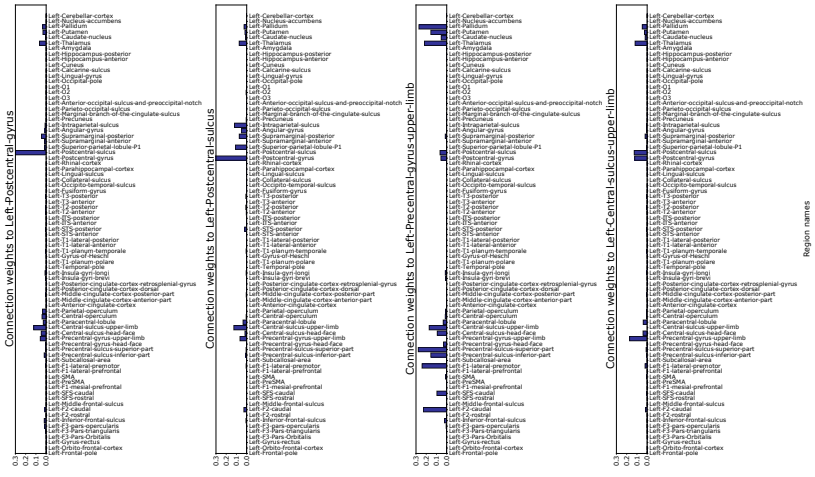

FIGURE 8.3 – Connection strengths to some main regions of the left hemisphere where refractory status epilepticus dynamics are observed. From left to right : Postcentral gyrus, Postcentral sulcus, Central sulcus upper limb, Precentral gyrus upper limb.

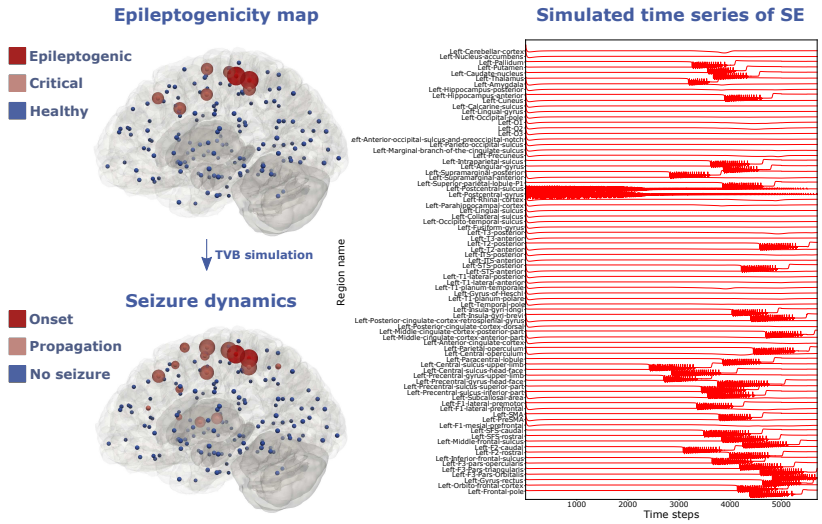

FIGURE 8.4 – Epileptogenicity map of x0 values on the 162 brain regions parcellated according to the VEP atlas. For epileptogenic zones, x0=-1.6, for zones close to the critical threshold for firing, x0=-2.1, for healthy zones x0=-2.2. Below, emerging spatiotemporal seizure dynamics from the combination of x0 parameter values and the structural connectivity, simulated with TVB. The radius of the point-like sources reflects the temporal evolution of the seizure (radius decreases as time increases). On the right, time series of the simulated SE on the brain region level. Time series are shown for all regions of the left hemisphere, there was no epileptogenic activity on the right hemisphere.

explains why absolute frequency and amplitude values appear different between empirical and simulated SE in Figure 8.2a. However, the signal power distribution of both empirical and simulated data is similar (Figure 8.2b), further supporting that the model captures the main features of the empirical SE.

We investigated the regions connected to the left Postcentral-sulcus and the left Postcentral-gyrus and observed that both the empirical and the simulated propagation patterns involve the regions connected to these two seizure onset areas (Figure 8.3). Importantly, the two onset regions are highly connected to each other. They have also strong connections with the left Central-sulcus-upper-limb, where the seizure first propagates in the simulated time series and the electrodes that sample this region show early seizure propagation in the empirical SEEG recordings. The recruitment of regions increases stepwise with time until it reaches most electrodes located within the left hemispheric parietal, motor-premotor, prefrontal and insulo-opercular corticies as well as within the sampled right hemispheric insulo-parietal regions, shortly before the SE termination. This is also reproduced in our simulation (Figure 8.4). A complete depiction of the complex connections between the regions is shown in Figure 8.5 (see also Supplementary figure 1).

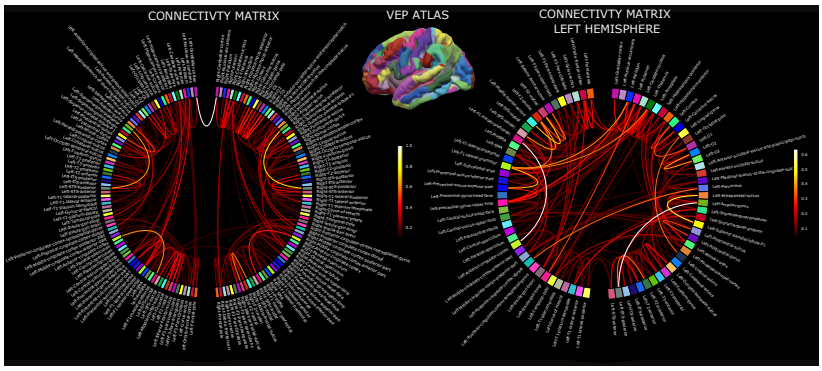

FIGURE 8.5 – Circular graph of 300 strongest region-to-region connection strengths for both hemispheres (left) and only for the left hemisphere (right). (Top center) VEP atlas is used to define the brain regions. The epileptogenic regions Left-postcentral-gyrus and Left-postcentral-sulcus are highly connected to each other. They also connect to regions of the sensory-motor cortex, which are highly connected to sub-cortical regions such as Left-Thalamus. Thus, we can observe the pathways for seizure propagation in the left hemisphere connectivity matrix.

8.3 Discussion

The present work shows the capability of personalised whole brain models in capturing SE propagation dynamics. However, there are a few limitations which we aim to address in future works.

First, the model is parametrized from one observation, thus choosing one set of excitability values over the regional map. However, neural mass models such as the Epileptor are shown to be degenerate [62], where multiple parameter configurations give rise to the same output. Bayesian inference methods provide a systematic exploration of the state space for parameters of choice [51, 137]. The application of this data inference method has not yet been applied to SE recordings, to our knowledge.

Second, neural mass models are widely used to model whole brain dynamics due to their low number of variables and fast computation time. However, these models do not take into account the brain's geometry. The representation of brain areas into points in space induces errors when computing the forward solution. Neural field models (NFM) take into account both the orientation and the distance between the dipoles and the sensor, providing more realistic source-to-sensor mapping [142]. Each vertex on the mesh represents one NFM, giving a millimetre scale resolution of the brain's surface. NFMs use a detailed connectivity, taking into account not only white matter connections but also shorter local connections between neighbouring points on the field. Third, recordings of spontaneous seizures and SE from the same patient would be an ideal case for comparing the spatiotemporal evolution of these two types of events. Unfortunately, that is extremely difficult to obtain in the clinic.

Understanding genesis and propagation of SE could open the way to test ways to stop it. It is possible to stimulate specific brain regions of axonal pathways in TVB. Varying the spatial and temporal parameters of the stimulation, one can test possible ways to abort SE in silico, in particular with non-invasive procedures such temporal interference [2, 48].

8.4 Conclusion

In this work, we demonstrate the capability of personalized whole brain modeling on capturing propagation dynamics of status epilepticus. These patterns emerge from the white matter connectivity between regions with different excitability levels. The complex interactions between epileptogenic and healthy regions give rise to these dynamics and they are constrained by the connectome. This first example opens an avenue of study for propagation patterns of status epilepticus.

8.5 Methods

8.5.1 Patient data

A 15-years old male patient with left parietal drug-resistant focal epilepsy since age 18 months and a history of neonatal CMV-encephalitis underwent standard presurgical protocol at La Timone hospital in Marseille. Informed written consent was obtained from the patient and his parents in compliance with the ethical requirements of the Declaration of Helsinki and the study protocol was approved by the local Ethics Committee (Comité de Protection des Personnes sud Méditerranée 1). The non-invasive evaluation included clinical history, neurological examination, neuropsychological testing, scalp video-EEG recordings, 3T and 7T brain MRI, magnetoencephalography (MEG) as well as FDG-PET. The 3T MRI protocol included T1-weighted imaging (MPRAGE sequence, repetition time = 1.9 or 2.3 s, echo time = 2.19 or 2.98 ms, voxel size 1.0 x 1.0 x 1.0 mm3) and diffusion MRI images (DTI-MR sequence, with an angular gradient set of 200 directions, repetition time = 3 s, echo time = 88 ms, voxel size 2.0 x 2.0 x 2.0 mm, b-weighting of 1800 s/mm2). The images were acquired on a Siemens Magnetom Verio 3T MR-scanner. The patient underwent invasive stereo-EEG (SEEG) recordings with the primary hypotheses of the left parietal or operculo-insular epilepsy, based on the non-invasive findings. His SEEG implantation comprised 14 left- and one right hemispheric depth electrodes, each containing 10-18 contacts 2 mm long and separated by 1.5 mm gaps. The SEEG signals were acquired on a 128 channel Deltamed/Natus system with at least 512 Hz sampling rate and recorded on a hard disk (16 bits/sample) using no digital filter. Two hardware filters were present in the acquisition procedure : a high-pass filter (cut-off frequency = 0.16 Hz at -3 dB), and an anti-aliasing low-pass filter (cut-off at one third of the respective sampling frequency). After the electrode implantation, a cranial CT scan was performed to obtain the location of the implanted electrodes and verify the absence of hemorrhagic complications.

8.5.2 Data processing

To construct the individual brain network models, we first preprocessed the T1-MRI and DW-MRI data, following the methods explained in [142]. Briefly, the recon-all pipeline of the FreeSurfer software package was used to reconstruct the cortical surface and segment the brain volume from the T1-MRI. The cortical surface was parcellated using the VEP atlas [140]. We used the MRtrix software package to

process the DW-MRI, using the iterative algorithm described in to derive the fibre orientation distribution functions. The iFOD2 algorithm was used to sample 15 million tracts. The structural connectome was constructed by assigning and counting the streamlines to and from each VEP brain region. The diagonal entries of the connectome matrix were set to 0 to exclude self-connections within areas and the matrix was normalised so that the maximum value was equal to one. We obtained the location of the SEEG contacts from post-implantation CT scans using GARDEL (Graphical user interface for automatic registration and depth electrodes localization), as part of the EpiTools software package. Then we coregistered the contact positions from the CT scan space to the T1-MRI scan space of each patient.

8.5.3 VEP model construction

In order to represent the brain's dynamics during epilepsy, we used whole brain neural models. The brain areas are represented as nodes, which are connected through edges of different strength, as informed by the reconstructed white matter fibres distribution. The activity of each node was modelled with a set of ODEs (Ordinary Differential Equation). These models are connected to each other and the connection strength is inferred from the structural connectome (derived from DW-MRI data). To model seizure-like activity we used the phenomenological 6D Epileptor model, which consists of 3 neural populations acting on fast, intermediate and slow time scales.

The Epileptor model consists of 6 coupled differential equations.

$$
\begin{aligned}
\dot{x}_1 &= y_1 - f_1(x_1, x_2) - z + I_{ext1} \\
\dot{y}_1 &= c - d x_1^2 - y_1 \\
\dot{x}_2 &= -y_2 + x_2 - x_2^3 + I_{ext2} + 0.002g - 0.3(z - 3.5) \\
\dot{y}_2 &= \frac{1}{\tau}(-y_2 + f_2(x_2)) \\
\dot{z} &= r(4(x_1 - x_0) - z + f_3(z) + K \sum_{j=1}^{N} C_{i,j}(x_1^j - x_1^i)) \\
\dot{g} &= -0.01(g - 0.1x_1)
\end{aligned}
\tag{8.1}
$$

where

$$
f_1(x_1, x_2) = \begin{cases} a x_1^3 - b x_1^2 & \text{if } x_1 < 0 \\ -(m - x_2 + 0.6(z-4)^2)x_1 & \text{if } x_1 \geq 0 \end{cases}
$$

$$
f_2(x_2) = \begin{cases} 0 & \text{if } x_2 < -0.25 \\ a_2(x_2 + 0.25) & \text{if } x_2 \geq -0.25 \end{cases}
$$

$$
f_3(z) = \begin{cases} -0.1z^7 & \text{if } z < 0 \\ 0 & \text{if } z \geq 0 \end{cases}
$$

The state variables x_1 and y_1 describe the activity of neural populations on a fast time scale and can model fast discharges. The state variable x_2 and y_2 operate

on an intermediate timescale and describe spike and wave events. The variable z, also called the slow permittivity variable operates on a slower time scale and drives the system autonomously between ictal and interictal states. This is done through the parameter x_0 which indicates the degree of excitability and directly controls the dynamics of the neural population to produce the seizure or not. The state variable g acts as a low-pass filter of the coupling from x_1 to x_2. The default parameters are $I_{ext1} = 3.1$, $I_{ext2} = 0.45$, $c = 1$, $d = 5$, $tau = 10$, $r = 1$, $K = -5$, $a = 1$, $m = 1$, $a_2 = 6$. The coupling between nodes of the network is defined by C_{ij} which comes from the structural connectivity. K scales the connectivity, which can vary the simulated output and is used to investigate different scenarios.

8.5.4 Neural mass modeling

To represent the macroscopic behaviour of neural populations we employ neural mass models. They are defined by a set of differential equations that describe the time evolution of brain region dynamics. Brain regions are connected through white matter fibres. Neural masses are also linked through the structural connectivity to form a brain network model. The global equation for this model is given by

$$\dot{\psi}_i(t) = F(\psi_i(t)) + K \sum_{j=1}^{L} W(i,j) S(\psi_i(t), \psi_j(t))$$

where $\psi_i(t)$ is a state vector of neural activity at brain region i and time t. $\dot{\psi}$ is the temporal derivative of the state vector. F is a function of the state and captures the local neural activity. In our case, F reflects the Epileptor model, described above. W is a matrix of heterogeneous connection strengths between node i and j. S is a coupling function of the local state ψ_i and the distant delayed state ψ_j. That a node receives input through the network is given by the sum across the number of nodes L and scaled by a constant K. In this paper, this set of differential equations is solved using a Euler integration scheme with a step size of 0.2 ms.

8.5.5 Modeling status epilepticus

To model status epilepticus, we based our work on El Houssaini et al., [33, 34]. It was shown that status epilepticus, depolarization block and refractory epilepsy can co-exist in the same model. In particular, we used the setting where status epilepticus co-exists with refractory epilepsy. We chose the following regions to be epileptogenic, based on the clinical hypothesis : Left-Postcentral-gyrus, Left-Postcentral-sulcus. For these regions we set $x_0 = -1.6$, $m = 0$ and initial conditions for the variable z to -1. Based on the propagation patterns observed in the SEEG recordings, and the VEP regions where the recruited electrodes were located, we set the following regions close to the critical threshold for seizure onset, but not enough for a seizure to start spontaneously : Left-Supramarginal-posterior, Left-Central-sulcus-head-face, Left-Precentral-gyrus-upper-limb, Left-Central-sulcus-upper-limb, Left-F2-caudal, Left-Precentral-gyrus-head-face. For these regions we set $x_0 = -2.1$, $m = 0$ and initial conditions for the variable z to 2.95. For the other remaining regions, we set $x_0 = -2.2$, $m = 0$ and initial conditions for the variable z to 2.95. All other variables

had the following initial conditions : $x_1 = -1.9$, $y_1 = -18.7$, $x_2 = -1.05$, $y_2 = 0$, $g = -0.2$. All other Epileptor parameters had default values. The neural mass models were coupled using the difference coupling, with global connectivity strength $K = 8$. The simulation was performed for a length of 10000 timesteps.

8.5.6 Forward solution

Mapping the neural activity from the brain sources (VEP brain regions) to the sensors (SEEG contacts) is done by solving the forward problem and estimating a source-to-sensor matrix (gain matrix). As sources for our model, we used the vertices of the pial surface and volume bounding surfaces for the cortical and subcortical regions respectively. Surfaces are represented as triangular meshes. We take the example for one region j which is has a surface composed of N_j vertices and area a_i. We estimate that the matrix $g_{j,k}$ from source brain region j to sensor k is equal to the sum of the inverse of the squared Euclidean distance $d_{i,k}$ from vertex i to sensor k, weighted by the area a_i of the vertex on the surface. The area a_i is obtained by summing up one third of the area of all the neighbouring triangles. Vertices belonging to the same brain region are summed to obtain the gain for a single region of our brain network model.

$$g_{j,k} = \sum_{i=0}^{N_j} \frac{a_i}{{d_{i,k}}^2}$$

The resulting gain matrix has dimensions $M \times N$, M being the number of regions and N the number of sensors. Matrix multiplication of the simulated source activity with the gain matrix yields the simulated SEEG signals.

8.6 Supplementary figures

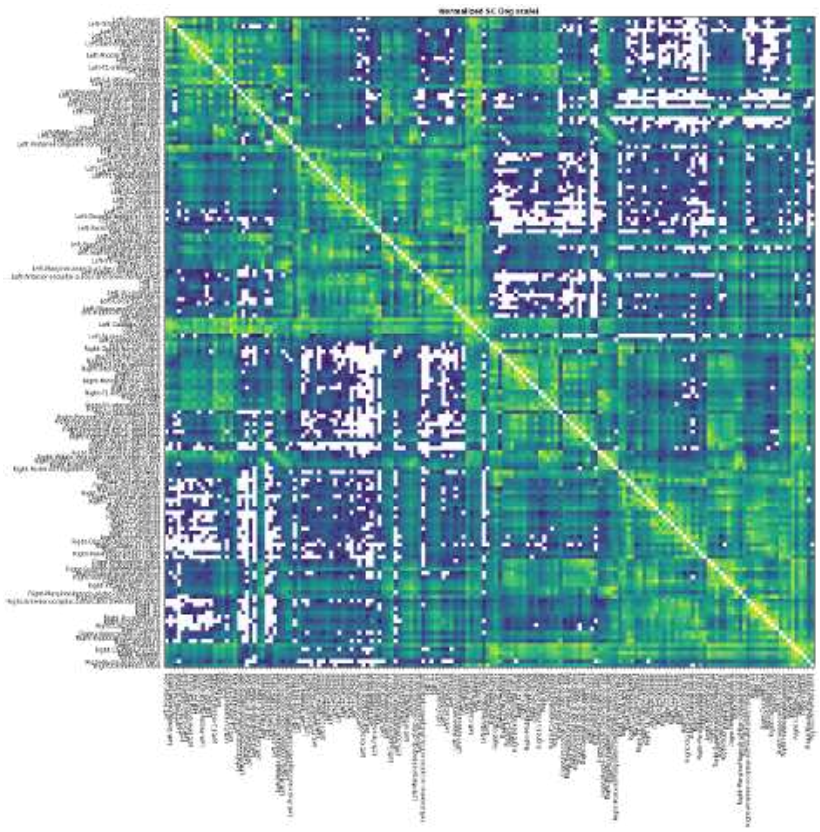

FIGURE 8.6 – Structural connectivity matrix of the patient with status epilepticus. The matrix is symmetrical, representing connection strength between two regions. The brain is parcellated in 162 regions using the VEP atlas.

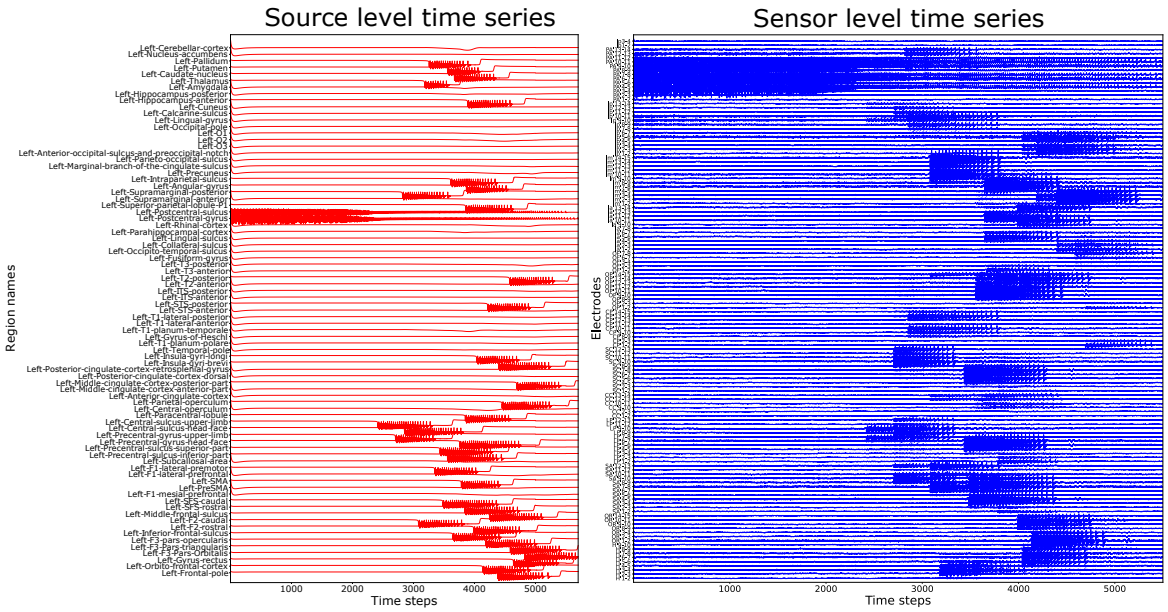

FIGURE 8.7 – Simulation time series on the source level and on the sensor level. The simulation is always performed on the source level. The time series show a status epilepticus event in the postcentral sulcus and postcentral gyrus followed by propagation in connected areas of the left hemisphere. The seizure did not propagate to the right hemisphere (not shown here). The source level time series are projected onto the sensor level through a matrix multiplication with the source-to-sensor gain matrix.

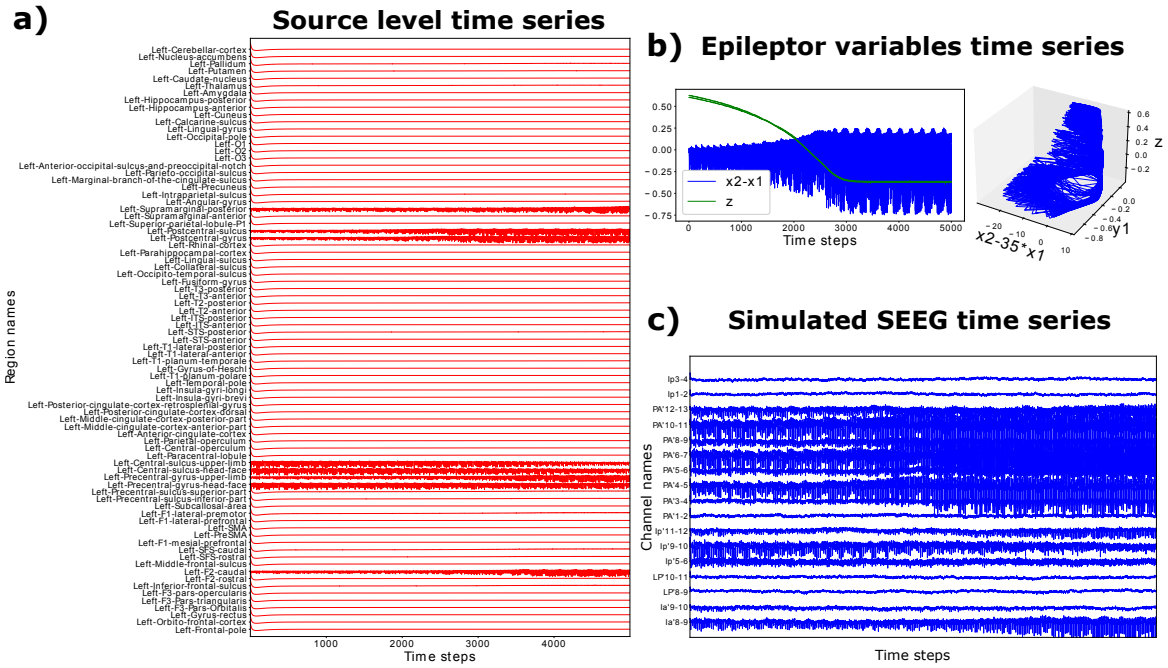

FIGURE 8.8 – Simulation of SE using a different set of parameters. Here, we show self-sustained SE in the epileptogenic regions. Here, global connectivity strength $K = 1$ and for propagation regions $x_0 = -1.9$. All other parameters are the same as the simulation shown in Figure 8.2. a) Time series of brain regions of the left hemisphere are shown. Time series of brain regions of the right hemisphere have a normal activity (not shown here). b) Variables of the Epileptor model for the epileptogenic brain areas. The variables $x_2 - x_1$ model the electrical brain activity of neural populations. The variable z is slow-evolving and guides the system between ictal and interictal brain states. After 2500 time steps, the variables $x_2 - x_1$ reach a periodic limit cycle (we plot in 3D $x_2 - 35x_1$ to show the oscillations, see also [34]). c) The simulated time series are mapped from the region level on the electrode level using the source-to-sensor map (a.k.a gain matrix).

Chapter 9

Conclusions

9.1 Summary

In this thesis, we have extended the Epileptor model to account for seizures induced by electrical brain stimulation. This model has been studied extensively and has been applied to model whole-brain seizure dynamics. Using Bayesian inference methods to fit empirical seizure recordings using 2D Epileptor model simulations, the epileptogenic zone network can be inferred. This approach is currently part of the clinical trial Epinov, aiming at improving surgery outcome for drug-resistant epilepsy. We used this well-established model to capture clinical seizures triggered via electrical brain stimulation. We extended the model to capture slow-evolving phenomena during stimulation which gave rise to seizures. Then, we used this extended model on personalized virtual brain twins and compared our simulations to empirical recordings. Based on retrospective data from 30 patients with drug-resistant epilepsy, we virtualized each patient and built synthetic copies of their spontaneous seizures, stimulated seizures and interictal activity with spikes. In addition, we built for the first time a complete methodology using high-resolution virtual brain models and temporal interference stimulation for drug-resistant epilepsy diagnosis.

Epileptor-stimulation model

The extended model for stimulated seizures in chapter 4 was based on empirical observations of stimulated seizures with SEEG electrodes. Our goal was to capture the response of neural populations following electrical stimulation. We implemented a very simple behavior in the model to account for state switching between the normal and epileptic states due to external brain stimulation. Although our approach was very simple, we could show that it could capture basic features of stimulated seizure recordings with SEEG. This was a very first step in modeling brain stimulation for drug-resistant epilepsy.

Virtual Epileptic Patient Cohort

The extended model was used alongside existing methods simulating spontaneous seizures and interictal activity, to build a complete virtual cohort of 30 patients with drug-resistant epilepsy (Chapter 5). The aim of this work was to provide the scientific

community a virtualized cohort, which reliably captures empirical data and contains ground truth information for hypothesis testing and validation. We developed simple metrics to compare spatio-temporal network dynamics of seizures and systematically tested the effects of stimulation location and stimulation amplitude.

High-resolution virtual epileptic patient and temporal interference stimulation

A future goal for drug-resistant epilepsy is the usage of purely non-invasive methods to diagnose and treat the disorder. Currently, invasive SEEG is used to record brain activity, notably in deep brain regions such as the hippocampus. In addition, brain surgery is the main treatment option for drug-resistant epilepsy. In chapter 6, we introduce a framework to diagnose epilepsy in a purely non-invasive fashion. Our pipeline used EEG to record seizures and TI stimulation to delineate the epileptogenic network. We compared this pipeline to our framework of SEEG recording and SEEG stimulation for epilepsy diagnosis, showing that non-invasive methods are theoretically possible.

Virtualized patient with status epilepticus

In chapter 8, we used our tools at hand to attempt to answer the following question : How does status epilepticus (SE) propagate in the brain ? Based on existing work that modeled SE with the Epileptor model, we attempted to model SE propagation for one patient. The patient had undergone non-invasive brain imaging and had a recorded SE with SEEG electrodes. We built a virtual brain model from their MRI data and ran simulations at the whole-brain level of an SE event, which we then mapped onto the reconstructed SEEG electrodes. In our model, the structural connectivity was used to allow for SE to propagate from its area of onset to the rest of the brain. We compared our simulated SEEG time series to the empirical recordings and noticed similar propagation patterns. This was an initial demonstration that SE may propagate following white matter fibers.

9.2 Discussion

We modeled the dynamical response to electrical brain stimulation by extending the Epileptor model. There are two main ways of perturbing a system and changing its dynamics : (i) changes in state space or (ii) changes in parameter space. In our approach, we chose the latter by modifying the variable m when a stimulus was applied. In the literature, models of electric fields and models of volume of tissue activated have become established methods to estimate the effects of electrical brain stimulation [3, 113]. However, modeling the dynamical brain response following brain stimulation is less straightforward and not well established. There is more investigation needed in this direction, in particular more experimental and clinical evidence in the way stimulation affects neural dynamic responses [77].

In this regard, we used a phenomenological model to link electrical perturbation to active tissue response. Our hypothesis, based on a slow accumulation of ion

imbalances, remains very broad and does not target specific biological mechanisms. For more narrow hypotheses, we would require biophysical models, which link neural dynamics to precise biological targets, such as specific ions. For instance, brain stimulation could influence potassium buffering, causing extracellular potassium accumulation, which in turn could trigger seizures in regions of high excitability.

In addition, we used a very basic method to estimate the electric field for SEEG stimulation. We assumed the stimulating electrodes were point-like charges and applied the quasi-static Maxwell equation for two point-charges in a homogeneous medium. We would need more precise models that take into account head models and electrode geometries, but this was not the main focus point in this thesis. Rather, we focused on dynamical brain responses from focal electrical brain stimulation. Also, we used neural mass models on large brain volumes. Therefore, any precision from the estimated electric field would be lost in most cases. On the other hand, to model TI stimulation, we used an open-source software, simNIBS, which did use personalized head models from T1-MRI and realistic electrode geometries. This was useful because we used high-resolution brain models to perform our simulations, where the spatial granularity is much smaller (mm scale). As a consequence, small differences in electric fields calculations would be noticeable on the simulated dynamical brain response.

Finally, the personalized empirical data were SEEG recordings and the patient-specific MRI. Such data allowed us to infer the epileptogenic networks for each patient, and tune our model's parameters to match empirical stimulated seizures. However, there are many ways to model such data. In order to constrain our methodology, we would require using larger patient cohorts and further experimental evidence on our accumulation hypothesis. In addition, our very first attempts at reproducing clinical stimulation responses in-silico were never 100% accurate. Precision needs to be increased in our models, but this will also increase the number of parameters that need to be tuned, and this increases the number of open questions.

The limitations of this work give rise to future potential for better approaches to the same problem. Firstly, using biophysical models can give more concrete physiological interpretations of the theoretical observations, which can lead to new experimental approaches. Secondly, using larger patient cohorts can give more solid proof or disproof of our hypothesis. We need to work with empirical data more, and we are limited by the tools we use to observe reality. Mathematical and computational models are a window to a perspective beyond the limited constraints of our tools, but without reality, models cannot be grounded nor validated. Theory and experiments should ideally go hand in hand, although it is not an easy task, and deviations are common. In this work, focused on modeling, we tried using the data at hand. Bringing empirical data and models together is easier said than done. We looked into a small subset of patients in order to demonstrate some predictive power of our modeling. There is still more to be done, but we can already see some future avenues suggested by this work.

9.3 Perspectives

One of the goals of our stimulation modeling for drug-resistant epilepsy was to build methods that can optimize stimulation parameter search. This could reduce both the burden on the patient, by stimulating their brain less, and reduce the time it would take clinicians to delineate the epileptogenic networks. For this, we still need to get a better grasp of the role of each stimulation parameter and their impact on brain responses. Employing models that link brain dynamics and behavior to quantifiable biophysical parameters is needed. Such models would give hypotheses on direct causal links between electrical brain stimulation and underlying biological mechanisms. This could lead to new experimental approaches. However, the challenge of such models is their complexity, which makes such models harder to analyze and more computationally expensive to fit against real data.

In addition, stimulation is currently performed via intracranial SEEG electrodes, but in the future, this could be done without requiring any invasive implantation. In addition, if focal stimulation could be delivered non-invasively, any target could be chosen instead of being limited to the limited locations of implanted electrodes. This is what TI stimulation aims to achieve, although it is still in its first stages of development. At the moment, TI is being applied experimentally to various brain disorders, such as epilepsy, Alzheimer's, Parkinson's disease, and depression.

In order for non-invasive diagnosis to be possible, source localization of deep brain activities from non-invasive brain recordings (EEG/MEG) needs to be improved. Currently, intracranial electrodes are implanted to record activities in deep brain structures such as the hippocampus, which EEG is still not able to do. On the other hand, MEG aims to achieve this [95]. In addition, MEG is slowly becoming smaller and cheaper, making it promising to be more widely applied and more flexible in performing various experiments [14].

If there is a better understanding of the effects of stimulation parameters on the brain and improved data imaging modalities for detecting deep brain activities, drug-resistant epilepsy could not just be diagnosed non-invasively, but also treated non-invasively. The advantage of brain stimulation is that it is flexible and reversible : if a certain stimulation treatment is not effective, it can be changed or stopped. The current most effective treatment is brain surgery, which is permanent. With a success rate of 40-80% depending on the epilepsy type, a non-negligible number of patients remain epileptic post-surgery. It is crucial to improve these treatments and find new ones. We hope that our research can contribute to ongoing efforts of using brain stimulation for a better diagnosis and treatment of epilepsy.

9.4 Personal thoughts

Researchers sometimes publish their thoughts on scientific research, and some of that has been very helpful, kind of like a hand the author lends to beginners in the scientific journey. In particular, [118], speaks of the realization that research is hard, and important research is even harder. The immersion into the unknown can be uncomfortable at times. Being comfortable with your own ignorance has been a challenge, as I can imagine, not only for me. But I am really glad to have experien-

ced research, to have kept struggling with it, and to have realized one important ingredient. As A. Culhane says it better than I, *"Science is weakened by the comic book myth of the lone powerful genius. I have yet to find one in science. Instead the best science comes when we work as a community that flounders, supports, and learns from each other, ventures and discovers together."*.

Bibliography

[1] E. Acerbo, B. Botzanowski, D. Dellavale, M. A. Stern, E. Cole, C.-A. Gutekunst et al. « Improved Temporal and Spatial Focality of Non-invasive Deep-brain Stimulation using Multipolar Single-pulse Temporal Interference with Applications in Epilepsy ». In : *bioRxiv* (2024), p. 2024-01.

[2] E. Acerbo, A. Jegou, C. Luff, P. Dzialecka, B. Botzanowski, F. Missey et al. « Focal non-invasive deep-brain stimulation with temporal interference for the suppression of epileptic biomarkers ». In : *Frontiers in neuroscience* 16 (2022), p. 945221.

[3] F. Alonso, B. Mercadal, R. Salvador, G. Ruffini, F. Bartolomei, F. Wendling et al. « Biophysical modeling of the electric field magnitude and distribution induced by electrical stimulation with intracerebral electrodes ». In : *Biomedical Physics & Engineering Express* 9.4 (2023), p. 045022.

[4] K. Amunts, C. Lepage, L. Borgeat, H. Mohlberg, T. Dickscheid, M.-E. Rousseau et al. « BigBrain : An Ultrahigh-Resolution 3D Human Brain Model ». In : *Science* 340 (6139 juin 2013), p. 1472-1475. doi : 10.1126/science.1235381.

[5] K. Ashkan, P. Rogers, H. Bergman et I. Ughratdar. « Insights into the mechanisms of deep brain stimulation ». In : *Nature Reviews Neurology* 13.9 (2017), p. 548-554.

[6] M. Azilinon, J. Makhalova, W. Zaaraoui, S. Medina Villalon, P. Viout, T. Roussel et al. « Combining sodium MRI, proton MR spectroscopic imaging, and intracerebral EEG in epilepsy ». In : *Human Brain Mapping* 44.2 (2023), p. 825-840.

[7] G. Baier, M. Goodfellow, P. N. Taylor, Y. Wang et D. J. Garry. « The importance of modeling epileptic seizure dynamics as spatio-temporal patterns ». In : *Frontiers in physiology* 3 (2012), p. 281.

[8] A. Balatskaya, N. Roehri, S. Lagarde, F. Pizzo, S. Medina, F. Wendling et al. « The "Connectivity Epileptogenicity Index"(cEI), a method for mapping the different seizure onset patterns in StereoElectroEncephalography recorded seizures ». In : *Clinical Neurophysiology* 131.8 (2020), p. 1947-1955.

[9] A. Bandyopadhyay, G. Rabuffo, C. Calabrese, K. Gudibanda, D. Depannemaecker, A. Ivanov et al. « Mean-field approximation of network of biophysical neurons driven by conductance-based ion exchange ». In : *bioRxiv* (2021), p. 2021-10.

[10] F. Bartolomei, P. Chauvel et F. Wendling. « Epileptogenicity of brain structures in human temporal lobe epilepsy : a quantified study from intracerebral EEG ». In : *Brain* 131.7 (2008), p. 1818-1830.

[11] F. Bartolomei, M. Guye et F. Wendling. « Abnormal binding and disruption in large scale networks involved in human partial seizures ». In : *EPJ Nonlinear Biomedical Physics* 1 (2013), p. 1-16.

[12] F. Bartolomei, A. Trébuchon, F. Bonini, I. Lambert, M. Gavaret, M. Woodman et al. « What is the concordance between the seizure onset zone and the irritative zone ? A SEEG quantified study ». In : *Clinical Neurophysiology* 127.2 (2016), p. 1157-1162.

[13] E. Beghi. « The epidemiology of epilepsy ». In : *Neuroepidemiology* 54.2 (2020), p. 185-191.

[14] E. Boto, S. S. Meyer, V. Shah, O. Alem, S. Knappe, P. Kruger et al. « A new generation of magnetoencephalography : Room temperature measurements using optically-pumped magnetometers ». In : *NeuroImage* 149 (2017), p. 404-414.

[15] B. Botzanowski, E. Acerbo, S. Lehmann, S. L. Kearsley, M. Steiner, E. Neufeld et al. « Controlling focality and intensity of non-invasive deep brain stimulation using multipolar temporal interference in non-human primates and rodents ». In : *bioRxiv* (2023), p. 2023-09.

[16] B. Botzanowski, E. Acerbo, S. Lehmann, S. L. Kearsley, M. Steiner, E. Neufeld et al. « Focal Control of Non-Invasive Deep Brain Stimulation Using Multipolar Temporal Interference ». In : *Available at SSRN 4640129* (2024).

[17] J. Bourien, F. Bartolomei, J. Bellanger, M. Gavaret, P. Chauvel et F. Wendling. « A method to identify reproducible subsets of co-activated structures during interictal spikes. Application to intracerebral EEG in temporal lobe epilepsy ». In : *Clinical Neurophysiology* 116.2 (2005), p. 443-455.

[18] D. T. Brocker et W. M. Grill. « Principles of electrical stimulation of neural tissue ». In : *Handbook of clinical neurology* 116 (2013), p. 3-18.

[19] R. J. Burman, R. E. Rosch, J. M. Wilmshurst, A. Sen, G. Ramantani, C. J. Akerman et al. « Why won't it stop ? The dynamics of benzodiazepine resistance in status epilepticus ». In : *Nature Reviews Neurology* 18.7 (2022), p. 428-441.

[20] S. S. Buss, P. J. Fried et A. Pascual-Leone. « Therapeutic noninvasive brain stimulation in Alzheimer's disease and related dementias ». In : *Current Opinion in Neurology* 32 (2 avr. 2019), p. 292-304. doi : 10.1097/WCO.0000000000000669.

[21] K. Butenko, C. Bahls, M. Schröder, R. Köhling et U. van Rienen. « OSS-DBS : Open-source simulation platform for deep brain stimulation with a comprehensive automated modeling ». In : *PLoS computational biology* 16.7 (2020), e1008023.

[22] W.-C. Chang, J. Kudlacek, J. Hlinka, J. Chvojka, M. Hadrava, V. Kumpost et al. « Loss of neuronal network resilience precedes seizures and determines the ictogenic nature of interictal synaptic perturbations ». In : *Nature neuroscience* 21.12 (2018), p. 1742-1752.

[23] P. Chauvel. « The voyage of SEEG ». In : *Journal of Clinical Neurophysiology* 41.5 (2024), p. 399-401.

[24] S. Coombes. « Waves, bumps, and patterns in neural field theories ». In : *Biological cybernetics* 93 (2005), p. 91-108.

[25] J. R. Cressman, G. Ullah, J. Ziburkus, S. J. Schiff et E. Barreto. « The influence of sodium and potassium dynamics on excitability, seizures, and the stability of persistent states : I. Single neuron dynamics ». In : *Journal of computational neuroscience* 26 (2009), p. 159-170.

[26] H. Cushing. « A note upon the faradic stimulation of the postcentral gyrus in conscious patients. » In : *Brain* 32.1 (1909), p. 44-53.

[27] F. L. Da Silva, W. Blanes, S. N. Kalitzin, J. Parra, P. Suffczynski et D. N. Velis. « Epilepsies as dynamical diseases of brain systems : basic models of the transition between normal and epileptic activity ». In : *Epilepsia* 44 (2003), p. 72-83.

[28] P. Davis et J. Gaitanis. « Neuromodulation for the Treatment of Epilepsy : A Review of Current Approaches and Future Directions ». In : *Clinical Therapeutics* 42 (7 juill. 2020), p. 1140-1154. doi : 10.1016/j.clinthera.2020.05.017.

[29] G. Deco, V. K. Jirsa, P. A. Robinson, M. Breakspear et K. Friston. « The dynamic brain : from spiking neurons to neural masses and cortical fields ». In : *PLoS computational biology* 4.8 (2008), e1000092.

[30] D. Depannemaecker, A. Destexhe, V. Jirsa et C. Bernard. « Modeling seizures : From single neurons to networks ». In : *Seizure* 90 (2021), p. 4-8.

[31] D. Depannemaecker, A. Ivanov, D. Lillo, L. Spek, C. Bernard et V. Jirsa. « A unified physiological framework of transitions between seizures, sustained ictal activity and depolarization block at the single neuron level ». In : *Journal of computational neuroscience* (2022), p. 1-17.

[32] *EBRAINS Infrastructure - Find neuroscience data, models and tools.* https://www.ebrains.eu/data/find-data/. Accessed : 2024-03-05. 2019.

[33] K. El Houssaini, C. Bernard et V. K. Jirsa. « The epileptor model : a systematic mathematical analysis linked to the dynamics of seizures, refractory status epilepticus, and depolarization block ». In : *Eneuro* 7.2 (2020).

[34] K. El Houssaini, A. I. Ivanov, C. Bernard et V. K. Jirsa. « Seizures, refractory status epilepticus, and depolarization block as endogenous brain activities ». In : *Physical Review E* 91.1 (2015), p. 010701.

[35] M. I. Falcon, V. Jirsa et A. Solodkin. « A new neuroinformatics approach to personalized medicine in neurology : The Virtual Brain ». In : *Current opinion in neurology* 29.4 (2016), p. 429-436.

[36] K. M. Fiest, K. M. Sauro, S. Wiebe, S. B. Patten, C.-S. Kwon, J. Dykeman et al. « Prevalence and incidence of epilepsy : a systematic review and meta-analysis of international studies ». In : *Neurology* 88.3 (2017), p. 296-303.

[37] R. Fisher, V. Salanova, T. Witt, R. Worth, T. Henry, R. Gross et al. « Electrical stimulation of the anterior nucleus of thalamus for treatment of refractory epilepsy ». In : *Epilepsia* 51.5 (2010), p. 899-908.

[38] R. S. Fisher, J. H. Cross, J. A. French, N. Higurashi, E. Hirsch, F. E. Jansen et al. « Operational classification of seizure types by the International League Against Epilepsy : Position Paper of the ILAE Commission for Classification and Terminology ». In : *Epilepsia* 58.4 (2017), p. 522-530.

[39] F. Fröhlich, M. Bazhenov, V. Iragui-Madoz et T. J. Sejnowski. « Potassium dynamics in the epileptic cortex : new insights on an old topic ». In : *The Neuroscientist* 14.5 (2008), p. 422-433.

[40] *Regulation (EU) 2016/679 of the European Parliament and of the Council (General Data Protection Regulation)*. http://data.europa.eu/eli/reg/2016/679/2016-05-04. Accessed : 2024-01-30. 2016.

[41] D. D. George, S. G. Ojemann, C. Drees et J. A. Thompson. « Stimulation mapping using stereoelectroencephalography : current and future directions ». In : *Frontiers in Neurology* 11 (2020), p. 320.

[42] M. Giuffrè et D. L. Shung. « Harnessing the power of synthetic data in healthcare : innovation, application, and privacy ». In : *NPJ Digital Medicine* 6.1 (2023), p. 186.

[43] V. Gnatkovsky, M. De Curtis, C. Pastori, F. Cardinale, G. Lo Russo, R. Mai et al. « Biomarkers of epileptogenic zone defined by quantified stereo-EEG analysis ». In : *Epilepsia* 55.2 (2014), p. 296-305.

[44] A. Gonzales, G. Guruswamy et S. R. Smith. « Synthetic data in health care : a narrative review ». In : *PLOS Digital Health* 2.1 (2023), e0000082.

[45] M. Goodfellow, C. Rummel, E. Abela, M. P. Richardson, K. Schindler et J. R. Terry. « Estimation of brain network ictogenicity predicts outcome from epilepsy surgery ». In : *Scientific reports* 6.1 (2016), p. 29215.

[46] O. Grinenko, J. Li, J. C. Mosher, I. Z. Wang, J. C. Bulacio, J. Gonzalez-Martinez et al. « A fingerprint of the epileptogenic zone in human epilepsies ». In : *Brain* 141.1 (2018), p. 117-131.

[47] N. Grossman. « Modulation without surgical intervention ». In : *Science* 361 (6401 août 2018), p. 461-462. doi : 10.1126/science.aau4915.

[48] N. Grossman, D. Bono, N. Dedic, S. B. Kodandaramaiah, A. Rudenko, H.-J. Suk et al. « Noninvasive deep brain stimulation via temporally interfering electric fields ». In : *cell* 169.6 (2017), p. 1029-1041.

[49] N. Grossman, M. S. Okun et E. S. Boyden. « Translating Temporal Interference Brain Stimulation to Treat Neurological and Psychiatric Conditions ». In : *JAMA Neurology* 75 (11 nov. 2018), p. 1307. doi : 10.1001/jamaneurol.2018.2760.

[50] A. Guerra, V. López-Alonso, B. Cheeran et A. Suppa. « Solutions for managing variability in non-invasive brain stimulation studies ». In : *Neuroscience letters* 719 (2020), p. 133332.

[51] M. Hashemi, A. N. Vattikonda, V. Sip, M. Guye, F. Bartolomei, M. M. Woodman et al. « The Bayesian Virtual Epileptic Patient : A probabilistic framework designed to infer the spatial map of epileptogenicity in a personalized large-scale brain model of epilepsy spread ». In : *NeuroImage* 217 (2020), p. 116839.

[52] W. A. Hauser et E. Beghi. « First seizure definitions and worldwide incidence and mortality ». In : *Epilepsia* 49 (2008), p. 8-12.

[53] T. M. Herrington, J. J. Cheng et E. N. Eskandar. « Mechanisms of deep brain stimulation ». In : *Journal of neurophysiology* 115.1 (2016), p. 19-38.

[54] *Summary of the HIPAA privacy rule*. https://www.hhs.gov/hipaa/for-professionals/privacy/laws-regulations/index.html. Accessed : 2024-01-30. 1996.

[55] A. L. Hodgkin et A. F. Huxley. « A quantitative description of membrane current and its application to conduction and excitation in nerve ». In : *The Journal of physiology* 117.4 (1952), p. 500.

[56] C. Holdgraf, S. Appelhoff et S. e. a. Bickel. « EEG-BIDS, extending the Brain Imaging Data Structure specification to human intracranial electrophysiology ». In : *Sci Data* 6 (2019). doi : 10.1038/s41597-019-0105-7.

[57] T. Hutson, D. Pizarro, S. Pati et L. D. Iasemidis. « Predictability and resetting in a case of convulsive status epilepticus ». In : *Frontiers in neurology* 9 (2018), p. 172.

[58] M. I. Iacono, E. Neufeld, E. Akinnagbe, K. Bower, J. Wolf, I. Vogiatzis Oikonomidis et al. « MIDA : a multimodal imaging-based detailed anatomical model of the human head and neck ». In : *PloS one* 10.4 (2015), e0124126.

[59] J. Isnard, D. Taussig, F. Bartolomei, P. Bourdillon, H. Catenoix, F. Chassoux et al. « French guidelines on stereoelectroencephalography (SEEG) ». In : *Neurophysiologie Clinique* 48.1 (2018), p. 5-13.

[60] M. Jedynak, A. Boyer, B. Chanteloup-Forêt, M. Bhattacharjee, C. Saubat, F. Tadel et al. « Variability of single pulse electrical stimulation responses recorded with intracranial electroencephalography in epileptic patients ». In : *Brain Topography* 36.1 (2023), p. 119-127.

[61] L. Jehi. « The epileptogenic zone : concept and definition ». In : *Epilepsy currents* 18.1 (2018), p. 12-16.

[62] J. Jha, M. Hashemi, A. N. Vattikonda, H. Wang et V. Jirsa. « Fully Bayesian estimation of virtual brain parameters with self-tuning Hamiltonian Monte Carlo ». In : *Machine Learning : Science and Technology* 3.3 (2022), p. 035016.

[63] V. Jirsa, H. Wang, P. Triebkorn, M. Hashemi, J. Jha, J. Gonzalez-Martinez et al. « Personalised virtual brain models in epilepsy ». In : *The Lancet Neurology* (2023).

[64] V. K. Jirsa. « Neural field dynamics with local and global connectivity and time delay ». In : *Philosophical Transactions of the Royal Society A : Mathematical, Physical and Engineering Sciences* 367.1891 (2009), p. 1131-1143.

[65] V. K. Jirsa, K. J. Jantzen, A. Fuchs et J. S. Kelso. « Spatiotemporal forward solution of the EEG and MEG using network modeling ». In : *IEEE transactions on medical imaging* 21.5 (2002), p. 493-504.

[66] V. K. Jirsa, T. Proix, D. Perdikis, M. M. Woodman, H. Wang, J. Gonzalez-Martinez et al. « The virtual epileptic patient : individualized whole-brain models of epilepsy spread ». In : *Neuroimage* 145 (2017), p. 377-388.

[67] V. K. Jirsa, W. C. Stacey, P. P. Quilichini, A. I. Ivanov et C. Bernard. « On the nature of seizure dynamics ». In : *Brain* 137.8 (2014), p. 2210-2230.

[68] P. Jiruska, J. Csicsvari, A. D. Powell, J. E. Fox, W.-C. Chang, M. Vreugdenhil et al. « High-frequency network activity, global increase in neuronal activity, and synchrony expansion precede epileptic seizures in vitro ». In : *Journal of Neuroscience* 30.16 (2010), p. 5690-5701.

[70] N. Kane, J. Acharya, S. Beniczky, L. Caboclo, S. Finnigan, P. W. Kaplan et al. « A revised glossary of terms most commonly used by clinical electroencephalographers and updated proposal for the report format of the EEG findings. Revision 2017 ». In : *Clinical neurophysiology practice* 2 (2017), p. 170.

[71] S. Kovac, P. Kahane et B. Diehl. « Seizures induced by direct electrical cortical stimulation - Mechanisms and clinical considerations ». In : *Clinical Neurophysiology* 127.1 (2016), p. 31-39. doi : https://doi.org/10.1016/j.clinph.2014.12.009.

[72] S. Kovac, P. Kahane et B. Diehl. « Seizures induced by direct electrical cortical stimulation–Mechanisms and clinical considerations ». In : *Clinical Neurophysiology* 127.1 (2016), p. 31-39.

[74] M. A. Kural, L. Duez, V. Sejer Hansen, P. G. Larsson, S. Rampp, R. Schulz et al. « Criteria for defining interictal epileptiform discharges in EEG : A clinical validation study ». In : *Neurology* 94.20 (2020), e2139-e2147.

[75] C. La Fougère, A. Rominger, S. Förster, J. Geisler et P. Bartenstein. « PET and SPECT in epilepsy : a critical review ». In : *Epilepsy & Behavior* 15.1 (2009), p. 50-55.

[76] B. Leeman-Markowski. « Review of MRI-negative epilepsy ». In : *Jama Neurology* 73.11 (2016), p. 1377-1377.

[77] G. Lepeu, E. van Maren, K. Slabeva, C. Friedrichs-Maeder, M. Fuchs, W. J. Z'Graggen et al. « The critical dynamics of hippocampal seizures ». In : *Nature Communications* 15.1 (2024), p. 6945.

[78] K. P. Lillis, M. A. Kramer, J. Mertz, K. J. Staley et J. A. White. « Pyramidal cells accumulate chloride at seizure onset ». In : *Neurobiology of disease* 47.3 (2012), p. 358-366.

[79] A. M. Lozano, N. Lipsman, H. Bergman, P. Brown, S. Chabardes, J. W. Chang et al. « Deep brain stimulation : current challenges and future directions ». In : *Nature Reviews Neurology* 15.3 (2019), p. 148-160.

[80] H. O. Lüders, I. Najm, D. Nair, P. Widdess-Walsh et W. Bingman. « The epileptogenic zone : general principles ». In : *Epileptic disorders* 8 (2006), S1-S9.

[81] J. Makhalova, S. Medina Villalon, H. Wang, B. Giusiano, M. Woodman, C. Bénar et al. « Virtual epileptic patient brain modeling : Relationships with seizure onset and surgical outcome ». In : *Epilepsia* 63.8 (2022), p. 1942-1955.

[83] P. Merton et H. Morton. « Stimulation of the cerebral cortex in the intact human subject ». In : *Nature* 285.5762 (1980), p. 227-227.

[84] E. Mirzakhalili, B. Barra, M. Capogrosso et S. F. Lempka. « Biophysics of temporal interference stimulation ». In : *Cell Systems* 11.6 (2020), p. 557-572.

[85] F. Missey, E. Rusina, E. Acerbo, B. Botzanowski, A. Trébuchon, F. Bartolomei et al. « Orientation of temporal interference for non-invasive deep brain stimulation in epilepsy ». In : *Frontiers in neuroscience* 15 (2021), p. 633988.

[86] D. R. Nair, K. D. Laxer, P. B. Weber, A. M. Murro, Y. D. Park, G. L. Barkley et al. « Nine-year prospective efficacy and safety of brain-responsive neurostimulation for focal epilepsy ». In : *Neurology* 95.9 (2020), e1244-e1256.

[87] S. Naze, C. Bernard et V. Jirsa. « Computational modeling of seizure dynamics using coupled neuronal networks : factors shaping epileptiform activity ». In : *PLOS Computational Biology* 11.5 (2015), e1004209.

[88] T. E. Nichols et A. P. Holmes. « Nonparametric permutation tests for functional neuroimaging : a primer with examples ». In : *Human brain mapping* 15.1 (2002), p. 1-25.

[89] M. A. Nitsche et W. Paulus. « Excitability changes induced in the human motor cortex by weak transcranial direct current stimulation ». In : *The Journal of physiology* 527.Pt 3 (2000), p. 633.

[90] C. C. Oderiz, N. von Ellenrieder, F. Dubeau, A. Eisenberg, J. Gotman, J. Hall et al. « Association of cortical stimulation–induced seizure with surgical outcome in patients with focal drug-resistant epilepsy ». In : *JAMA neurology* 76.9 (2019), p. 1070-1078.

[91] R. Oostenveld et P. Praamstra. « The five percent electrode system for high-resolution EEG and ERP measurements ». In : *Clinical Neurophysiology* 112 (4 2001), p. 713-719. DOI : https://doi.org/10.1016/S1388-2457(00)00527-7.

[92] A. Palmini. « The concept of the epileptogenic zone : a modern look at Penfield and Jasper's views on the role of interictal spikes ». In : *Epileptic disorders* 8 (2006), S10-S15.

[93] C. P. Panteliadis, P. Vassilyadi, J. Fehlert et C. Hagel. « Historical documents on epilepsy : From antiquity through the 20th century ». In : *Brain and Development* 39.6 (2017), p. 457-463.

[94] W. Penfield et H. Jasper. « Epilepsy and the functional anatomy of the human brain. » In : (1954).

[95] F. Pizzo, N. Roehri, S. Medina Villalon, A. Trébuchon, R. Carron, M. Gavaret et al. « Deep brain activities can be detected with magnetoencephalography ». In : *Nature communications* 10.1 (2019), p. 971.

[96] R. Polania, M. A. Nitsche et C. C. Ruff. « Studying and modifying brain function with non-invasive brain stimulation ». In : *Nature neuroscience* 21.2 (2018), p. 174-187.

[97] T. Proix, V. Jirsa, F. Bartolomei, M. Guye et W. Truccolo. « Predicting the spatiotemporal diversity of seizure propagation and termination in human focal epilepsy ». In : *Nature Communications* (2018).

[98] T. Proix, F. Bartolomei, M. Guye et V. K. Jirsa. « Individual brain structure and modelling predict seizure propagation ». In : *Brain* 140.3 (2017), p. 641-654.

[99] O. Puonti, K. Van Leemput, G. B. Saturnino, H. R. Siebner, K. H. Madsen et A. Thielscher. « Accurate and robust whole-head segmentation from magnetic resonance images for individualized head modeling ». In : *Neuroimage* 219 (2020), p. 117044.

[100] R. Q. Quiroga, Z. Nadasdy et Y. Ben-Shaul. « Unsupervised spike detection and sorting with wavelets and superparamagnetic clustering ». In : *Neural computation* 16.8 (2004), p. 1661-1687.

[101] J. V. Raimondo, R. J. Burman, A. A. Katz et C. J. Akerman. « Ion dynamics during seizures ». In : *Frontiers in cellular neuroscience* 9 (2015), p. 419.

[102] F. Rattay. « Analysis of models for external stimulation of axons ». In : *IEEE transactions on biomedical engineering* 10 (1986), p. 974-977.

[103] S. Rich, H. M. Chameh, J. Lefebvre et T. A. Valiante. « Loss of neuronal heterogeneity in epileptogenic human tissue impairs network resilience to sudden changes in synchrony ». In : *Cell Reports* 39.8 (2022).

[104] C. Runfola, H. Sheheitli, F. Bartolomei, H. Wang et V. Jirsa. « In pursuit of the epileptogenic zone in focal epilepsy :a dynamical network biomarker approach ». In : *Communications in Nonlinear Science and Numerical Simulation* 117 (2023), p. 106973. doi : https://doi.org/10.1016/j.cnsns.2022.106973.

[105] P. Ryvlin, J. H. Cross et S. Rheims. « Epilepsy surgery in children and adults ». In : *The Lancet Neurology* 13.11 (2014), p. 1114-1126.

[106] P. Ryvlin, S. Rheims, L. J. Hirsch, A. Sokolov et L. Jehi. « Neuromodulation in epilepsy : state-of-the-art approved therapies ». In : *The Lancet Neurology* 20.12 (2021), p. 1038-1047.

[107] M. L. Saggio, D. Crisp, J. M. Scott, P. Karoly, L. Kuhlmann, M. Nakatani et al. « A taxonomy of seizure dynamotypes ». In : *Elife* 9 (2020), e55632.

[108] M. L. Saggio et V. K. Jirsa. « Phenomenological Mesoscopic for Seizure Activity Models ». In : *A Complex Systems Approach to Epilepsy : Concept, Practice, and Therapy* (2023), p. 41.

[109] V. Salanova, T. Witt, R. Worth, T. R. Henry, R. E. Gross, J. M. Nazzaro et al. « Long-term efficacy and safety of thalamic stimulation for drug-resistant partial epilepsy ». In : *Neurology* 84.10 (2015), p. 1017-1025.

[110] V. Santhakumar, I. Aradi et I. Soltesz. « Role of mossy fiber sprouting and mossy cell loss in hyperexcitability : a network model of the dentate gyrus incorporating cell types and axonal topography ». In : *Journal of neurophysiology* 93.1 (2005), p. 437-453.

[111] P. Sanz Leon, S. A. Knock, M. M. Woodman, L. Domide, J. Mersmann, A. R. McIntosh et al. « The Virtual Brain : a simulator of primate brain network dynamics ». In : *Frontiers in neuroinformatics* 7 (2013), p. 10.

[112] P. Sanz-Leon, S. A. Knock, A. Spiegler et V. K. Jirsa. « Mathematical framework for large-scale brain network modeling in The Virtual Brain ». In : *Neuroimage* 111 (2015), p. 385-430.

[113] G. B. Saturnino, O. Puonti, J. D. Nielsen, D. Antonenko, K. H. Madsen et A. Thielscher. « SimNIBS 2.1 : a comprehensive pipeline for individualized electric field modelling for transcranial brain stimulation ». In : *Brain and human body modeling : computational human modeling at EMBC 2018* (2019), p. 3-25.

[114] H. E. Scharfman. « The neurobiology of epilepsy ». In : *Current neurology and neuroscience reports* 7.4 (2007), p. 348-354.

[115] I. E. Scheffer, S. Berkovic, G. Capovilla, M. B. Connolly, J. French, L. Guilhoto et al. « ILAE classification of the epilepsies : Position paper of the ILAE Commission for Classification and Terminology ». In : *Epilepsia* 58.4 (2017), p. 512-521.

[116] S. R. Schreglmann, D. Wang, R. L. Peach, J. Li, X. Zhang, A. Latorre et al. « Non-invasive suppression of essential tremor via phase-locked disruption of its temporal coherence ». In : *Nature Communications* 12 (1 jan. 2021), p. 363. doi : 10.1038/s41467-020-20581-7.

[117] G. M. Schroeder, F. A. Chowdhury, M. J. Cook, B. Diehl, J. S. Duncan, P. J. Karoly et al. « Multiple mechanisms shape the relationship between pathway and duration of focal seizures ». In : *Brain Communications* 4.4 (2022), fcac173.

[118] M. A. Schwartz. « The importance of stupidity in scientific research ». In : *Journal of Cell Science* 121.11 (2008), p. 1771-1771.

[119] S. Simula, M. Daoud, G. Ruffini, M. C. Biagi, C.-G. Benar, P. Benquet et al. « Transcranial current stimulation in epilepsy : A systematic review of the fundamental and clinical aspects ». In : *Frontiers in Neuroscience* 16 (2022), p. 909421.

[120] S. S. Spencer. « Neural networks in human epilepsy : evidence of and implications for treatment. » In : *Epilepsia (Series 4)* 43.3 (2002).

[121] P. Sudbrack-Oliveira, M. Z. Barbosa, S. Thome-Souza, L. B. Razza, J. Gallucci-Neto, L. da Costa Lane Valiengo et al. « Transcranial direct current stimulation (tDCS) in the management of epilepsy : A systematic review ». In : *Seizure* 86 (mars 2021), p. 85-95. doi : 10.1016/j.seizure.2021.01.020.

[122] J. Talairach et J. Bancaud. « Stereotaxic approach to epilepsy ». In : *Progress in neurological surgery*. T. 5. Karger Publishers, 1973, p. 297-354.

[123] J. Talairach et J. Bancaud. « Lesion," irritative" zone and epileptogenic focus ». In : *Stereotactic and Functional Neurosurgery* 27.1-3 (1966), p. 91-94.

[124] F. Tergau, U. Naumann, W. Paulus et B. J. Steinhoff. « Low-frequency repetitive transcranial magnetic stimulation improves intractable epilepsy ». In : *The Lancet* 353.9171 (1999), p. 2209.

[125] R. D. Thijs, R. Surges, T. J. O'Brien et J. W. Sander. « Epilepsy in adults ». In : *The lancet* 393.10172 (2019), p. 689-701.

[126] S. A. D. Tissot. *Traité de l'epilepsie : faisant le tome troisieme du Traité des nerfs & leurs maladies*. T. 3. Chez PF Didot, le jeune, 1770.

[127] A. Trebuchon, R. Racila, F. Cardinale, S. Lagarde, A. McGonigal, G. L. Russo et al. « Electrical stimulation for seizure induction during SEEG exploration : a useful predictor of postoperative seizure recurrence ? » In : *Journal of Neurology, Neurosurgery & Psychiatry* 92.1 (2021), p. 22-26.

[128] A. Trébuchon et P. Chauvel. « Electrical stimulation for seizure induction and functional mapping in stereoelectroencephalography ». In : *Journal of Clinical Neurophysiology* 33.6 (2016), p. 511-521.

[129] A. J. Trevelyan, R. T. Graham, R. R. Parrish et N. K. Codadu. « Synergistic Positive Feedback Mechanisms Underlying Seizure Initiation ». In : *Epilepsy Currents* (sept. 2022), p. 153575972211271. doi : 10.1177/15357597221127163.

[130] E. Trinka, H. Cock, D. Hesdorffer, A. O. Rossetti, I. E. Scheffer, S. Shinnar et al. « A definition and classification of status epilepticus–Report of the ILAE Task Force on Classification of Status Epilepticus ». In : *Epilepsia* 56.10 (2015), p. 1515-1523.

[131] *The Virtual Brain : The Documentation Website*. https://docs.thevirtualbrain.org/manuals/UserGuide/UserGuide-UI.html. Accessed : 2024-02-01. 2024.

[133] G. Ullah, J. R. Cressman Jr, E. Barreto et S. J. Schiff. « The influence of sodium and potassium dynamics on excitability, seizures, and the stability of persistent states : II. Network and glial dynamics ». In : *Journal of computational neuroscience* 26 (2009), p. 171-183.

[134] M. Ursino et G.-E. La Cara. « Travelling waves and EEG patterns during epileptic seizure : analysis with an integrate-and-fire neural network ». In : *Journal of theoretical biology* 242.1 (2006), p. 171-187.

[135] A. Valentin. « Responses to single pulse electrical stimulation identify epileptogenesis in the human brain in vivo ». In : *Brain* 125 (8 août 2002), p. 1709-1718. doi : 10.1093/brain/awf187.

[136] A. Valentín, G. Alarcón, M. Honavar, J. J. G. Seoane, R. P. Selway, C. E. Polkey et al. « Single pulse electrical stimulation for identification of structural abnormalities and prediction of seizure outcome after epilepsy surgery : a prospective study ». In : *The Lancet Neurology* 4 (11 nov. 2005), p. 718-726. doi : 10.1016/S1474-4422(05)70200-3.

[137] A. N. Vattikonda, M. Hashemi, V. Sip, M. M. Woodman, F. Bartolomei et V. K. Jirsa. « Identifying spatio-temporal seizure propagation patterns in epilepsy using Bayesian inference ». In : *Communications biology* 4.1 (2021), p. 1244.

[138] S. M. Villalon, R. Paz, N. Roehri, S. Lagarde, F. Pizzo, B. Colombet et al. « EpiTools, A software suite for presurgical brain mapping in epilepsy : Intracerebral EEG ». In : *Journal of neuroscience methods* 303 (2018), p. 7-15.

[139] I. R. Violante, K. Alania, A. M. Cassarà, E. Neufeld, E. Acerbo, R. Carron et al. « Non-invasive temporal interference electrical stimulation of the human hippocampus ». In : *Nature neuroscience* 26.11 (2023), p. 1994-2004.

[140] H. E. Wang, J. Scholly, P. Triebkorn, V. Sip, S. M. Villalon, M. M. Woodman et al. « VEP atlas : An anatomic and functional human brain atlas dedicated to epilepsy patients ». In : *Journal of neuroscience methods* 348 (2021), p. 108983.

[141] H. E. Wang, P. Triebkorn, M. Breyton, B. Dollomaja, J.-D. Lemarechal, S. Petkoski et al. « Virtual brain twins : from basic neuroscience to clinical use ». In : *National Science Review* 11.5 (2024), nwae079.

[142] H. E. Wang, M. Woodman, P. Triebkorn, J.-D. Lemarechal, J. Jha, B. Dollomaja et al. « Delineating epileptogenic networks using brain imaging data and personalized modeling in drug-resistant epilepsy ». In : *Science Translational Medicine* 15.680 (2023), eabp8982.

[143] F. Wendling, P. Benquet, F. Bartolomei et V. Jirsa. « Computational models of epileptiform activity ». In : *Journal of neuroscience methods* 260 (2016), p. 233-251.

[144] M. Wenzel, J. P. Hamm, D. S. Peterka et R. Yuste. « Acute focal seizures start as local synchronizations of neuronal ensembles ». In : *Journal of Neuroscience* 39.43 (2019), p. 8562-8575.

[145] H. G. Wieser, W. T. Blume, D. Fish, E. Goldensohn, A. Hufnagel, D. King et al. « Proposal for a New Classification of Outcome with Respect to Epileptic Seizures Following Epilepsy Surgery ». In : *Epilepsia* 42 (2 juill. 2008), p. 282-286. doi : 10.1046/j.1528-1157.2001.35100.x.

[146] H. R. Wilson et J. D. Cowan. « Excitatory and inhibitory interactions in localized populations of model neurons ». In : *Biophysical journal* 12.1 (1972), p. 1-24.

[147] M. Windhoff, A. Opitz et A. Thielscher. *Electric field calculations in brain stimulation based on finite elements : an optimized processing pipeline for the generation and usage of accurate individual head models*. Rapp. tech. Wiley Online Library, 2013.

[149] M. Zijlmans, W. Zweiphenning et N. van Klink. « Changing concepts in presurgical assessment for epilepsy surgery ». In : *Nature Reviews Neurology* 15.10 (2019), p. 594-606.

[150] K. Zilles et K. Amunts. « Cytoarchitectonic and receptorarchitectonic organization in Broca's region and surrounding cortex ». In : *Current Opinion in Behavioral Sciences* 21 (juin 2018), p. 93-105. doi : 10.1016/j.cobeha.2018.02.011.